

Louisiana Tech University

Louisiana Tech Digital Commons

Doctoral Dissertations

Graduate School

Summer 8-16-2018

Investigating the Role of Operating Parameters and Surface Treatments of Carbon Based Electrodes in Capacitive Deionization

Md Ashique Ahmed
Louisiana Tech University

Follow this and additional works at: <https://digitalcommons.latech.edu/dissertations>

Recommended Citation

Ahmed, Md Ashique, "" (2018). *Dissertation. 22.*
<https://digitalcommons.latech.edu/dissertations/22>

This Dissertation is brought to you for free and open access by the Graduate School at Louisiana Tech Digital Commons. It has been accepted for inclusion in Doctoral Dissertations by an authorized administrator of Louisiana Tech Digital Commons. For more information, please contact digitalcommons@latech.edu.

Summer 8-16-2018

Investigating the Role of Operating Parameters and Surface Treatments of Carbon Based Electrodes in Capacitive Deionization

Md Ashique Ahmed
Louisiana Tech University

Follow this and additional works at: <https://digitalcommons.latech.edu/dissertations>

Recommended Citation

Ahmed, Md Ashique, "" (2018). *Dissertation*. 22.
<https://digitalcommons.latech.edu/dissertations/22>

This Dissertation is brought to you for free and open access by the Graduate School at Louisiana Tech Digital Commons. It has been accepted for inclusion in Doctoral Dissertations by an authorized administrator of Louisiana Tech Digital Commons. For more information, please contact digitalcommons@latech.edu.

INVESTIGATING THE ROLE OF OPERATING PARAMETERS AND
SURFACE TREATMENTS OF CARBON BASED ELECTRODES
IN CAPACITIVE DEIONIZATION

by

Md Ashique Ahmed, B.Sc., M.S.

A Dissertation Presented in Partial Fulfillment
of the Requirements for the Degree
Doctor of Philosophy

COLLEGE OF ENGINEERING AND SCIENCE
LOUISIANA TECH UNIVERSITY

August 2018

LOUISIANA TECH UNIVERSITY

THE GRADUATE SCHOOL

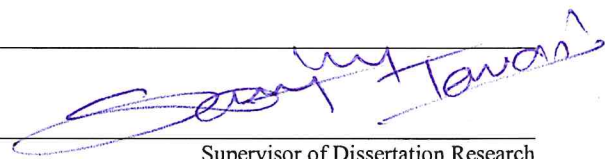
June 21, 2018

Date

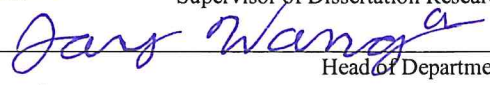
We hereby recommend that the dissertation prepared under our supervision
by Md Ashique Ahmed

entitled INVESTIGATING THE ROLE OF OPERATING PARAMETERS AND
SURFACE TREATMENTS OF CARBON BASED ELECTRODES
IN CAPACITIVE DEIONIZATION

be accepted in partial fulfillment of the requirements for the Degree of
PhD - Engineering



Supervisor of Dissertation Research



Head of Department


Engineering

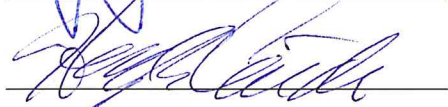
Department

Recommendation concurred in:



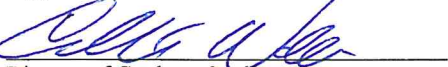






Advisory Committee

Approved:



Director of Graduate Studies

Approved:



Dean of the Graduate School



Dean of the College

ABSTRACT

This research focused on studying salt ion removal behavior and regeneration of electrodes used in capacitive deionization (CDI). CDI is a novel deionization technology that utilizes electrochemical processes to extract ions from water and either hold them electrostatically on the electrode surface or trap them in a double layer formed next to surface of electrodes. The use of porous carbon materials as electrodes in CDI enhances ion removal capacity because of availability of high surface area, conductivity, porosity, non-corrosive behavior, and other favorable properties. Experiments were conducted with a synthetic NaCl solution prepared in the laboratory. The first part of this dissertation focused on studying the adsorption and desorption behavior of CDI electrodes under various operating parameters. The effects of applied voltage, ambient temperature, flow rate, and initial concentration of solution on the salt removal behavior of CDI electrodes during the adsorption stage were studied. An isotherm study was conducted to model the data obtained during adsorption stage. Regeneration of saturated/exhausted CDI electrodes was achieved through desorption with observed variables being applied reverse potential, duration of applied reverse potential, ambient temperature, and flow rate. The second part of this research focused on studying salt removal behavior of CDI electrodes before and after surface treatment. Two types of surface treatments were studied – nitric acid treatment and gold deposition on electrode surface. This is the first study to use novel gold deposited carbon/aerogel fiber paper-based electrodes in CDI

experiments. The salt removal behavior of treated electrodes was studied for two symmetric (same electrode on both sides as positive and negative) and two asymmetric (treated electrode on one side and untreated on the other side) electrode configurations. The results from these configurations were compared with symmetric configuration of untreated electrodes (both positive and negative electrodes are untreated). The characteristics of the electrodes before and after surface treatment were assessed based on scanning electron microscopy (SEM), three-dimensional laser confocal microscopy, cyclic voltammetry (CV), Fourier transform spectroscopy (FTIR), and surface area and porosity measurement from BET isotherm analysis. The highest salt removal capacity achieved was 8.0 mg/g of NaCl when a gold-deposited electrode was used as an anode and an untreated electrode was used as a cathode.

DEDICATION

To

My parents and wife

TABLE OF CONTENTS

| | |
|--|-----|
| ABSTRACT..... | iii |
| DEDICATION..... | v |
| LIST OF TABLES..... | x |
| LIST OF FIGURES..... | xii |
| ACKNOWLEDGMENTS..... | xvi |
| CHAPTER 1 INTRODUCTION..... | 1 |
| 1.1 Background..... | 1 |
| 1.2 Hypotheses..... | 3 |
| 1.3 Objective..... | 5 |
| CHAPTER 2 LITERATURE REVIEW..... | 7 |
| 2.1 Introduction..... | 8 |
| 2.2 Process of Capacitive Deionization..... | 12 |
| 2.2.1 Basic operation..... | 12 |
| 2.2.2 Electrode materials..... | 16 |
| 2.3 Digging Deeper into the Science of Capacitive Deionization..... | 16 |
| 2.3.1 Effect of porosity of electrodes..... | 16 |
| 2.3.2 Effect of charge efficiency of electrical double layer..... | 20 |
| 2.3.3 Constant voltage and constant current methods..... | 21 |
| 2.4 Electrode and other development approaches in capacitive deionization process..... | 23 |
| 2.4.1 Electrode preference and surface modification..... | 25 |

| | | |
|--|---|----|
| 2.4.2 | Graphene based electrodes..... | 34 |
| 2.4.3 | Inclusion of membrane, polymer, resins, ion selective materials etc. | 36 |
| 2.4.4 | Energy recovery & energy efficient electrode development | 39 |
| 2.4.5 | Suspended electrodes (FCDI systems) and inverted CDI (i-CDI systems) .. | 41 |
| 2.4.6 | Targeted removal | 43 |
| 2.4.7 | Pilot scale studies..... | 44 |
| 2.5 | Conclusion | 45 |
| CHAPTER 3 MATERIALS AND METHODOLOGY..... | | 48 |
| 3.1 | Materials and equipment for CDI operation..... | 48 |
| 3.2 | Peristaltic pump calibration | 51 |
| 3.3 | Cell preparation..... | 52 |
| 3.4 | Capacitive deionization test setup for adsorption..... | 54 |
| 3.5 | Salt removal capacity measurement from adsorption..... | 55 |
| 3.6 | Acetone wash of electrodes | 57 |
| 3.7 | Experimental set up and methods for chapter-4 (adsorption)..... | 58 |
| 3.7.1 | Applied voltage adsorption experiments | 58 |
| 3.7.2 | Varying temperature level adsorption experiments | 58 |
| 3.7.3 | Varying flow adsorption experiments..... | 59 |
| 3.7.4 | Varying initial concentration adsorption experiments..... | 59 |
| 3.7.5 | Statistical analysis of adsorption data | 59 |
| 3.7.6 | Retention time and drift velocity related calculations | 60 |
| 3.7.7 | Isotherm modelling of data | 61 |
| 3.8 | Experimental set up and methods for chapter-4 (desorption)..... | 62 |
| 3.8.1 | Multi-pass method (Re-circulating Flow)..... | 62 |
| 3.8.2 | Single-pass Method (No Re-circulation Flow)..... | 64 |

| | | |
|---|---|----|
| 3.9 | Experimental setup and methods for surface treatment (chapter-5)..... | 67 |
| 3.9.1 | Acid treatment process..... | 67 |
| 3.9.2 | Gold deposition process..... | 68 |
| 3.9.3 | Scanning electron microscopy..... | 68 |
| 3.9.4 | Laser scanning microscopy..... | 68 |
| 3.9.5 | Surface area and porosity analysis..... | 68 |
| 3.9.6 | Cyclic voltammetry test set up..... | 69 |
| 3.9.7 | Fourier transform infrared spectroscopy (FTIR)..... | 69 |
| 3.9.8 | Symmetric and asymmetric configuration using acid treated electrode..... | 70 |
| 3.9.9 | Symmetric and asymmetric configuration in gold deposited cell..... | 70 |
| 3.9.10 | Capacitive deionization experiments..... | 71 |
| CHAPTER 4 EFFECT OF OPERATING PARAMETERS..... | | 73 |
| 4.1 | Effect of operating parameter on adsorption..... | 73 |
| 4.1.1 | Effect of applied voltage on salt removal capacity of CDI electrodes..... | 73 |
| 4.1.2 | Effect of temperature on salt removal capacity of CDI electrodes..... | 78 |
| 4.1.3 | Effect of flow rate on salt removal capacity..... | 81 |
| 4.1.4 | Effect of initial concentration on salt removal capacity..... | 84 |
| 4.1.5 | Adsorption Isotherms..... | 87 |
| 4.2 | Effect of operating parameter on desorption..... | 91 |
| 4.2.1 | Effect of applied reverse potential using multi-pass method..... | 91 |
| 4.2.2 | Effect of duration of applied reverse voltage using multi-pass method..... | 92 |
| 4.2.3 | Effect of applied reverse potential using single-pass method..... | 94 |
| 4.2.4 | Effect of duration of applied reverse voltage using single-pass method..... | 96 |
| 4.2.5 | Effect of variation temperature using single-pass method..... | 97 |
| 4.2.6 | Effect of flow rate on regeneration using single-pass method..... | 99 |

| | |
|---|-------------------------------------|
| CHAPTER 5 SURFACE MODIFICATION AND SALT REMOVAL BEHAVIOR OF CDI ELECTRODES | 101 |
| 5.1 Results and discussion: nitric acid treatment | 101 |
| 5.2 Results and Discussion: gold deposition on electrodes | 109 |
| CHAPTER 6 CONCLUSION AND RECOMMENDATIONS | 117 |
| 6.1 Conclusions..... | 117 |
| 6.2 Recommendations..... | 120 |
| REFERENCES | Error! Bookmark not defined. |
| APPENDIX A..... | 122 |
| APPENDIX B..... | 159 |

LIST OF TABLES

| | |
|--|----|
| Table 2.1: Removal by different electrodes with different SSA and pore openings. | 19 |
| Table 2.2: Key parameters and their significance in selection of CDI electrodes selection based on physical, chemical and other characteristics..... | 24 |
| Table 2.3: Capacitance of different electrodes under different specific current..... | 25 |
| Table 2.4: Capacitance of different electrodes under different scan rates..... | 26 |
| Table 2.5: Removal per electrode mass by different electrodes under variable conditions..... | 27 |
| Table 2.6: Percentage of salt removal by different electrodes under variable conditions..... | 28 |
| Table 2.7: Specific Surface Area of different electrodes..... | 32 |
| Table 2.8: Other methods of carbon-based electrode development and corresponding changes..... | 33 |
| Table 2.9: Graphene based electrode and their modified forms | 35 |
| Table 2.10: 3D graphene-based electrode's performance at asymmetric electrode systems..... | 36 |
| Table 2.11: Energy and power density by different carbon-based electrodes | 41 |
| Table 3.1: Operating parameters for variation of applied reverse voltage experiments with multi-pass method..... | 63 |
| Table 3.2: Parameters for variation of duration of applied voltage experiments with multi-pass method..... | 64 |
| Table 3.3: Parameters for variation of applied reverse voltage experiments with single-pass method..... | 65 |
| Table 3.4: Parameters for variation of applied voltage duration experiments with single-pass method..... | 66 |

| | |
|---|-----|
| Table 3.5: Parameters for variation of temperature experiments with single-pass method..... | 67 |
| Table 3.6: Parameters for variation of flow rate experiments with Single-pass Method..... | 67 |
| Table 4.1: Average removal capacity of electrodes at different voltages and 95% confidence limits..... | 75 |
| Table 4.2: Average removal capacity of electrodes at different temperature and 95% confidence limits..... | 81 |
| Table 4.3: Average removal capacity of electrodes at different flow rates and 95% confidence limits..... | 83 |
| Table 4.4: Average removal capacity of electrodes at different initial concentrations and 95% confidence limits..... | 86 |
| Table 4.5: Parameter values from isotherm models..... | 89 |
| Table 4.6: Regeneration percentages for various applied reverse voltages using multi-pass method..... | 91 |
| Table 4.7: Regeneration percentages for various time lengths of applying reverse voltages using multi-pass method..... | 93 |
| Table 4.8: Regeneration percentages for various applied reverse voltages using single-pass method..... | 95 |
| Table 4.9: Regeneration percentages for various time lengths of applying reverse voltages using single-pass method..... | 96 |
| Table 4.10: Regeneration percentages for various temperature levels using single-pass method..... | 98 |
| Table 4.11: Regeneration percentages for various flow rates using single-pass method..... | 99 |
| Table 5.1: Results from N ₂ gas adsorption- desorption | 104 |
| Table 5.2: Results from N ₂ gas adsorption- desorption | 111 |
| Table 5.3: Salt removal capacities by different electrodes | 114 |

LIST OF FIGURES

| | |
|--|----|
| Figure 2-1: Process of batch mode CDI experiments - Reprinted from [2], Copyright (2013), with permission from Elsevier. | 12 |
| Figure 2-2: Basic idea of adsorption in CDI process. | 14 |
| Figure 2-3: Regeneration of electrodes in CDI process. | 14 |
| Figure 2-4: Process of membrane capacitive deionization during desorption. | 15 |
| Figure 2-5: Electro-sorption capacity vs micro-porosity at various applied voltages and ionic strength – Reprinted from [23], Copyright (2014), with permission from Elsevier. | 17 |
| Figure 2-6: Possible ion-diffusion path in three different pore structures (a) 2D-hexagonal (b)3D symmetry cube (c) 3D-bincontinuous-Reprinted (adapted) with permission from [35]. Copyright 2011 American Chemical Society. | 18 |
| Figure 2-7: Comparison of removal rate by carbon aerogel electrode with PMCG and RMCG – Reprinted (adapted) with permission from [36]. Copyright 2011 American Chemical Society. | 18 |
| Figure 2-8: Charge efficiency of electrodes- Reprinted (adapted) with permission from [39]). Copyright 2012 American Chemical Society. | 20 |
| Figure 2-9: Physical adsorption and electro-sorption performance of the electrode- Reprinted (adapted) with permission from [39]). Copyright 2012 American Chemical Society. | 21 |
| Figure 2-10: Effluent concentration in (a) CV and (b) CC mode – Reprinted from [41]. | 22 |
| Figure 2-11: Adsorption efficiency (a), charge efficiency (b) and energy consumption (c) at different cell potential for CV and CC mode – Reprinted from [41]. | 23 |
| Figure 2-12: Diagram of suspension electrodes in capacitive deionization (used with permission) [80]. | 42 |
| Figure 3-1: Carbon aerogel/fiber paper used as electrode in this study. | 48 |

| | |
|--|----|
| Figure 3-2: Flexible graphite sheet with no insert used as current collector. | 49 |
| Figure 3-3: Power supplier used. | 50 |
| Figure 3-4: (a) Multimeter used for data collection (b) conductivity probe (c) pH probe | 50 |
| Figure 3-5: (a) Magnetic stirrer (b) Deionized water producing system. | 51 |
| Figure 3-6: A peristaltic pump used in this study. | 52 |
| Figure 3-7: (a) Electrode assembly with acrylic sheet and current collector (b) top view of the assembly..... | 53 |
| Figure 3-8: Schematic diagram of the CDI experimental setup. | 54 |
| Figure 3-9: Calibration curve for NaCl solution..... | 56 |
| Figure 3-10: Drift velocity (V_x) and flow velocity (V_y) in the ion path. | 61 |
| Figure 3-11: Different configurations of CDI experiments (a) Symmetric with both electrode with no deposition (b) Symmetric with both electrode with gold deposition (c) Asymmetric with gold deposited as negative (cathode) (d) Asymmetric with gold deposited as positive (anode). | 71 |
| Figure 4-1: The change in conductivity of reservoir solution with time at applied DC voltages of (a) 0.6 V (b) 0.8 V (c) 1 V (d) 1.2 V. | 74 |
| Figure 4-2: Salt removal capacity of electrodes as mg of salt removed per g of electrode at different applied voltages. | 75 |
| Figure 4-3: (a) Unknown brown solution (b) XRF data (c) NMR spectroscopy..... | 78 |
| Figure 4-4: The change in conductivity of reservoir solution with time at temperature values of (a) 9.7°C (b) 23°C (c) 34°C. | 79 |
| Figure 4-5: Salt removal capacity of CDI electrodes at various temperatures. | 81 |
| Figure 4-6: Salt removal capacity of CDI electrodes at flow rate of (a) 12 mL/min (b) 18 mL/min (c) 24 ml/min (d) 30 mL/min. | 82 |
| Figure 4-7: Salt removal capacity at different flow rates. | 83 |
| Figure 4-8: Salt removal capacity at different flow rates (a) 100 mg/L (b) 200 mg/L (c) 300 mg/L (d) 400 mg/L. | 85 |
| Figure 4-9: Salt removal capacity at initial concentrations. | 86 |
| Figure 4-10: Freundlich isotherm model. | 89 |

| | |
|--|-----|
| Figure 4-11: Langmuir isotherm model..... | 90 |
| Figure 4-12: Dubinin-Radushkevich isotherm model..... | 90 |
| Figure 4-13: Regeneration rates for different reverse voltages using multi-pass Method..... | 92 |
| Figure 4-14: Regeneration rates for different time lengths of applying voltage using multi-pass method..... | 93 |
| Figure 4-15: Regeneration rates for various applied reverse voltage using single-pass method..... | 95 |
| Figure 4-16: Regeneration rates for various duration of applying reverse voltage using single-pass method..... | 97 |
| Figure 4-17: Regeneration rates for various temperature level using single -pass method..... | 98 |
| Figure 4-18: Regeneration rates for various flow rates using single-pass method..... | 99 |
| Figure 5-1: SEM image of electrodes before (left) and after (right) nitric acid treatment. | 102 |
| Figure 5-2: Surface profile by 3D laser confocal microscope – untreated electrode (left) and electrode after nitric acid treatment (right). | 103 |
| Figure 5-3: FTIR spectra of electrodes before and after nitric acid treatment..... | 103 |
| Figure 5-4: Cyclic voltammogram of electrodes before and after nitric acid treatment. | 105 |
| Figure 5-5: Specific capacitance (F/g) for electrodes before and after acid treatment... .. | 105 |
| Figure 5-6: Conductivity and pH change with time for both electrodes untreated..... | 106 |
| Figure 5-7: Conductivity and pH change with time for - both electrodes acid treated... .. | 107 |
| Figure 5-8: Conductivity and pH change with time for nitric acid treated electrode as cathode and untreated electrode as anode..... | 107 |
| Figure 5-9: Conductivity and pH change with time for nitric acid treated electrode as anode and untreated electrode as cathode..... | 108 |
| Figure 5-10: SEM images of electrode without (left) and with (right) gold deposition. | 109 |
| Figure 5-11: Surface profile by 3D laser confocal microscope (a) Electrode without deposition (b) Electrode with gold deposition..... | 110 |

Figure 5-12: (a) Cyclic voltammogram of electrodes before and after gold deposition
(b) Specific capacitance (F/g) for electrodes before and after gold deposition. 112

Figure 5-13: Conductivity drop with time in configuration where, (a) both electrodes are unmodified (without gold deposition), (b) both electrodes are modified (gold deposited), (c) gold treated electrode is cathode and no gold deposited one is anode
(d) gold treated electrode is anode and no gold deposited one is cathode. 113

ACKNOWLEDGMENTS

First, I would like to thank Almighty God for all the blessings and privileges I have been given in life.

I would like to express my deepest gratitude to Dr. Sanjay Tewari for his constant support, mentorship, guidance and patience throughout this journey. Without his active involvement in every aspect of this dissertation, it would not have been possible. It was an honor to have him as chair of my doctoral dissertation committee.

I would also like to thank Dr. Cardenas, Dr. Eklund, Dr. Wasi and Dr. Sherer for serving on my doctoral committee and for their guidance and help during this course of research, fruitful discussion on my work during the presentations and the corrections, which have widened my outlook as a researcher.

I would also like to thank Shams Arafat and Chandramouli Tummala for their help in laboratory experiments and their constant support as colleagues and friends.

I would like to thank my parents, who sacrificed their dreams to make the lives of their children better. I would also like to thank my in-laws, specially Colonel Belayet Hossain for his unconditional support all these years.

Lastly, I would like to thank my wife Mahjabin Chowdhury Tiny. She has been the source of my strength since the day we met. Without her, I would have given up this journey at the half-way point. I am here today because of her unwavering faith in me. She keeps me strong when I feel doubt.

CHAPTER 1

INTRODUCTION

1.1 Background

Capacitive deionization (CDI) is an emerging electrochemical technology. It has been used for various applications starting from water purification to water desalination. It has proved to be energy and cost efficient specifically in comparison with traditional membrane-based technologies to desalinate brackish water (salt concentration less than 10 g/L) or low saline water. In CDI, salts are removed through adsorption process aided by electrostatic forces.

A CDI cell is analogous to a capacitor. In its simplest configuration, there are two electrically conductive, flat and thin electrodes that are separated by a distance of a couple of millimeters. An electrical low voltage (direct current) of about 1.2 V is applied across these electrodes. Water contaminated with charged ions or impurities is allowed to pass through the narrow space between the electrodes. As charged ions navigate the electrical field between the electrodes, they are attracted to oppositely charged electrodes and are removed from the flow stream. These ions usually get adsorbed on the surface of the electrode. Water coming out of a CDI cell is relatively cleaner compared to water entering the CDI cell. As available surface area of each electrode is being occupied by ions that are being removed from the flow stream over a duration of time, electrodes start

to get saturated. The water purification/desalination process slows down and stops when electrodes are completely saturated (exhausted). The saturated electrodes can be regenerated through desorption process and reused for adsorption.

Due to high conductivity, relative inertness in chemical environment, highly porous structure, high surface area and other such qualities, carbon-based electrodes have been a popular choice as electrode material and there is enough evidence in the literature to support the choice as discussed in Chapter 2. Carbon aerogel is one of the allotropes showing remarkable applicability as electrodes in CDI applications. Low density, high porosity, and pore sizes mostly in mesoporous range etc., make carbon aerogel a suitable candidate to adsorb more ions in the electrochemical environment.

Carbon aerogel is usually prepared through sol-gel process. In this process, 1, 3-dihydroxybenzene called resorcinol-formaldehyde (RF), is mixed with methanol to enter a polymerization reaction. The reaction can either go on for weeks or can be completed in two to three days at higher temperatures. Following this reaction, nanoparticles get crosslinked and a mesoporous framework structure evolves and physically appears as a gel. When this gel is dried, it becomes aerogel. This RF aerogel goes through carbonization. This process converts most of the non-carbon content to a carbonized skeleton of similar structure. Carbon aerogel appears in powder form, which is bound to a conductive surface like metal or graphite by using a suitable binder. This kind of surface allows carbon aerogel to be used as adsorption agent in electrochemical deionization processes like CDI. In this dissertation, the electrode materials used is carbon aerogel bound together with carbon fibers and produced in paper form. For ease it is called carbon aerogel/fiber paper.

In CDI literature as discussed in Section 2.4 of this dissertation, research efforts mostly focus on developing new and highly efficient electrode material. Efficient materials can provide high salt removal capacity in CDI process. Another way to improve salt removal capacity of electrodes is to use an optimized condition based on their performance at various operating conditions. For this improvement, a rigorous study was required to observe effects of operating parameters on salt removal capacity. Since some of the synthesized electrode material can be expensive, the regeneration of saturated electrodes is also highly desirable in CDI process because it reduces the overall cost of the CDI process. Therefore, Chapter 4 of this dissertation focuses on exploring various effects of several operating parameters on adsorption as well as desorption.

Various chemical treatments such as metal coatings, modification with metal oxides, composite development, and other surface modification methods can improve ion removal capacity of these electrodes. The salt removal capacity of carbon/aerogel/fiber paper electrodes following acid treatment and highly conductive metal coating is discussed in Chapter 5 of this dissertation.

1.2 Hypotheses

The adsorption (salt removal capacity) performance of electrodes in CDI applications depends on electrode surface morphology, pore openings, flow velocity of ions to be removed, concentration of the solution, ambient temperature, and factors that are specific to configuration of CDI cells and electrodes such as available electrical field between electrodes, separation distance of electrodes, travel distance of ions before exiting the electrical field and so many other factors. Two groups of hypotheses

(adsorption and desorption) are tested in this investigation. The adsorption-specific major hypotheses are listed below:

1. As applied potential across electrodes is increased, the salt removal capacity of electrodes should also increase. However, the electrochemical environment present in CDI cells may pose a limit restricting the amount of applied potential.
2. Since temperature affects the activation forces of ions and surface properties of electrodes, an increase in temperature can increase the salt removal capacity of electrodes.
3. Flow velocity of the ions within a CDI cell can affect the availability of ions near electrodes. Thus, increased flow rate can decrease the salt removal capacity.
4. A high initial concentration will lead to a higher concentration gradient, which should result in higher mass transfer of ions onto electrodes.
5. Treating the electrode surface with a strong acid can alter electrode surface and bonding in the chemical structure and can increase the salt removal capacity of the electrodes.
6. Having dissimilar electrodes in a CDI cell with an acid treated electrode as one electrode and an untreated electrode as opposite one can increase the salt removal capacity as compared to CDI cell with two treated or two untreated electrodes.
7. Deposition of a conductive metal can change electrochemical properties and behavior of electrodes in CDI environment and should enhance the salt removal capacity of electrodes.

8. viii. Having dissimilar electrodes with metal-deposited electrode as one electrode and untreated electrode as opposite one can increase the salt removal capacity compared to CDI cell with two metal-deposited or two untreated electrodes.

The desorption-specific major hypotheses tested in this dissertation are listed below:

1. Applying reverse potential should detach ions from electrode surface and push them out of the deep pores of the electrodes before they are flushed out of CDI. However, if the reverse potential is applied too long, the desorbed ions could reabsorb onto the opposite electrode before being flushed out of the CDI cell.
2. Duration of applied reverse voltage may affect the ability of ions to get reabsorbed on oppositely charged electrode. Higher applied voltage can decrease the desorption capacity.
3. Temperature may affect the activation of ions and morphology of the surface, which in turn can increase the desorption capacity when temperature is increased.
4. The flow rate of the deionized water used in the desorption process effects the flow speed over electrodes with retention time of the wash water in the CDI cell determining the time ions are in electrical field. This can increase the desorption capacity.

1.3 Objective

Experiments are designed to obtain the information needed to support or reject each of the hypotheses. After each of the objectives were met, rational conclusions of the

adsorption and desorption behavior under varying operating conditions and after surface modification are made. The specific objectives of this study are as follows:

1. Study the effect of applied voltage on salt removal capacity.
2. Study the effect of temperature on salt removal capacity.
3. Study the effect of flow rate on salt removal capacity.
4. Study the effect of initial concentration solution on salt removal capacity.
5. Study isotherm behavior in applied conditions to understand how ions are being adsorbed onto electrode surface.
6. Study the effect of surface modifications with nitric acid treatment on salt removal capacity of electrodes.
7. Study various configurations of electrode arrangement (acid treated electrode on one side, untreated on the other side or both acid treated electrodes, etc.) to assess the ion removal behavior under acid treated conditions.
8. Study how gold layer deposition on the electrodes affects salt removal capacity.
9. Study various configurations of the electrode arrangement (gold deposited electrode on one side, untreated on the other side or both gold deposited electrodes, etc.) to assess the ion removal behavior under gold deposited conditions.

CHAPTER 2

LITERATURE REVIEW

Capacitive deionization (CDI) is a new technology that has been successfully utilized for many water treatment/purification applications. The CDI technology has shown increased efficiency compared to the other contemporary technologies. Recent developments (discussed later in this chapter) in the CDI technology have enhanced the adsorption capacity of electrode materials. Different types of carbon electrodes, such as traditional and latest forms of porous-carbon and graphene-based electrodes, have been used in the CDI technology. This has further increased the effectiveness of CDI by facilitating mass transfer in the form of adsorption of salt ions on to modified electrodes. This chapter aims to review basic concepts, electrode saturation-regeneration processes, various types of materials used for electrodes and assess the overall state of CDI technology. In addition, this chapter reviews the recent progress made in electrode surface modifications by metals or metal oxides, membrane, polymer, organics and other compounds, which have resulted in increased efficiency of ion extraction from water. The evaluation of past and present research in using low-cost carbon forms as electrode materials to reduce the overall cost and eliminate the need to regenerate saturated electrodes is also part of the chapter.

2.1 Introduction

The demand for more quantity of potable water has always existed. Researchers have explored many possible ways to meet this demand. Seawater is the focus of recent research in potable water as it is available in huge quantities throughout the world. Additionally, brackish water is common in coastal areas all over the world. Countries with desert lands and little fresh water seek more cost effective and innovative approaches for the desalination of water. The huge amounts of energy, high production costs, and the constant need to fine tune design flaws, etc., have made it difficult for existing desalination technologies, such as multi-effect desalination (MED), reverse osmosis (RO), and multistage flash (MSF) etc., to become sustainable solution options [1, 2]. CDI has emerged as an effective alternative for these existing technologies in terms of energy efficiency, environmental friendliness and of course the ion removal efficiency [3]. In typical production of CDI of salt water, porous carbon is used in electrodes, a DC voltage is applied, and saline water is pumped into the cell. The electrodes eventually extract the salt ions from water. After adsorption of salt ions, the applied voltage is either reversed or the electrochemical cell is short-circuited to regenerate the electrodes by desorption of ions [1, 2, 4-8]. There is no need for application of any external pressure to extract ions, as is required in membrane filtration and some other desalination processes, because ions are extracted by electrostatic force. In the case of brackish water, where salt ions are fewer with respect to the amount of water in which they are dissolved, it is more energy efficient to remove these ions rather than it is to extract the water, as in reverse osmosis. Therefore, for low salt concentrated waters CDI is more efficient than RO, but optimization of operating conditions is still required in large scale production. The same

is true for seawater desalination using CDI. Since there is a desorption stage associated in CDI operations, there is good chance of energy recovery, which has attracted the attention of many researchers. The latest research approaches in CDI as discussed later in this chapter are therefore focused on solving specific issues such as the need to optimize of operational parameters, to improve of co-ion adsorption, and to enhance the surface area and porosity of the electrodes.

Modification of surface area of activated carbon, carbon aerogel, graphene, carbon nanotube, carbon nanofoam and other carbon-based electrodes is an approach to increase efficiency of CDI operations. Studies [3, 9] have shown that a greater surface area and appropriate pore size distribution (with respect of the size of target ions) are very important for higher removal efficiency in CDI cells. Usually, two same type electrodes were used in classical CDI cells, which is termed as "symmetric" operation of CDI in the research literature. However, modifying each electrode with different metal oxides and consequently shifting the potential zero charge (PZC) location increased the removal efficiency of preferred ions to a significant extent [6]. This is termed as "asymmetric" operation of CDI in the research literature, because of the electrochemical dissimilarity of the electrodes. Some studies focused on selective ion removal from a solution of mixed salts. For example, fabrication of nitrate selective carbon electrode using resins has shown significant improvement in nitrate removal in one of these studies [7]. High surface area and high electrical conductivity are the most important requirements of CDI electrodes. Synthesis method and activation process are also crucial factors in controlling properties of the surfaces in carbon-based electrodes. The resorcinol-formaldehyde method allows control which synthesizing carbon aerogel (CA)

with desired surface area by varying the mixing ratio and pyrolysis temperature. Thermal activation by CO₂ of CA electrodes resulted in ion removal, specifically nitrates and phosphates from agricultural fertilizers in CDI operation [9]. Carbon aerogel/fiber paper electrodes washed with Acetone and Nitric Acid also exhibited higher removal capacity in CDI operation [10].

Another attempt to improve the efficiency of CDI operation involves introducing of ion exchange membranes between the electrodes and spacer channel (the space between two electrodes), which is termed membrane capacitive deionization (MCDI). These membranes restrict the adsorption of co-ions (ions which have the same charge with respect to an electrode in the removal stage and become oppositely charged in regeneration stage) during the regeneration process, thus improving the adsorption capacity of electrodes after regeneration [11]. Recent approaches in this research aimed to make MCDI a better alternative for RO in desalination of seawater. MCDI can be more energy efficient than RO for salinity concentrations less than 60 mM [4]. A possibility energy recovery during regeneration stage results in overall low energy consumption in MCDI cells [11]. In one of the modified MCDI methods, electrodes are coated with ion exchange polymers, which improves the contact adhesion between the electrodes and ion exchange membranes, resulting in a lower contact resistance and lower bulk resistivity. Consequently, energy consumption falls compared to conventional MCDI operation [12]. Models have also been developed that can successfully help predict steady state in CDI operation [13]. The model describes the CDI operation in terms of different operational parameters, i.e., flow rate, water quantity, CDI capacitance, resistance, spacer volume, applied potential, initial concentration, etc.

The concept of charge efficiency, defined as a ratio of charge equivalent of total salt adsorbed at equilibrium over charge supplied to an electrode, was developed to give more accurate understanding of the CDI process [14]. Recent electrode modification studies aimed to increase the charge efficiency of CDI cell by surface treatment of electrodes with metal oxides. One of these studies used surface treated electrodes and a "third" electrode of activated carbon fiber to increase the charge efficiency [15].

Statistical models such as Box-Behnken and ANOVA were used in two studies to optimize the operational conditions such as initial concentration, flow rate and cell voltage which maximize the electro-sorption of ions in CDI cells [2, 16]. The Box-Behnken statistical model was used to predict the removal percentage of arsenic in a solar panel based CDI setup with activated carbon electrodes. The method predicted the removal to be 84.2% and 100% at different experimental conditions, while actual values were observed to be 82.6% and 98% respectively [16].

This chapter reviews the latest CDI processes, the recent trend of electrode development using a combination of materials, and the current state of the technology. It provides comparative analysis of results achieved in recent research studies in this field. There are some recent publications that reviewed the technology and presented some interesting information [3, 17-22]. However, this chapter presents in-depth discussion of a broader range of key parameters and accounts for latest progress in this field. It will help in developing a better understanding of CDI technology and its operational parameters.

2.2 Process of Capacitive Deionization

2.2.1 Basic operation

The capacitive deionization process includes two electrodes supported on glass/plexiglass and placed face to face in a parallel configuration with very little separation. The space between electrodes is either kept as open channel [10] or a spacer material is used. Spacer material can be a woven/non-woven fabric [23] or a polymeric mesh [24] or any other mesh material is made of an electrically insulated, chemically inert, and anti-corrosive material [25]. The spacer should permit the solution to flow through and ions to pass through it in order to reach the electrical double layer region. In some cases, ion exchange membranes [4] are used between the electrode and spacer/open channel. Anion exchange membranes only allow anions to go through while cation exchange membrane does the opposite. A schematic diagram of the typical batch mode CDI experiment is shown in the Figure 2-1.

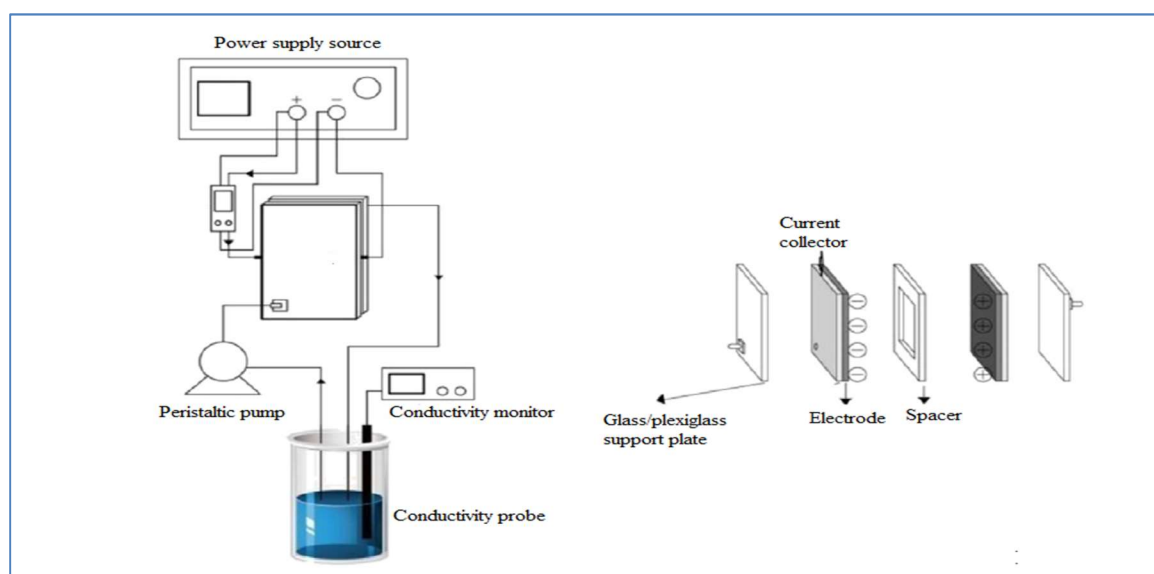


Figure 2-1: Process of batch mode CDI experiments - Reprinted from [2], Copyright (2013), with permission from Elsevier.

A current collector is also used to provide required charges to electrodes from an external power supply. Typically, a graphite current collector is used to ensure inertness and a corrosion-free environment. The use of copper wire as current collector resulted in corrosive reactions in one of the studies [26]. A CDI cell is analogous to a capacitor. The electrodes in a CDI cell are arranged exactly they are in capacitor plates and DC voltage is applied across the electrodes. In CDI cells, aqueous solution with ions to be removed can flow between electrodes. Under applied electrical field, the ions from the solution are attracted on to oppositely charged electrodes, as shown in Figure 2-2. In the outlet, deionized water appears. The CDI cell could be fed with water in a single-pass configuration (water travels between electrodes of the cell just once before exiting the cell) or in cyclic configuration (water exiting the CDI cell is repeatedly directed back to the CDI cell). The single-pass configuration is used with multiple CDI cells arranged in a series while the cyclic rotation is used with a single cell (lesser number of cells) where the solution from a reservoir is cyclically pumped through the electrodes using a peristaltic pump. The conductivity (Figure 2-1) of the reservoir is observed in real time to measure concentration of ions. Equilibrium is achieved when the electrodes are saturated and can no longer adsorb ions because all adsorption sites are taken by the adsorbed ions. At this point, the conductivity of the solution no longer changes.

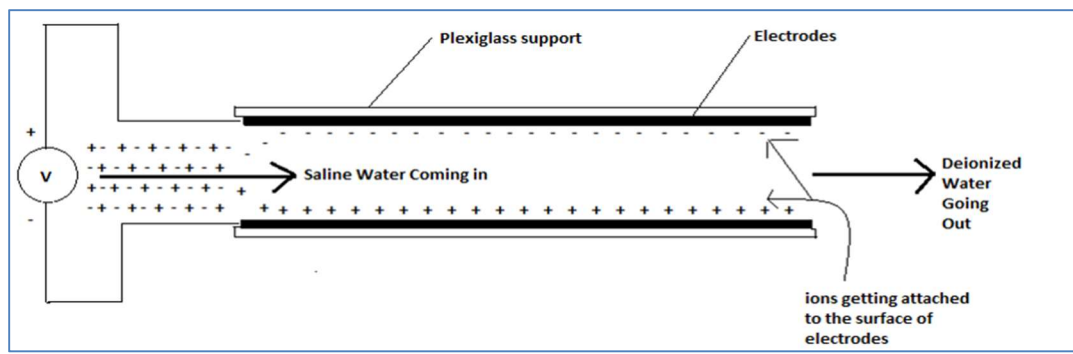


Figure 2-2: Basic idea of adsorption in CDI process.

After the adsorption process the saturated electrodes can undergo a regeneration/desorption process. This regenerated electrode can be used for adsorption process again, as needed. The process of regeneration is the opposite of the adsorption process in the case of CDI cells. In this process, the electrodes are either shorted or the polarity of the electrodes is reversed. Additionally, this process forces adsorbed ions dislodge and emerge in bulk liquid between electrodes before they are flushed out of the CDI cell. Deionized water or salt solution (typically with lower concentration than that of the preceding adsorption) stream are pumped through the system to wash out these ions, resulting in an ion saturated stream (Figure 2-3).

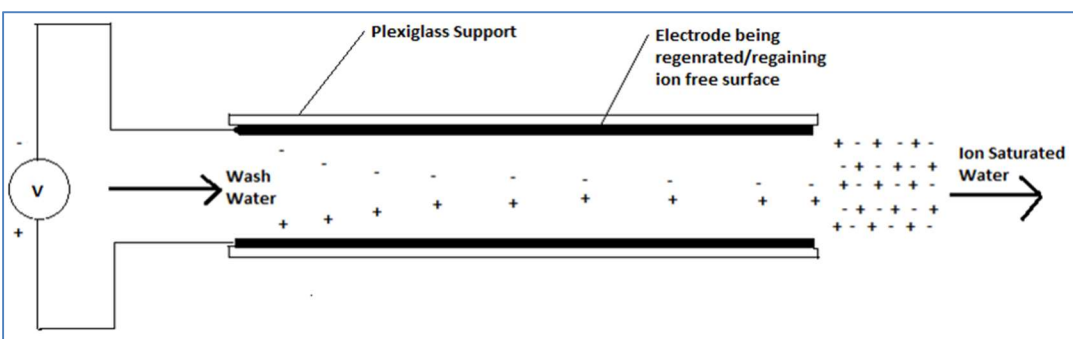


Figure 2-3: Regeneration of electrodes in CDI process.

There is a possibility for ions to get reabsorbed in the oppositely charged electrodes during this regeneration process. This reabsorption is not ideal for regeneration and can be avoided by applying a lower voltage for a brief period of time. Alternatively, electrodes can simply be short circuited, and wash-water is pumped at a higher flow rate. To overcome this challenge of re-adsorption some researchers developed membrane capacitive deionization in which an ion exchange membrane is used between the electrode and the spacer/open channel. These membranes free ions which then pass through into the spacer, preventing reabsorption on the other electrode (as membrane on the other side would not allow this ion to pass through). This membrane also helps to increase the charge efficiency [14] of the system by allowing counter ion adsorption and preventing co-ion exclusion (details discussed in membrane and charge efficiency sections). The typical process of MCDI is shown in Figure 2-4.

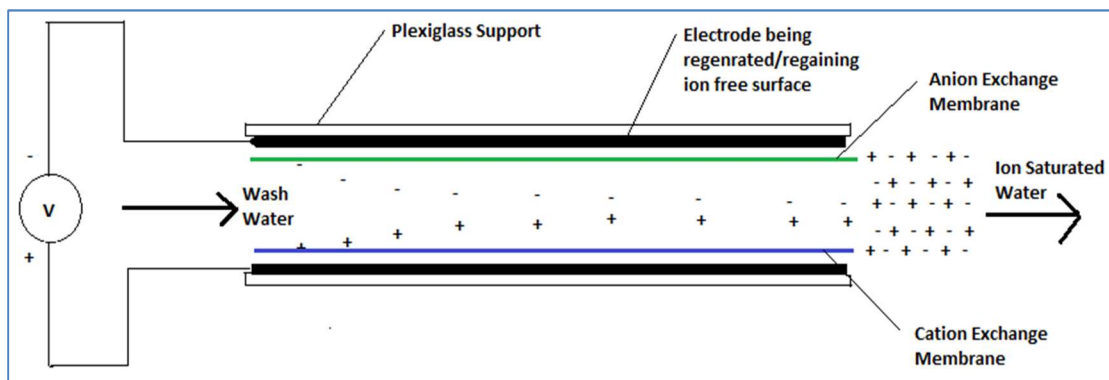


Figure 2-4: Process of membrane capacitive deionization during desorption.

2.2.2 Electrode materials

Carbon based electrodes are widely used in CDI applications due to their high conductivity, low contact resistance (a voltage drop from electrode to the current collector), good wetting behavior, low cost, good process-ability, bio-inertness, and chemical stability [3]. Various forms of carbon, its allotropes, and carbon composites are used in CDI applications such as activated carbon [27], carbon cloth [28], carbon aerogel [10], carbon nanotube [29], carbide derived carbons [30], graphene [31] etc. These materials are chosen due to their high specific surface areas and porous structures, which ensure plenty of available area for electro-sorption. In case of graphene its selection is based on the ease with which saturated electrodes regenerate. Metal oxides and carbon composites are used by some researchers due to their enhanced electrochemical performance [32]. Examples of electrode materials used can be seen in section 2.4.1.

2.3 **Future Analysis of the Science of Capacitive Deionization**

2.3.1 Effect of porosity of electrodes

The porosity of the electrode material plays a vital role in adsorption and electro-sorption performance. The relationship between the pore opening and hydrated radius of different ions is discussed in many recent articles. Though previous studies [33-36] of the traditional electrical double layer (EDL) have mentioned the contribution of the mesopores for most of the electro-sorption, in fact significant electro-sorption happened in micropores, too [23]. Instead of traditional EDL theories it was explained using modern EDL theories which consider ion hydration and water-water interaction phenomena. In these new models, ions are expected to form a single layer in the middle

of the pore, whereas the classical model says overlapping diffuse layer eliminates all electro-sorption in these micropores. Also, it was found that electro-sorption capacity increased with increase in applied potential and ionic strength as the diffuse layer in the EDL shrinks (Figure 2-5).

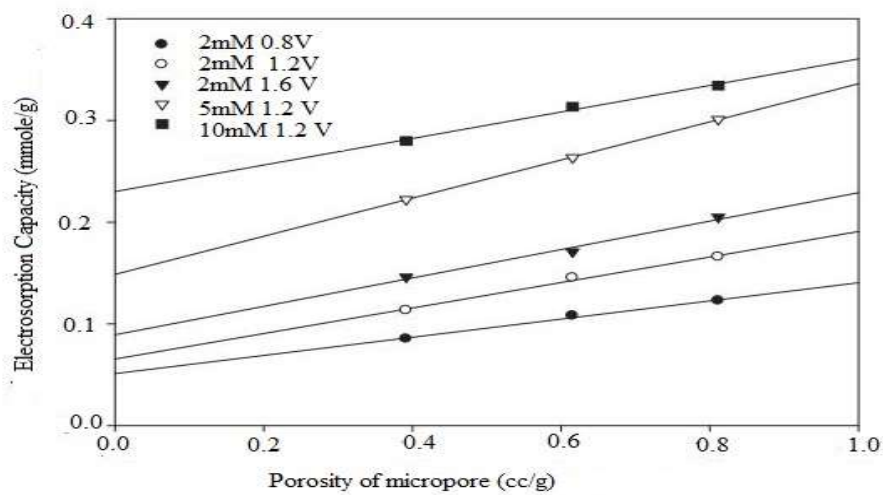


Figure 2-5: Electro-sorption capacity vs micro-porosity at various applied voltages and ionic strength – Reprinted from [23], Copyright (2014), with permission from Elsevier.

Three mesoporous carbons with 2D-hexagonal, 3D-cubic and 3D-bicontinuous pore opening were used as electrodes [35]. The average pore openings of these materials were 7.57 nm, 3.42 nm, and 3.25 nm respectively. From an electro-sorption study of capacitive deionization, it was seen that due to 2D-hexagonal structure, this electrode favors the absorption of monovalent ions in the pore walls. The electrode with 3D-cubic space favored monovalent and trivalent ions. The third electrode with a 3D-bicontinuous pore opening did not show significant electro-sorption compared to the performance of

first two electrodes. The probable reason is the bi-continuous path of its pore structure (Figure 2-6).

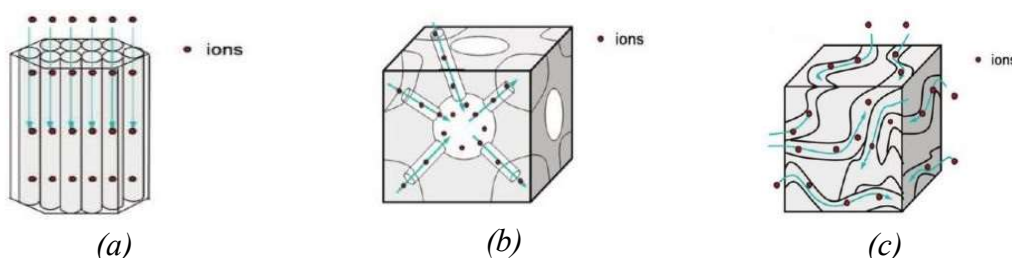


Figure 2-6: Possible ion-diffusion path in three different pore structures (a) 2D-hexagonal (b) 3D symmetry cube (c) 3D-bicontinuous-Reprinted (adapted) with permission from [35]. Copyright 2011 American Chemical Society.

Resorcinol based mesoporous carbon graphite electrodes (RMCG) and phloroglucinol based mesoporous carbon graphite electrodes (PMCG) were synthesized and their performances were compared to carbon aerogel electrodes [36]. The pores of the PMCG has narrower distribution compared to RMCG electrodes. At around 5000 ppm salt concentration, carbon aerogel electrodes exhibited a lower removal rate than PMCG and RMCG electrodes in CDI experiments (Figure 2-7).

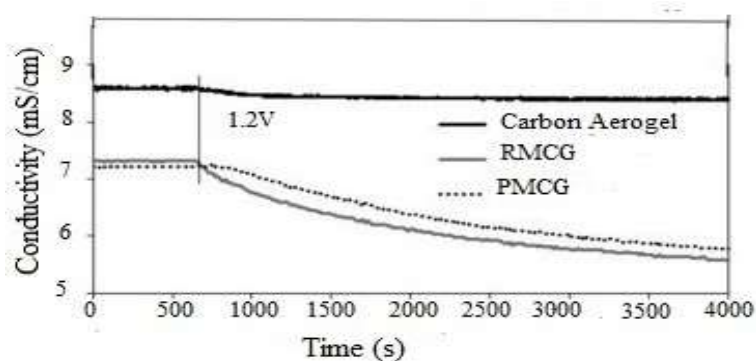


Figure 2-7: Comparison of removal rate by carbon aerogel electrode with PMCG and RMCG – Reprinted (adapted) with permission from [36]. Copyright 2011 American Chemical Society.

The performance comparison of some electrode materials with different specific surface area (SSA) and pore openings is presented in Table 2.1. It is hard to conclude from this comparison whether the difference in percent removal was the result of material alone or if the variation in SSA and pore openings played some role in it. The basic understanding is that pore openings and high surface area can contribute to higher removal capacity. The pore structures and pore size distributions also must be taken into consideration along with other variables as contributing to the difference in percent removal.

Table 2.1: Removal by different electrodes with different SSA and pore openings.

| Ref. | Electrode Materials | % removal or mg/g | SSA (m ² /g) | Average Pore size (nm) |
|------|--|----------------------|----------------------------|---------------------------|
| [27] | Pure activated carbon (parent) | 50% | 932.4 | 4.2 |
| | Activated carbon treated with KOH | 55% | 889.1 | 4.19 |
| | Activated carbon treated with CO ₂ | 60% | 851.3 | 4.07 |
| [37] | Reduced graphene oxide and activated carbon fiber composite (RGO/ACF-10) | 7.2 mg/g | 621 | 2.2 |
| | RGO/ACF-1 | - | 584 | 2 |
| | RGO-ACF-5 | - | 612 | 2.2 |
| | RGO/ACF-15 | - | 456 | 2.2 |
| | RGO | - | 53 | 15.3 |
| | ACF (parent) | 4.7 mg/g | 630 | 1.9 |
| [38] | OMC-S (nickel sulfate based ordered mesoporous Carbon) | 0.93 mg/g | 1491 | 3.7 |
| | OMC-N (nickel nitrate based) | 0.54 mg/g | 1594 | 3.3 |
| | OMC-W (without nickel salt) | 0.602 mg/g | 950 | 4 |
| | Activated carbon (AC) | 0.275 mg/g | 845 | - |
| [29] | Multiwalled carbon nanotube | 13.07 mg/g | 208 | 13.7 |
| | AC | 6.03 mg/g | 964 | 2.1 |

2.3.2 Effect of charge efficiency of electrical double layer

The concept of charge efficiency was first defined as the ratio of equilibrium salt adsorption and total electrode charge [14]. In ideal conditions, it is expected that for supply of one unit of charge to the electrode, one oppositely charged ion with same unit charge would be adsorbed. Therefore, the charge efficiency value will be equal to 1. But this is not the case in the double layer phenomena. The idea of charge efficiency arose from the fact that in the electrical double layer, formed near electrode surface, inclusion of counter ions takes place, but the exclusion of co-ions also occurs. This reduces the overall efficiency less than 1 for the system.

Later, based on this concept, it was demonstrated that electro-sorption capacity of the electrodes can also be increased by focusing on improving the charge efficiency [39]. The electrode with highest BET surface area (denoted by A15 in Figure 2-8) showed the lowest electro-sorption capacity in CDI experiments.

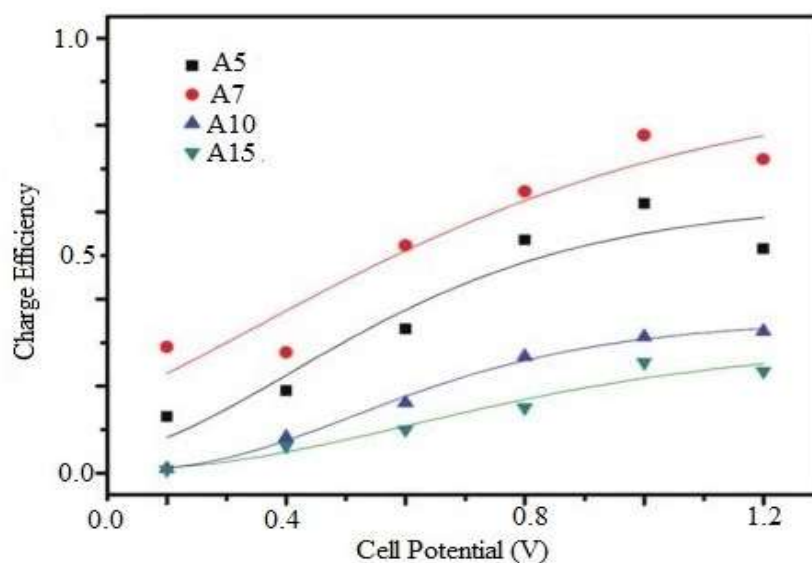


Figure 2-8: Charge efficiency of electrodes- Reprinted (adapted) with permission from [39]). Copyright 2012 American Chemical Society.

The lowest electro-sorption rate was attributed to the lower charge efficiency showed by A15 compared to other electrodes. The lower charge efficiency value by A15 electrodes may have been caused by higher pore volume and a smaller graphitized structure (as reported by analyzing FTIR spectra). In Figure 2-9, it is evident that A15 showed highest physical adsorption capacity, as expected, due to its higher surface area. But when it came to electrosorption performance, the trend followed the same as charge efficiency.

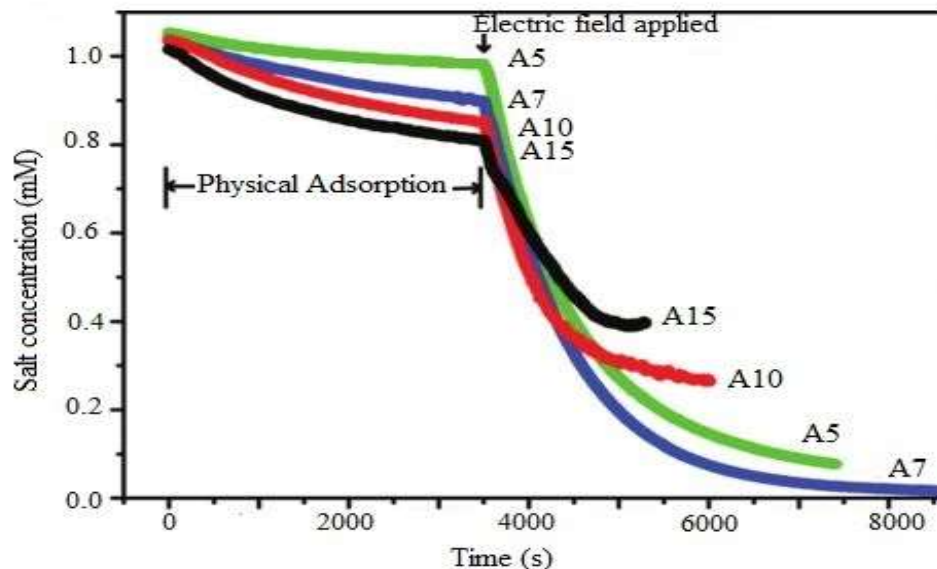


Figure 2-9: Physical adsorption and electro-sorption performance of the electrode- Reprinted (adapted) with permission from [39]). Copyright 2012 American Chemical Society.

2.3.3 Constant voltage and constant current methods

Constant voltage (CV) and constant current (CC) mode are both widely used in CDI operation [3]. Sometimes these modes can be used simultaneously in different parts of the CDI system to ensure optimized performance by each part [40]. The pros and cons

of both CV mode and CC mode under same operating conditions were also discussed [41]. The Figure 2-10 shows effluent concentration at CV and CC mode.

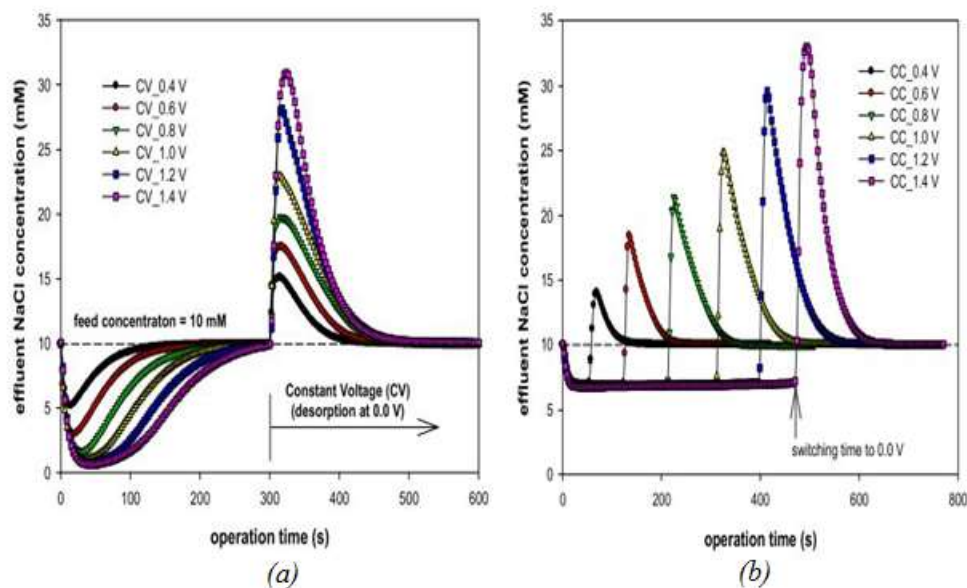


Figure 2-10: Effluent concentration in (a) CV and (b) CC mode – Reprinted from [41].

With varying current density in constant voltage mode, the effluent concentration gradually decreases during adsorption but gradually increases during desorption. The final concentration is dependent on applied voltage. As voltage increases, the final concentration decreases in the adsorption process. (Figure 2-10a). Since CC mode is operated at a predetermined current density, the effluent concentration remains constant throughout adsorption process depending on this applied current density (Figure 2-10b).

Therefore, CC mode is a better fit in situations where a desired concentration of effluent is required. On the other hand, if maximum removal of ions is required for a process, CV mode is suggested to be used as it can deliver higher adsorption rate at the same operating condition (Figure 2-11a). Charge efficiency values are higher for CV

mode than for CC mode in voltage range less than 0.8V and lower in voltage range greater than 0.8V. For both modes, charge efficiency gradually decreases at higher voltage range (Figure 2-11b). Though adsorption efficiency is greater for CV at same operating conditions, it comes at a cost of higher energy consumption. Figure 2-11c shows the energy requirement per ion removal at different cell potentials for both CV and CC modes. MCDI system was also demonstrated to be much more energy efficient when it was operated in CC mode [4].

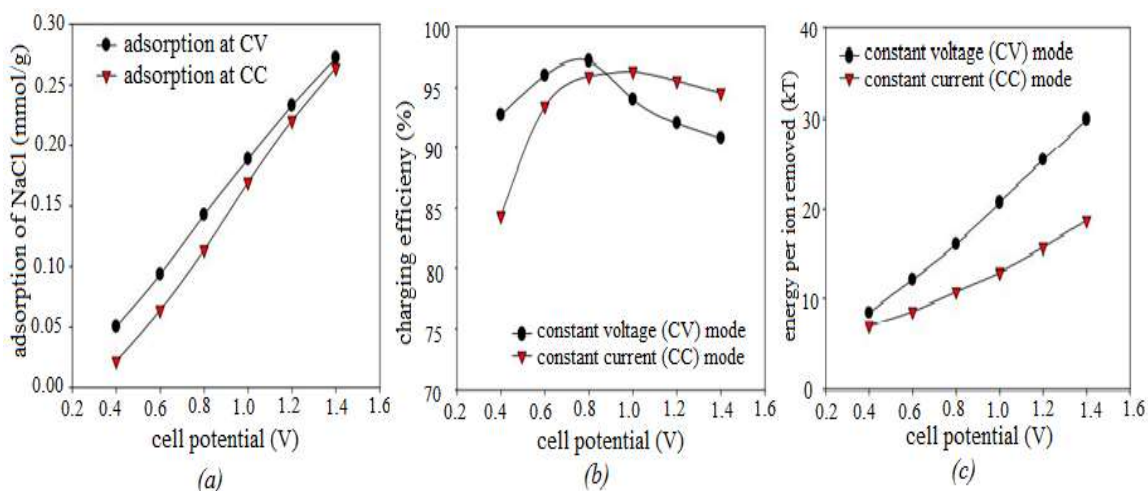


Figure 2-11: Adsorption efficiency (a), charge efficiency (b) and energy consumption (c) at different cell potential for CV and CC mode – Reprinted from [41].

2.4 Electrode and other development approaches in capacitive deionization process

Electrode development and improvement of electrode characteristics has in recent years been the most focused research area in CDI literature. Oftentimes, electrode material choice in CDI is influenced by the performance of electrodes in supercapacitor

literature. Table 2.2 provides a summary of selection criteria for electrodes in CDI based on some key performance parameters and their significance for CDI electrodes selection.

Table 2.2: Key parameters and their significance in selection of CDI electrodes selection based on physical, chemical and other characteristics.

| Parameter | Significance |
|-----------------------------|---|
| Specific surface area (SSA) | Needed to provide space for ions to be adsorbed onto the electrode surface. Essential for obtaining higher specific capacitance. |
| Pore size distribution | Pore sizes and their distribution is important for removal of ions with a certain radius and to overcome electrical double layer overlapping. Pore smaller than target ions will contribute in overall surface area but would not be effective in removal of target ions. |
| Conductivity | Higher conductivity or lower resistance values lead to faster charge transfer and hence faster ion adsorption-desorption. |
| Electroactive surface | The more ion accessible surface an electrode has the more it would be efficient in ion removal. Higher SSA increases possibility of more accessible surface but doesn't guarantee the material highly efficient as electrode. Pore openings, physical arrangement of pore paths etc. also affects the availability of active or accessible surface. |
| Stability | An electrode must be stable at applied voltage ranges and its surrounding chemical environment. |
| Cost | Constraints of cost and corresponding efficiency of electrodes must be considered |

Carbon based electrodes have been the most popular choice in supercapacitor applications as well as CDI because of their low cost, corrosion resistivity, high surface area, good conductivity, and good stability. From activated carbon to carbon nanotube have been used as carbon cloth electrodes. Also, carbon allotropes like carbon aerogel, carbon nanofiber, and graphene etc. have been used as electrodes for CDI operations. Recent research efforts are focused on minimizing the cost of production, enhancing efficiency, and regeneration of these materials.

2.4.1 Electrode preference and surface modification

One of the research efforts is to coat the carbon substrate with a metal oxide to improve the electrode's specific capacitance, which in turn increases ion removal efficiency. However, the maximum capacitance of carbon-based electrodes is limited to 150 F/g, which is also evident in the literature data provided in Table 2.3 and Table 2.4. Generally, oxides of transition metals, such as RuO₂, MnO₂, NiO, SnO₂, ZnO, TiO₂, V₂O₅, CuO, and Fe₂O₃, are used to fabricate composite electrodes of carbon substrates [42]. Specific capacitance of metal oxides is much higher than carbon counterparts. Therefore, when incorporated with carbon substrates, composites show better specific capacitance (Table 2.3 and Table 2.4) and higher percent removal and mass removed per unit mass efficiency (Table 2.5 and Table 2.6) when compared to the parent carbon substrate. Issues regarding metal oxide deposition on carbon substrates leaves room for more research and improvement of electrodes, such as high resistivity of metal oxides which increases the sheet resistance and lowers charge transfer rate, cracking of electrodes due to strains in metal oxides caused by charge-discharge, and poor control over SSA and pore size distribution during fabrication process.

Table 2.3: Capacitance of different electrodes under different specific current.

| Ref. | Electrode Materials | Capacitance (F/g) at Specific Current (A/g) | |
|------|--|---|-------|
| | | 0.05 A/g | 1 A/g |
| [37] | Reduced graphene-oxide and activated carbon fiber composite (RGO/ACF-10) | 256 | 193 |
| | RGO | 135 | 98 |
| | ACF | 214 | 148 |
| [43] | Graphene-Oxide & porous carbon nanofiber composite (GO-PCNF) | 151.6 | - |
| | PCNF | 105.9 | - |

Table 2.4: Capacitance of different electrodes under different scan rates.

| Ref. | Electrode Materials | Capacitance (F/g) for given Scan Rate (mV/s) | | | | | |
|------|--|--|-----------|-----------|----------------|------------|------------|
| | | 1 mV/s | 3 mV/s | 5 mV/s | 10 mV/ s | 20 mV/s | 50 mV/s |
| [44] | Activated carbon cloth (ACC) grafted with ZnO nanorod | 95 | 70 | - | - | - | 30 |
| | ACC grafted with ZnO microsheet | 74 | 63 | - | - | - | 24 |
| | ACC grafted with ZnO nanoparticle | 75 | 55 | - | - | - | 21 |
| | ACC grafted with ZnO microsphere | 73 | 62 | - | - | - | 20 |
| [38] | OMC-S (nickel sulfate based ordered mesoporous carbon) | 192 | - | 150 | 125 | - | - |
| | OMC-N (OMC based on Nickel Nitrate) | 174 | - | 135 | 110 | - | - |
| | OMC-W (OMC without Nickel salt) | 140 | - | 133 | 95 | - | - |
| | OMC-S (nickel sulfate based ordered mesoporous carbon) | 108 | - | 82 | 40 | - | - |
| [45] | Carbon nanofiber (CNF-based on Phenolic resin) -600 | - | - | - | 1.6 | 1.1 | 0.7 |
| | CNF-800 | - | - | - | 41.8 | 37.7 | 30.5 |
| | CNF-1000 | - | - | - | 52.1 | 48.8 | 41.4 |
| [46] | ACC | 100 | - | - | 70 | - | 40 |
| | ACC-ZnO nanorod | 80 | - | - | 60 | - | 50 |
| [32] | Graphene and MnO ₂ nanorod composite | - | - | - | 292 | - | - |
| | Graphene and MnO ₂ nanoparticle composite | - | - | - | 180 | - | - |
| | Pristine graphene | - | - | - | 144 | - | - |
| | Activated carbon (AC) | - | - | - | 205 | - | - |
| | GO-PCNF | - | - | - | 151.6 | - | - |
| | PCNF | - | - | - | 105.9 | - | - |
| [29] | Multiwalled carbon nanotube (MWCNT) | - | - | 47.4 | - | - | - |
| | AC | - | - | 72.5 | - | - | - |

Table 2.5: Removal per electrode mass by different electrodes under variable conditions.

| Ref. | Operating Conditions | Electrode Type | Removal (mg/g) |
|------|--|---|----------------|
| [44] | Solution: 100 mg/L NaCl; applied voltage: 1.2 V; flow rate: 2 mL/min; electrode area: 8.4 cm ² ; temp: N/R | Activated carbon cloth (ACC) | 5.8 |
| | | ACC grafted with ZnO nanorod | 8.5 |
| | | ACC grafted with ZnO microsheet | 8.5 |
| | | ACC grafted with ZnO nanoparticle | 1 |
| | | ACC grafted with ZnO microsphere | 2.5 |
| [6] | Solution: 500 mL 233 mg/L NaCl; applied voltage: 1.2 V; temp: N/R; electrode mass: 0.75 g; spacer: 3 mm; flow rate: 8.4 mL/min; electrode area: 40 cm ² | Carbon xerogel (CX) | 1.9 |
| | | CX-SiO ₂ as cathode & CX as anode | 3 |
| | | CX-COOH (oxidized CX) as cathode & CX as anode | 3.8 |
| [36] | Solution: 100 mL 5000 mg/L NaCl; applied voltage: 1.2 V; temp: 25 ⁰ C; electrode mass: N/R; spacer: 6 mm; flow rate: 30 mL/min; electrode area: 110 cm ² | Carbon aerogel | 5.8 |
| | | Resorcinol based mesoporous carbon on graphite | 13.8 |
| | | Phloroglucinol based mesoporous carbon on graphite | 12.4 |
| [31] | Solution: 25 mg/L NaCl; applied voltage: 2 V; temp: N/R; electrode mass: N/R; spacer: N/R; flow rate: 25 mL/min; electrode area: 98 cm ² | Activated carbon | 0.8 |
| | | Graphene like nanoflakes (GNFs) | 1.35 |
| [43] | Solution: 100 mg/L NaCl; applied voltage: 1.2 V; temp: N/R; electrode mass: N/R; spacer: N/R; flow rate: 6 mL/min; electrode area: N/R | Graphene oxide-porous carbon nanofiber | 7.8 |
| | | PCNF | 5.9 |
| | | Activated carbon (AC) | 2.5 |
| [45] | Solution: 2000 mg/L; applied voltage: 1.2 V; temp: 25 ⁰ C; electrode mass: N/R; spacer: N/R; flow rate: 6 mL/min; electrode area: 9 cm ² | Carbon nanofiber (CNF-based on phenolic resin) -600 | 20.1 |
| | | CNF-800 | 35.9 |
| | | CNF-1000 | 50.1 |
| [46] | Solution: 1000 mg/L NaCl; applied voltage: 1.6 V; temp: N/R; electrode mass: N/R; spacer: N/R; flow rate: 3 mL/min; electrode area: 8.4 cm ² | ACC | 1.92 |
| | | ACC-ZnO nanorod | 3.6 |
| [47] | Solution: 5 mg/L 200 mL NaCl; applied voltage: 450 mV; temp: 20 ⁰ C; electrode mass: N/R; spacer: 3 mm; flow rate: 4 mL/min; electrode area: 60 cm ² | Carbon nanotube (CNT) | 1.36 |
| | | Air plasma treated CNT | 2.4 |

Table 2.6: Percentage of salt removal by different electrodes under variable conditions.

| Ref. | Operating Conditions | Electrode | Removal (%) |
|------|---|---|-------------|
| [24] | Solution: 40 mL 220 mg/L CaCl ₂ ; applied voltage: 1.5 V; temp: N/R; electrode mass: N/R; spacer: 0.1 mm (mesh); flow rate: 0 (stagnant); electrode area: 25.8 cm ² | Carbon fiber sheet (as cathode & anode) | 19 |
| | | CF-SiO ₂ as cathode and CF-Al ₂ O ₃ as anode | 75 |
| [32] | Solution: 50 mL 45 mg/L NaCl; applied voltage: 1.2 V; temp: room; electrode mass: N/R; spacer: N/R; flow rate: N/R; electrode area: N/R | Graphene and MnO ₂ nanorod composite | 93 |
| | | Graphene and MnO ₂ nanoparticle composite | 75.3 |
| | | Pristine graphene | 67.5 |
| | | Activated carbon | 38.1 |

Other approaches to improve electro-sorption performance of electrodes includes the activation of surfaces through chemical treatment or oxidation with acids or other reagents. Some approaches focused on synthesis methods in order to exact better control over key parameters and improve efficiency. Coal tar pitch (CTP) based activated carbon and its modified form was used as a low cost alternative for the most promising electrode material carbon aerogel [8]. Commercial CTP was used to prepare the electrode which was activated using KOH with KOH/carbon at 5:1 proportion. The activated carbon was then modified in following three ways: (i) thermal treatment at 600°C and 1000°C under nitrogen flow, (ii) thermal treatment using H₂ and (iii) thermal treatment using CO₂. The removal efficiency was 55% when parent activated carbon was used as electrode. This efficiency was reduced when the electrodes were treated thermally at 600°C and 1000°C (30% and 20% respectively). This low efficiency was attributed to the resulting lower surface area in these treated forms. Activated carbon modified by treatment with CO₂ also showed a lower efficiency than parent activated carbon, though it has got higher surface area and larger pore sizes. This low efficiency was due to the removal of oxygenated groups in this treated form. The best removal efficiency was observed in the

case of activated carbon treated thermally using H₂, which was about 60%. This form of activated carbon showed high charge capacity with high surface area and a large quantity of oxygenated groups.

Conventional activated carbon and its KOH and TiO₂ activated forms were also compared as electrodes in CDI process [27]. It was observed that there was no notable change in surface area (from 932 m²/g to 889 m²/g) and porosity when activated with KOH, but a significant decrease to 851 m²/g in surface area was noted when activated with TiO₂. In both cases it was found that activated electrodes performed higher compared to original form electrodes. This improvement was attributed to the increased hydrophilic nature of activated materials. But these traditional methods of producing activated carbon don't offer good control over pore size distribution.

Two carbide derived carbon (CDC) electrodes derived from metal carbides (TiC or SiC) enabling a control over porosity in sub-angstrom range (depending on synthesis conditions and parent metal carbide) were compared to two types of activated carbon as electrodes in CDI process [30]. This control is important for measuring and controlling the salt adsorption rate in CDI operation. These electrodes were named as AC-1, AC-2, CDC-1 and CDC-2 and tested as electrodes in CDI cell for voltage range of 1.2-1.4 V and initial salt concentration of 5 mM. Observing the salt adsorption rate, it was found that CDC-2 has 15% and 33% higher efficiency than AC-1 and AC-2 respectively at cell voltage 1.2 V, which becomes even higher (18% and 35%) when cell voltage is increased to 1.4 V. On the other hand, CDC-1 has 28% and 44% higher efficiency than AC-1 and AC-2 respectively at the entire voltage range (1.2-1.4 V). These results suggest CDC-1 to be the most efficient electrode in the experimental conditions and salt used. It was

observed that a difference in the structure of the material has only minor effects on the charge storage capacity. This leads to a hypothesis that materials which are suitable for high charge storage in super-capacitor applications may also be suitable for efficient CDI application. However, the charge efficiency was found to be 0.8, a value close to unity which is important for charge efficient CDI operation. The charge storage capacity was found to be highest for CDC-1 and lowest for AC-2 and followed a trend as shown here: CDC-1>CDC-2>AC-1>AC-2, which is exactly same as the sequence in salt removal capacity. The contradiction of experimental data with the general view from classical double layer theory was that salt removal capacity would be proportional to BET surface area. In this experiment, it was found AC-1 and AC-2 had larger BET surface area and larger total pore volume than the CDCs. But the salt adsorption capacity was much higher in the case of CDCs.

Measurement of the electro-sorption capacitance of environmentally concerning chlorides, nitrates, and phosphate ions using a carbon aerogel electrode synthesized by resorcinol formaldehyde was also done [9]. Carbon aerogel activated by thermal treatment with CO₂ and was chemically activated by KOH. This thermal activation with CO₂ yielded a material with high surface area with large pore volumes. It was observed that there is a close relationship between ionic radii and capacitance values. These values were 75.8 F/g and 78.3 F/g for smaller chloride and nitrate ions respectively and 61.2 F/g for larger phosphate ions. The resulting increase in the surface area due to activation also increased these capacitance values, which were recorded as 120.3, 100.5 and 86.9 F/g for chloride, nitrate, and phosphate ions respectively. The theoretical hypothesis that larger

ions are hard to be adsorbed in smaller diameter pores was confirmed by lower capacitance rate in larger phosphate ions.

Activated carbon (AC) has a larger surface than many other composites forms, so the electrosorption capacity was much lower for AC. This high capacity may be attributed to the more accessible interlayer structure of composites for adsorbing ions, while AC has small micropores that are inaccessible to some ions.

The examples of various electrode materials and their corresponding specific surface areas (SSAs) are provided in Table 2.7. The table illustrate the wide variation of SSA value, which ranges very low value of $1.88 \text{ m}^2/\text{g}$ for carbon fiber sheet to $1300 \text{ m}^2/\text{g}$ for activated carbon cloth electrodes.

Table 2.7: Specific Surface Area of different electrodes.

| Ref. | Electrode Materials | SSA (m ² /g) |
|------|---|-------------------------|
| [44] | Activated carbon cloth (ACC) | 1200 |
| | ACC grafted with ZnO nanorod | 700 |
| | ACC grafted with ZnO microsheet | 1300 |
| | ACC grafted with ZnO nanoparticle | 300 |
| | ACC grafted with ZnO microsphere | 500 |
| [6] | Carbon xerogel (CX) | 196.2 |
| | CX-SiO ₂ as cathode & CX as anode | 218.3 |
| | CX-COOH (oxidized CX) as cathode & CX as anode | 196.9 |
| [24] | Carbon fiber sheet | 1.88 |
| | CF-SiO ₂ as cathode and CF-Al ₂ O ₃ as anode | 25.6 & 18 |
| [36] | Carbon aerogel | 289 |
| | Resorcinol based mesoporous carbon on graphite | 488 |
| | Phloroglucinol based mesoporous carbon on graphite | 610 |
| [31] | Activated carbon | 989.54 |
| | Graphene like nanoflakes (GNFs) | 222.01 |
| [43] | Graphene oxide-porous carbon nanofiber (GO-PCNF) | 474 |
| | PCNF | 583 |
| | AC | 1047 |
| [45] | Carbon nanofiber (CNF-Based on Phenolic Resin) -600 | 481 |
| | CNF-800 | 579 |
| | CNF-1000 | 617 |
| [46] | Activated carbon cloth (ACC) | 1228 |
| | ACC-ZnO nanorod | 587 |
| [47] | Carbon nanotube (CNT) | 95 |
| | Air plasma treated CNT | 106 |

Many recent research approaches focused on developing new low-cost methods of synthesizing carbon based porous electrodes for CDI. In one study, calcinated watermelon peels were used as carbon source. They were activated with KHCO₃ then washed in HCl [48]. The resulting materials had very high specific surface area (2360 m²/g) and electrosorption capacity (17.38 mg/g). A three-dimensional foam like carbon (3DFCN) with a simple photochemical method was developed. It had electrosorption

capacity of 20.0 mg/g. Nitrogen doped hollow carbon spheres (N-PHCS) prepared by mixing polystyrene and dopamine hydrochloride (as carbon and nitrogen source) had very high specific capacitance (152 F/g at 5 mV/s scan rate) with good electrosorption capacity (12.95 mg/g) [49]. Ordered mesoporous carbon and carbon nanotube (OMC/CNT) electrodes had higher electrosorption capacity (10.74 $\mu\text{mol/g}$) than OMC (9.19 $\mu\text{mol/g}$) and activated carbon (3.69 $\mu\text{mol/g}$) [50]. KOH-activated OMC/CNT in a later work by the same group had improved electrosorption performance (11.83 $\mu\text{mol/g}$) than that of pristine OMC/CNT [51]. Table 2.8 lists some other approaches by different research groups to develop carbon-based electrodes for CDI.

Table 2.8: Other methods of carbon-based electrode development and corresponding changes.

| Ref. | Electrodes Compared for Performance | Adsorption capacity (mg/g) | Capacitance (F/g) |
|------|--|----------------------------|-----------------------------|
| [52] | N, P doped meso/microporous carbon | 20.78 | 207 at 1 mV/s |
| | KHCO ₃ treated meso/microporous carbon | 16.63 | 150 at 1 mV/s |
| | NH ₄ H ₂ PO ₄ treated meso/microporous carbon | 15.2 | 115 at 1 mV/s |
| | Calcinated meso/microporous carbon | 9.95 | 109 at 1 mV/s |
| [53] | N-doped bimetallic zeolite imidazolate framework | 12.25 | |
| | Zeolite imidazolate framework -8 | 6.12 | |
| | Zeolite imidazolate framework- 67 | 11.38 | |
| [54] | Dodecahedron-like carbon framework derived from metal organic frameworks | 20.05 | |
| | ZiF-8 | 13.01 | |
| [55] | 3D hierarchical carbon architectures (3DHCA) | 17.83 | 142 at 5 mV/s |
| | Calcinated carbon | 6.88 | 64 at 5 mV/s |
| [56] | 3D hierarchical porous carbon with a bimodal pore arrangement | 2.16 | 60 (No scan rate mentioned) |
| | Ordered mesoporous carbon (OMC) | 1.94 | 40 (No scan rate mentioned) |
| [57] | N-doped hollow multi yolk shell carbon (N doped-HMYSC) | 16.1 | 204 at 1 mV/s |
| | Hollow carbon | 12.7 | 150 1 mV/s |

2.4.2 Graphene based electrodes

In recent years many graphene-based electrodes have been developed for CDI applications. Graphene, a carbon-based material with excellent conductivity, inertness, low density, and high surface area, is an ideal material to host for composite electrode materials [17, 58, 59]. A novel method of graphene production via dispersion of graphene oxide and ethanol in pyridine was described. The resulting material showed electrosorption capacity of 0.88 mg/g [60]. Three dimensional macroporous graphene architectures (3DMGA) have been synthesized and used as CDI electrodes [61]. These 3DMGA electrodes resulted in better capacitance (58.4 F/g) than traditional graphene electrodes (35/3 F/g) at 5 mV/s scan rate. 3DMGA consequently produced better electrosorption capacity (3.9 mg/g) than traditional 3D graphene (2.5 mg/g) and activated Carbon (2.9 mg/g).

Another study [62] synthesized 3D graphene-based, hierarchically porous carbon structure. This structure resulted in improved specific capacitance (from 101.5 F/g to 151.7 F/g) and electrosorption capacity (6.2 mg/g to 14.7 mg/g) when compared to using pristine 3D graphene as an electrode in CDI. This porous graphene framework (PGF), developed through UV-assisted polymerization with high specific capacitance (190 F/g), yielded better electrosorption capacity (19.1 mg/g) when compared to mesoporous carbon nanofiber (15.2 mg/g) [63]. Furthermore, PGF calcinated at low temperature resulted in better electrosorption capacity (17.1 mg/g) than that of PGF calcinated at high temperature (12.7 mg/g). Graphene carbon nanostructure (GCNS) was synthesized from glucose (as carbon precursors), $\text{Fe}(\text{NO}_3)_3 \cdot 9\text{H}_2\text{O}$ (as graphitization precursor) and NH_4Cl (as a blowing agent) [64]. The resulting material showed a high electrosorption capacity of 38.63 $\mu\text{mol/g}$ and specific capacitance of 54.68 F/g. Graphene-mesoporous Carbon

nanosphere grafted (GN/MCS) electrodes showed higher capacitance (211 F/g) compared to graphene (73 F/g) and mesoporous Carbon (164 F/g) [65] without nanospheres. These GN/MCS electrodes, developed for supercapacitors, can also be used as electrodes in CDI cell in some future endeavors. Table 2.9 lists all other approaches related that improves the performance of CDI electrodes.

Table 2.9: Graphene-based electrode and their modified forms.

| Ref. | Modified form of Graphene used | Performance by different electrodes | | | | |
|------|---|-------------------------------------|---------------------|---------------------|-------------------------|----------------|
| | | Type of Electrode | Adsorption capacity | Capacitance (F/g) | SSA (m ² /g) | Pore size (nm) |
| | | MC | 590 µg/g | 36 at 5 mV/s | 685.2 | 3.16 |
| [66] | Graphene-Mesoporous Carbon (GE/MC) composite | GE/5%MC | 731 µg/g | 57.5 at 5 mV/s | 567.7 | 2.5 |
| | | GR | 1.10 mg/g | 30 at 10 mV/s | 479.5 | |
| [67] | Graphene and Carbon Nanotube Composite (GR/CNT) | GR/10%CNT | 1.41 mg/g | 70 at 10 mV/s | 342.9 | |
| | | 3DG | 4.41 mg/g | | 250.3 | |
| [68] | 3D graphene and hierarchically porous Carbon composite (3DGHPC) | 3DGHPC | 6.18 mg/g | | 384.4 | |
| | | GHMCS | 2.3 mg/g | 43.33 at 1 mV/s | | |
| [69] | Graphene coated with hollow mesoporous Carbon Structure (GHMCS) | Compact Graphene | 1 mg/g | 23.33 at 1 mV/s | | |
| | | HMCS | 2 mg/g | 32.39 F/g at 1 mV/s | | |

In another study, heavy metal lead (Pb) removal was also examined [70]. Using ethylenediamine (EDTA) and 3-aminopropyltriethoxysilane grafted 3D graphene at pH=6,

99.9% Pb^{2+} was removed and 98.7% Na^+ was removed. The concept of the work was to adsorb lead ions by EDTA through chelation reaction and to adsorb sodium ions through electrosorption.

Sulfonic functional group grafted graphene (3DSGR) and amine functional group grafted graphene (3DNGR) electrodes were developed and compared in CDI cell for different cathode-anode configuration (asymmetric electrode configuration) in conjunction with 3D graphene (3DGR) electrodes. Electrosorption capacity by different configurations of electrodes are shown in Table 2.10.

Table 2.10: 3D graphene-based electrode performance at asymmetric electrode systems.

| Ref. | Applied conditions | Cathode -Anode | Electrosorption Capacity (mg/g) |
|------|--------------------|----------------|---------------------------------|
| [71] | 1.4 V, 40 mL/min | 3DGR-3DGR | 2.91 |
| | 50 mg/L NaCl | 3DNGR-3DGR | 3.82 |
| | | 3DSGR-3DGR | 5.33 |
| | 1.4 V, 40 mL/min | 3DNGR-3DSGR | 13.72 |
| | 500 mg/L NaCl | 3DGR-3DGR | 9.48 |

2.4.3 Inclusion of membrane, polymer, resins, ion selective materials, etc.

In membrane capacitive deionization (MCDI), the ion exchange membranes are placed in front of the electrodes to block the co-ions from getting re-adsorbed in the regeneration phase, which occurs when the applied voltage is reversed. In one study [2], experimental and theoretical results for desalination capacity as well as the rates of constant voltage and constant current methods were reported as functions of adsorption/desorption time, salt concentration in the feed, electrical current, and cell voltage. It was observed that the duration of desalination cycles depends on influent salt

concentration. Lower influent salt concentration led to shorter duration. In other words, the cell voltage reaches the final voltage level quickly. On the other hand, adsorption capacity decreases if desorption time is decreased. This was because shorter duration resulted in incomplete regeneration, which in turn decreased the ion removal efficiency of the next adsorption phase. In another work [72] it was proved that varying the water flow rate cases control and finetuning of the effluent salt concentration to desired level. All these observations led to the introduction of a new performance indicator in CDI operation, which was named average salt adsorption rate (ASAR). ASAR is the salt adsorption per cycle, per gram of total mass of electrode. ASAR can be maximized by maintaining an influent salt concentration of around 20 mM, adsorption current of 1 A, water flow rate higher than 40 mL/min, and desorption time of 50 s.

An even more advanced MCDI system is also going through further development. A recent improvement in this system is the introduction of ion exchange polymers. In one study [12], polyethyleneimine (PEI) was used as a cation exchange polymer and dimethyl diallyl ammonium chloride (DMDAAC) as anion exchange polymer. These polymers were cast into the electrodes. The resulting removal efficiency was 93% for NaCl solution, which was superior to both the traditional MCDI system with an efficiency of 74% and the conventional CDI system with an efficiency of only 25% at the same experimental conditions.

Much recent work focuses on developing the CDI technique by using inexpensive activated carbon fiber. At one point, activated carbon was once thought to yield less desalination rate and charge efficiency compared to novel carbonaceous materials with high surface area, porosity, and favorable pore structures. The incorporation of ion

exchange polymers, membrane, resins, etc., has generated new potential for this low-cost electrode material. Three CDI cells with an electrode system that was modified with ion exchange felt (IEF), ion exchange membranes (IEM), and ion exchange resins (IER) were tested as electrodes [73]. All used low-cost activated carbon fiber as electrodes in all three systems dealing with NaCl solution with effluent flow rate of 1000 mg/L and applied voltage of 1.2 V. The regeneration phase of each electrode system included both short circuiting and discharge desorption. The removal rate and efficiency was found to be in the following order: CDI-IER (670 ± 20 mg/Lh and $90 \pm 1\%$ /h) > CDI-IEM (440 ± 15 mg/Lh and $60 \pm 2\%$ /h). Removal rate of 24% by CDI-IEF was poor compared to CDI-IER and CDI-IEM's performances. Both the desalination rate and efficiency increased significantly (270 to 670 mg/Lh and 83% to 90 /h) in CDI-IER with increasing applied voltage then decreased slightly with decrease in effluent flow rate.

A hybrid system comprised of reverse osmosis (RO) and CDI to produce ultrapure water (UPW) from seawater was also developed [74]. Researchers found the RO-constant current CDI hybrid system to be superior to the RO-constant voltage CDI system in terms of quality and quantity of UPW produced while both systems consumed same amount of energy at similar operational conditions. Another study [75] used the asymmetric model of CDI in a case of MCDI operation. This research reported that the best performance of MCDI cell occurred at conditions where cathode was configured at 0.5 V PZC and anode at -0.1 V PZC.

Box-Behnken design based on response surface methodology (RSM), a statistical tool to optimize the operational parameters in physical processes, was used in one study [2]. This research conducted experiments with CDI cell at applied voltage range 1.2-1.6

V, initial concentration of NaCl solution 200-1000 mg/L, and flow rate 10-40 mL/min. It used activated carbon-based electrodes which have a good range of mesopores for overcoming the electrical double layer effect. The polynomial statistical fit presented in the publication predicted the optimal value of electrosorption capacity would be 10.67 mg/g with $R^2 = 0.9945$ and $p\text{-value} < 0.0001$. Experimental values showed maximum electrosorption of 10.53 ± 2.1 mg/g at cell voltage, initial concentration and flow rate of 1.57 V, 1000 mg/L, and 25 mL/min respectively. Four activated carbon fibers (ACF) with different BET surface areas were used by one study [39]. Though physical adsorption rate increases with increasing BET surface area, the electro-sorption performance in this CDI cell did not follow the same sequence, because the electrosorption capacity also depends on the charge efficiency of electrical double layers, as discussed in section 2.3.2. A polypyrrole-coated multiwalled carbon nanotube doped with nitrogen as electrodes was used in CDI cell and showed high specific capacitance (103.1 F/g), high energy density (161 mWh/g), and high power density (14.4 W/g) [76]. The material exhibited high energy storage in super-capacitor applications as well as high electro-sorption capacity in CDI with 0.5 M Na_2SO_4 as electrolyte.

2.4.4 Energy recovery & energy efficient electrode development

Quantifying the amount of energy that can be recovered in MCDI operation was focused by another study [11]. Energy recovery leads to higher charge efficiency which is the ratio between the ionic charge removed and electrical charge supplied close to unity. This value is far below unity for other conventional CDI systems. There are different forms of energy that are consumed during MCDI operation. One of them is the thermodynamic energy, which is needed to separate the feed water into diluted and

concentrated streams. This energy cannot be recovered as it is the minimal energy required for desalination. The energy that can be recovered was determined in this study by charging and discharging electrodes. There was a combined resistance caused by the graphite current collector, electrodes, membranes, and spacer compartments used in the experiment which caused an initial jump in the cell voltage. This jump was higher when the electrodes were charged at high current. Part of this energy was stored in the electrical double layers that could be recovered, but the other part was used to overcome an internal resistance and was not recoverable. There were other energy losses due to redistribution of ions in the pores and Faradaic reactions. The experimental data suggested that charging electrodes at lower current not only required less energy but also increased the potential of more energy recovery during the regeneration step. On the other hand, higher initial salt concentration lowered the initial resistance which implied that in this case recoverable energy should have been even higher. In their study, they found 25% of energy recovery at 12 A and salt concentration of 8.6 mM which became higher up to 63% with the salt concentration 273 mM while the current remained the same. Again, this energy recovery went up to 73% when charging was done at 2 A and discharging at 12 A. The estimated recoverable energy by extrapolating the values of charging and discharging currents was found to be $84\% \pm 1\%$, which was not dependent on the salt concentration of water. These observations led to an estimated energy consumption rate of 0.26 kW-h/m^3 of produced water, which was much lower than energy consumed by reverse osmosis for brackish water. Another group [4] aimed at quantifying the energy efficiency in terms of influent concentration, flow rate, and water recovery. They observed that MCDI energy consumption should be less than 1 kWh/m^3 of fresh water

produced in order to be a strong alternative to reverse osmosis. Experimental data showed that MCDI is more energy efficient at salinity levels lower than 60 mM.

Most electrode development research has focused on energy efficient electrodes with less resistivity and thus good ion and charge transport capability in the deionization process. Energy density and power density values increases in many electrodes after some form of modification (Table 2.11).

Table 2.11: Energy and power density by different carbon-based electrodes.

| Ref. | Electrode | Energy Density (Wh/Kg) | Power Density (W/Kg) |
|------|---|------------------------|----------------------|
| [66] | Mesoporous Carbon | 1.31 | 67.37 |
| | Graphene-Mesoporous Carbon Composite | 1.97 | 70.9 |
| [67] | Graphene | 4.07 | |
| | Graphene-Carbon Nanotube Composite | 5.49 | |
| [61] | Traditional Graphene | | 42.42 |
| | 3D Macroporous Graphene Architecture | | 45.34 |
| [50] | Carbon Nanotube (CNT) | | 54.88 |
| | Ordered Mesoporous Carbon-CNT composite | | 56.81 |
| [77] | Co ₃ O ₄ nanosheet, Ag dot grown on 3D graphene | 26.7 | 600 |

One study [78] focusing on TDS removal from one on-site pilot scale CDI unit for groundwater treatment found that the energy requirement of their system went down with the flow rate. The energy consumption was reduced to as low as 1.52 kWh/m³ at 9 L/min from 10.5 kWh/m³ at 1 L/min.

2.4.5 Suspended electrodes (FCDI systems) and inverted CDI (i-CDI systems)

Suspended type or flow-able electrode (also known as FCDI) is a fairly new concept in supercapacitor application [79]. The basic advantage of suspended electrodes is that the electrode material can be replenished with fresh sorbent material without

interrupting the system, while in traditional CDI the process must undergo regeneration once the electrode is saturated with ions. Other advantages include overcoming the challenge of enlarging the CDI system for real world applications, ability to separate clean and ion saturated stream, energy efficient recovery, etc. The same concept was applied in CDI applications by mixing anisometric activated carbon powder (capacitance of 92 F/g as revealed by cyclic voltammetry and specific surface area of $1800\text{m}^2/\text{g}$) and acetylene black (AB) as a conductive additive along with NaCl electrolyte solution. An electrochemical impedance study revealed an ohmic resistance around $1.6\ \Omega$, which is fairly comparable with traditional electrodes. A salt removal efficiency of 68% was achieved in this study. The results indicate that if the total system is developed with much more efficient materials, it could desalinate seawater in one charging period [1]. The Figure 2-12 shows the schematic diagram of a suspended electrode in a CDI application.

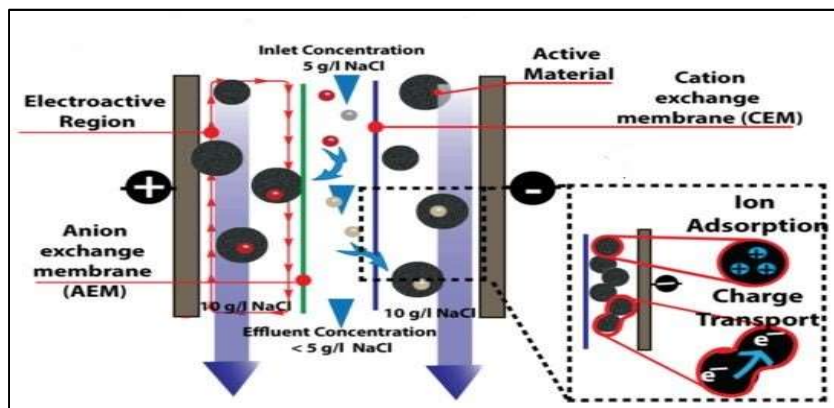


Figure 2-12: Diagram of suspension electrodes in capacitive deionization (used with permission) [80].

In typical constant voltage operations with carbon based electrodes, after long (50-500) hours of adsorption-desorption cycles the CDI cell shows a loss in performance

due to oxidation reaction at the surface of the electrodes [81]. This oxidation leads to formation of $-\text{COO}^-$ groups resulting in a net negative charge at the electrode surface. The concept of inverted CDI (i-CDI) has been developed to utilize this phenomenon. In the i-CDI systems, electrodes were modified chemically, so the cathode (with NH_3^+) could have a net positive charge and the anode (with COO^-) could have a net negative charge [81, 82]. These innate surface charges on electrode surfaces help in adsorption and desorption of ions (desorbed when connected to oppositely charged DC power terminals and adsorbed when the electrodes are shorted). The behavior of the i-CDI unit is completely opposite to the conventional CDI system, but it still maintained salt separation for 600 hours of operation. Further studies are required to develop in-depth understanding of i-CDI systems so that it can be applied to large scale processes.

2.4.6 Targeted removal

Targeted ion removal or selective ion removal is also being investigated by some research groups. This approach helps in removing a specific ion when there are competing ions in the system. This method is useful in developing novel techniques for water softening [83] or metal ion removal [6]. A chemical vapor deposition method was successfully used to increase selectivity of monovalent ions over divalent ions following adsorption/electro-sorption [33]. The researchers focused on adjusting pore openings between the sizes of monovalent and divalent ions so that only monovalent ions can get adsorbed into the pores. Another study [7] aimed at removing only nitrate ions from solution, which they termed "selective" removal. In that study, BHP55 resin was used to coat CDI carbon electrodes. The BHP55 resin was selected as a coating material based on the understanding from literature and adsorption tests. The publication lists the adsorption

performance of removal of the ions in the following order: nitrate > sulphate > chloride. These coated materials were used as electrodes in a constant current CDI operation and the effluent was a mixture of NaCl, NaNO₃ and Na₂SO₄ salt solutions. The same test was repeated under the same experimental conditions using uncoated carbon electrodes. The total adsorption was 34% higher and nitrate removal was 100% higher when nitrate selective electrodes were used as opposed to the uncoated electrodes. The results of this study indicate the potential of the selective removal of other ions; for example, chelating resin coated electrodes may be able to selectively remove Ca²⁺ or other heavy metal ions. Another study [84] used activated carbon to target the selective removal of copper ions. At low voltages, these researchers achieved only limited electrosorption, but removal still occurred due to electrostatic forces. The higher the initial concentration and applied voltage, the higher the removal rate and electrosorption capacity became. At 0.8 V, they found the electrosorption capacity to be 24.57 mg/g and electrosorption constant rate 0.038 min⁻¹ (based on Langmuir model). Both values are much higher than formerly reported values for copper ion.

2.4.7 Pilot scale studies

Some pilot scale studies have also suggested the application of CDI in real world conditions. In one of them, CDI technology was applied to remove total dissolved solid (TDS) on site from groundwater [78]. The study found water recovery rate to be 75-80% and significantly removed nitrate, fluoride, and arsenic along with calcium, magnesium, and sodium ions. One of the problems in any on-site application of water treatment technology is fouling. Another pilot scale study [85] conducted in Australia at sites of Wilora and Mawson Lakes found that TDS removal efficiency of CDI electrodes

decreased with time due to fouling issues. The decrease in removal efficiency was much worse (from 86% to 55% in 15 days) for Mawson Lake than that of Wilora Lake (82% to 75% in 15 days). This decrease was attributed to presence of high organic content in Mawson Lakes. A mild cleansing solution of 0.01 M citric acid was found to be effective for removal of calcium and magnesium scaling, while 0.01 M sodium hydroxide helped to minimize organic fouling. These solutions restored the actual capacity of the CDI unit. In another study [86], TiO₂ coated reduced graphene oxide (TiO₂-RGO) electrodes were developed. They demonstrated an ability to minimize fouling by humic-acid through photocatalytic process. These studies provide a good base of knowledge for this problems but more such studies are needed to develop a greater understanding of the issues related to fouling under various conditions with electrodes of different materials in a large-scale CDI based water treatment plant.

2.5 Conclusion

Various technologies such as Reverse Osmosis (RO), Membrane Filtration, and Multistage Flash etc. are commonly used in desalinating water. CDI technology has shown increased efficiency compared to these contemporary technologies used in water purification. This process is theoretically less energy consuming compared to Reverse Osmosis for many reasons, such as the fact that CDI is operated at low voltages and pressure while RO uses high pressure to overcome resistance to membranes. Most of the research efforts have focused improving electrode characteristics and optimizing operational conditions in order to increase the efficiency of CDI operations.

Different forms and composites of carbon have shown remarkable efficiency, ranging from as low as 0.275 mg/g (for activated carbon) to 50.1 mg/g (phenolic resin

based carbon nanofiber), which is more than 180 times the capacity of activated carbon. Inclusion of membranes, polymers, and resin has improved the ion removal capacity of the electrodes. Yet, the research on CDI is on-going and there are many important issues that will need attention in the near future. Some of the issues and unanswered questions are listed below.

- In most of the adsorption and desorption CDI studies the electrodes were studied in a solution of one or two sample salts. A comprehensive study with more complex solutions containing competing ions is needed for full understanding of CDI electrodes' behavior.
- There is not much secondary pollution in CDI process. However, wastewater is produced that is saturated with the salt ions that are removed from CDI systems during regeneration. There is no significant study that focused on characterizing and analyzing the salt ions that saturated the wastewater stream. Very little, if any, work has been done in minimizing this wastewater stream and maximizing the production of net treated water.
- While high surface area is required for effective adsorption, still some materials with inherent high surface area showed lower removal capacity. Selection of electrodes with desired pore size distribution for more efficient adsorption of ions is also a critical issue in upcoming CDI related research.
- The cost associated with materials, manpower, capital investment, maintenance, and operation depend on various factors such as source water quality, location of sites, quality of the treated water, and other similar factors.

- Even though CDI operates at a low voltage range with low current, safety issues related to large scale plant have not been addressed. It is expected that next thrust of the CDI research would be in this direction that would cover instrumentation and automation of the technology for the utility systems of the future smart cities.
- Large scale application of CDI process to deionize surface water for industrial as well as municipal purposes would require additional pre-processing and post-processing. As carbon electrodes can host many organic and inorganic materials through physical adsorption, there remains a chance of fouling, which is common issue in regular water treatment plants. Pre-filtering or other options need to be explored so that water is free of unwanted substances in the CDI influent stream.
- Carbon electrodes also store energy (like supercapacitors) along with ions. This aspect of the CDI technology has not been thoroughly investigated. A good understanding of this area would help in recovering wasted energy, which in turn will help to alleviate the cost and energy requirements of the CDI systems.

There has been noteworthy progress in terms of various types of materials used as CDI electrodes and configurations of electrodes for better yield in this field. The knowledge base has been created and the effectiveness of the technology has been demonstrated in many studies directed for specific cases. CDI technology is paving a path for being an alternative option for deionization/desalination in the future where cost and energy savings will be vital, and sources of freshwater will be scarce.

CHAPTER 3

MATERIALS AND METHODOLOGY

In this chapter, materials, equipment and methods used in the experiments conducted in this study are described. The discussion also includes calibration methods and other processes used.

3.1 Materials and equipment for CDI operation

The electrode material used in this study is a composite of carbon aerogel and carbon fiber. The material is available in a paper-like sheet form. These sheets were purchased from Marketech International (Port Townsend, WA). Each sheet came in 10 inches by 3.5 inches (254 mm x 88.9 mm) pieces with 7 mils (0.1778 mm) thickness (Figure 3-1).



Figure 3-1: Carbon aerogel/fiber paper used as electrode in this study.

Flexible graphite sheets with no insert (Figure 3-2) were purchased from Equalseal (through Amazon.com) and were used as current collectors. Acrylic plastic sheets of thickness 0.7 mm were purchased from Home Depot (Allen, TX). These plastic sheets were used in various ways in cell preparation stages. Glass plates of 5 inches by 12 inches were acquired locally (courtesy of Ruston Glass, Ruston, LA) to be used as cell wall.



Figure 3-2: Flexible graphite sheet with no insert used as current collector.

Non-conductive Silicon II Clear Sealant was purchased from Lowe's (Ruston, LA) and was used to seal the cell to make it water tight and attach different components during cell assembly. A peristaltic pump (Model: 3387, Fisher Scientific) was used to control flow of the solution in and out of the CDI cell. A power supplier (TP1803D, TEK-POWER) was used to apply DC voltage across the electrodes (Figure 3-3).



Figure 3-3: Power supplier used.

HQ40d multimeter (Figure 3-4a) and a CDC401 conductivity probe (Figure 3-4b) were used to monitor and record conductivity of the solutions used in this study. The conductivity probe was calibrated using $1000 \mu S/cm$ standard NaCl solution provided by the manufacturer. HACH pH101 probe was used to measure pH as needed. The pH probe was calibrated every month using standard solutions with pH values of 4.0, 7.0, and 10.0 provided by the manufacturer. (Figure 3-4c).

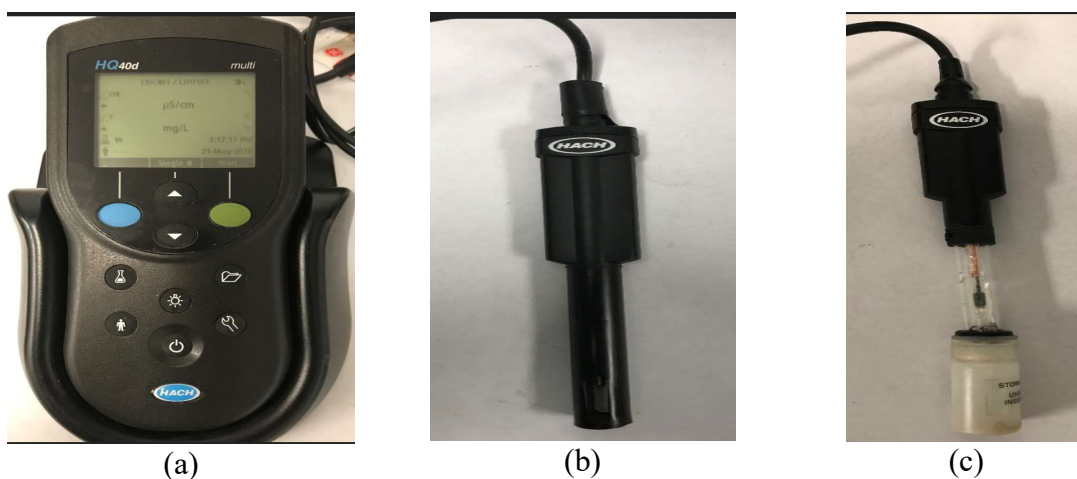


Figure 3-4: (a) Multimeter used for data collection, (b) conductivity probe, and (c) pH probe

A magnetic stirrer was used to ensure a well-mixed was present in reservoirs used in this study (Figure 3-5a). A Barnstead MP-6A machine was used to produce deionized water (Figure 3-5b).

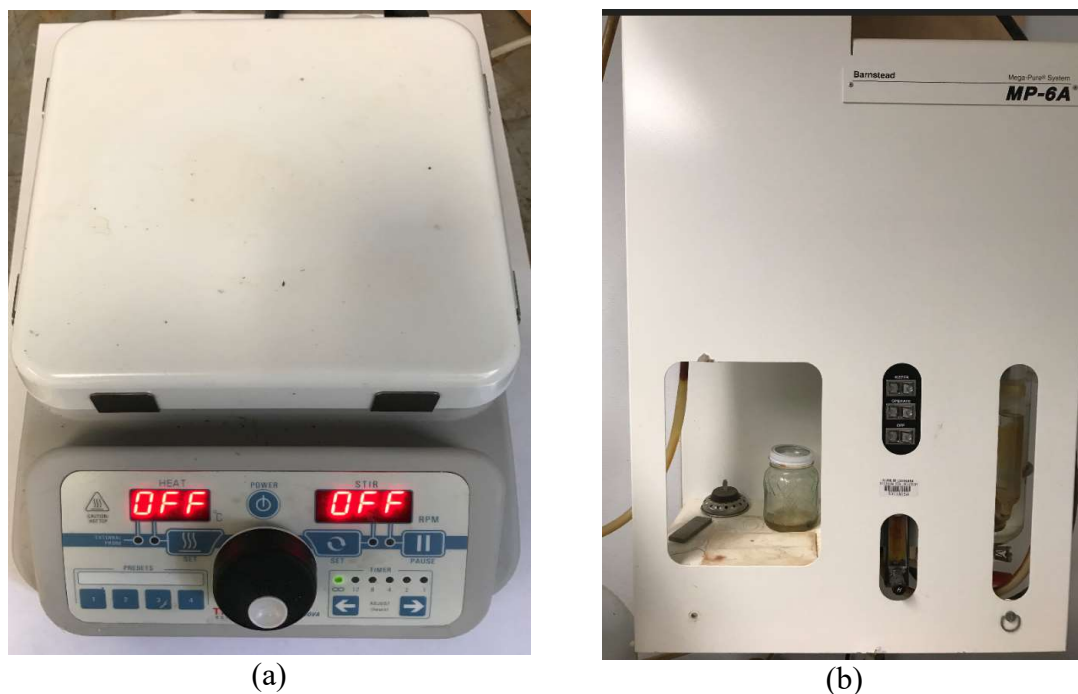


Figure 3-5: (a) Magnetic stirrer, and (b) Deionized water producing system.

3.2 Peristaltic pump calibration

The peristaltic pumps used in this study were calibrated to mark specific flow rates associated with each dial position referring to pump speed. The deionized water present in one beaker was pumped to another beaker using the peristaltic pump. The time it took the pump to transfer 50 mL was recorded. The experiment was repeated five times. An average flow rate (ml/min) was calculated from the collected data for each dial position, which referred to pump speed. Detailed calculations are show in Appendix-A1.

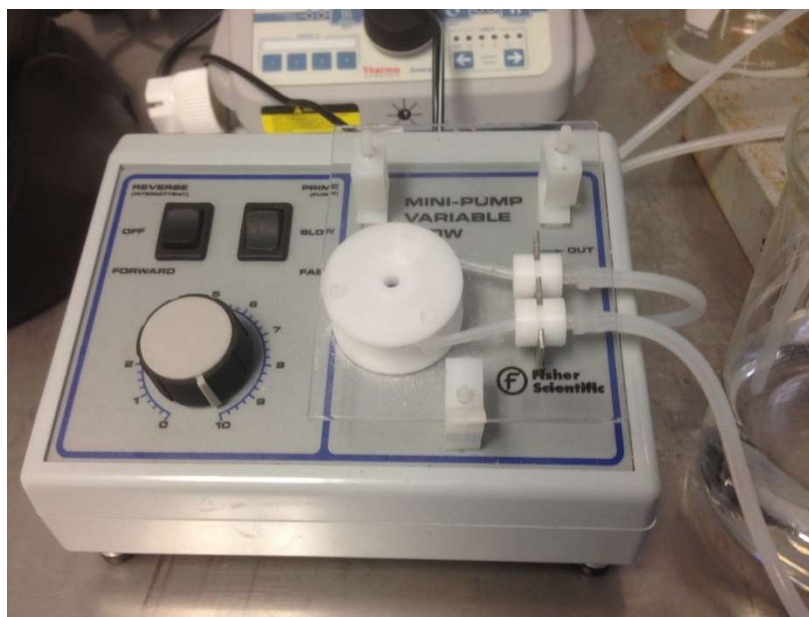


Figure 3-6: A peristaltic pump used in this study.

3.3 Cell preparation

Purchased carbon aerogel/fiber paper sheets were cut into pieces of 3.5 inches by 2 inches (88.9 mm by 50.8 mm) to be used as electrodes. Two long (approximately 150-160 mm) pieces of acrylic sheets, each with approximately 5 mm width and 0.7 mm thickness, were cut and a graphite sheet of similar dimension was pasted on each, as shown in Figure 3-7. The total thickness of this layer, comprised of acrylic sheet, graphite and glue, was between 1.5-1.6 mm. This assembly was used to provide both spacing between the electrodes and electrical connectivity. The assembly was placed in between the electrodes so each electrode touched acrylic sheet on one side and graphite sheet on the other. After the assembly was placed, the dimension of the exposed electrodes was 88.9 mm by 40 mm. The exposed area of electrodes participated in active electrosorption.

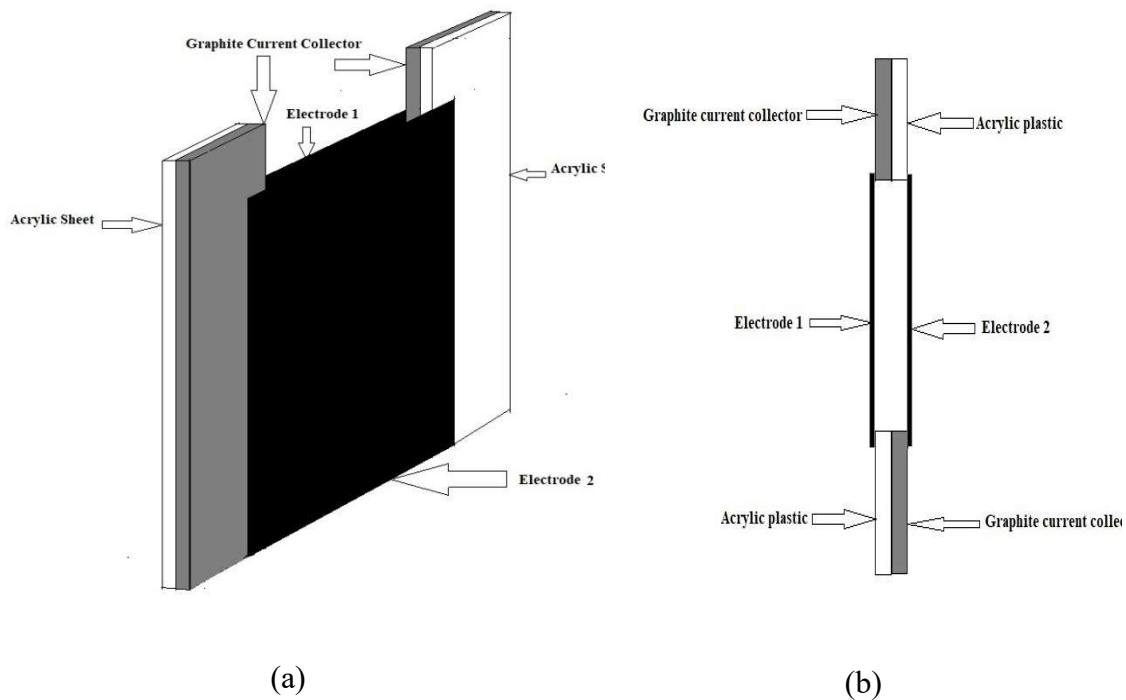


Figure 3-7: (a) Electrode assembly with acrylic sheet and current collector and (b) Top view of the assembly.

The assembly was then inserted into the cell made with glass walls (as shown in Figure 3.8). The space between glass walls was kept approximately 1.8-1.9 mm. The acrylic sheets and the graphite collectors together act as a separator between electrodes. The whole electrode assembly fit snugly inside the glass-walled container. The cell was then sealed from all sides to make it water tight with only two extensions of graphite pasted on acrylic sheet coming out of the cell to serve as current collector (as shown in Figure 3-8).

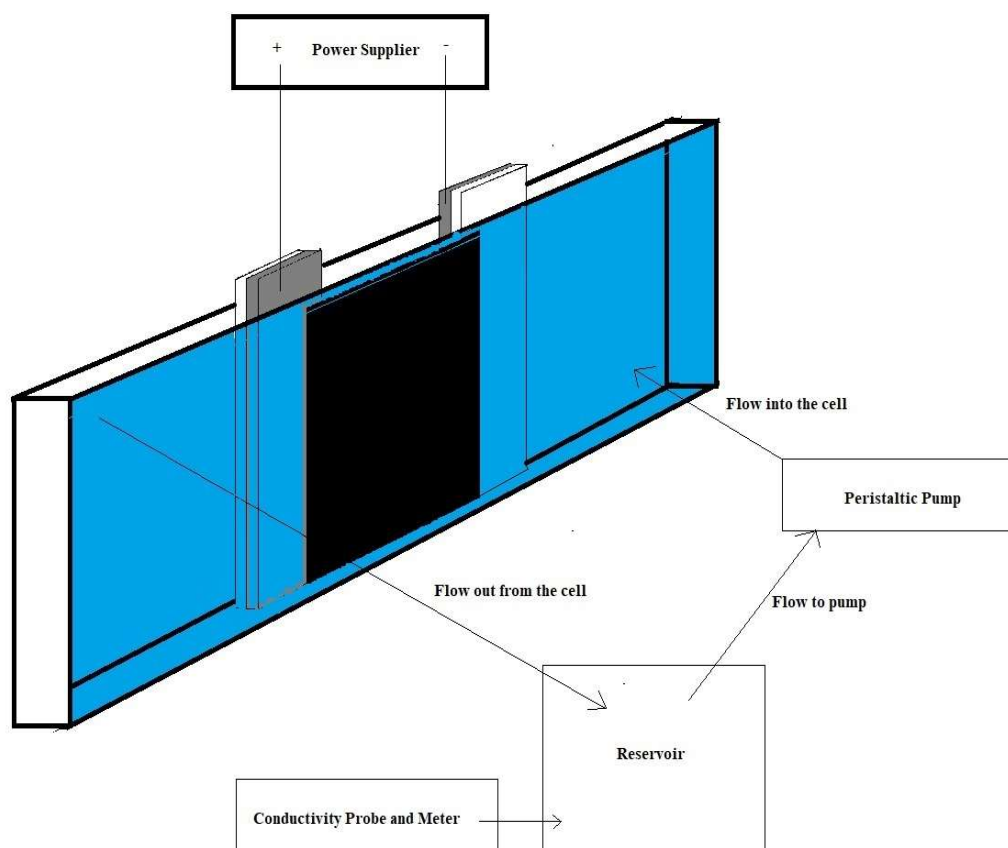


Figure 3-8: Schematic diagram of the CDI experimental setup.

3.4 Capacitive deionization test setup for adsorption

A schematic diagram of the batch mode CDI experimental setup is shown in Figure 3.8. The initial concentrations of NaCl solutions (determined by specific experimental conditions) were 100, 200, 300 or 400 mg/L. The solution was circulated in and out of the CDI cell and between the cell and a reservoir. A magnetic stirrer was used to provide a well-mixed solution in the reservoir. An electrical voltage of 0.6, 0.8, 1, and 1.2 V (depending on experimental condition) was applied to the electrodes via graphite current collectors. A peristaltic pump was used to maintain flow rate of 12, 18, 24, or 30

mL/min (depending on the experimental condition) throughout the entire experiment period. A total of 160 mL solution was circulating through the system (total solution in reservoir, connecting tubes and the CDI cell unit). Experiments were run at least 500 minutes to make sure equilibrium has been achieved in the study. The tube around peristaltic pump rotating unit was changed after every experiment which ran at flow = 12 mL/min. For other flows the tube was changed in between the experiment to ensure there was no leakage due to tube damage. Temperature was controlled using an ice bath for low-temperature ($9.7 \pm 1.24^\circ\text{C}$) experiments, and using a hot plate for high-temperature experiments ($34 \pm 1.21^\circ\text{C}$). No temperature control was used for experiments conducted at room temperature ($23 \pm 0.43^\circ\text{C}$). A dedicated probe measured the temperature and conductivity of the solution every minute. The conductivity was used to calculate the concentration of the salt in the solution. Once the equilibrium stage was achieved, the conductivity (as a result concentration) did not change with time, indicating that the electrodes were saturated.

3.5 Salt removal capacity measurement from adsorption

The initial conductivity values of the reservoir solutions at the start of CDI experiments were recorded. Once the adsorption cycles of CDI tests were completed, the final conductivity values at equilibrium were recorded. The initial and final conductivity values were used to calculate the electrodes' salt removal capacity of the electrodes using the following equation. Here, 0.5057 is the slope of calibration curve of salinity vs conductivity of NaCl (Figure 3-9).

$$q = s * (S_0 - S_1) * \frac{V}{m} \dots \dots \dots (3.1)$$

where,

q = Salt removal capacity (mg/g)

s = slope of salinity vs conductivity curve = 0.5057 (mg cm / L μ S)

S_0 =Initial Conductivity (μ S/cm)

S_1 = Final Conductivity (μ S/cm)

V = Volume of total solution (L)

m = total mass of both electrodes (g)

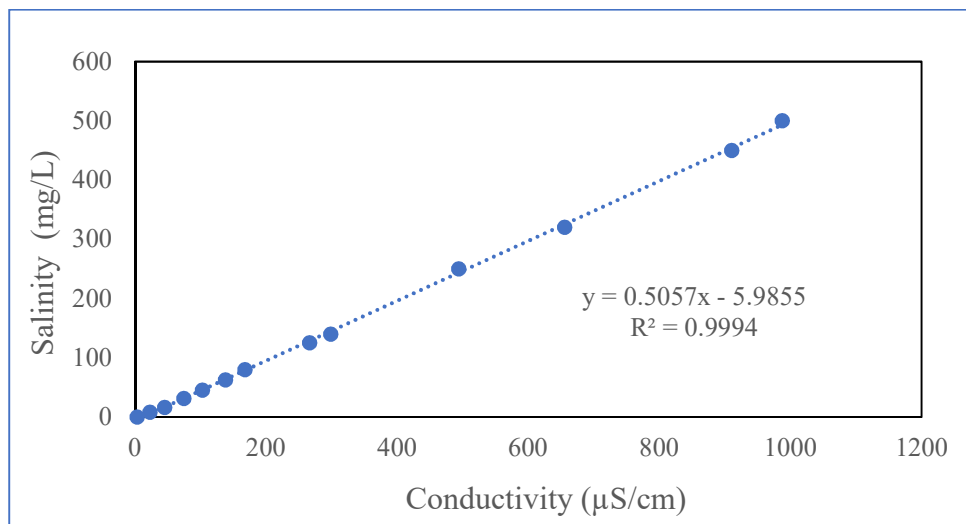


Figure 3-9: Calibration curve for NaCl solution.

Various concentrations of NaCl solutions were prepared to prepare calibration curve for NaCl's salinity vs. conductivity. Each solution was prepared 3 times and conductivity was measured for each of them. The average of these conductivity values was used as prepared salinity level (in mg/L). The detailed data is shown in Appendix A2.

3.6 Acetone wash of electrodes

In this study, electrodes were washed with acetone before being used for experiments to study the effect of operating parameters on surface treatment. The goal was to wash off the impurities and clean the electrodes. The acetone wash process is described below.

- A volume of 50 mL acetone was taken for carbon block and 20 mL was taken for carbon aerogel and each material was dipped into the liquid for 15 mins and gently stirred using a magnetic stirrer.
- Each electrode was then washed for 5 minutes with deionized water.
- Each electrode was then kept at room temperature for air drying.
- Each electrode was washed again with DI water and then dried in a vacuum at about 60°C for 6 hours.

Three experiments under the same applied conditions were conducted using a CDI cell with unwashed electrodes. Unwashed electrodes showed salt removal capacities of 2.19 mg/g, 2.78 mg/g, and 2.78 mg/g (data shown in Appendix B1) while acetone washed electrode showed average salt removal capacity of 3.47 mg/g (described in section 4.1.1 of chapter 4). This 34.5% increase in capacity provided greater salt removal. A decision was made to wash all electrodes used in this study with acetone following the above stated method.

3.7 Experimental set up and methods for chapter 4 (adsorption)

3.7.1 Applied voltage adsorption experiments

Different values of applied voltages across CDI electrodes were used these experiments (0.6, 0.8, 1, and 1.2 V). Experiments for each voltage were repeated for five times. The other applied conditions were kept constant (flow rate = 12 mL/min, initial concentration = 300 mg/L, and room/water temperature at $23 \pm 0.43^\circ\text{C}$).

3.7.2 Varying temperature level adsorption experiments

These experiments were conducted at three different temperatures. The first set of experiments was done at lower temperature level. This lower temperature level was achieved by putting the reservoir in an ice bath during the CDI experiments. Water produced from melted ice was replaced with new ice cubes every 30 mins to maintain a constant low temperature. The average temperature achieved in this test was 9.7°C with a standard deviation of 1.24°C . A second set of experiments was done at room temperature. The average room/water temperature in these experiments was 23°C with standard deviation of 0.43°C . The last set of experiments was done at higher temperature level. This temperature was achieved by setting the hot-plate temperature around $65\text{-}70^\circ\text{C}$ for the duration of the experiment. The average temperature of the water in reservoir in these experiments was 34°C with standard deviation of 1.21°C . Experiments for each temperature level were repeated five times. Other experimental conditions were kept constant (initial concentration of solution = 300 mg/L, applied voltage = 1 V, and flow rate = 12 mL/min).

3.7.3 Varying flow adsorption experiments

In these experiments flow rate was varied as 12, 18, 24, and 30 mL/min by setting peristaltic pump speeds at previously calibrated positions. The tube around the rotating peristaltic pump head was changed after every experiment if it was run at 12 mL/min. For other flow rates, the tube was changed in between the experiment to ensure the flow was not interrupted by rupture of the tube. For 18 mL/min flow rate the tube was changed after 5/6 hours, for 24 mL/min flow rate the tube was changed every 4 hours, and for 30 mL/min flow rate the tube was changed every 2 hours. Other operating conditions were kept constant (applied voltage = 1 V, initial concentration = 300 mg/L, and room/solution temperature at $23 \pm 0.43^\circ\text{C}$). Experiments for each flow were repeated five times.

3.7.4 Varying initial concentration adsorption experiments.

Four different initial concentrations (100 mg/L, 200 mg/L, 300 mg/L, and 400 mg/L) were used in these experiments. Experiments for each concentration were repeated five times. Other operating conditions were kept constant (applied voltage = 1 V, flow rate = 12 mL/min, and room/water temperature at $23 \pm 0.43^\circ\text{C}$).

3.7.5 Statistical analysis of adsorption data

The average and sample standard deviation of recorded values for each experimental parameter were calculated. Limits with 95% confidence interval of the mean were calculated using standard t-table method. Hypothesis testing for mean comparison was done to check whether any significant difference exists between the two consecutive means of same variable.

3.7.6 Retention time and drift velocity related calculations

Consider an ion entering the area between two electrodes as shown in Figure 3-10. The ion has a flow velocity in upward direction (V_y) due to constant circulation of salt water by the peristaltic pump and a drift velocity toward the electrode (V_x) due to electrostatic forces between the ion and the oppositely charged electrode. If the time (t_y) taken by the ion to travel distance Y (retention time) in an upward direction due to V_y is smaller than time (t_x) taken by the ion to travel distance X toward the oppositely charged electrode due to V_x , then the ion may be out of the electrode area before it gets a chance to be adsorbed in the electrode surface. V_y and V_x are calculated from equation 3.2 and 3.3.

$$V_y = \frac{Q}{A} \dots \dots \dots (3.2)$$

where,

Q = Flow rate in m³/s

A = cross sectional area of flow = (0.127 x 0.0016) m²

$$V_x = \mu E \dots \dots \dots (3.3)$$

where,

μ = ionic mobility

($\mu = 5.19 \times 10^{-8}$ m²/Vs for Na⁺ ions and $\mu = 7.92 \times 10^{-8}$ m²/Vs for Cl⁻ ions at 25°C)

[87]

$$E = \text{applied electric field in } \text{Vm}^{-1} = \frac{V}{d} = \frac{\text{Applied voltage}}{\text{distance between electrodes}}$$

The time taken by the ion to travel in both directions is then calculated from the velocity in each direction and approximate travel distance, using equations 3.4 and 3.5.

$$t_y = \frac{Y}{V_y} \dots \dots \dots (3.4)$$

where,

Y = total distance in upward direction = 0.0889 m

$$t_x = \frac{X}{V_y} \dots \dots \dots (3.5)$$

where,

X = total distance in the direction of electrode = 0.0008 m

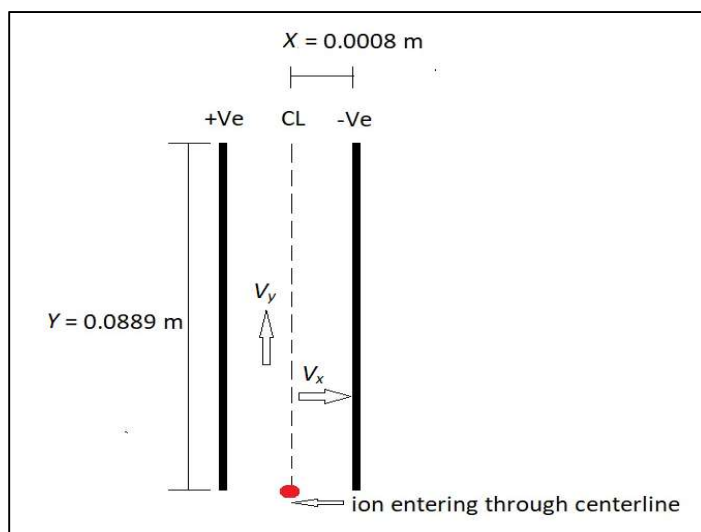


Figure 3-10: Drift velocity (V_x) and flow velocity (V_y) in the ion path.

3.7.7 Isotherm modeling of data

Experimental data obtained for different concentrations were fitted with Freundlich, Langmuir, and Dubini-Radushkevich isotherms to study how the adsorption process. The details of the calculations and respective graphs are discussed in section 4.1.5 of chapter 4.

3.8 Experimental set up and methods for chapter 4 (desorption)

Saturated CDI electrodes were used for desorption experiments. The purpose of the desorption experiments was to explore the extent of regeneration of saturated electrodes and study their desorption behavior. Two different methods of desorption were used to study the effect of operating parameters. The four specific operating parameters explored were variation in applied reverse voltage, duration of applied voltage, flow rate, and temperature. The term “applied reverse voltage” refers to reversing polarity of electrodes in the preceding adsorption cycle. The two desorption methods had one fundamental difference related to the way flushing (DI) water was used during desorption. In one method, the water was circulated (multi-pass) for a long duration (about 10 hours), meaning the water exiting the CDI cell was collected in a reservoir and then was continuously recirculated into the same CDI cell. The conductivity values of the solution in the reservoir were continuously measured. Meanwhile, in the second method a single pass process was used, meaning that the flushing water was held in the two separate reservoir, one for source water feeding to the CDI cell and other for receiving water exiting the CDI cell. In this method, the conductivity values of the solution in the receiving reservoir were measured. The detailed descriptions of both methods are provided in following sections.

3.8.1 Multi-pass method (re-circulating flow)

In this method, 160 mL of deionized water was pumped through the CDI cell for about 500 minutes for desorption to reach equilibrium. Water was pumped through the inlet located at the bottom of the CDI cell using the peristaltic pump. The flow rate was set according to the appropriate applied and experimental parameters of each experiment.

The temperature was set either at room environment or controlled using a stirring hot plate to a value appropriate to the experiment. The duration of applied reverse voltage was controlled manually using a stopwatch. The operating conditions for each set of experiments are shown in the tables below. Only the applied reverse voltages were varied in the experiments described in Table 3.1 and all other parameters were kept constant, as shown in the table. Experiments for each applied reverse voltage were repeated three times.

Table 3.1: Operating parameters for variation of applied reverse voltage experiments with multi-pass method.

| Parameter | Value |
|-------------------------------------|--|
| Variable: | |
| Applied reverse voltages (V) | 0, 0.2, 0.4, 0.6, 0.8, 1, and 1.2 |
| Constant: | |
| Duration of applied reverse voltage | 3 seconds |
| Flow rate | 12 mL/min |
| Temperature | Room environment ($23 \pm 0.43^\circ\text{C}$) |

The effect of variation in the duration of applied reverse voltage and applied conditions are investigated and are presented in Table 3.2. A constant value of 0.8 V was used for reverse potential in these experiments. The experiments for each duration were repeated three times. Since CDI cells are of capacitive nature, the electrodes usually retain some residual charge even when applied voltages are reduced to zero. This residual charge may be responsible for retention of some ions. Externally shorting electrodes free this residual charge and should help in desorption, resulting in greater regeneration of electrodes. For this reason, applying voltage for “0 sec”, which is applying no voltage at

all, was done in two different ways – (i) without shorting electrodes, (ii) with shorting electrodes.

Table 3.2: Parameters for variation of duration of applied voltage experiments with multi-pass method.

| Parameter | Value |
|---------------------------------|---|
| Variable: | |
| Time length of applying voltage | 0 sec, 3 sec, 30 sec, 1 min, 3 min, 5 min, 10 min, and 15 min |
| Constant: | |
| Applied reverse voltage | 0.8 V |
| Flow rate | 12 mL/min |
| Temperature | Room environment ($23 \pm 0.43^\circ\text{C}$) |

In this method the percentage of regeneration was measured by using following equation:

$$\text{percent regeneration} = \frac{(\text{Final conductivity} - \text{initial conductivity in desorption})}{\text{conductivity drop in preceeding adsorption}} * 100 \dots \dots \dots (3.6)$$

The initial conductivity values during the desorption depend on the conductivity of deionized water, which was found to be around 1-2 $\mu\text{S}/\text{cm}$. This value was probably due to impurities in pipes and fixtures of the deionized water producing system or in the storage bucket.

3.8.2 Single-pass Method (No Re-circulation Flow)

In this method, 160 mL of deionized water was passed once through the cell from one reservoir to another. The conductivity of the water collected in the receiving reservoir was measured. Percent regeneration of the CDI electrodes, saturated in the preceding adsorption experiment, was calculated using the following equation.

$$\text{percent regeneration} = \frac{\text{Conductivity in the collection reservoir}}{\text{Final conductivity} - \text{initial conductivity in the preceeding adsorption}} * 100 \dots (3.7)$$

In this method, operating parameters the same as Multi-pass method were observed. Details are shown in the following tables. Only the applied reverse voltages were varied in the experiments described in Table 3.3 while all other parameters were kept as constant, as shown in the table. Experiments for each applied reverse voltage were repeated 3 times. Five different applied reverse potentials were used in this study, they are 0 V, 0.3 V, 0.6 V, 0.9 V, and 1.2 V.

Table 3.3: Parameters for variation of applied reverse voltage experiments with single-pass method.

| Parameter | Value |
|---------------------------------|------------------------------|
| Variable: | |
| Applied reverse voltages (V) | 0, 0.3, 0.6, 0.9, and 1.2 |
| Constant: | |
| Time length of applying voltage | 3 seconds |
| Flow rate | 12 mL/min |
| Temperature | Room environment (23±0.43°C) |

The effect of variation in the duration of applied reverse voltage was studied by applying the same voltage for six different durations, as shown in Table 3.4. Other experimental conditions are also presented in Table 3.4. A constant value of 0.6 V of reverse potential was applied for different durations. Experiments for each duration were repeated 3 times.

Table 3.4: Parameters for variation of applied voltage duration experiments with single-pass method.

| Parameter | Value |
|---------------------------------|--|
| Variable: | |
| Time length of applying voltage | 0 sec, 3 sec, 30 sec, 1 min, 3 min, and 5 min |
| Constants: | |
| Applied reverse voltage | 0.6 V |
| Flow rate | 12 mL/min |
| Temperature | Room environment ($23 \pm 0.43^\circ\text{C}$) |

The effect of variation in temperature on the regeneration of exhausted CDI electrodes was investigated by a series of experiments conducted at three different temperature levels. Deionized water was kept refrigerated for more than two hours before it was used in desorption experiments conducted at low temperature experiments. The reservoir containing the pre-cold water was then placed in an ice-bath to maintain the temperature at $9.7 \pm 1.24^\circ\text{C}$. Experiments conducted at room temperature did not require ice-bath or heating. The average maintained temperature was $23 \pm 0.43^\circ\text{C}$. Experiments conducted at high temperature were conducted by heating the reservoir using a hot plate equipped with a magnetic stirrer, and the average maintained temperature was $34 \pm 1.21^\circ\text{C}$. All experimental and applied parameters are presented in Table 3.5. Experiments for each temperature level were repeated 3 times.

Table 3.5: Parameters for variation of temperature experiments with single-pass method.

| Parameter | Value |
|---------------------------------|--------------------------------|
| Variable: | |
| Temperature (°C) | 9.7±1.24, 23±0.43, and 34±1.21 |
| Constants: | |
| Applied reverse voltage | 0.6 V |
| Flow rate | 12 mL/min |
| Time length of applying voltage | 3 seconds |

The effect of variation of flow rates on the regeneration of CDI electrodes was investigated by a series of experiments conducted with four different flow rates of 12 mL/min, 18 mL/min, 24 mL/min, and 30 mL/min. All other conditions were kept constant as shown in Table 3.6. Experiments for each flow rate were repeated three times.

Table 3.6: Parameters for variation of flow rate experiments with single-pass method.

| Parameter | Value |
|---------------------------------|------------------------------|
| Variable: | |
| Flow rate (mL/min) | 12, 18, 24, and 30 |
| Constants: | |
| Applied reverse voltage | 0.6 V |
| Time length of applying voltage | 3 seconds |
| Temperature | Room environment (23±0.43°C) |

3.9 Experimental setup and methods for surface treatment (chapter 5)

3.9.1 Acid treatment process

Carbon aerogel/fiber paper electrodes that were pre-treated with acetone as described in section 3.6. were dipped into a 2 M nitric acid solution. The electrodes remained in the acid and were heated at 75°C for 1 hour. The electrodes were then removed from the acid and washed with deionized water until the pH of the wash-water

was around 7. The electrodes were then air-dried at room temperature before they were assembled into CDI cells. Comparisons of electrodes with acid treatment were made to electrodes that were not subject to acid treatment. All electrodes used in this phase of study were pretreated with acetone.

3.9.2 Gold deposition process

Sheet electrodes of 88.9 mm by 50.8 mm were deposited with 15 nm gold layer with a 10 nm chromium layer as binder through e-beam deposition using CHA BEC-600-RAP e-beam evaporator, a four-pocket, electron-beam deposition system under high vacuum. Before deposition, each sheet was washed with acetone, isopropanol, and deionized water and then dried using a nitrogen gun.

3.9.3 Scanning electron microscopy

A Hitachi S-4800 Scanning Electron Microscope (SEM) was used to analyze the surface morphology of the untreated and treated electrodes.

3.9.4 Laser scanning microscopy

A VK-X150 3D laser scanning confocal microscope was used to generate high resolution optical images of the surfaces of electrodes.

3.9.5 Surface area and porosity analysis

A NOVA2200e surface area and porosity analyzer was used to measure surface area, pore volume, and pore opening of surface-modified electrodes and untreated electrodes using N₂ adsorption-desorption isotherm at 77 K. Surface area was measured using the Brunauer-Emmet-Teller (BET) method. Pore volume and pore openings were measured using the Barret-Joyner-Halenda (BJH) model.

3.9.6 Cyclic voltammetry test setup

Cyclic Voltammetry (CV) was done using an Ag/AgCl reference electrode and a platinum electrode as counter electrode. The untreated and treated electrodes (which are to be used in CDI cell) were used as working electrodes. 0.5 M NaCl solution was used with scan rate of 5 mv/s and voltage range of -0.4 V to 1 V. Specific Capacitance (SC) in F/g unit was calculated using equation:

$$SC = Q / (2 * v * k * m) \dots \dots \dots (3.8)$$

where,

Q = area enclosed by CV curves with current in A and applied potential in V,

v = working voltage range (V),

k = scan rate (V/s) and

m = working electrode mass (g).

Detailed calculations are shown in Appendix A34.

3.9.7 Fourier transform infrared spectroscopy (FTIR)

Untreated and acid treated samples were tested using FTIR for the presence of any chemical bond formation/destruction that resulted from acid treatment. A small sample of the electrode material (5 mg) was mixed with 100 mg of KBr and ground together thoroughly. Then, this ground mixture was put under 8000 psi pressure for a minute to form a pellet. Then the pellet was analyzed using a Genesis II FTIR machine and the resulting spectra was obtained using OMNIC software. A background spectra was obtained by preparing a pellet using only 100 mg KBr.

3.9.8 Symmetric and asymmetric configuration using acid treated electrodes

Four types of electrode configurations were used in this study. In the first configuration, electrodes were used in the CDI cell without any treatment. These electrodes were washed with acetone and deionized water and then air-dried for 6 hours before they were assembled into a cell. In the second configuration, both electrodes were treated with nitric acid. In third configuration, a nitric acid treated electrode was used as cathode and an untreated electrode was used as anode. In fourth configuration, the polarity was switched so that the acid treated electrode was used as anode and the untreated electrode was used as cathode. The first two configurations had cathode and anode treated and prepared with the same type of electrodes used on opposite sides and are termed symmetric configurations, while in the third and fourth configurations the electrodes on both sides were not same and are therefore termed asymmetric configurations.

3.9.9 Symmetric and asymmetric configuration in a gold deposited cell

Four types of electrode configurations were used in this study. In the first configuration, electrodes were used in the CDI cell without any gold deposition. These electrodes were washed with acetone and deionized water and then air-dried for 6 hours before they were assembled into a cell. In the second configuration, both electrodes were coated with gold deposition as stated previously. In third configuration, a gold deposited electrode was used as cathode and an electrode without gold deposition was used as anode. In fourth configuration, polarity is switched so that the gold deposited electrode was used as anode and the electrode without gold deposition was used as cathode. A schematic diagram of these configurations is shown in Figure 3-11.

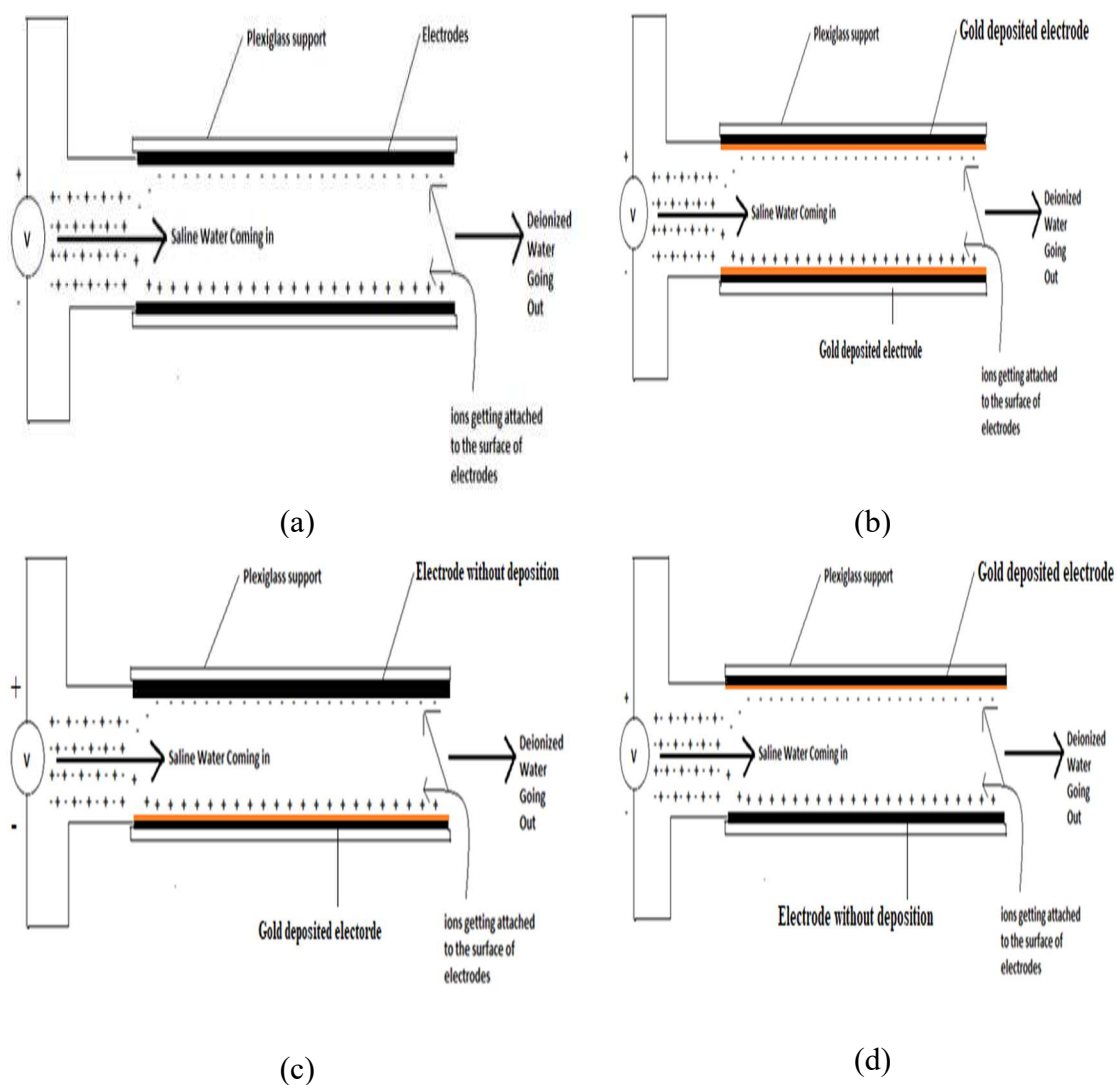


Figure 3-11: Different configurations of CDI experiments (a) Symmetric with both electrode with no deposition (b) Symmetric with both electrode with gold deposition (c) Asymmetric with gold deposited as negative (cathode) (d) Asymmetric with gold deposited as positive (anode).

3.9.10 Capacitive deionization experiments

All the CDI adsorption experiments described in this chapter were run under the same conditions but different the types of electrodes were used. 160 mL of 300 mg/L

NaCl solution was circulated for at least 500 mins. 1 V DC voltage was applied across the electrodes and flow rate was maintained at 12 mL/min. Temperature was maintained under room temperature ($23 \pm 0.43^\circ\text{C}$) setting. After the conductivity reached equilibrium condition, the adsorption cycle was stopped, and the cell went through wash cycles until the wash water conductivity was less than $5 \mu\text{S}/\text{cm}$, which occurred after 500 mins of wash.

CHAPTER 4

EFFECT OF OPERATING PARAMETERS

In this chapter effect of operating parameters on the salt removal behavior of CDI electrodes used in various experiments is discussed. The discussion includes both adsorption and desorption capacities as observed by the collected data from multiple series of experiments.

4.1 Effect of operating parameters on adsorption

4.1.1 Effect of applied voltage on salt removal capacity of CDI electrodes

The effect of applied DC voltages on the salt removal capacity of CDI electrodes was studied by applying four different voltages across electrodes of a CDI cell. The experiments for each applied voltage were repeated five times. The description of the CDI cell used along with the values of applied variables in these experiments is provided in section 3.7. The adsorption data set from one of the five repeated experiments for each applied voltage is presented in Figure 4-1 and the remaining four sets for each applied voltage are presented in Appendices B2-B5.

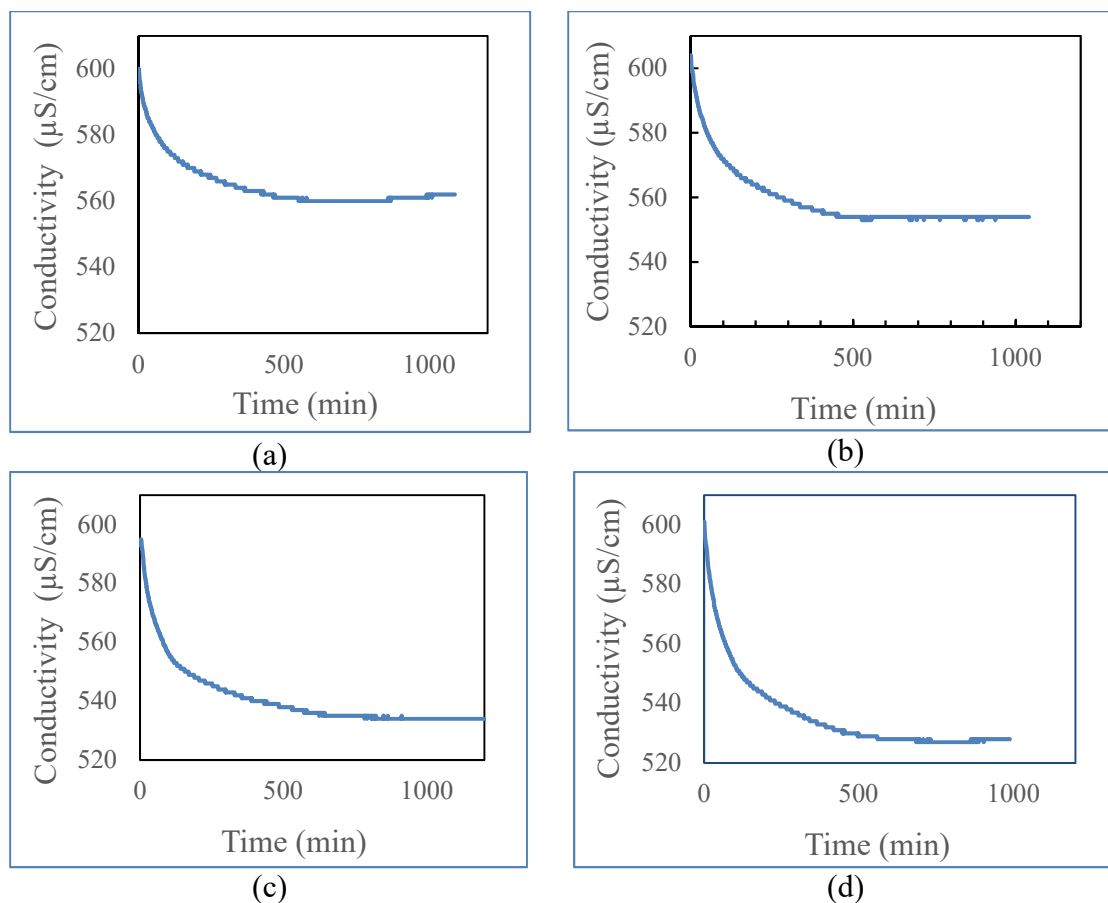


Figure 4-1: The change in conductivity of reservoir solution with time at applied DC voltages of (a) 0.6 V (b) 0.8 V (c) 1 V (d) 1.2 V.

The quantity of salt removed from each experiment was calculated based on initial concentration and concentration at equilibrium of the liquid in the reservoir. These concentrations were calculated from initial and final conductivity values using the calibration plot of conductivity vs. salinity for NaCl solution. A constant volume (160ml) of NaCl solution was used in all experiments. Following mass-balance calculations, the amount of salt removed (in milligrams) per unit mass of electrodes (in g) was calculated to get the salt removal capacity in mg/g unit. The applied voltages, corresponding average salt removal capacities, and their 95% confidence interval limits calculated following t-test, are presented in Table 4.1 and Figure 4-2.

Table 4.1: Average removal capacity of electrodes at different voltages and 95% confidence limits.

| Applied Voltage (V) | Average Salt Removal Capacity (mg/g) | 95% Confidence Interval Limits | |
|---------------------|--------------------------------------|--------------------------------|-------|
| | | Lower | Upper |
| 0.6 | 2.52 | 2.28 | 2.76 |
| 0.8 | 3.02 | 2.83 | 3.22 |
| 1.0 | 3.47 | 3.18 | 3.76 |
| 1.2 | 4.15 | 4.01 | 4.28 |

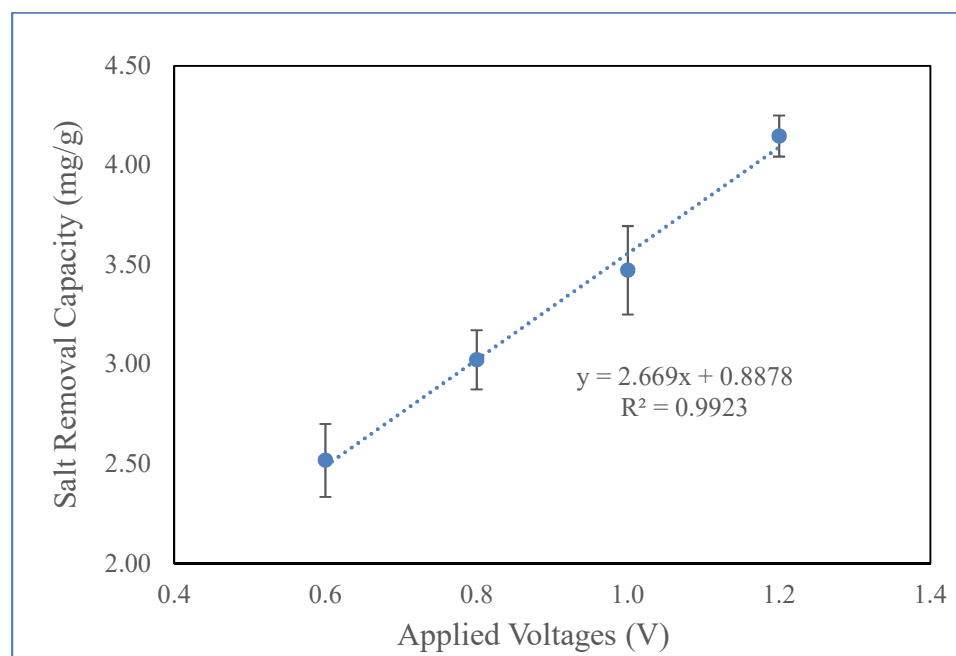


Figure 4-2: Salt removal capacity of electrodes as mg of salt removed per g of electrode at different applied voltages.

From Figure 4-2 it is evident that the salt removal capacity increased with the increase in applied voltage. This increase could be attributed to increased electrostatic attraction forces between the ions and the adsorbing electrode. Additionally, a decrease in electrical double layer overlapping with increase in applied voltage could be a factor for increased salt removal capacity as it will result in pores that were previously inaccessible for ions to become accessible for adsorption, this providing more surface area for more

ions to be adsorbed. An extended version of Table 4.1 is presented in Appendix A3, which shows details of all five sets of experiments for each applied voltage. As observed from the 95% confidence limits, there is a minimal difference between the means of salt removal capacities at 0.8 V and at 1 V. A hypothesis test was done at 95% confidence level to compare the expected means from these two CDI test conditions. This test confirmed that there is enough evidence of both mean being different. The test details are shown in Appendix A4. A significance test done on the slope of linear regression shown in Figure 4-2 indicates that a significant correlation exists between the applied voltage and salt removal capacity. Details of the calculations are shown in Appendix A5.

An analysis was conducted on an ion entering through centerline of the space between electrodes to compare the time it took to cover the distance along the flow to the time it took to drift towards the electrode surface. In experiments with voltage being the study variable, a constant flow rate of 12 mL/min was used, which gave an average flow velocity of $9.84 \times 10^{-5} \text{ ms}^{-1}$. This axial velocity means the ion needed approximately 91 secs to enter and exit the space between the electrodes before it is removed from the flow stream because of the electric field between the electrodes. The ion would be exerted with two different forces – 1) attraction force between the ion and the oppositely charged electrode, which would make the ion move towards that electrode and, 2) repulsion force between the ion and the electrode with the same polarity, which would make the ion move away from that electrode. The combination of these two movement results in drift (lateral) velocity.

In this simplistic analysis, only the force of attraction is considered in calculating drift velocity. This provided a very conservative estimate of drift velocity. At applied

voltages 0.6, 0.8, 1, and 1.2 V, the time needed for Na^+ ions to reach the negative electrode surface from centerline were 41, 31, 25, and 21 secs (approximately) respectively. Since the time needed for ion to hit oppositely charged electrode is lower than time needed for ion to escape the CDI cell, it is highly likely that this ion will be removed from the flow stream. Drift velocity was higher at higher applied voltages, resulting in shorter times required for the ion to hit the electrode, resulting in a higher chance of adsorption. Similarly, for Cl^- ions the time needed to get adsorbed was lower than time needed to flow out of the area (detail calculation shown in Appendix A6).

Even though increasing voltage led to higher salt removal capacities, the applied voltage beyond a certain value started creating issues with the stability of the electrode material and the participating ions. In initial stages of this study, relatively high voltages (ranging from 2 to 4 V) were applied. This resulted in unwanted chemical reactions between salt ions and electrodes that produced a brown colored solution as shown in Figure 4-3a. The resulting solution was analyzed using X-ray fluorescence (XRF) and nuclear magnetic resonance spectroscopy (NMR) as shown in Figure 4-3b and Figure 4-3c. The spectroscopy of the brown material suggested it to be of an organic nature containing chlorine, but the identity of the substance could not be determined. Fe and Cu were also present as shown by the XRF spectra. The source of Fe was the steel spatula which was used to collect dried sample from the drying dish. The source of Cu ions was probably the copper wire used in the initial design of the CDI cells. Though, copper was not in direct contact with water, there may be some infiltration of Cu ions due to reaction with water vapor or other ions present in the deionization system.

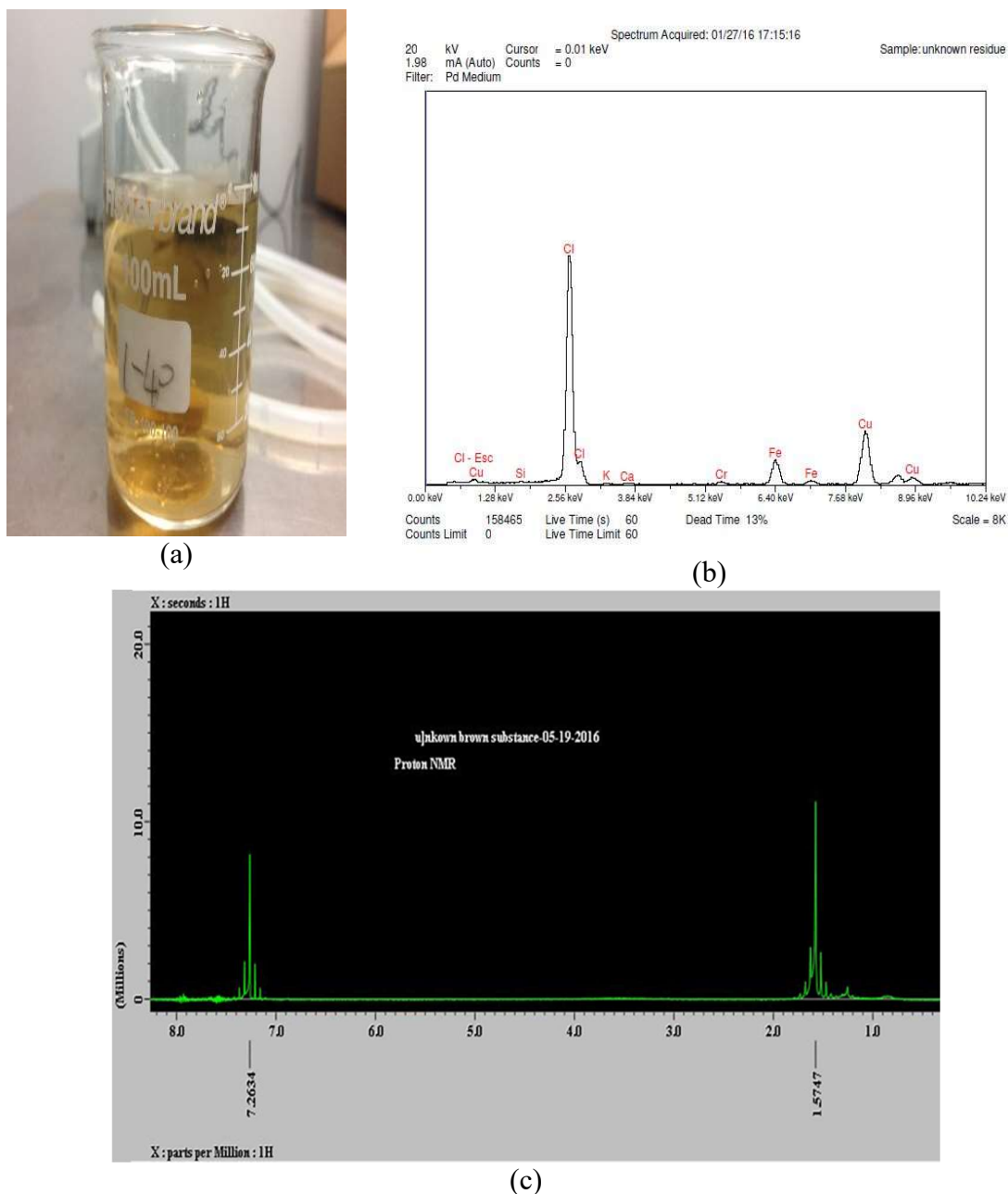


Figure 4-3: (a) Unknown brown solution (b) XRF data (c) NMR spectroscopy.

4.1.2 Effect of temperature on salt removal capacity of CDI electrodes

The effect of variation in temperature on salt removal capacity of CDI electrodes was studied by conducting the experiments at three different temperatures levels. The experiments were repeated five times for each temperature. The description of the CDI

cell used along with the values of applied variables in these experiments is provided in chapter 3.

The adsorption data set from one of the five repeated experiments for each temperature value is presented in Figure 4-4 and the remaining four sets for each applied voltage are presented in Appendices B6-B8.

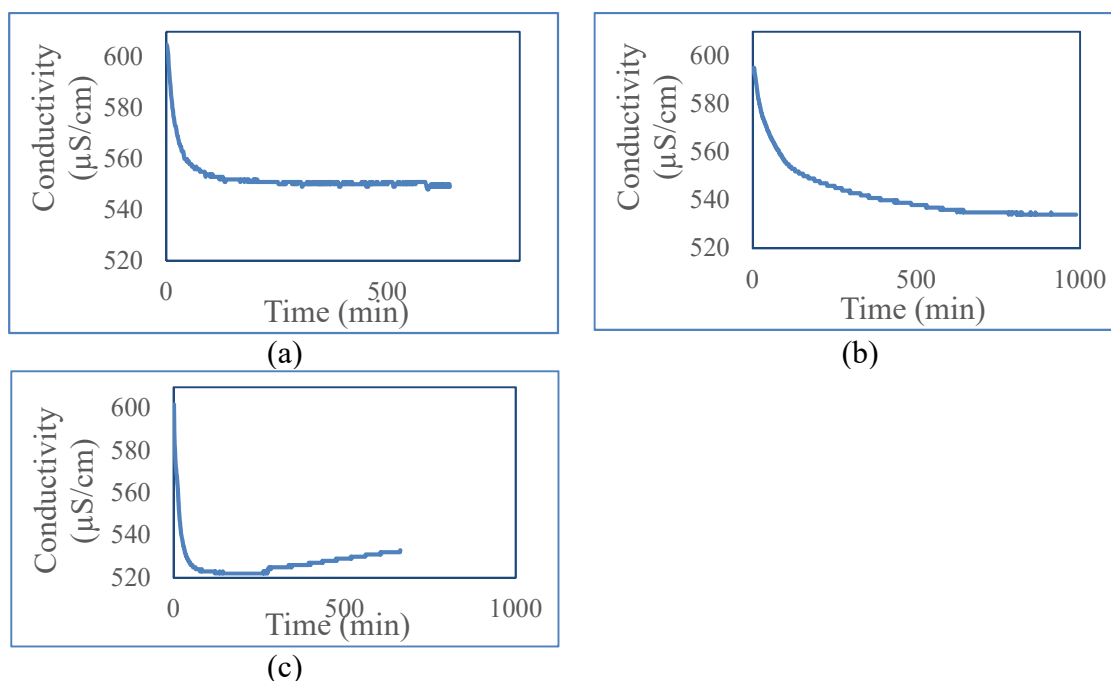


Figure 4-4: The change in conductivity of reservoir solution with time at temperature values of (a) 9.7°C (b) 23°C (c) 34°C.

Table 4.2 presents temperatures, average salt removal capacities observed, standard deviation, and 95% confidence interval limits based on data collected from each set of five experiments for temperature values explored in these experiments. Figure 4-5 shows the average salt removal capacity (mg of salt removed per unit g of CDI electrodes) at temperature values investigated in these experiments. The data show that salt removal capacity increased with increase in temperature. This increase in adsorption

capacity could be attributed to increased movements of ions with increase in temperature resulting in greater number of ions having more contact with electrodes and thus increasing their chances to get adsorbed. CDI electrodes have limited freedom for expansion in vertically because on one end a graphite strip was attached and on the other end there was a plastic strip as discussed in chapter 3. However, the electrodes were unrestricted and free to expand horizontally. The thermal expansion could result into greater pore opening, which could be another possible reason for the increase in salt removal capacity with increase of temperature. Also, diffusion coefficient increases with increase in temperature for liquids, resulting in more mass transfer into pores. An extended version of Table 4.2 is presented in the Appendix A7, which shows salt removal capacities of all different runs. As observed from the 95% confidence limits, there is an overlap between the upper limit of mean at 9.7°C and lower limit of mean 23°C. Also, upper limit of mean at 23°C and lower limit of mean at 34°C are close. Hypothesis tests were done at 95% confidence level to compare the expected means from these CDI test conditions. The test confirmed that there is enough evidence of these means being different. The test details are shown at Appendices A8-A9. A significance test done on the slope of linear regression shown in Figure 4-5 indicates that a significant correlation exists between temperature and salt removal capacity. Details of the calculations are shown in Appendix A10.

Table 4.2: Average removal capacity of electrodes at different temperature and 95% confidence limits.

| Average Attained Temperature (°C) | Average Salt Removal Capacity (mg/g) | Standard Deviation | 95% Confidence Interval Limits | |
|-----------------------------------|--------------------------------------|--------------------|--------------------------------|-------|
| | | | Lower | Upper |
| 9.7 | 3.00 | 0.15 | 2.82 | 3.18 |
| 23 | 3.47 | 0.23 | 3.18 | 3.76 |
| 34 | 4.29 | 0.36 | 3.85 | 4.74 |

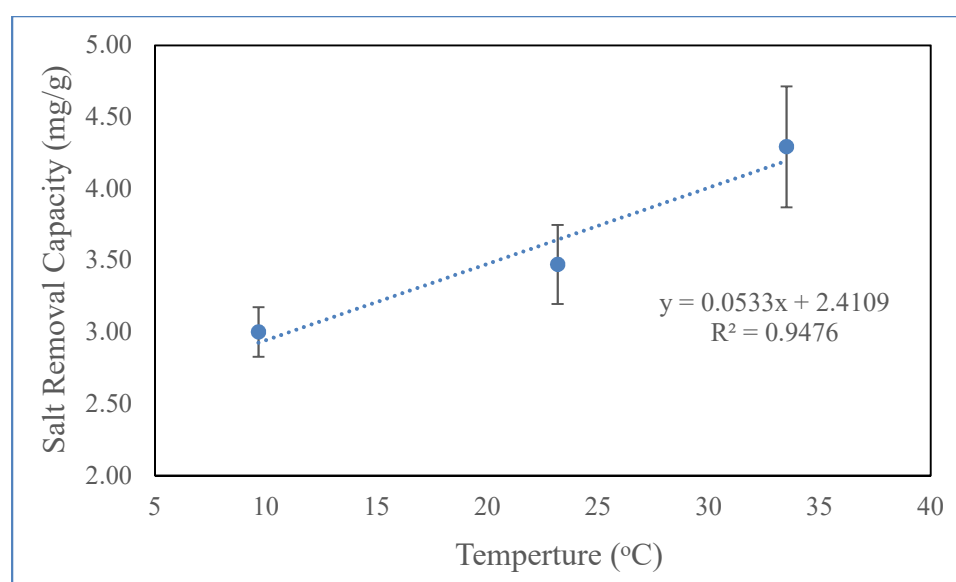


Figure 4-5: Salt removal capacity of CDI electrodes at various temperatures.

4.1.3 Effect of flow rate on salt removal capacity

The effect of variation in flow rate on salt removal capacity of CDI electrodes was studied by conducting a series of four experiments with four different flow rates of 12 ml/min, 18 ml/min, 24 ml/min, and 30 ml/min. Experiments for each flow rate were repeated five times. One data set from each set of five experiments for each flow rate is presented in Figure 4-6. The remaining four data sets for each flow rate are presented in Appendices B9-B12.

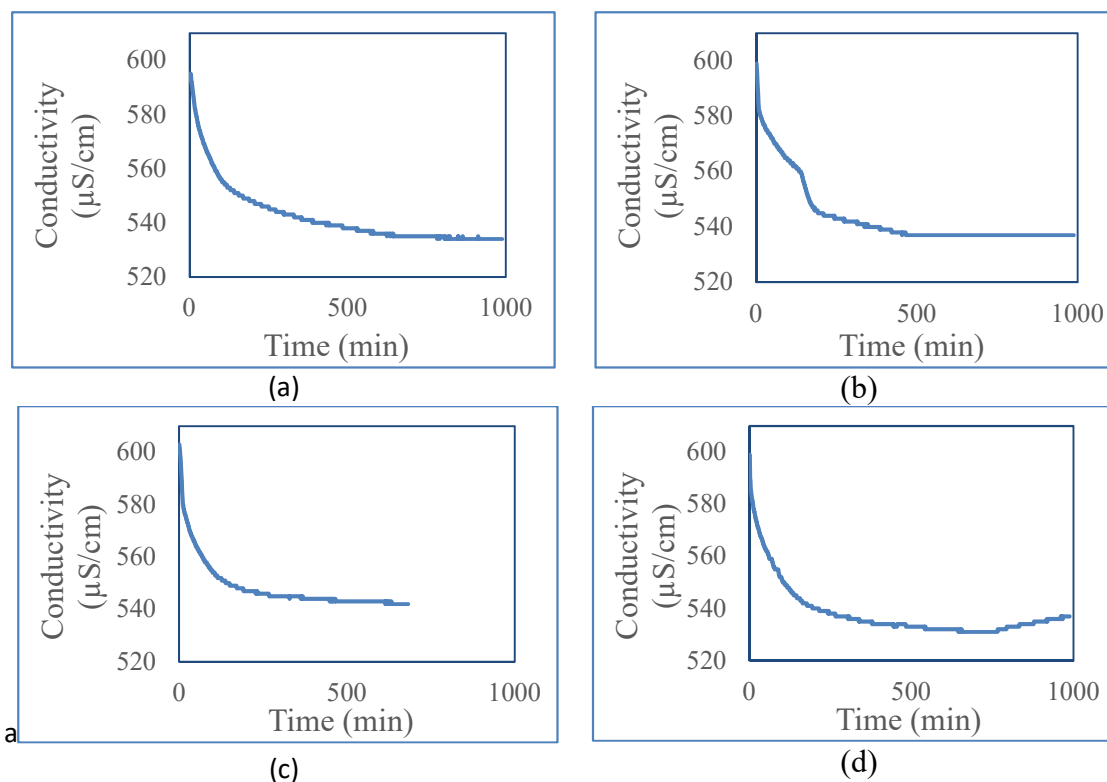


Figure 4-6: Salt removal capacity of CDI electrodes at flow rate of (a) 12 mL/min (b) 18 mL/min (c) 24 mL/min (d) 30 mL/min.

Table 4.3 shows the average salt removal capacity and range of expected mean at 95% confidence limit as per t-test. An extended Table 4.3 is added in Appendix A11 which also shows the salt removal capacities of all different runs. As observed from the 95% confidence limits, there is huge overlap between the range of means from different conditions. Hypothesis tests were done at 95% confidence level to compare the expected means from these CDI test conditions. The tests confirmed that there is not enough evidence of these means being different. The test details are shown in Appendix A12-A15.

Table 4.3: Average removal capacity of electrodes at different flow rates and 95% confidence limits.

| Flow (mL/min) | Average Salt Removal Capacity (mg/g) | Standard Deviation | 95% Confidence Interval Limits | |
|------------------|---|-----------------------|-----------------------------------|-------|
| | | | Lower | Upper |
| 12 | 3.47 | 0.15 | 3.29 | 3.66 |
| 18 | 3.52 | 0.19 | 3.29 | 3.75 |
| 24 | 3.54 | 0.20 | 3.29 | 3.79 |
| 30 | 3.58 | 0.17 | 3.38 | 3.79 |

The average salt removal capacities (mg/g) at various flow rates are also presented in Figure 4-7. It is evident from the presented data that the average salt removal capacity did not change significantly over the flow rates used in the experiments. A significance test done on the slope of linear regression shown in Figure 4-7 indicates that a significant correlation does not exist between flow rate and salt removal capacity.

Details of the calculations are shown in Appendix A16.

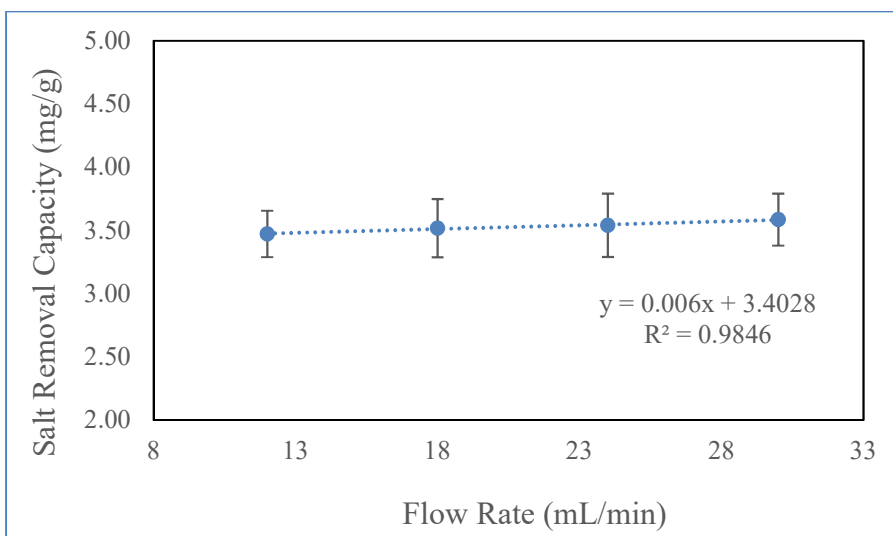


Figure 4-7: Salt removal capacity at different flow rates.

For experiments at different flow rates, the applied voltage was kept constant at 1 V, which resulted in a constant drift velocity. For Na^+ ion drift velocity was 3.24×10^{-5} m/s, which resulted in a constant time needed to reach the electrode represented as $t_x = 25$ secs. Drift velocity for Cl^- ions was 4.95×10^{-6} m/s and resulting constant time needed to reach the electrode as $t_x = 16$ secs. Retention time or time needed to flow out of the space between electrodes in vertical directions were 91, 60, 45, and 36 secs at 12, 18, 24, and 30 mL/min flow rates respectively. Therefore, both ions had higher chances to get adsorbed and thus removed from the flow stream. Resulting average salt removal capacities were 3.47, 3.52, 3.54, and 3.58 mg/g respectively. Since there is no significant statistical difference between the salt removal capacities, it can be concluded that electrodes were reaching their saturation capacities in the flow range used. A slight increase with flow perhaps occurred because, in a semi-batch mode operation (where flow is recycled) at high flow rate, a particular ion comes to the electrode vicinity more often than at low flow rate. This increases the chance of ions getting adsorbed and thus there is a possible increase in salt removal capacity. Here, the salt removal capacity is increased at a very low gradient. A wider range of flow rate (such as 10-100 mL/min) probably could have provided a more definite trend. The peristaltic pumps used in these experiments were designed with a maximum flow rate 32 mL/min and for that reason a wider range of flow rates could not be explored. In future work exploration of a wide range of flow rates and their effect on salt removal capacity is recommended.

4.1.4 Effect of initial concentration on salt removal capacity

Four different initial concentrations were used to assess the effect on salt removal capacity of electrodes in CDI operations. Each initial concentration was used in five

different runs. Example of runs are shown in Figure 4-8 and rest of the runs are shown in Appendix B13-B16.

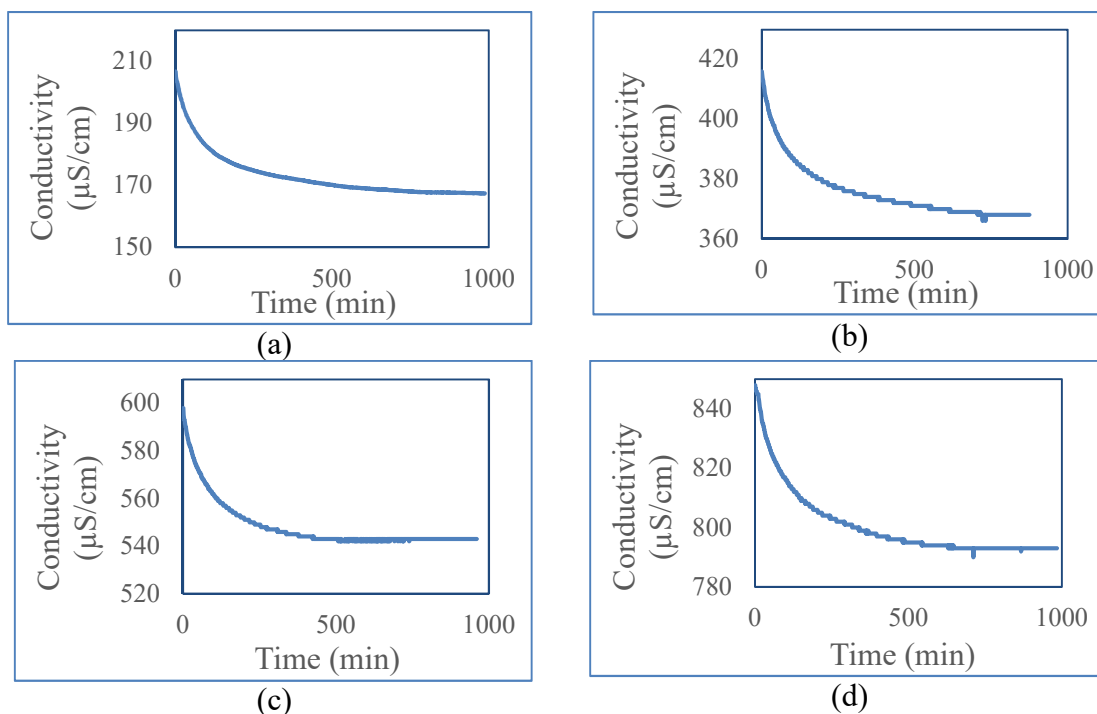


Figure 4-8: Salt removal capacity at different flow rates (a) 100 mg/L (b) 200 mg/L (c) 300 mg/L (d) 400 mg/L.

Table 4.4 and Figure 4-9 shows the average salt removal capacity (mg/g) for different initial concentrations. The average capacity increased with increasing initial concentration. The increase in removal capacity of the specific CDI electrodes used could be attributed to the higher concentration gradient near the electrodes. A higher concentration gradient leads to a higher mass transfer rate. Thus, more salt removal occurs during the same period. 95% confidence intervals from t-test shown in Table 4.4 shows, there is overlap in lower and upper limits of mean salt removal at initial concentrations of 100

mg/L and 200 mg/L. This is also the case with initial concentrations of 300 mg/L and 400 mg/L. An extended version of Table 4.4 is presented in Appendix A17.

Table 4.4: Average removal capacity of electrodes at different initial concentrations and 95% confidence limits.

| Initial Concentration (mg/L) | Average Salt Removal Capacity (mg/g) | Standard Deviation | 95% Confidence interval limits | |
|------------------------------|--------------------------------------|--------------------|--------------------------------|-------|
| | | | Lower | Upper |
| 100 | 2.52 | 0.21 | 2.25 | 2.78 |
| 200 | 2.81 | 0.10 | 2.69 | 2.93 |
| 300 | 3.47 | 0.15 | 3.29 | 3.66 |
| 400 | 3.66 | 0.28 | 3.32 | 4.01 |

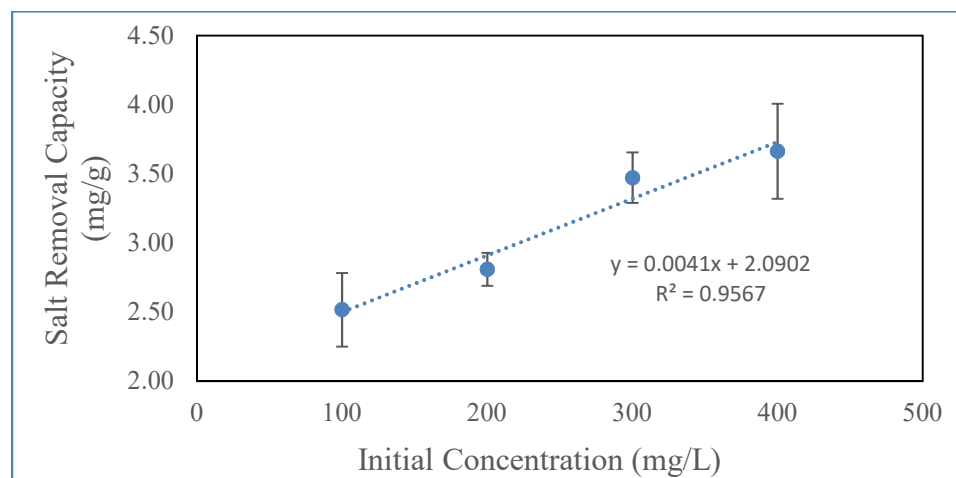


Figure 4-9: Salt removal capacity at initial concentrations.

Appendices A18-20 show the hypothesis tests for mean comparisons. From the tests it is concluded that means of salt removal capacities at 100 mg/L, 200 mg/L, and 300 mg/L initial concentrations are significantly different. But there is not enough evidence to prove the significant difference between mean salt removal capacities

between 300 mg/L and 400 mg/L initial concentrations. A significance test done on the slope of linear regression shown in Figure 4-9 indicates that a significant correlation exists between the initial concentration and salt removal capacity. Details of the calculations are shown in Appendix A21.

4.1.5 Adsorption Isotherms

Freundlich, Langmuir and Dubinin-Radushkevich isotherm models were used to simulate the experimental data for adsorption of NaCl in the electrodes at different concentration levels. A Freundlich equation was used in this study in the non-linear form as follows:

$$q_e = K_f C_e^{\frac{1}{n}} \dots\dots\dots (4.1)$$

Where, q_e is the adsorption capacity (mg/g), C_e is the equilibrium concentration (mg/L), K_f and n are constants related to adsorption capacity and intensity. A linearized Freundlich model is used in this study. The equation is as follows:

$$\ln q_e = \ln K_f + \frac{1}{n} \ln C_e \dots\dots\dots (4.2)$$

Original Langmuir equation is a non-linear equation as follows:

$$q_e = q_m K_L \frac{C_e}{1 + K_L C_e} \dots\dots\dots (4.3)$$

Where, q_m is a constant related to adsorption capacity and K_L is a constant related to energy or net enthalpy of adsorption. A linearized form of Langmuir equation was used in this study to simulate the data:

$$\frac{C_e}{q_e} = \frac{1}{q_m K_L} + \frac{C_e}{q_m} \dots\dots\dots (4.4)$$

Actual Dubinin-Radushkevich isotherm model is a non-linear equation as follows:

$$q_e = q_s \exp(-K_D \varepsilon^2) \dots\dots\dots (4.5)$$

Where, q_s is constant related to adsorption capacity, K_D is constant related to mean free energy and ε is given by following equation:

$$\varepsilon = RT \ln\left(1 + \frac{1}{C_e}\right) \dots\dots\dots (4.6)$$

Where, R is the ideal gas constant and T is the absolute temperature.

A linearized form of the Dubinin-Radushkevich isotherm used in this study is:

$$\ln q_e = \ln q_s - K_D \varepsilon^2 \dots\dots\dots (4.7)$$

Table 4.5 shows different parameters values from the models used. Figure 4-10, Figure 4-11 and Figure 4-12 shows the adsorption isotherm models fitted with experimental data. It is evident from R^2 value that the Langmuir isotherm fit well with the data presented in this study. This means monolayer adsorption is taking place in the electrode surface as per assumptions behind Langmuir modelling.

Table 4.5: Parameter values from isotherm models.

| Model Name | Parameters | | |
|----------------------|------------|---------|--------|
| Freundlich | K_F | n | R^2 |
| | 1.10637 | 5.05561 | 0.6931 |
| Langmuir | q_m | K_L | R^2 |
| | 3.79939 | 0.02851 | 0.9821 |
| Dubinin-Radushkevich | q_s | K_D | R^2 |
| | 3.4373 | 0.0003 | 0.6057 |

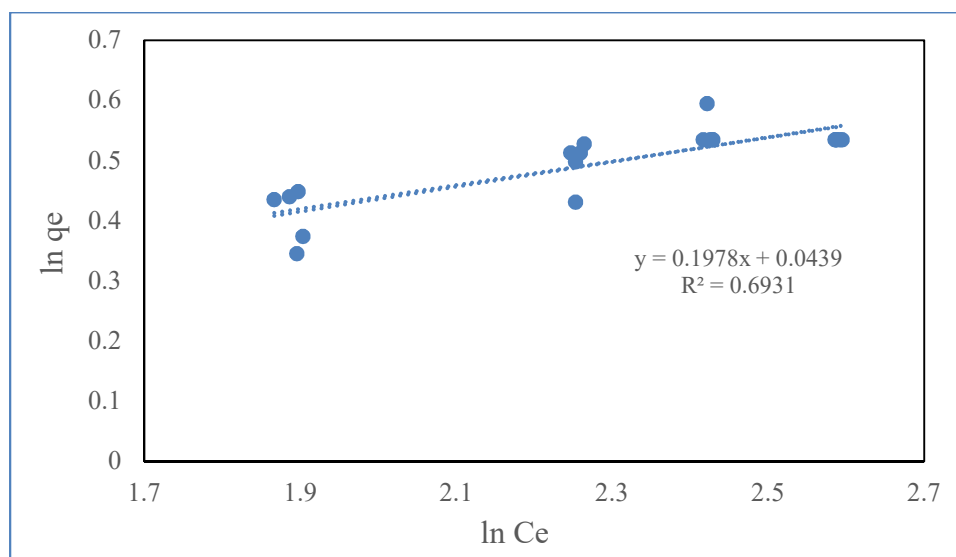


Figure 4-10: Freundlich isotherm model.

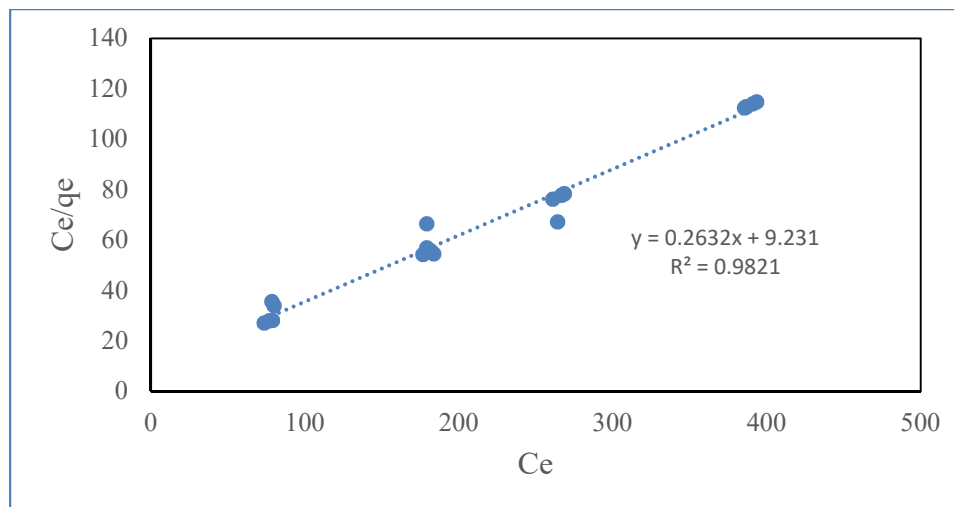


Figure 4-11: Langmuir isotherm model.

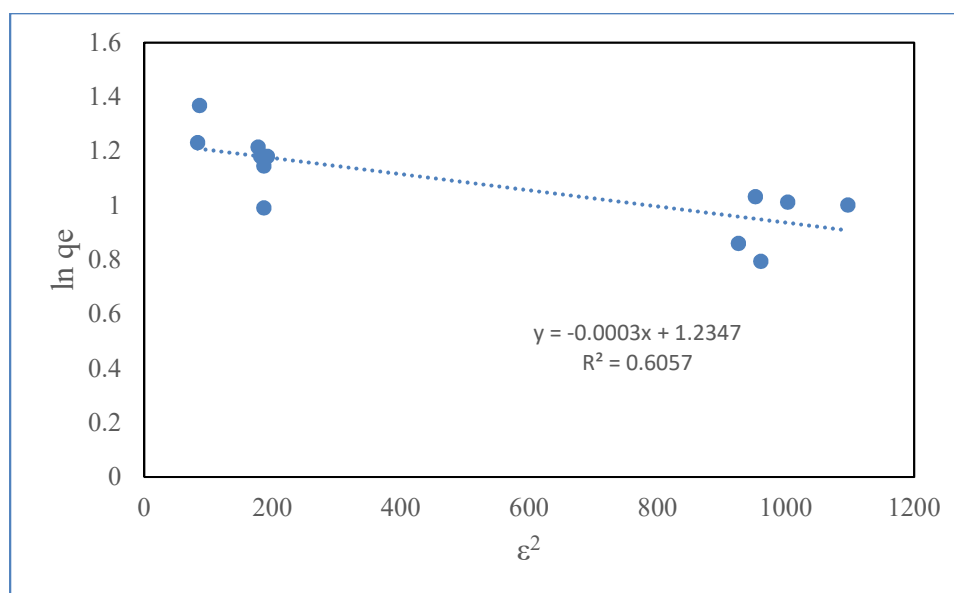


Figure 4-12: Dubinin-Radushkevich isotherm model.

In Langmuir isotherm the parameter q_m is considered as the maximum adsorption capacity, which in this case is 3.7993 mg/g. In the voltage experiments, the highest value achieved for adsorption at 1 V with 300 mg/L initial concentration was 3.82 mg/g, which can be accurately predicted by the Langmuir isotherm model derived in this study.

4.2 Effect of operating parameters on desorption

4.2.1 Effect of applied reverse potential using multi-pass method

Experiments were conducted with seven different voltages to study the effect of applied reverse potential in the single-pass regeneration method. Experiments were repeated three times except for voltages of 0 V, 0.2 V, and 1.2 V, which were repeated twice. Average percentage regeneration, their standard deviation, and 95% confidence limits are presented in Table 4.6. An extended version of this table with regeneration percentages from all experiments conducted are presented in Appendix A22.

Table 4.6: Regeneration percentages for various applied reverse voltages using multi-pass method.

| Applied voltage | Average regeneration (%) | Standard deviation | 95% confidence interval | |
|-----------------|--------------------------|--------------------|-------------------------|-------|
| | | | Lower | Upper |
| 0 | 53 | 11 | 27 | 79 |
| 0.2 | 68 | 14 | 34 | 102 |
| 0.4 | 88 | 7 | 72 | 104 |
| 0.6 | 76 | 12 | 47 | 105 |
| 0.8 | 81 | 6 | 65 | 97 |
| 1 | 82 | 5 | 70 | 94 |
| 1.2 | 78 | 12 | 47 | 109 |

The regeneration percentages plotted against applied reverse voltages as shown in Figure 4-13 shows no observable difference in regeneration percentages. A significance test done on the slope of linear regression shown in Figure 4-13 indicates that a significant correlation does not exist between the applied reverse voltage and percent regeneration. Details of the calculations are shown in Appendix A23.

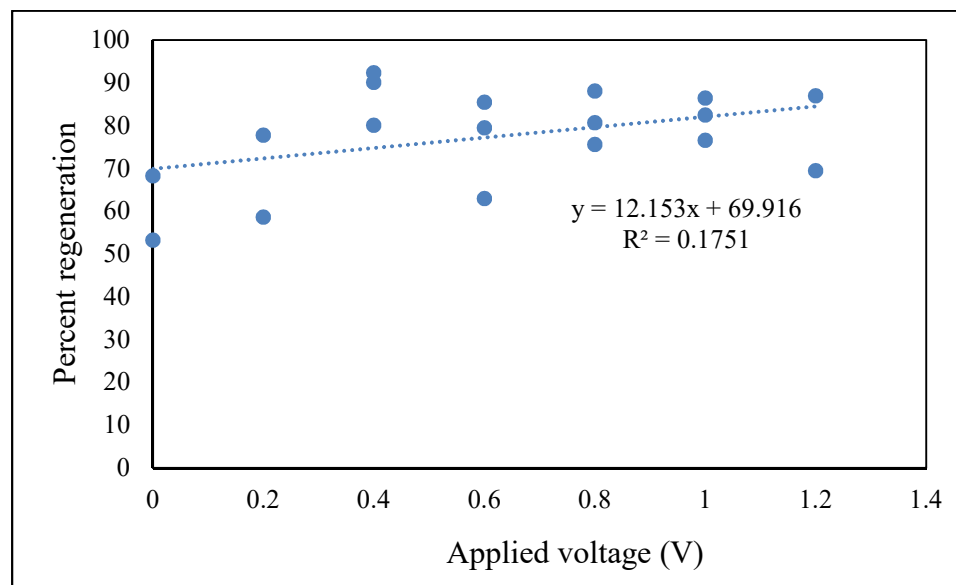


Figure 4-13: Regeneration rates for different reverse voltages using multi-pass method.

4.2.2 Effect of duration of applied reverse voltage using multi-pass method

Eight different time lengths were applied to study the effect of duration. Each time length was applied 3 times (except for 0 sec, 10 min, and 15 min, which were run twice). In addition, an experiment with shorted electrodes was also studied. Table 4.7 presents the average regeneration rates for different time lengths and electrode-shortened condition along with their standard deviation and 95% confidence intervals. An extended version of this table with regeneration percentages from all experiments conducted are presented in Appendix A24.

Table 4.7: Regeneration percentages for various time lengths of applying reverse voltages using multi-pass method.

| Time Applied/Condition | Voltage | Average Regeneration (%) | Standard Deviation | 95% Confidence Interval Lower - Upper |
|------------------------|---------|--------------------------|--------------------|--|
| No Voltage | 0 | 61 | 11 | 35 - 87 |
| Shorted | 0 | 79 | 8 | 58 - 100 |
| 3 S | 0.8 | 83 | 2 | 78 - 88 |
| 30 S | 0.8 | 71 | 20 | 21 - 121 |
| 1 min | 0.8 | 76 | 3 | 70 - 82 |
| 3 min | 0.8 | 74 | 4 | 65 - 83 |
| 5 min | 0.8 | 85 | 8 | 64 - 106 |
| 10 min | 0.8 | 91 | 10 | 65 - 117 |
| 15 min | 0.8 | 65 | 4 | 56 - 74 |

Even when all percent regenerations were plotted against the applied reverse potential, no observable difference in regeneration percentages was observed as depicted by the scatter plot provided in Figure 4-14. On all the experiments in multi-pass method, the duration of applied reverse voltages was varied between 0-15 mins and the total duration of the regeneration (desorption) experiments was more than 500 mins.

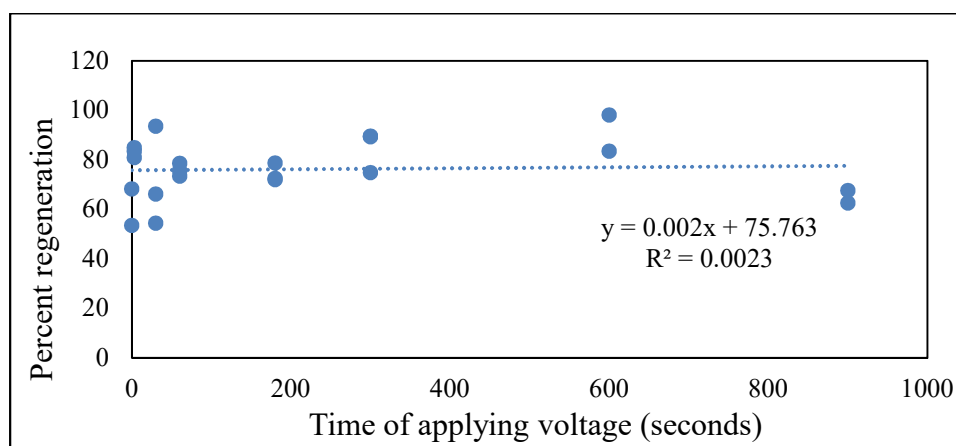


Figure 4-14: Regeneration rates for different time lengths of applying voltage using multi-pass method.

Effectively, the CDI cell was without any applied voltages and continuously circulated with same solution for more than 485 mins (485 mins in the case of 15 mins of applied reverse voltage, 500 mins in the case of 0 minutes of applied reverse voltage) for each experiment. A significance test done on the slope of linear regression shown in Figure 4-14 indicates that a significant correlation does not exist between the time duration of applying reverse voltage and percent regeneration. Details of the calculations are shown in Appendix A25.

Since experiments following multi-pass method did not show a definitive trend, the rest of the regeneration (desorption) experiments in this study were conducted with single-pass method to reduce the overall time needed for regenerating and preparing the CDI cell for next set of experiments. The time required for single-pass experiments was between 5-10 minutes depending on the flow rate versus more than 500 minutes in multi-pass experiments.

4.2.3 Effect of applied reverse potential using single-pass method

Five different reverse voltages were applied for 3 seconds, a flow rate of 12 mL/min was maintained and the experiments were conducted at room temperature conditions. Experiments for each voltage were repeated three times. The detailed results for the runs are shown in Appendix A26. From the results shown in Table 4.8 and Figure 4-15 it is evident that no observable difference in the regeneration values are found for various applied voltages using single-pass method. A significance test done on the slope of linear regression shown in Figure 4-15 indicates that a significant correlation does not

exist between the applied reverse potential and percent regeneration. Details of the calculations are shown in Appendix A27.

Table 4.8: Regeneration percentages for various applied reverse voltages using single-pass method.

| Applied Voltage | Average Regeneration (%) | Standard Deviation | 95% Confidence Interval Lower - Upper |
|-----------------|--------------------------|--------------------|--|
| 0 | 44 | 0.38 | 43 - 45 |
| 0.3 | 43 | 4 | 34 - 52 |
| 0.6 | 40 | 2 | 34 - 46 |
| 0.9 | 43 | 4 | 32 - 54 |
| 1.2 | 43 | 5 | 32 - 54 |

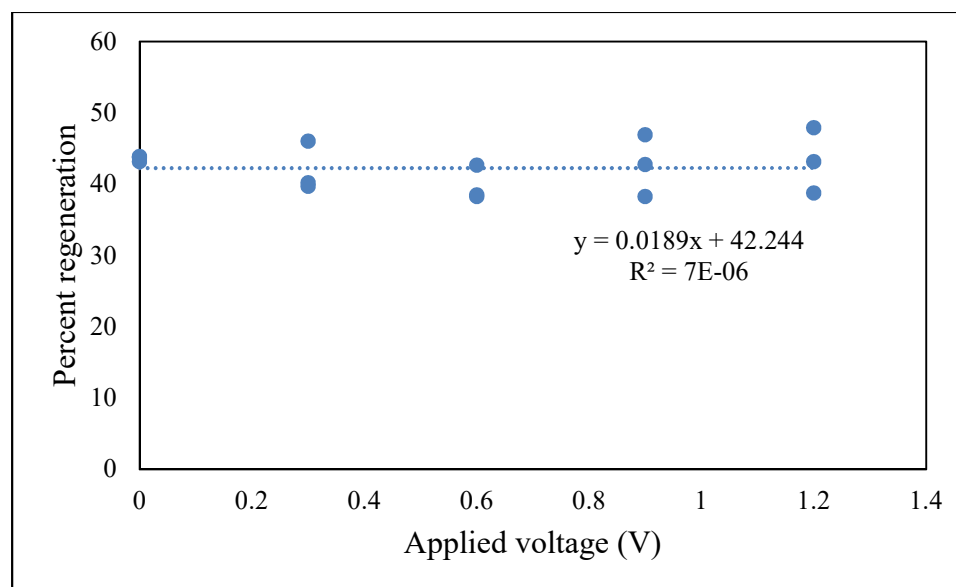


Figure 4-15: Regeneration rates for various applied reverse voltage using single-pass method.

4.2.4 Effect of duration of applied reverse voltage using single-pass method

Six different durations of applied reverse voltage were studied to see the effect on regeneration percentage. Each experiment was repeated three times. Table 4.9 shows the corresponding data, while the same data are presented in graphical form in Figure 4.-6. The detailed data for each run is presented in Appendix A28. A reverse voltage of 0.6 V was applied in all these experiments with a flow rate of 12 mL/min, and temperature was maintained at room setting. Experiments were repeated three times for each duration. From the data presented, no observable difference in regeneration percentages for different time lengths could be found.

Table 4.9: Regeneration percentages for various time lengths of applying reverse voltages using single-pass method.

| Time Length | Average Regeneration (%) | Standard Deviation | 95% Confidence Interval Lower - Upper |
|--------------------|-------------------------------------|-------------------------------|--|
| 0 | 42 | 9 | 20 - 64 |
| 3 sec | 72 | 6 | 56 - 88 |
| 30 sec | 65 | 11 | 37 - 93 |
| 1 min | 65 | 9 | 43 - 87 |
| 3 min | 67 | 7 | 50 - 84 |
| 5 min | 70 | 8 | 51 - 89 |

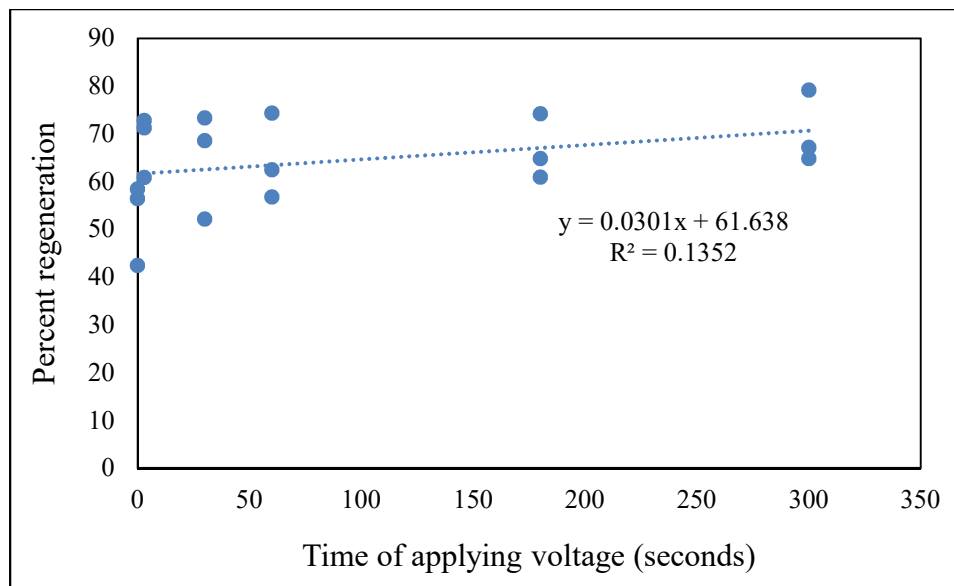


Figure 4-16: Regeneration rates for various duration of applying reverse voltage using single-pass method.

A significance test done on the slope of linear regression shown in Figure 4-16 indicates that a significant correlation does not exist between the varying time duration of applied reverse potential and percent regeneration. Details of the calculations are shown in Appendix A29.

4.2.5 Effect of temperature variation using single-pass method

Three different temperature levels were studied for studying effect on regeneration percentages. Experiments for each level were repeated three times. In these tests, a voltage of 0.6 V was applied for 3 secs with flow rate of 12 mL/min. Table 4.10 shows the average regeneration rates along with standard deviation and 95% confidence level for different temperature levels. Appendix A30 shows detailed data for these runs. From data presented in Figure 4-17 and Table 4.10, no observable difference in regeneration percentages was found in the regeneration percentages. A significance test done on the slope of linear

regression shown in Figure 4-17 indicates that a significant correlation does not exist between temperature variation and percent regeneration. Details of the calculations are shown in Appendix A31.

Table 4.10: Regeneration percentages for various temperature levels using single-pass method.

| Temperature (°C) | Average Regeneration (%) | Standard Deviation | 95% Confidence Interval Lower – Upper |
|------------------|--------------------------|--------------------|--|
| 9.7±1.24 | 61 | 4 | 51 - 71 |
| 23±0.43 | 57 | 18 | 13 -101 |
| 34±1.21 | 65 | 11 | 37 - 93 |

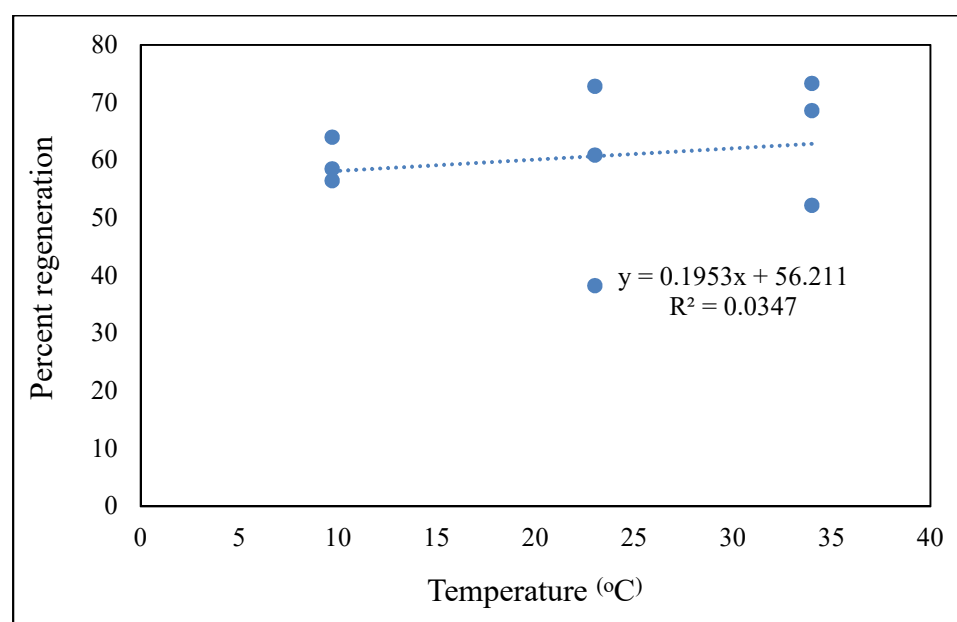


Figure 4-17: Regeneration rates for various temperature level using single-pass method.

4.2.6 Effect of flow rate on regeneration using single-pass method

Four different flow rates were observed to study the effect on regeneration percentages. In these experiments, 0.6 Voltage was applied for 3 secs and room temperature was maintained. Each flow rate related experiments were repeated 3 times. The average regeneration rate, standard deviation, and 95% confidence intervals are shown in Table 4.11 and Figure 4-18. Detailed data for all the runs are shown in Appendix A32.

Table 4.11: Regeneration percentages for various flow rates using single-pass method.

| Flow Rate (mL/min) | Average Regeneration (%) | Standard Deviation | 95% Confidence Interval Lower – Upper |
|--------------------|--------------------------|--------------------|--|
| 12 | 71 | 6 | 55 - 87 |
| 18 | 40 | 2 | 34 - 46 |
| 24 | 39 | 8 | 19 - 59 |
| 30 | 43 | 13 | 11 - 75 |

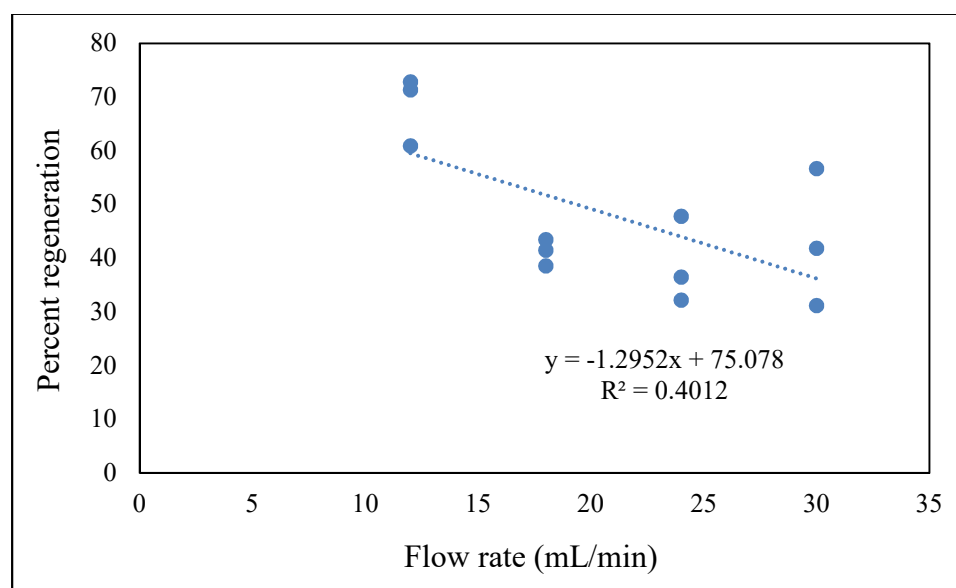


Figure 4-18: Regeneration rates for various flow rates using single-pass method.

A significance test done on the slope of linear regression shown in Figure 4-18 indicates that a significant correlation exists between flow rate and percent regeneration (details of the calculations are shown in Appendix A33). While R^2 value is not significant as observed regeneration rate is high for low flow rate of 12 mL/min, there is no observable difference in the percent regenerations for other flow rates presented in Figure 4-18. In future studies, it is recommended to observe the salt removal behavior at very low flow rates (around 2-10 mL/min) and at very high flow rates (such as 50, 100, 150 mL/min, etc.) in order to record any definitive trend.

The focus of the overall study was to study the adsorption behavior of CDI electrodes. The plan of this experiment was designed to optimize the time and number of adsorption experiments. After each adsorption experiment, CDI electrodes were regenerated following multiple wash cycles and the CDI cells were made ready for the next adsorption experiment. The opportunity to study desorption behavior existed during these wash cycles but the ideal conditions were not met because starting salt concentrations for desorption experiments were not same simply because different conditions were applied for adsorption experiments to accommodate the primary focus of the research. This is one possible reason for not having an observable trend in any of the desorption experiments (multi-pass and single-pass experiments). In future studies, all the preceding adsorptions should be done under same operating conditions to achieve a similar conductivity drop, i.e., similar salt amount present on electrodes. This may lead to a set of meaningful data.

CHAPTER 5

SURFACE MODIFICATION AND SALT REMOVAL

BEHAVIOR OF CDI ELECTRODES

Discussion in this chapter is focused on salt removal behavior of CDI electrodes used in this study after two types of surface modification processes – (I) surface treatment with nitric acid, and (II) deposition of gold. Post-modification characteristics of the electrode material are also discussed. All electrode materials were pretreated with acetone to ensure removal of impurities as discussed in chapter 4 before they went through any CDI experiments or surface modification process. The electrodes without any acid treatment or gold deposition are referred as untreated despite being pre-washed with acetone. Chapter specific methodology is discussed before going deeper into the discussion of material characteristics and salt removal behavior.

5.1 Results and discussion: nitric acid treatment

The SEM images of electrodes with and without acid treatment were captured with Hitachi S-4800 following standard protocol and are presented in Figure 5-1. The images obtained look similar with no notable changes upon visual comparison. However, when several pore openings were measured as shown in Figure 5-1, there seems to be some difference in pore openings post acid treatment. Generally, however, pore openings seemed to be in the similar range for both untreated and treated surfaces.

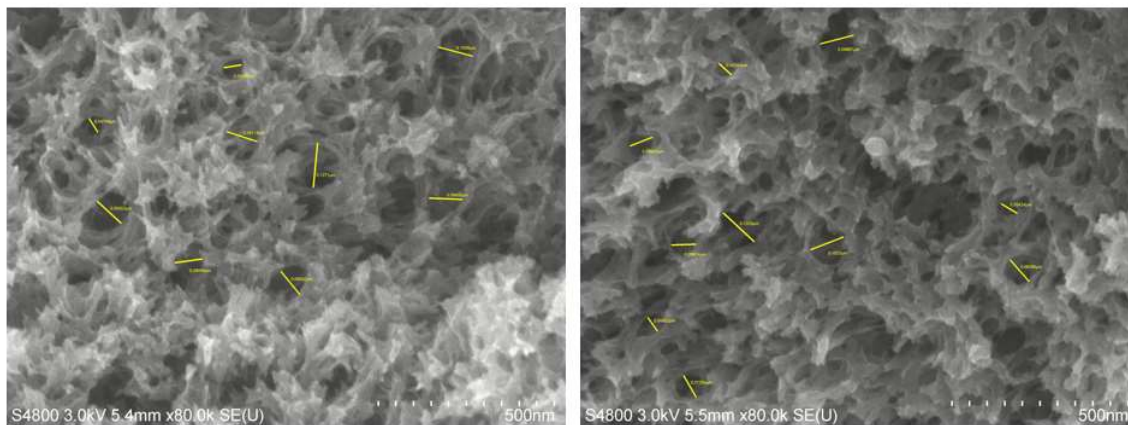


Figure 5-1: SEM image of electrodes before (left) and after (right) nitric acid treatment.

Surface profiles of both types of electrodes (with and without acid treatment) were also observed using 3D laser microscopic optical images as presented in Figure 5-2. A surface area analysis on the obtained profile gave the extent of increase in surface area per area due to the presence of cracks, pores, and other surface morphology features. An area of 0.0723 cm^2 of electrodes without acid treatment was scanned and the resulting surface area after the analysis was calculated to be 0.1068 cm^2 . It is 1.47 times greater than the flat area scanned. In case of electrodes with acid treatment when the same size area was scanned, the resulting surface area after the analysis was calculated to be 0.1029 cm^2 , which is 1.42 times greater than the flat area scanned. The numbers remained almost the same even when different locations and different sizes of areas were scanned. It is evident that there was a slight decrease in the surface area of electrodes after acid treatment, possibly due to change in chemical composition. This chemical change is also observed by Fourier-Transform Infrared Spectroscopy (FTIR) results shown in Figure 5-3.

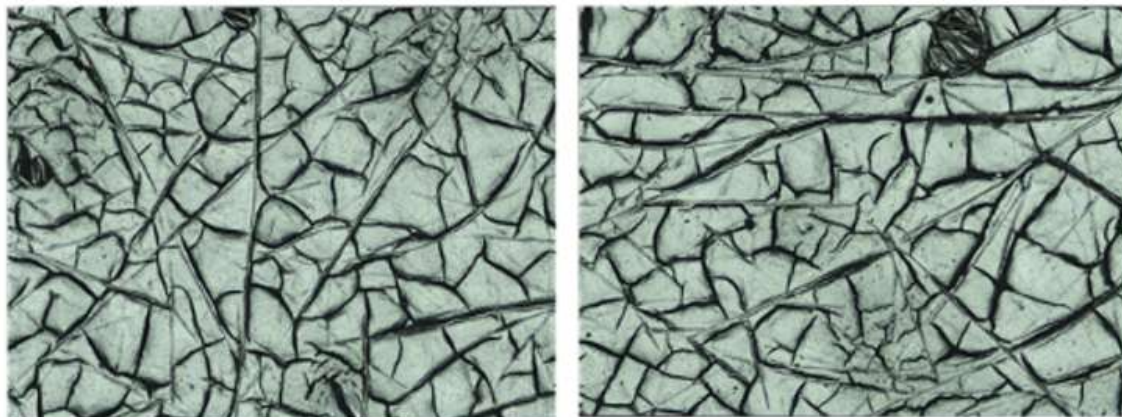


Figure 5-2: Surface profile by 3D laser confocal microscope – untreated electrode (left) and electrode after nitric acid treatment (right).

From FTIR spectra it is evident that a peak at around 3200 cm^{-1} , corresponding to O-H bond, disappeared after nitric acid treatment. New peaks associated with C-H bond were observed at around $2700\text{-}2800\text{ cm}^{-1}$ in FTIR spectra of acid-treated electrodes.

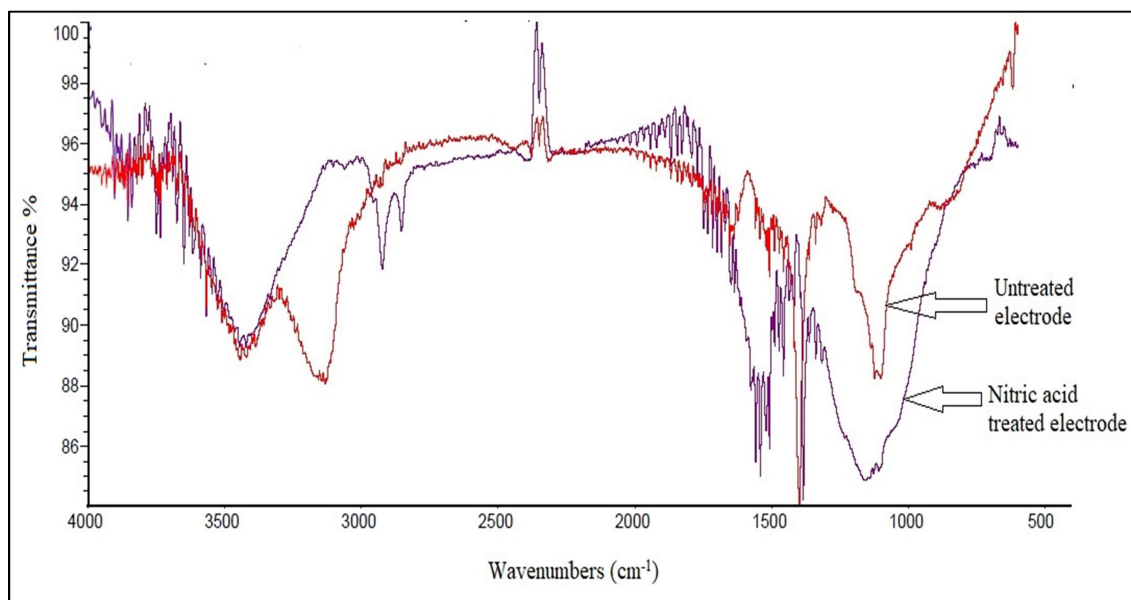


Figure 5-3: FTIR spectra of electrodes before and after nitric acid treatment.

Nitrogen gas adsorption data obtained from BET surface area and porosity analyzer NOVA2200e are presented in Table 5.1.

Table 5.1: Results from N₂ gas adsorption- desorption.

| Type | Observed parameters | | |
|-------------------------------|--|-------------------------------------|-----------------------|
| | Specific surface area (m ² /g) | Pore Volume (cm ³ /g) | Pore diameter (nm) |
| Untreated electrode | 39.5 | 0.274 | 3.6 |
| Nitric acid treated electrode | 24.5 | 0.170 | 3.3 |

A decrease in the value of observed parameters occurred after acid treatment of electrodes. The BET surface area of electrodes without acid treatment was 39.5 m²/g. When the same electrode was treated with nitric acid, the BET surface area was found to be 24.5 m²/g. The Barrett-Joyner-Halenda (BJH) pore volume and average pore diameter also decreased after acid treatment.

The cyclic voltammogram of untreated and (nitric) acid-treated electrodes along with their corresponding specific capacitance values under the applied conditions (as described in Materials and Methods) are shown in Figure 5-4 and Figure 5-5. There is a decrease in peak current for acid-treated electrodes as compared to the electrode with no acid treatment. The corresponding specific capacitance is also lower for acid treated electrodes, which supports the lower electrosorption performance (presented later) of nitric acid-treated electrodes for different configurations of CDI operations. Detailed calculations of specific capacitance are shown in Appendix A34.

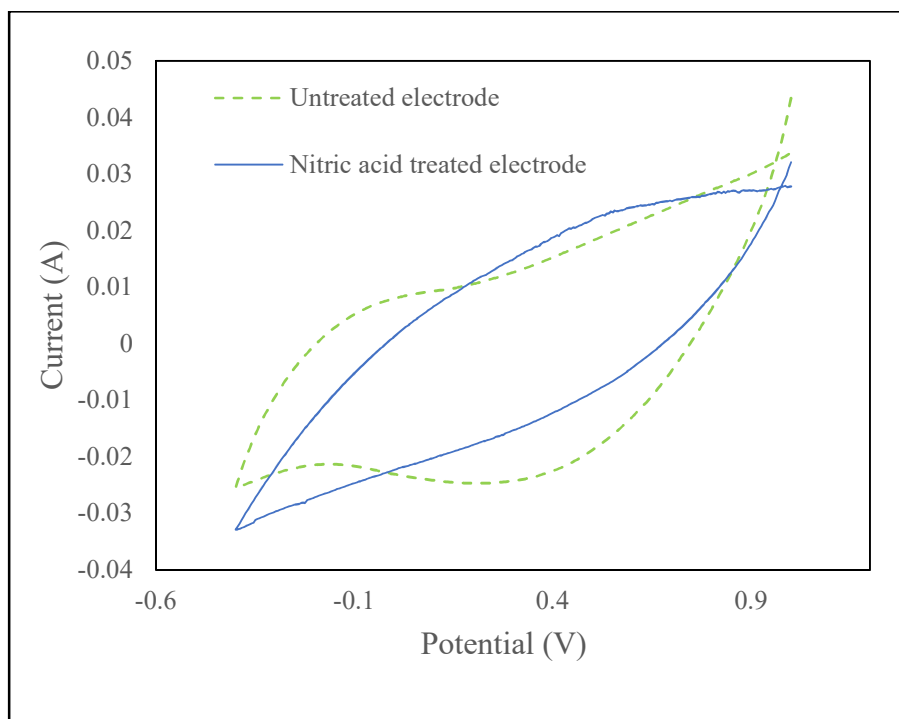


Figure 5-4: Cyclic voltammogram of electrodes before and after nitric acid treatment.

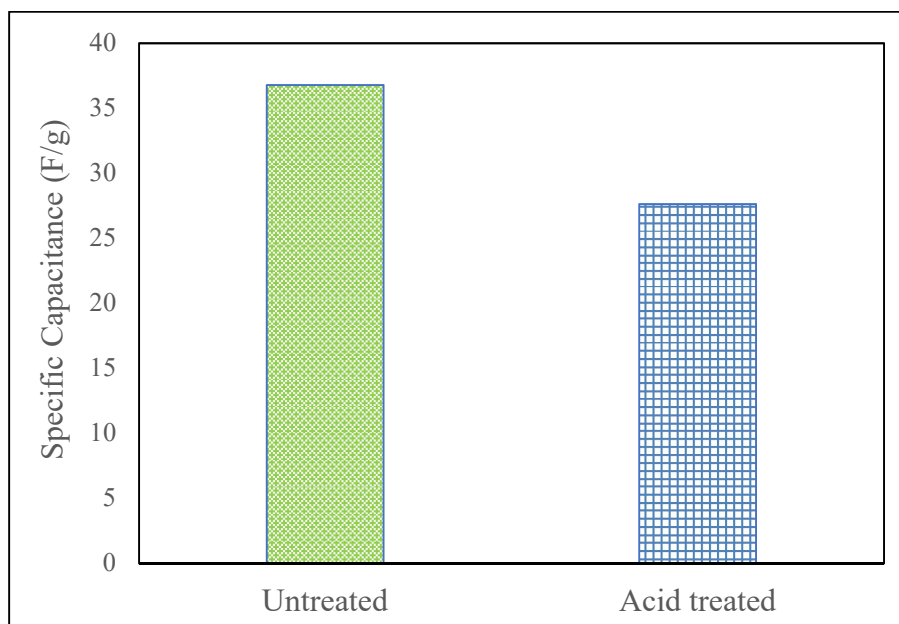


Figure 5-5: Specific capacitance (F/g) for electrodes before and after acid treatment.

Multiple replicated experiments were conducted to compare the salt removal capacities of four different combinations of electrodes in CDI cells. These CDI cells were prepared in following combinations:

1. both electrodes untreated (symmetric)
2. both electrodes acid treated (symmetric)
3. nitric acid-treated electrode as cathode and untreated electrode as anode
4. nitric acid-treated electrode as anode and untreated electrode as cathode

The data from a series of experiments conducted to measure the effect of variation in applied voltage at 1 V presented in section 4.1.1 showed that the salt removal capacity of untreated electrodes was 3.47 mg/g. One data set for change in conductivity and pH with time from CDI cells with each of the above listed combinations of electrodes is presented in Figure 5-6. Results from one run in combination 2, 3 and 4 are presented in Figure 5-7, Figure 5-8 and Figure 5-9. The remaining runs are shown in Appendices B17-B19.

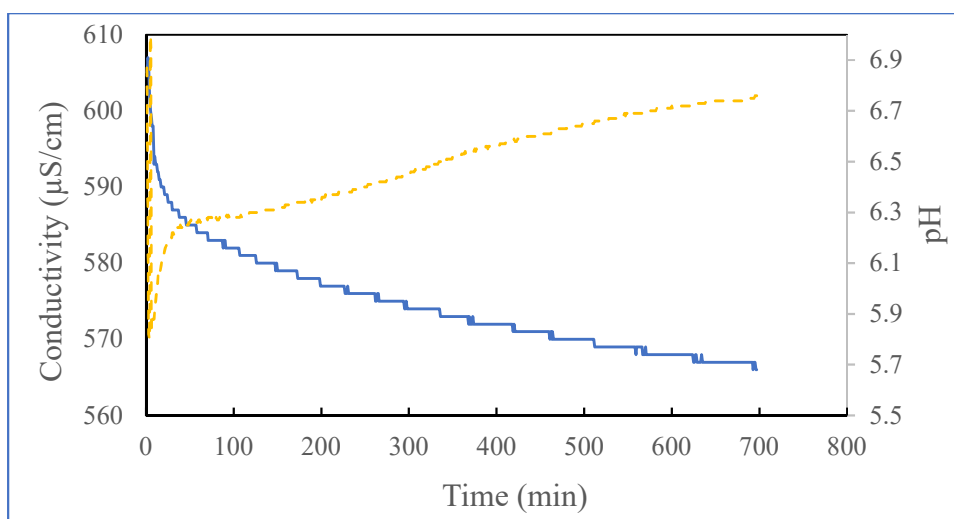


Figure 5-6: Conductivity and pH change with time for symmetric untreated electrodes.

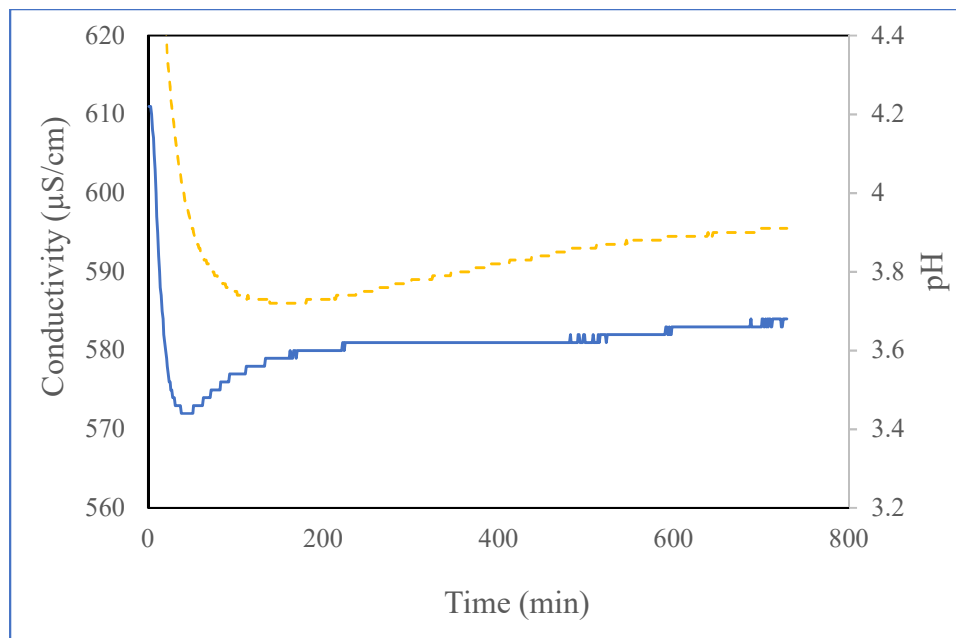


Figure 5-7: Conductivity and pH change with time for symmetric acid-treated electrodes.

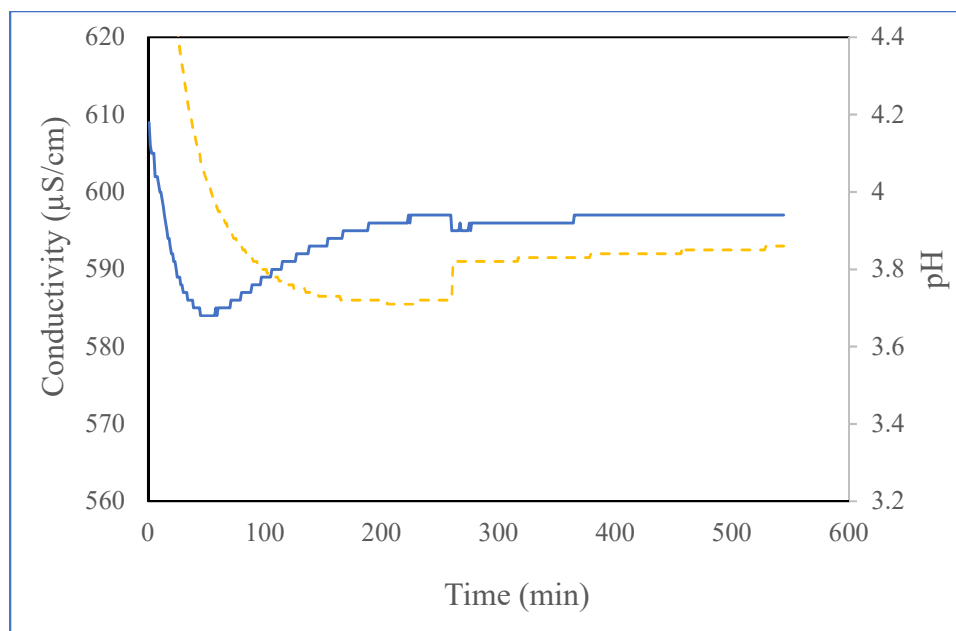


Figure 5-8: Conductivity and pH change with time for nitric acid-treated electrode as cathode and untreated electrode as anode.

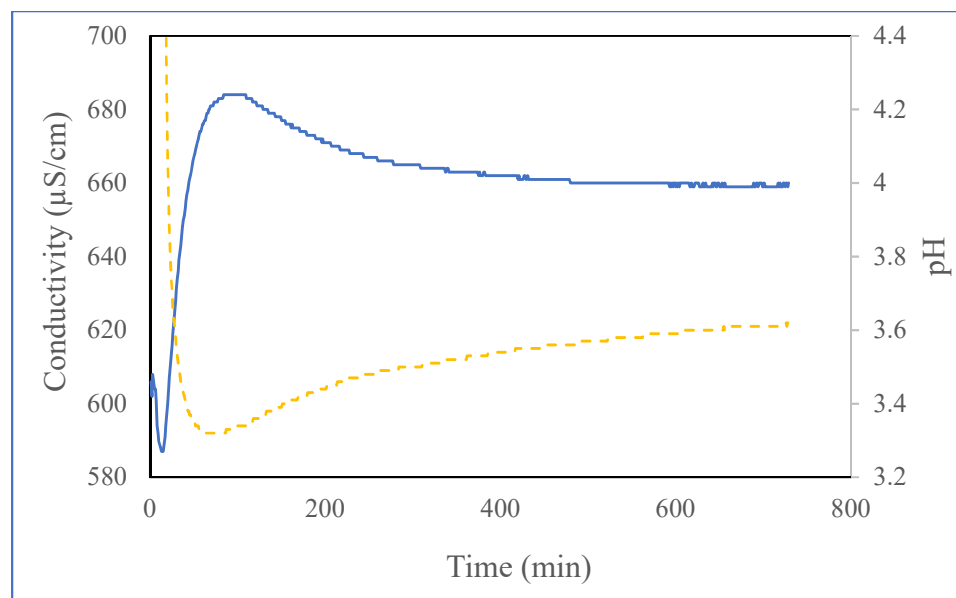


Figure 5-9: Conductivity and pH change with time for nitric acid-treated electrode as anode and untreated electrode as cathode.

When both electrodes were acid-treated and used as opposite electrodes in a CDI cell (symmetrical configuration), the average salt removal capacity achieved was 2.23 mg/g, a decrease of about 36% with respect to symmetric untreated electrodes used as opposite electrodes. In the case of nitric acid-treated electrode used as cathode and untreated electrode as anode configuration, also called asymmetrical configuration, the average salt removal capacity was 1.37 mg/g. In this specific configuration, the pH value of the solution dropped significantly during experiments. The measured conductivity values may have not truly represented the salt concentration in the solution because of an increased H^+ concentration. Therefore, it is not possible to definitively conclude that how much of the final conductivity data occurred solely because of Na^+ and Cl^- ions and how much was because of H^+ ions. In case of nitric acid-treated electrode as anode and untreated electrode as cathode the final conductivity went much higher than the initial

value, suggesting that desorption was taking place instead of adsorption, which was not desirable. In this case, the high increase in concentration of H^+ ions resulted in a measurement of too much conductivity. In future studies, quantification of individual ions is needed to observe the actual adsorption capacity of the electrodes and generation rate of H^+ ions.

5.2 Results and discussion: gold deposition on electrodes

The SEM images taken with the Hitachi S-4800 are presented in Figure 5-10. These images reveal that gold is uniformly deposited over the surface of the electrodes. The quality of SEM images was much better for gold-deposited electrodes due to possible conductivity improvement, which facilitated electron beam scattering. Pore openings seemed to be in the range of 60-100 nanometers for electrodes without gold deposition and between 25-70 nanometer for electrodes with gold deposition.

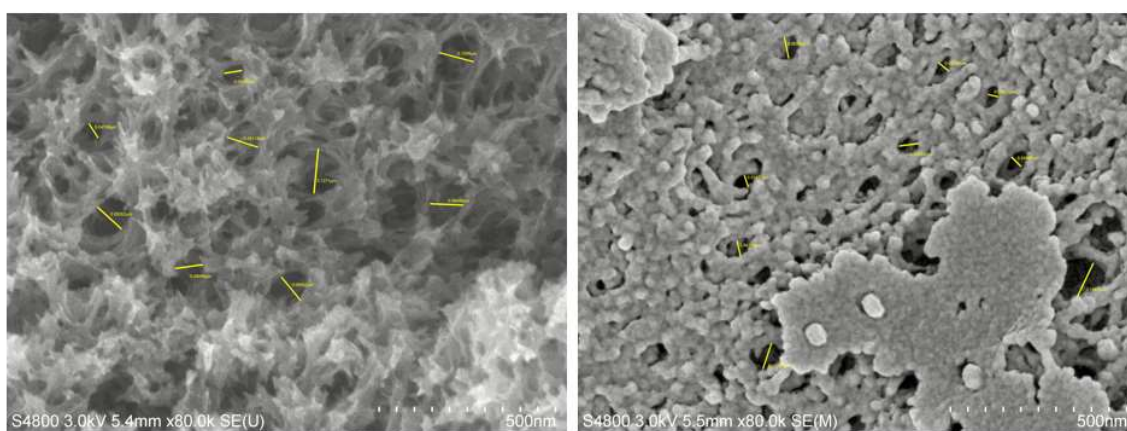


Figure 5-10: SEM images of electrode without (left) and with (right) gold deposition.

In addition to SEM images, the surface profiles of both electrodes were also observed using 3D laser microscopic optical images, as presented in Figure 5-11.

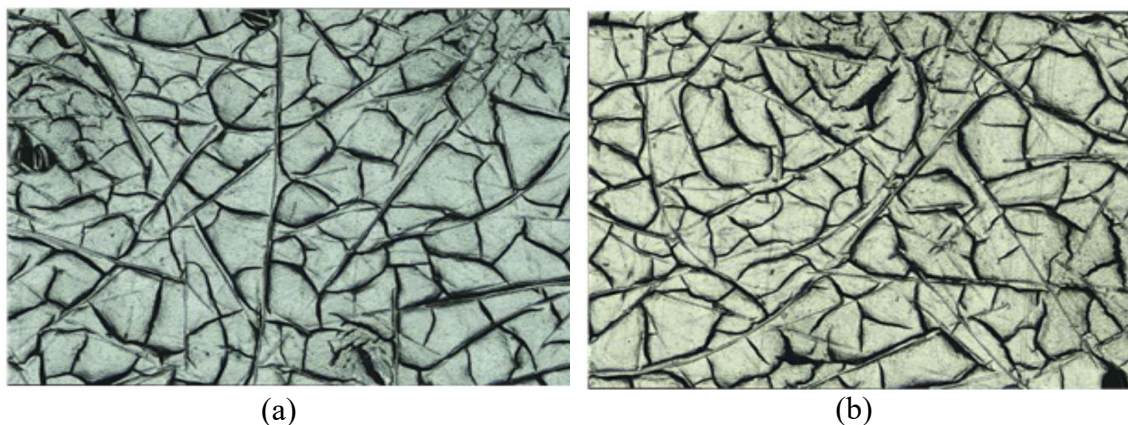


Figure 5-11: Surface profile by 3D laser confocal microscope (a) Electrode without deposition (b) Electrode with gold deposition.

The change of color in optical images depicts the uniform deposition of gold layer throughout the exposed surface. A surface area analysis on the obtained profile gave the extent of increase in surface area per area due to presence of cracks, depths of deposited layers, pores, and other surface morphology features. For unmodified electrodes, an area of 0.0723 cm^2 was scanned and the resulting surface area after the analysis was 0.1068 cm^2 . It is 1.47-fold increase compared to scanned flat area. In case of the gold-deposited electrode, it was observed that for the same scanned area the resulting surface area after analysis was 0.1002 cm^2 , a 1.38-fold increase compared to the scanned flat area. From observed numbers, it is evident that the surface area has decreased for gold-deposited electrodes, possibly due to filling up of some cracks and pores with the gold layer. The decrease in the surface area was also observed while analyzing N_2 gas adsorption data from NOVA2200e surface area and porosity analyzer as presented in Table 5.2.

Table 5.2: Results from N₂ gas adsorption-desorption.

| Type | Observed parameters | | |
|--------------------------------|--|-------------------------------------|-----------------------|
| | Specific Surface Area (m ² /g) | Pore Volume (cm ³ /g) | Pore Diameter (nm) |
| Electrode without deposition | 39.5 | 0.274 | 3.6 |
| Electrode with gold deposition | 29.1 | 0.222 | 3.6 |

The BET surface area was observed to be 29.1 m²/g for the gold-deposited electrode, which was lower than 39.5 m²/g, observed surface area for the electrode with no deposition. The BJH pore volume also decreased while average pore diameter remained same. The performance of the CDI cells with gold-deposited electrodes (symmetric as well as asymmetric) showed better salt removal despite having lower BET surface areas and lower pore volumes. The presence of a conductive gold layer may have helped in increasing current for the same applied voltage, as observed in a Cyclic Voltammetry (CV) test. This increase might possibly result in higher adsorption capacity.

Cyclic voltammetry has been an indispensable tool for evaluating adsorption-desorption performance in CDI operations. Cyclic voltammogram of with/without gold-deposited electrodes and their corresponding specific capacitance values under the applied conditions are shown in Figure 5-12a. As peak current increases, it is evident that gold-deposited electrodes have a higher electrosorption performance than the electrode without any deposition. This better performance can be attributed to the improvement of conductivity in the composite electrode. Specific capacitance measured from CV analysis also shows that specific capacitance value is higher for gold-deposited electrodes, as illustrated in Figure 5-12b.

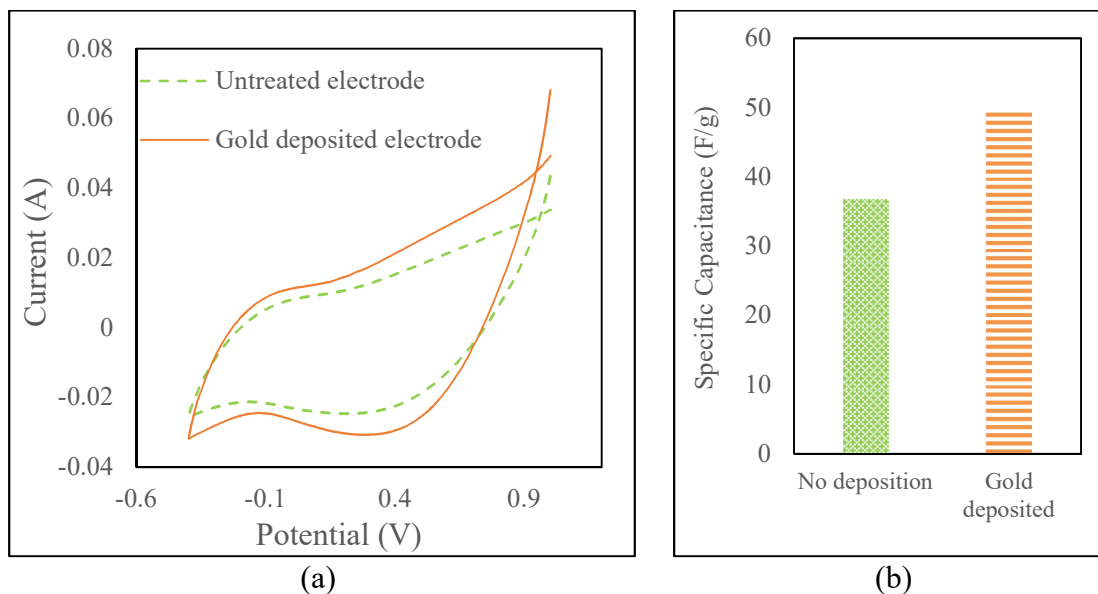


Figure 5-12: (a) Cyclic voltammogram of electrodes before and after gold deposition (b) Specific capacitance (F/g) for electrodes before and after gold deposition.

Conductivity values were recorded in CDI tests every minute using a dedicated conductivity probe. Five sets of experiments were conducted for every configuration of electrodes. Figure 5-13 presents one set of data from each configuration.

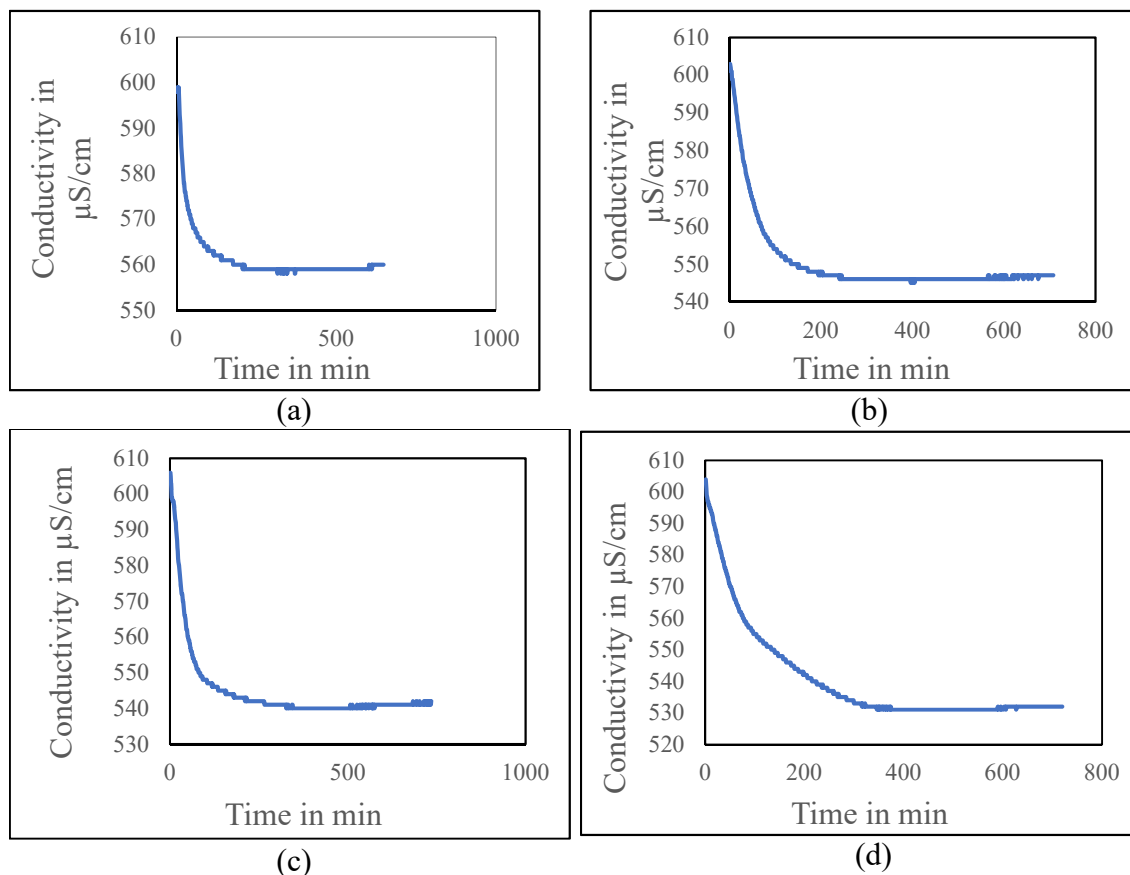


Figure 5-13: Conductivity drop with time in configuration where (a) both electrodes are unmodified (without gold deposition), (b) both electrodes are modified (gold-deposited), (c) gold-treated electrode is cathode and no gold-deposited one is anode (d) gold-treated electrode is anode and no gold-deposited one is cathode.

The salt removal capacities of each configuration from each set of experiments are shown in Table 5.3. The capacity was little lower (average value of 6.50 mg/g) when a gold treated electrode was connected to the negative end of the DC voltage source as compared to when a gold deposited electrode was connected to the positive end of the DC voltage source (average value of 7.61 mg/g). The results indicate that the gold-deposited electrode may have favored chloride ions and slightly repelled sodium ions. The reason behind such behavior can be attributed to modification in electrochemical

characteristics of gold deposited electrodes when they are subject to opposite applied potentials.

Table 5.3: Salt removal capacities by different electrodes.

| Type | Configuration | Data Set | Salt Removed per mass of electrode (mg/g) | Average Salt Removal Capacity (mg/g) | Standard Deviation | 95% Confidence interval | |
|------------|---|----------|---|--------------------------------------|--------------------|-------------------------|-------|
| | | | | | | Lower- | Upper |
| Symmetric | Electrode without deposition as anode and cathode | Set 1 | 4.37 | 3.90 | 0.32 | 3.50 | 4.30 |
| | | Set 2 | 3.98 | | | | |
| | | Set 3 | 3.78 | | | | |
| | | Set 4 | 3.88 | | | | |
| | | Set 5 | 3.48 | | | | |
| | Gold deposited electrode as anode and cathode | Set 1 | 5.15 | 5.09 | 0.48 | 4.50 | 5.68 |
| | | Set 2 | 4.84 | | | | |
| | | Set 3 | 4.95 | | | | |
| | | Set 4 | 5.88 | | | | |
| | | Set 5 | 4.64 | | | | |
| Asymmetric | Gold deposited electrode as cathode and electrode without deposition as anode | Set 1 | 6.07 | 6.50 | 0.25 | 6.18 | 6.81 |
| | | Set 2 | 6.48 | | | | |
| | | Set 3 | 6.68 | | | | |
| | | Set 4 | 6.68 | | | | |
| | | Set 5 | 6.58 | | | | |
| | Gold deposited electrode as anode and electrode without deposition as cathode | Set 1 | 8 | 7.61 | 0.25 | 7.30 | 7.93 |
| | | Set 2 | 7.59 | | | | |
| | | Set 3 | 7.69 | | | | |
| | | Set 4 | 7.39 | | | | |
| | | Set 5 | 7.39 | | | | |

Salt removal capacity increases after electrodes are treated with gold. In the configuration where both electrodes are same (no gold deposit) the average capacity was 3.47 mg/g. When both electrodes are gold deposited, the average capacity went up to 5.09 mg/g. The removal capacity went up when asymmetric configurations were used. The

highest capacity achieved was 8.00 mg/g, where a gold deposited electrode was connected to the positive end of the DC voltage supplier and functioned as an anode.

The results of these experiments indicated that removal of NaCl increased when gold deposited electrodes were incorporated into the CDI system. The average capacity increased from 3.47 mg/g (in case of symmetric set up with no deposition) to 5.09 mg/g (symmetric set up with gold deposited electrodes). Asymmetric configurations showed even higher removal capacity. Average capacities were 6.50 mg/g and 7.61 mg/g in cases where gold deposited electrodes were used as cathodes and anodes respectively with the opposite electrode being an unmodified electrode (without gold deposition). The higher capacity of gold deposited electrodes can be attributed to increased conductivity and capacitance. SEM images confirmed a uniform deposition of gold layer throughout the surface. Cyclic voltammetry showed that peak current was higher for gold deposited electrodes and specific capacitance was also higher compared to electrodes without deposition. Even though BET surface area was decreased after gold deposition, the electrodes still performed better, possibly because of increased electrical conductivity of the gold deposited electrodes which is a couple of orders higher than carbon-based electrodes. The higher exchange current density of gold could contribute to this high salt removal capacity. Exchange current density occurs when oxidation and reduction rate are at equilibrium condition between an electrode surface and an electrolyte [88]. The exchange current density of gold in acidic solutions was found to be about 10^{-5} A/cm² [88]. In one study [89] the exchange current densities of graphite and carbon felt electrodes in acidic solutions were found to be around 10^{-8} and 1.9×10^{-6} A/cm², which are lower than the corresponding exchange current density of gold. Gold deposited anode configurations

showed higher removal capacity. A greater affinity of modified electrodes towards chloride ions when used as anode could explain this increased adsorption capacity. However, no ion specific concentration measurement was performed to verify it in this study. Further investigation is required to assess this affinity. Additional investigation is also required to assess the relationship between the thickness of deposited layers and overall salt removal capacities of electrodes.

CHAPTER 6

CONCLUSION AND RECOMMENDATIONS

6.1 Conclusions

The following the results and discussion as presented previously in the conclusion of this study are summarized below:

- The variation in applied voltages across CDI electrodes directly influences the adsorption capacity of CDI electrodes. The average capacity at 1.2 V (4.15 mg/g) was 65% higher than at 0.6 V (2.52 mg/g). However, higher potential (more than activation potential of participating ions) may lead to unwanted reactions, which can affect electrode materials and further contaminate water instead of treating it.
- Higher temperature increases the salt removal capacity of CDI cells. Adsorption capacity at the higher temperature of $34 \pm 1.21^\circ\text{C}$ was found to be 4.29 mg/g. This was 43% higher than capacity of 3.00 mg/g at $9.7 \pm 1.24^\circ\text{C}$ and 24% higher than capacity of 3.47 mg/g at $23 \pm 0.43^\circ\text{C}$, respectively.
- For the same configuration of CDI cells, salt removal capacities did not show a definitive trend in terms of change in flow rates. The range of flow used in this study was 12 to 30 mL/min. A wider range such as – 2 to 100 mL/min is recommended for exploration in future studies.

- Salt removal capacity increased with an increase in initial concentration of solution as more and more ions were available to strengthen the diffusion process. Capacity with initial solution concentration of 400 mg/L (3.66 mg/g) was 45% higher than capacity with initial solution concentration of 100 mg/L (2.52 mg/g).
- The highest adsorption capacity achieved by varying operating conditions was 4.61 mg/g at 34°C temperature with 300 mg/L initial concentration, 12 mL/min flow rate, and 1 V applied voltage.
- Isotherm studies based on data obtained by varying operating parameters indicated that the adsorption process in CDI fitted well with Langmuir Isotherm. This indicates that a monolayer adsorption has taken place on the electrode surface.
- Desorption studies did not provide good correlation between regeneration and the different applied conditions examined in this study.
- Acid treatment decreased the BET surface area of electrodes. A confocal microscopy analysis also confirmed the reduction in surface area after nitric acid treatment. The reduction was found to be about 38% (24.5 m²/g for treated electrodes as compared to 39.5 m²/g for untreated electrodes). Specific capacitance of the materials also decreased after treatment with nitric acid. Surface properties of nitric acid-treated electrodes were different than that of untreated.
- An FTIR spectra confirmed that O-H bond disappeared and C-H bond evolved after nitric acid treatment. Therefore, some chemical change happened in the electrode materials before and after this treatment.

- Salt treatment of CDI electrodes leads to lower salt removal capacities. In this study, acid treatment resulted in a 36% decrease of salt removal capacity. When both electrodes were untreated, the removal capacity was 3.47 mg/g, but when both electrodes were treated with nitric acid, the capacity was 2.23 mg/g. Since the concentration measurements were based on the conductivity of the solution and the H^+ concentration increased significantly during these experiments, concentrations clearly would have affected conductivity values. This means the true salt removal capacity may not have been achieved.
- Asymmetric configuration with a nitric acid-treated electrode as cathode showed very low removal capacity (1.37 mg/g). Again, the resulting solution had an acidic pH level, which indicates that the process was dominated by H^+ ion production. So true salt removal capacity was not achieved.
- Asymmetric configuration with a nitric acid-treated electrode as anode showed higher final conductivity of the solution than initial conductivity. Also, like other acid related tests, the resulting solution had an acidic pH level, which indicates that the process was dominated by H^+ ion production. In this case, salt removal capacity could not be determined at all.
- BET surface area of electrodes decreased upon gold deposition treatment (29.1 m^2/g) compared to untreated electrodes 39.5 m^2/g), and SEM image analysis confirmed that average pore opening decreased on gold treated surfaces. In symmetric CDI configuration of gold-treated electrodes, the average salt removal capacity increased to 5.09 mg/g when compared to 3.47 mg/g when both electrodes were untreated. This

is a increase of a little more than 46%. Therefore, salt removal capacity increases in CDI systems when gold-deposited electrodes are used.

- Salt removal capacity of CDI cells farther increased to an average of 6.50 mg/g (about 28%) and 7.61 mg/g (about 50%) when gold-treated electrodes were used as cathode or anode in asymmetric CDI configurations with untreated opposite electrodes.
- Highest removal capacity achieved in this study was 8.00 mg/g with gold deposited electrodes as anode and untreated electrode as cathode configuration. As the configuration where a gold-treated electrode was used as an anode shows highest removal capacity, it suggests that gold deposition favors Chlorine ions removal over Sodium ion removal. Further investigation is required to reach a definitive conclusion.

6.2 Recommendations

The results described in this dissertation provide an insight into the salt removal behavior of one specific type of carbon-based electrodes in capacitive deionization. The conclusions presented here help in gaining a deeper understanding of CDI desalination. At the same time, the study also identified issues that need to be investigated further. Specific recommendations for future research are as follows:

- Further investigations are required to establish the effect of flow rate within in a CDI cell on salt removal capacity. A wider range of flowrate, possibly ranging from 2 mL/min to 100 mL/min depending the CDI cell, should be investigated.

- Experiments with nitric acid-treated electrodes should be conducted with ion specific analysis for better understanding the adsorption behavior of CDI electrodes. This may lead to better quantification of salt removed and the specific contribution of the H^+ in conductivity-based CDI adsorption experiments.
- Since acid treatment in this study was conducted with only one specific concentration, the effect of variation of acid strength on salt removal capacity should be explored to determine the specific strength of acid needed for optimized salt removal ability.
- Experiments with gold-deposited electrodes should be conducted with ion specific analysis to quantify individual amounts of Na^+ and Cl^- ions that have been removed by CDI electrodes and to discover if there is a true affinity between Cl^- ions and gold-deposited electrodes.
- Different amounts and thicknesses of gold layers can be deposited on the electrodes to further investigate their effect on salt removal capacity.
- Solutions with competing ion types should be investigated to better understand adsorption of these ions on acid-treated electrodes as well as gold-deposited electrodes.
- Some of the operating parameters not investigated in this study, such as ionic size of contaminants, separation distance of electrodes, etc., can be explored for their effect on salt removal capacity in CDI process.
- The combined effect of varying two or more variables at the same time also needs to be explored.

APPENDIX A

A1: Peristaltic pump calibration

| Dial Position | | 0 | |
|-------------------|--------------------|------------------|--------------------|
| Fluid used | | Deionized water | |
| Volume Range (mL) | Volume Filled (mL) | Time taken (min) | Flow rate (mL/min) |
| 50-100 | 50 | 4.067 | 12.29 |
| 100-150 | 50 | 3.833 | 13.04 |
| 150-200 | 50 | 4.1 | 12.20 |
| 200-250 | 50 | 4.067 | 12.29 |
| 250-300 | 50 | 4 | 12.50 |
| Average | | | 12.47 |

| Dial Position | | 1 | |
|-------------------|--------------------|------------------|--------------------|
| Fluid used | | Deionized water | |
| Volume Range (mL) | Volume Filled (mL) | Time taken (min) | Flow rate (mL/min) |
| 50-100 | 50 | 3.858 | 12.96 |
| 100-150 | 50 | 3.723 | 13.43 |
| 150-200 | 50 | 3.663 | 13.65 |
| 200-250 | 50 | 3.859 | 12.96 |
| 250-300 | 50 | 3.902 | 12.81 |
| Average | | | 13.16 |

| Dial Position | | 2 | |
|-------------------|--------------------|------------------|--------------------|
| Fluid Used | | Deionized water | |
| Volume Range (mL) | Volume Filled (mL) | Time taken (min) | Flow rate (mL/min) |
| 50-100 | 50 | 3.159 | 15.83 |
| 100-150 | 50 | 3.085 | 16.21 |
| 150-200 | 50 | 2.963 | 16.87 |
| 200-250 | 50 | 3.179 | 15.73 |
| 250-300 | 50 | 3.155 | 15.85 |
| Average | | | 16.10 |

| Dial Position | | 3 | |
|-------------------|--------------------|------------------|--------------------|
| Fluid used | | Deionized water | |
| Volume Range (mL) | Volume Filled (mL) | Time taken (min) | Flow rate (mL/min) |
| 50-100 | 50 | 2.854 | 17.52 |
| 100-150 | 50 | 2.739 | 18.25 |
| 150-200 | 50 | 2.838 | 17.62 |
| 200-250 | 50 | 2.555 | 19.57 |
| 250-300 | 50 | 2.77 | 18.05 |
| Average | | | 18.20 |

A1: Continues...

| Dial Position | | 4 | |
|-------------------|--------------------|------------------|--------------------|
| Fluid Used | | Deionized water | |
| Volume Range (mL) | Volume Filled (mL) | Time taken (min) | Flow rate (mL/min) |
| 50-100 | 50 | 2.517 | 19.86 |
| 100-150 | 50 | 2.387 | 20.95 |
| 150-200 | 50 | 2.542 | 19.67 |
| 200-250 | 50 | 2.235 | 22.37 |
| 250-300 | 50 | 2.438 | 20.51 |
| Average | | | 20.67 |

| Dial Position | | 5 | |
|-------------------|--------------------|------------------|--------------------|
| Fluid Used | | Deionized water | |
| Volume Range (mL) | Volume Filled (mL) | Time taken (min) | Flow rate (mL/min) |
| 50-100 | 50 | 2.121 | 23.57 |
| 100-150 | 50 | 2.195 | 22.78 |
| 150-200 | 50 | 2.158 | 23.17 |
| 200-250 | 50 | 2.198 | 22.75 |
| 250-300 | 50 | 2.109 | 23.71 |
| Average | | | 23.20 |

| Dial Position | | 6 | |
|-------------------|--------------------|------------------|--------------------|
| Fluid Used | | Deionized water | |
| Volume Range (mL) | Volume Filled (mL) | Time taken (min) | Flow rate (mL/min) |
| 50-100 | 50 | 2.01 | 24.88 |
| 100-150 | 50 | 2.079 | 24.05 |
| 150-200 | 50 | 2.043 | 24.47 |
| 200-250 | 50 | 2.147 | 23.29 |
| 250-300 | 50 | 1.97 | 25.38 |
| Average | | | 24.41 |

| Dial Position | | 7 | |
|-------------------|--------------------|------------------|--------------------|
| Fluid Used | | Deionized water | |
| Volume Range (mL) | Volume Filled (mL) | Time taken (min) | Flow rate (mL/min) |
| 50-100 | 50 | 1.946 | 25.69 |
| 100-150 | 50 | 1.818 | 27.50 |
| 150-200 | 50 | 1.889 | 26.47 |
| 200-250 | 50 | 1.879 | 26.61 |
| 250-300 | 50 | 1.791 | 27.92 |
| Average | | | 26.84 |

A1: Continues...

| Dial Position | | 8 | |
|-------------------|--------------------|------------------|--------------------|
| Fluid Used | | Deionized water | |
| Volume Range (mL) | Volume Filled (mL) | Time taken (min) | Flow rate (mL/min) |
| 50-100 | 50 | 1.643 | 30.43 |
| 100-150 | 50 | 1.736 | 28.80 |
| 150-200 | 50 | 1.677 | 29.82 |
| 200-250 | 50 | 1.706 | 29.31 |
| 250-300 | 50 | 1.717 | 29.12 |
| Average | | | 29.50 |

| Dial Position | | 9 | |
|-------------------|--------------------|------------------|--------------------|
| Fluid Used | | Deionized water | |
| Volume Range (mL) | Volume Filled (mL) | Time taken (min) | Flow rate (mL/min) |
| 50-100 | 50 | 1.59 | 31.45 |
| 100-150 | 50 | 1.624 | 30.79 |
| 150-200 | 50 | 1.544 | 32.38 |
| 200-250 | 50 | 1.575 | 31.75 |
| 250-300 | 50 | 1.605 | 31.15 |
| Average | | | 31.50 |

| Dial Position | | 10 | |
|-------------------|--------------------|------------------|--------------------|
| Fluid Used | | Deionized water | |
| Volume Range (mL) | Volume Filled (mL) | Time taken (min) | Flow rate (mL/min) |
| 50-100 | 50 | 1.5 | 33.33 |
| 100-150 | 50 | 1.487 | 33.62 |
| 150-200 | 50 | 1.557 | 32.11 |
| 200-250 | 50 | 1.488 | 33.60 |
| 250-300 | 50 | 1.651 | 30.28 |
| Average | | | 32.59 |

A2: Salinity vs. conductivity calibration data for NaCl.

| Salinity (mg/L) | 500 | | 450 | | 320 | | 250 | | 140 | | 125 | |
|-----------------------------|-------|-----|-------|-----|-------|-----|------|-----|------|-----|------|-----|
| Conductivity ($\mu S/cm$) | 996 | 996 | 893 | 893 | 651 | 651 | 501 | 501 | 293 | 293 | 258 | 258 |
| | 996 | | 893 | | 651 | | 501 | | 293 | | 258 | |
| | 996 | | 892 | | 651 | | 501 | | 293 | | 258 | |
| | 984 | 984 | 925 | 925 | 658 | 658 | 506 | 506 | 302 | 301 | 268 | 268 |
| | 984 | | 925 | | 658 | | 506 | | 301 | | 268 | |
| | 984 | | 925 | | 658 | | 506 | | 301 | | 268 | |
| | 982 | 982 | 912 | 912 | 657 | 657 | 474 | 474 | 300 | 300 | 272 | 272 |
| | 982 | | 912 | | 657 | | 474 | | 300 | | 273 | |
| 982 | 912 | | 657 | | 474 | | 300 | | 272 | | | |
| Salinity (mg/L) | 80 | | 62.5 | | 45 | | 31 | | 16 | | 8 | |
| Conductivity ($\mu S/cm$) | 182.7 | 183 | 137.3 | 137 | 93.3 | 93 | 74.5 | 75 | 45.8 | 46 | 20.4 | 20 |
| | 182.7 | | 137.3 | | 93.3 | | 74.5 | | 45.9 | | 20.5 | |
| | 182.8 | | 137.3 | | 93.3 | | 74.5 | | 45.8 | | 20.5 | |
| | 152.6 | 153 | 129.7 | 130 | 108.7 | 109 | 77.6 | 78 | 42.4 | 42 | 24 | 24 |
| | 152.6 | | 129.7 | | 108.7 | | 77.7 | | 42.4 | | 24 | |
| | 152.7 | | 129.7 | | 108.8 | | 77.6 | | 42.5 | | 24 | |
| | 167.4 | 167 | 145.4 | 145 | 106.1 | 106 | 70.5 | 71 | 47 | 47 | 23.1 | 23 |
| | 167.4 | | 145.5 | | 106.2 | | 70.6 | | 47 | | 23.1 | |
| | 167.4 | | 145.5 | | 106.2 | | 70.6 | | 47.1 | | 23.7 | |

A3: Extended Table-4.1

| Applied Voltage (V) | Data Set | Initial Conductivity ($\mu\text{S/cm}$) | Equilibrium/ Lowest Conductivity ($\mu\text{S/cm}$) | Conductivity Drop ($\mu\text{S/cm}$) | Salt Removed per mass of electrode (mg/g) | Average Salt Removal Capacity (mg/g) | Standard Deviation | 95% Confidence interval limits | |
|---------------------|----------|---|---|--|---|--------------------------------------|--------------------|--------------------------------|-------|
| | | | | | | | | Lower | Upper |
| 0.6 | Set-1 | 600 | 560 | 40 | 2.25 | 2.52 | 0.19 | 2.28 | 2.76 |
| | Set-2 | 601 | 558 | 43 | 2.42 | | | | |
| | Set-3 | 606 | 557 | 49 | 2.75 | | | | |
| | Set-4 | 596 | 550 | 46 | 2.58 | | | | |
| | Set-5 | 599 | 553 | 46 | 2.58 | | | | |
| 0.8 | Set-1 | 604 | 554 | 50 | 2.81 | 3.02 | 0.16 | 2.83 | 3.22 |
| | Set-2 | 598 | 542 | 56 | 3.15 | | | | |
| | Set-3 | 596 | 543 | 53 | 2.98 | | | | |
| | Set-4 | 595 | 542 | 53 | 2.98 | | | | |
| | Set-5 | 601 | 544 | 57 | 3.20 | | | | |
| 1 | Set-1 | 594 | 534 | 60 | 3.37 | 3.47 | 0.23 | 3.18 | 3.76 |
| | Set-2 | 602 | 543 | 59 | 3.32 | | | | |
| | Set-3 | 600 | 542 | 58 | 3.26 | | | | |
| | Set-4 | 603 | 539 | 64 | 3.60 | | | | |
| | Set-5 | 596 | 528 | 68 | 3.82 | | | | |
| 1.2 | Set-1 | 601 | 527 | 74 | 4.16 | 4.15 | 0.11 | 4.01 | 4.28 |
| | Set-2 | 591 | 520 | 71 | 3.99 | | | | |
| | Set-3 | 596 | 520 | 76 | 4.27 | | | | |
| | Set-4 | 598 | 523 | 75 | 4.21 | | | | |
| | Set-5 | 598 | 525 | 73 | 4.10 | | | | |

A4: Test - mean comparison for 0.8 V and 1 V data

| Hypothesis | $H_0: \mu_1 = \mu_2; \Delta = 0$ $H_1: \mu_1 \neq \mu_2$ | Test statistics: |
|---|---|--|
| Given Data | | $t_o = \frac{\bar{x}_1 - \bar{x}_2 - \Delta}{\sqrt{\left(\frac{s_1^2}{n_1} + \frac{s_2^2}{n_1}\right)}}$ |
| n_1 | 5 | $= -3.59$ |
| n_2 | 5 | |
| \bar{x}_1 | 3.02 | Degrees of Freedom: |
| | | $v = \frac{\left(\frac{s_1^2}{n_1} + \frac{s_2^2}{n_2}\right)^2}{\frac{\left(\frac{s_1^2}{n_1}\right)^2}{n_1 - 1} + \frac{\left(\frac{s_2^2}{n_1}\right)^2}{n_2 - 1}}$ |
| \bar{x}_2 | 3.47 | $= 7.14 \approx 8$ |
| s_1 | 0.16 | $t_{\frac{\alpha}{2}, v} = t_{0.025, 8}$ |
| s_2 | 0.23 | $= 2.306$ (From standard t-table) |
| Reject criteria: $ t_o > t_{\frac{\alpha}{2}, v} \Rightarrow 3.59 > 2.306$ | | |

Comment: We reject null hypothesis and conclude that there is enough evidence that mean from the two conditions are different at 95% confidence level.

A5: Regressions analysis of varying voltage adsorption data:

| <i>Regression Statistics</i> | |
|------------------------------|------------|
| Multiple R | 0.96260605 |
| R Square | 0.9266104 |
| Adjusted R Square | 0.9225332 |
| Standard Error | 0.17704207 |
| Observations | 20 |

| ANOVA | | | | | |
|------------|-----------|-------------|------------|------------|-----------------------|
| | <i>df</i> | <i>SS</i> | <i>MS</i> | <i>F</i> | <i>Significance F</i> |
| Regression | 1 | 7.123412723 | 7.12341272 | 227.266368 | 1.1853E-11 |
| Residual | 18 | 0.564190074 | 0.03134389 | | |
| Total | 19 | 7.687602797 | | | |

| | <i>Coefficients</i> | <i>Standard Error</i> | <i>t Stat</i> | <i>P-value</i> | <i>Lower 95%</i> | <i>Upper 95%</i> |
|-----------------|---------------------|-----------------------|-------------------|----------------|------------------|------------------|
| Intercept | 0.88778444 | 0.164182057 | 5.40731709 | 3.8782E-05 | 0.54285074 | 1.23271815 |
| Applied voltage | 2.66897222 | 0.177042066 | 15.0753563 | 1.1853E-11 | 2.29702064 | 3.0409238 |

| | | | |
|-----------------------------|--------------|---------|-----------------------------|
| $t_{\frac{\alpha}{2}, n-2}$ | 2.101 | Comment | t-stat greater, significant |
|-----------------------------|--------------|---------|-----------------------------|

A6: Retention time and drift velocity related calculations

| Drift velocity analysis at different voltages for Na ions | | | | | | Drift velocity analysis at different voltages for Cl ions | | | | | |
|---|-------------------|-----------------|--------------------|--------------------------------|---|---|-------------------|-----------------|--------------------|--------------------------------|---|
| Flow rate | Flow velocity, Vy | Applied voltage | Drift Velocity, Vx | Retention time ,t _y | Time needed to get adsorbed ,t _x | Flow rate | Flow velocity, Vy | Applied voltage | Drift Velocity, Vx | Retention time ,t _y | Time needed to get adsorbed ,t _x |
| (mL/min) | (m/s) | (V) | (m/s) | (seconds) | (seconds) | (mL/min) | (m/s) | (V) | (m/s) | (seconds) | (seconds) |
| 12 | 0.000984 | 0.8 | 0.00002595 | 90.32 | 30.83 | 12 | 0.000984 | 0.8 | 0.0000396 | 90.32 | 20.20 |
| 12 | 0.000984 | 1 | 3.24375E-05 | 90.32 | 24.66 | 12 | 0.000984 | 1 | 0.0000495 | 90.32 | 16.16 |
| 12 | 0.000984 | 1.2 | 0.000038925 | 90.32 | 20.55 | 12 | 0.000984 | 1.2 | 0.0000594 | 90.32 | 13.47 |
| | | | | | | | | | | | |
| | | | | | | | | | | | |
| Drift velocity analysis at different flow rates for Na ions | | | | | | Drift velocity analysis at different flow rates for Cl ions | | | | | |
| Flow rate | Flow velocity, Vy | Applied voltage | Drift Velocity, Vx | Retention time ,t _y | Time needed to get adsorbed ,t _x | Flow rate | Flow velocity, Vy | Applied voltage | Drift Velocity, Vx | Retention time ,t _y | Time needed to get adsorbed ,t _x |
| (mL/min) | (m/s) | (V) | (m/s) | (seconds) | (seconds) | (mL/min) | (m/s) | (V) | (m/s) | (seconds) | (seconds) |
| 18 | 0.001476 | 1 | 3.24375E-05 | 60.21 | 24.66 | 18 | 0.001476 | 1 | 0.0000495 | 60.21 | 16.16 |
| 24 | 0.001969 | 1 | 3.24375E-05 | 45.16 | 24.66 | 24 | 0.001969 | 1 | 0.0000495 | 45.16 | 16.16 |
| 30 | 0.002461 | 1 | 3.24375E-05 | 36.13 | 24.66 | 30 | 0.002461 | 1 | 0.0000495 | 36.13 | 16.16 |

A7: Extended Table-4.2

| Average Attained Temperature (°C) | Data Set | Initial Conductivity (μS/cm) | Equilibrium/ Lowest Conductivity (μS/cm) | Conductivity Drop (μS/cm) | Salt Removed per mass of electrode (mg/g) | Average Salt Removal Capacity (mg/g) | Standard Deviation | 95% Confidence Interval Limits | |
|-----------------------------------|----------|------------------------------|--|---------------------------|---|--------------------------------------|--------------------|--------------------------------|-------|
| | | | | | | | | Lower | Upper |
| 10 | Set-1 | 605 | 549 | 56 | 3.15 | 3.00 | 0.15 | 2.82 | 3.18 |
| | Set-2 | 598 | 542 | 56 | 3.15 | | | | |
| | Set-3 | 590 | 537 | 53 | 2.98 | | | | |
| | Set-4 | 601 | 551 | 50 | 2.81 | | | | |
| | Set-5 | 597 | 545 | 52 | 2.92 | | | | |
| 23 | Set-1 | 594 | 534 | 60 | 3.37 | 3.47 | 0.23 | 3.18 | 3.76 |
| | Set-2 | 602 | 543 | 59 | 3.32 | | | | |
| | Set-3 | 600 | 542 | 58 | 3.26 | | | | |
| | Set-4 | 603 | 539 | 64 | 3.60 | | | | |
| | Set-5 | 596 | 528 | 68 | 3.82 | | | | |
| 34 | Set-1 | 602 | 522 | 80 | 4.50 | 4.29 | 0.36 | 3.85 | 4.74 |
| | Set-2 | 605 | 535 | 70 | 3.93 | | | | |
| | Set-3 | 609 | 527 | 82 | 4.61 | | | | |
| | Set-4 | 599 | 518 | 81 | 4.55 | | | | |
| | Set-5 | 602 | 533 | 69 | 3.88 | | | | |

A8: Test - mean comparison for 10°C data and 23°C data

| Hypothesis | $H_0: \mu_1 = \mu_2; \Delta = 0$ $H_1: \mu_1 \neq \mu_2$ | Test statistics: |
|---|---|--|
| Given Data | | $t_o = \frac{\bar{x}_1 - \bar{x}_2 - \Delta}{\sqrt{\left(\frac{s_1^2}{n_1} + \frac{s_2^2}{n_2}\right)}}$ |
| n_1 | 5 | $= -3.83$ |
| n_2 | 5 | |
| \bar{x}_1 | 3.00 | Degrees of Freedom: |
| | | $v = \frac{\left(\frac{s_1^2}{n_1} + \frac{s_2^2}{n_2}\right)^2}{\frac{\left(\frac{s_1^2}{n_1}\right)^2}{n_1 - 1} + \frac{\left(\frac{s_2^2}{n_2}\right)^2}{n_2 - 1}}$ |
| \bar{x}_2 | 3.47 | $= 6.88 \approx 7$ |
| s_1 | 0.15 | $t_{\frac{\alpha}{2}, v} = t_{0.025, 7}$ |
| s_2 | 0.23 | $= 2.365$ (From standard t-table) |
| Reject criteria: $ t_o > t_{\frac{\alpha}{2}, v} \Rightarrow 3.83 > 2.365$ | | |

Comment: We reject null hypothesis and conclude that there is enough evidence that mean from the two conditions are different at 95% confidence level.

A9: Test - mean comparison for 23°C data and 34°C data

| Hypothesis | $H_0: \mu_1 = \mu_2; \Delta = 0$ $H_1: \mu_1 \neq \mu_2$ | Test statistics: |
|---|---|--|
| Given Data | | $t_o = \frac{\bar{x}_1 - \bar{x}_2 - \Delta}{\sqrt{\left(\frac{s_1^2}{n_1} + \frac{s_2^2}{n_1}\right)}}$ |
| n_1 | 5 | $= -4.29$ |
| n_2 | 5 | |
| \bar{x}_1 | 3.47 | Degrees of Freedom: |
| | | $v = \frac{\left(\frac{s_1^2}{n_1} + \frac{s_2^2}{n_2}\right)^2}{\frac{\left(\frac{s_1^2}{n_1}\right)^2}{n_1 - 1} + \frac{\left(\frac{s_2^2}{n_2}\right)^2}{n_2 - 1}}$ |
| \bar{x}_2 | 4.29 | $= 6.80 \approx 7$ |
| s_1 | 0.23 | $t_{\frac{\alpha}{2}, v} = t_{0.025, 7}$ |
| s_2 | 0.36 | $= 2.365$ (From standard t-table) |
| Reject criteria: $ t_o > t_{\frac{\alpha}{2}, v} \Rightarrow 4.29 > 2.365$ | | |

Comment: We reject null hypothesis and conclude that there is enough evidence that mean from the two conditions are different at 95% confidence level.

A10: Regressions analysis of varying temperature adsorption data:

| <i>Regression Statistics</i> | |
|------------------------------|-------------|
| Multiple R | 0.896797479 |
| R Square | 0.804245718 |
| Adjusted R Square | 0.789187697 |
| Standard Error | 0.276809504 |
| Observations | 15 |

| ANOVA | | | | | |
|------------|-----------|-------------|-------------|------------|-----------------------|
| | <i>df</i> | <i>SS</i> | <i>MS</i> | <i>F</i> | <i>Significance F</i> |
| Regression | 1 | 4.092444833 | 4.092444833 | 53.4097862 | 5.9325E-06 |
| Residual | 13 | 0.99610552 | 0.076623502 | | |
| Total | 14 | 5.088550352 | | | |

| | <i>Coefficients</i> | <i>Standard Error</i> | <i>t Stat</i> | <i>P-value</i> | <i>Lower 95%</i> | <i>Upper 95%</i> |
|-----------|---------------------|-----------------------|--------------------|----------------|------------------|------------------|
| Intercept | 2.419710828 | 0.175184456 | 13.81236034 | 3.8023E-09 | 2.041247821 | 2.798173835 |
| Temp | 0.052573593 | 0.007193781 | 7.308199928 | 5.9325E-06 | 0.037032373 | 0.068114812 |

| | | | |
|-----------------------------|-------------|---------|-----------------------------|
| $t_{\frac{\alpha}{2}, n-2}$ | 2.16 | Comment | t-stat greater, significant |
|-----------------------------|-------------|---------|-----------------------------|

A11: Extended Table-4.3

| Flow (mL/min) | Data Set | Initial Conductivity ($\mu\text{S/cm}$) | Equilibrium/ Lowest Conductivity ($\mu\text{S/cm}$) | Conductivity Drop ($\mu\text{S/cm}$) | Salt Removed per mass of electrode (mg/g) | Average Salt Removal Capacity (mg/g) | Standard Deviation | 95% Confidence Interval Limits | |
|------------------|-------------|---|--|---|---|---|-----------------------|--------------------------------------|-------|
| | | | | | | | | Lower | Upper |
| 12 | Set-1 | 594 | 534 | 60 | 3.37 | 3.47 | 0.15 | 3.29 | 3.66 |
| | Set-2 | 602 | 543 | 59 | 3.32 | | | | |
| | Set-3 | 600 | 542 | 58 | 3.26 | | | | |
| | Set-4 | 603 | 539 | 64 | 3.60 | | | | |
| | Set-5 | 596 | 528 | 68 | 3.82 | | | | |
| 18 | Set-1 | 599 | 537 | 62 | 3.48 | 3.52 | 0.19 | 3.29 | 3.75 |
| | Set-2 | 606 | 540 | 66 | 3.71 | | | | |
| | Set-3 | 602 | 541 | 61 | 3.43 | | | | |
| | Set-4 | 604 | 546 | 58 | 3.26 | | | | |
| | Set-5 | 603 | 537 | 66 | 3.71 | | | | |
| 24 | Set-1 | 603 | 542 | 61 | 3.43 | 3.54 | 0.20 | 3.29 | 3.79 |
| | Set-2 | 603 | 539 | 64 | 3.60 | | | | |
| | Set-3 | 599 | 531 | 68 | 3.82 | | | | |
| | Set-4 | 600 | 540 | 60 | 3.37 | | | | |
| | Set-5 | 603 | 541 | 62 | 3.48 | | | | |
| 30 | Set-1 | 599 | 531 | 68 | 3.82 | 3.58 | 0.17 | 3.38 | 3.79 |
| | Set-2 | 602 | 541 | 61 | 3.43 | | | | |
| | Set-3 | 598 | 533 | 65 | 3.65 | | | | |
| | Set-4 | 605 | 538 | 67 | 3.76 | | | | |
| | Set-5 | 604 | 546 | 58 | 3.26 | | | | |

A12: Test - mean comparison for 12 mL/min data and 18 mL/min data

| Hypothesis | $H_0: \mu_1 = \mu_2; \Delta = 0$ $H_1: \mu_1 \neq \mu_2$ | Test statistics: |
|---|---|--|
| Given Data | | $t_o = \frac{\bar{x}_1 - \bar{x}_2 - \Delta}{\sqrt{\left(\frac{s_1^2}{n_1} + \frac{s_2^2}{n_2}\right)}}$ |
| n_1 | 5 | $= -0.46$ |
| n_2 | 5 | |
| \bar{x}_1 | 3.47 | Degrees of Freedom: |
| | | $v = \frac{\left(\frac{s_1^2}{n_1} + \frac{s_2^2}{n_2}\right)^2}{\frac{\left(\frac{s_1^2}{n_1}\right)^2}{n_1 - 1} + \frac{\left(\frac{s_2^2}{n_2}\right)^2}{n_2 - 1}}$ |
| \bar{x}_2 | 3.52 | $= 7.59 \approx 8$ |
| s_1 | 0.15 | $t_{\frac{\alpha}{2}, v} = t_{0.025, 8}$ |
| s_2 | 0.19 | $= 2.306$ (From standard t-table) |
| Reject criteria: $ t_o > t_{\frac{\alpha}{2}, v} \Rightarrow 0.46 < 2.306$ | | |

Comment: We cannot reject null hypothesis and conclude that there is not enough evidence that mean from the two conditions are different at 95% confidence level.

A13: Test - mean comparison for 18 mL/min data and 24 mL/min data

| Hypothesis | $H_0: \mu_1 = \mu_2; \Delta = 0$ $H_1: \mu_1 \neq \mu_2$ | Test statistics: |
|---|---|--|
| Given Data | | $t_o = \frac{\bar{x}_1 - \bar{x}_2 - \Delta}{\sqrt{\left(\frac{s_1^2}{n_1} + \frac{s_2^2}{n_2}\right)}}$ |
| n_1 | 5 | $= -0.16$ |
| n_2 | 5 | |
| \bar{x}_1 | 3.52 | Degrees of Freedom: |
| | | $v = \frac{\left(\frac{s_1^2}{n_1} + \frac{s_2^2}{n_2}\right)^2}{\frac{\left(\frac{s_1^2}{n_1}\right)^2}{n_1 - 1} + \frac{\left(\frac{s_2^2}{n_2}\right)^2}{n_2 - 1}}$ |
| \bar{x}_2 | 3.54 | $= 7.98 \approx 8$ |
| s_1 | 0.19 | $t_{\frac{\alpha}{2}, v} = t_{0.025, 8}$ |
| s_2 | 0.2 | $= 2.306$ (From standard t-table) |
| Reject criteria: $ t_o > t_{\frac{\alpha}{2}, v} \Rightarrow 0.16 < 2.306$ | | |

Comment: We cannot reject null hypothesis and conclude that there is not enough evidence that mean from the two conditions are different at 95% confidence level.

A14: Test - mean comparison for 24 mL/min data and 30 mL/min data

| Hypothesis | $H_0: \mu_1 = \mu_2; \Delta = 0$ $H_1: \mu_1 \neq \mu_2$ | Test statistics: |
|---|---|--|
| Given Data | | $t_o = \frac{\bar{x}_1 - \bar{x}_2 - \Delta}{\sqrt{\left(\frac{s_1^2}{n_1} + \frac{s_2^2}{n_1}\right)}}$ |
| n_1 | 5 | $= -0.34$ |
| n_2 | 5 | |
| \bar{x}_1 | 3.54 | Degrees of Freedom: |
| | | $v = \frac{\left(\frac{s_1^2}{n_1} + \frac{s_2^2}{n_2}\right)^2}{\frac{\left(\frac{s_1^2}{n_1}\right)^2}{n_1 - 1} + \frac{\left(\frac{s_2^2}{n_1}\right)^2}{n_2 - 1}}$ |
| \bar{x}_2 | 3.58 | $= 7.80 \approx 8$ |
| s_1 | 0.2 | $t_{\frac{\alpha}{2}, v} = t_{0.025, 8}$ |
| s_2 | 0.17 | $= 2.306$ (From standard t-table) |
| Reject criteria: $ t_o > t_{\frac{\alpha}{2}, v} \Rightarrow 0.34 < 2.306$ | | |

Comment: We cannot reject null hypothesis and conclude that there is not enough evidence that mean from the two conditions are different at 95% confidence level.

A15: Test - mean comparison for 12 mL/min data and 30 mL/min data

| Hypothesis | $H_0: \mu_1 = \mu_2; \Delta = 0$ $H_1: \mu_1 \neq \mu_2$ | Test statistics: |
|---|---|--|
| Given Data | | $t_o = \frac{\bar{x}_1 - \bar{x}_2 - \Delta}{\sqrt{\left(\frac{s_1^2}{n_1} + \frac{s_2^2}{n_1}\right)}}$ |
| n_1 | 5 | $= -1.08$ |
| n_2 | 5 | |
| \bar{x}_1 | 3.47 | Degrees of Freedom: |
| | | $v = \frac{\left(\frac{s_1^2}{n_1} + \frac{s_2^2}{n_2}\right)^2}{\frac{\left(\frac{s_1^2}{n_1}\right)^2}{n_1 - 1} + \frac{\left(\frac{s_2^2}{n_1}\right)^2}{n_2 - 1}}$ |
| \bar{x}_2 | 3.58 | $= 7.88 \approx 8$ |
| s_1 | 0.15 | $t_{\frac{\alpha}{2}, v} = t_{0.025, 8}$ |
| s_2 | 0.17 | $= 2.306$ (From standard t-table) |
| Reject criteria: $ t_o > t_{\frac{\alpha}{2}, v} \Rightarrow 1.08 < 2.306$ | | |

Comment: We cannot reject null hypothesis and conclude that there is not enough evidence that mean from the two conditions are different at 95% confidence level.

A16: Regressions analysis of varying flow rate adsorption data:

| <i>Regression Statistics</i> | |
|------------------------------|------------|
| Multiple R | 0.20777469 |
| R Square | 0.04317032 |
| Adjusted R Square | - |
| Standard Error | 0.19952111 |
| Observations | 20 |

| ANOVA | | | | | | |
|------------|-----------|-------------|------------|------------|-----------------------|--|
| | <i>df</i> | <i>SS</i> | <i>MS</i> | <i>F</i> | <i>Significance F</i> | |
| Regression | 1 | 0.032329638 | 0.03232964 | 0.81212548 | 0.3793928 | |
| Residual | 18 | 0.716556123 | 0.03980867 | | | |
| Total | 19 | 0.748885761 | | | | |

| | <i>Coefficients</i> | <i>Standard Error</i> | <i>t Stat</i> | <i>P-value</i> | <i>Lower 95%</i> | <i>Upper 95%</i> |
|-----------------------------|---------------------|-----------------------|-------------------|---------------------------------|------------------|------------------|
| Intercept | 3.40279911 | 0.146617474 | 23.2086873 | 7.277E-15 | 3.09476723 | 3.71083099 |
| Flow rate | 0.00599348 | 0.006650704 | 0.90118005 | 0.3793928 | 0.00797913 | 0.01996609 |
| $t_{\frac{\alpha}{2}, n-2}$ | 2.101 | | Comment | t-stat smaller, not significant | | |

A17: Extended Table-4.4

| Initial Concentration (mg/L) | Data Set | Initial Conductivity ($\mu\text{S}/\text{cm}$) | Equilibrium/ Lowest Conductivity ($\mu\text{S}/\text{cm}$) | Conductivity Drop ($\mu\text{S}/\text{cm}$) | Salt Removed per mass of electrode (mg/g) | Average Salt Removal Capacity (mg/g) | Standard Deviation | 95% Confidence interval limits | |
|------------------------------|----------|--|--|---|---|--------------------------------------|--------------------|--------------------------------|------|
| 100 | Set-1 | 207 | 167 | 39 | 2.21 | 2.52 | 0.21 | 2.25 | 2.78 |
| | Set-2 | 206 | 157 | 49 | 2.73 | | | | |
| | Set-3 | 212 | 170 | 42 | 2.37 | | | | |
| | Set-4 | 211 | 168 | 43 | 2.42 | | | | |
| | Set-5 | 215 | 164 | 51 | 2.87 | | | | |
| 200 | Set-1 | 416 | 366 | 50 | 2.81 | 2.81 | 0.10 | 2.69 | 2.93 |
| | Set-2 | 415 | 366 | 49 | 2.75 | | | | |
| | Set-3 | 419 | 371 | 48 | 2.70 | | | | |
| | Set-4 | 421 | 375 | 46 | 2.58 | | | | |
| | Set-5 | 418 | 361 | 57 | 3.20 | | | | |
| 300 | Set-1 | 594 | 534 | 60 | 3.37 | 3.47 | 0.15 | 3.29 | 3.66 |
| | Set-2 | 602 | 543 | 59 | 3.32 | | | | |
| | Set-3 | 600 | 542 | 58 | 3.26 | | | | |
| | Set-4 | 603 | 539 | 64 | 3.60 | | | | |
| | Set-5 | 596 | 528 | 68 | 3.82 | | | | |
| 400 | Set-1 | 851 | 790 | 61 | 3.43 | 3.66 | 0.28 | 3.32 | 4.01 |
| | Set-2 | 844 | 774 | 70 | 3.93 | | | | |
| | Set-3 | 846 | 785 | 61 | 3.43 | | | | |
| | Set-4 | 845 | 776 | 69 | 3.88 | | | | |
| | Set-5 | 842 | 777 | 65 | 3.65 | | | | |

A18: Test - mean comparison for 100 mg/L data to 200 mg/L data

| Hypothesis | $H_0: \mu_1 = \mu_2; \Delta = 0$ $H_1: \mu_1 \neq \mu_2$ | Test statistics: |
|---|---|--|
| Given Data | | $t_o = \frac{\bar{x}_1 - \bar{x}_2 - \Delta}{\sqrt{\left(\frac{s_1^2}{n_1} + \frac{s_2^2}{n_1}\right)}}$ |
| n_1 | 5 | $= -2.79$ |
| n_2 | 5 | |
| \bar{x}_1 | 2.52 | Degrees of Freedom: |
| | | $v = \frac{\left(\frac{s_1^2}{n_1} + \frac{s_2^2}{n_2}\right)^2}{\frac{\left(\frac{s_1^2}{n_1}\right)^2}{n_1 - 1} + \frac{\left(\frac{s_2^2}{n_1}\right)^2}{n_2 - 1}}$ |
| \bar{x}_2 | 2.81 | $= 5.73 \approx 6$ |
| s_1 | 0.21 | $t_{\frac{\alpha}{2}, v} = t_{0.025, 6}$ |
| s_2 | 0.10 | $= 2.447$ (From standard t-table) |
| Reject criteria: $ t_o > t_{\frac{\alpha}{2}, v} \Rightarrow 2.79 > 2.306$ | | |

Comment: We reject null hypothesis and conclude that there is enough evidence that mean from the two conditions are different at 95% confidence level.

A19: Test - mean comparison for 200 mg/L data and 300 mg/L data

| Hypothesis | $H_0: \mu_1 = \mu_2; \Delta = 0$ $H_1: \mu_1 \neq \mu_2$ | Test statistics: |
|---|---|--|
| Given Data | | $t_o = \frac{\bar{x}_1 - \bar{x}_2 - \Delta}{\sqrt{\left(\frac{s_1^2}{n_1} + \frac{s_2^2}{n_1}\right)}}$ |
| n_1 | 5 | $= -8.19$ |
| n_2 | 5 | |
| \bar{x}_1 | 2.81 | Degrees of Freedom: |
| | | $v = \frac{\left(\frac{s_1^2}{n_1} + \frac{s_2^2}{n_2}\right)^2}{\frac{\left(\frac{s_1^2}{n_1}\right)^2}{n_1 - 1} + \frac{\left(\frac{s_2^2}{n_1}\right)^2}{n_2 - 1}}$ |
| \bar{x}_2 | 3.47 | $= 6.97 \approx 7$ |
| s_1 | 0.10 | $t_{\frac{\alpha}{2}, v} = t_{0.025, 7}$ |
| s_2 | 0.15 | $= 2.365$ (From standard t-table) |
| Reject criteria: $ t_o > t_{\frac{\alpha}{2}, v} \Rightarrow 8.19 > 2.365$ | | |

Comment: We reject null hypothesis and conclude that there is enough evidence that mean from the two conditions are different at 95% confidence level.

A20: Test - mean comparison for 300 mg/L data and 400 mg/L data

| Hypothesis | $H_0: \mu_1 = \mu_2; \Delta = 0$ $H_1: \mu_1 \neq \mu_2$ | Test statistics: |
|---|---|--|
| Given Data | | $t_o = \frac{\bar{x}_1 - \bar{x}_2 - \Delta}{\sqrt{\left(\frac{s_1^2}{n_1} + \frac{s_2^2}{n_1}\right)}}$ |
| n_1 | 5 | $= -1.34$ |
| n_2 | 5 | |
| \bar{x}_1 | 3.47 | Degrees of Freedom: |
| | | $v = \frac{\left(\frac{s_1^2}{n_1} + \frac{s_2^2}{n_2}\right)^2}{\frac{\left(\frac{s_1^2}{n_1}\right)^2}{n_1 - 1} + \frac{\left(\frac{s_2^2}{n_1}\right)^2}{n_2 - 1}}$ |
| \bar{x}_2 | 3.66 | $= 6.12 \approx 7$ |
| s_1 | 0.15 | $t_{\frac{\alpha}{2}, v} = t_{0.025, 7}$ |
| s_2 | 0.28 | $= 2.365$ (From standard t-table) |
| Reject criteria: $ t_o > t_{\frac{\alpha}{2}, v} \Rightarrow 1.34 < 2.365$ | | |

Comment: We cannot reject null hypothesis and conclude that there is not enough evidence that mean from the two conditions are different at 95% confidence level.

A21: Regressions analysis of varying initial concentration adsorption data:

| <i>Regression Statistics</i> | |
|------------------------------|---------|
| Multiple R | 0.88631 |
| R Square | 0.78554 |
| Adjusted R Square | 0.77362 |
| Standard Error | 0.25258 |
| Observations | 20 |

| ANOVA | | | | | |
|------------|-----------|-------------|------------|----------|-----------------------|
| | <i>df</i> | <i>SS</i> | <i>MS</i> | <i>F</i> | <i>Significance F</i> |
| Regression | 1 | 4.206168022 | 4.20616802 | 65.9312 | 1.9819E-07 |
| Residual | 18 | 1.148333596 | 0.06379631 | | |
| Total | 19 | 5.354501618 | | | |

| | <i>Coefficients</i> | <i>Standard Error</i> | <i>t Stat</i> | <i>P-value</i> | <i>Lower 95%</i> | <i>Upper 95%</i> |
|--------------|---------------------|-----------------------|-------------------|----------------|------------------|------------------|
| Intercept | 2.09023 | 0.138343389 | 15.108974 | 1.1E-11 | 1.79957799 | 2.38087534 |
| Initial Conc | 0.0041 | 0.000505159 | 8.11980362 | 2E-07 | 0.00304049 | 0.00516309 |

| | | | |
|-----------------------------|--------------|---------|-----------------------------|
| $t_{\frac{\alpha}{2}, n-2}$ | 2.101 | Comment | t-stat greater, significant |
|-----------------------------|--------------|---------|-----------------------------|

A22: Regeneration percentages for different applied reverse voltage tests using multi-pass method.

| Applied Voltage | Trials | Results (%) | Average Regeneration (%) | Standard Deviation | STDV at 95% Confidence Interval |
|-----------------|--------|-------------|--------------------------|--------------------|---------------------------------|
| 0 | Set-1 | 53 | 53 | 10.63 | 26.40 |
| | Set-2 | 68 | | | |
| | Set-3 | Not done | | | |
| 0.2 | Set-1 | 59 | 68 | 13.58 | 33.73 |
| | Set-2 | 78 | | | |
| | Set-3 | Not done | | | |
| 0.4 | Set-1 | 80 | 88 | 6.55 | 16.27 |
| | Set-2 | 90 | | | |
| | Set-3 | 92 | | | |
| 0.6 | Set-1 | 63 | 76 | 11.66 | 28.98 |
| | Set-2 | 79 | | | |
| | Set-3 | 85 | | | |
| 0.8 | Set-1 | 88 | 81 | 6.28 | 15.61 |
| | Set-2 | 76 | | | |
| | Set-3 | 81 | | | |
| 1 | Set-1 | 77 | 82 | 4.97 | 12.35 |
| | Set-2 | 86 | | | |
| | Set-3 | 82 | | | |
| 1.2 | Set-1 | 69 | 78 | 12.39 | 30.78 |
| | Set-2 | 87 | | | |
| | Set-3 | Not done | | | |

A23: Regressions analysis of varying voltage desorption data in multi-pass method:

| <i>Regression Statistics</i> | |
|------------------------------|---------|
| Multiple R | 0.41844 |
| R Square | 0.17509 |
| Adjusted R Square | 0.12353 |
| Standard Error | 10.3669 |
| Observations | 18 |

| ANOVA | | | | | |
|------------|-----------|-----------|-----------|----------|-----------------------|
| | <i>df</i> | <i>SS</i> | <i>MS</i> | <i>F</i> | <i>Significance F</i> |
| Regression | 1 | 364.98 | 364.98 | 3.39601 | 0.08396 |
| Residual | 16 | 1719.57 | 107.473 | | |
| Total | 17 | 2084.55 | | | |

| | <i>Coefficients</i> | <i>Standard Error</i> | <i>t Stat</i> | <i>P-value</i> | <i>Lower 95%</i> | <i>Upper 95%</i> |
|-----------|---------------------|-----------------------|----------------|----------------|------------------|------------------|
| Intercept | 69.9158 | 4.77588 | 14.6393 | 1.1E-10 | 59.7914 | 80.0402 |
| Voltage | 12.1531 | 6.59483 | 1.84283 | 0.08396 | -1.8273 | 26.1335 |

| | | | |
|-----------------------------|-------------|---------|---|
| $t_{\frac{\alpha}{2}, n-2}$ | 2.12 | Comment | absolute value of t-stat smaller, not significant |
|-----------------------------|-------------|---------|---|

A24: Regeneration percentages for different duration of applying reverse voltage with multi-pass method.

| Time Applied/Condition | Voltage | Results (%) | | Average Regeneration (%) | Standard Deviation | 95% Confidence Interval |
|------------------------|---------|-------------|----------|--------------------------|--------------------|-------------------------|
| No Voltage | 0 | Set-1 | 53 | 61 | 10.50 | 26.09 |
| | | Set-2 | 68 | | | |
| | | Set-3 | Not done | | | |
| Shorted | 0 | Set-1 | 83 | 79 | 8.44 | 20.96 |
| | | Set-2 | 69 | | | |
| | | Set-3 | 85 | | | |
| 3 S | 0.8 | Set-1 | 85 | 83 | 2.01 | 4.98 |
| | | Set-2 | 83 | | | |
| | | Set-3 | 81 | | | |
| 30 S | 0.8 | Set-1 | 94 | 71 | 20.11 | 49.95 |
| | | Set-2 | 54 | | | |
| | | Set-3 | 66 | | | |
| 1 min | 0.8 | Set-1 | 73 | 76 | 2.61 | 6.48 |
| | | Set-2 | 76 | | | |
| | | Set-3 | 79 | | | |
| 3 min | 0.8 | Set-1 | 79 | 74 | 3.76 | 9.33 |
| | | Set-2 | 72 | | | |
| | | Set-3 | 72 | | | |
| 5 min | 0.8 | Set-1 | 90 | 85 | 8.45 | 20.99 |
| | | Set-2 | 75 | | | |
| | | Set-3 | 89 | | | |
| 10 min | 0.8 | Set-1 | 83 | 91 | 10.35 | 25.72 |
| | | Set-2 | 98 | | | |
| | | Set-3 | Not done | | | |
| 15 min | 0.8 | Set-1 | 63 | 65 | 3.54 | 8.78 |
| | | Set-2 | 68 | | | |
| | | Set-3 | Not done | | | |

A25: Regressions analysis of varying time duration of voltage desorption data in multi-pass method:

| <i>Regression Statistics</i> | |
|------------------------------|---------|
| Multiple R | 0.04818 |
| R Square | 0.00232 |
| Adjusted R Square | -0.0502 |
| Standard Error | 12.1403 |
| Observations | 21 |

| ANOVA | | | | | | |
|------------|-----------|-----------|-----------|----------|-----------------------|--|
| | <i>df</i> | <i>SS</i> | <i>MS</i> | <i>F</i> | <i>Significance F</i> | |
| Regression | 1 | 6.51592 | 6.51592 | 0.04421 | 0.8357 | |
| Residual | 19 | 2800.33 | 147.386 | | | |
| Total | 20 | 2806.85 | | | | |

| | <i>Coefficients</i> | <i>Standard Error</i> | <i>t Stat</i> | <i>P-value</i> | <i>Lower 95%</i> | <i>Upper 95%</i> |
|-----------|---------------------|-----------------------|----------------|----------------|------------------|------------------|
| Intercept | 75.7629 | 3.39131 | 22.3403 | 4.2E-15 | 68.6648 | 82.861 |
| Time | 0.00198 | 0.00942 | 0.21026 | 0.8357 | -0.0177 | 0.0217 |

| $t_{\frac{\alpha}{2}, n-2}$ | 2.093 | Comment | absolute value of t-stat smaller, not significant |
|-----------------------------|--------------|---------|---|
| | | | |

A26: Desorption data for applied voltage tests – single pass method.

| Voltage | Conductivity drop in adsorption ($\mu S/cm$) | Conductivity rise in desorption ($\mu S/cm$) | % Regeneration | Conductivity drop in adsorption ($\mu S/cm$) | Conductivity rise in desorption ($\mu S/cm$) | % Regeneration | Conductivity drop in adsorption ($\mu S/cm$) | Conductivity rise in desorption ($\mu S/cm$) | % Regeneration |
|---------|--|--|----------------|--|--|----------------|--|--|----------------|
| | Set 1 | | | Set 2 | | | Set 3 | | |
| 0 | 51 | 22.3 | 44 | 46 | 19.85 | 43 | 38 | 16.67 | 44 |
| 0.3 | 55 | 25.3 | 46 | 50 | 19.85 | 40 | 45 | 18.09 | 40 |
| 0.6 | 54 | 20.67 | 38 | 47 | 18.09 | 38 | 75 | 32 | 43 |
| 0.9 | 58 | 22.2 | 38 | 45 | 19.23 | 43 | 39 | 18.3 | 47 |
| 1.2 | 51 | 19.77 | 39 | 43 | 18.56 | 43 | 71 | 34 | 48 |

| Applied Voltage | Trials | Results (%) | Average Regeneration (%) | Standard Deviation | 95% Confidence Interval |
|-----------------|--------|-------------|--------------------------|--------------------|-------------------------|
| 0 | Set-1 | 44 | 44 | 0.38 | 0.94 |
| | Set-2 | 43 | | | |
| | Set-3 | 44 | | | |
| 0.3 | Set-1 | 46 | 43 | 3.50 | 8.70 |
| | Set-2 | 40 | | | |
| | Set-3 | 40 | | | |
| 0.6 | Set-1 | 38 | 40 | 2.48 | 6.15 |
| | Set-2 | 38 | | | |
| | Set-3 | 43 | | | |
| 0.9 | Set-1 | 38 | 43 | 4.32 | 10.74 |
| | Set-2 | 43 | | | |
| | Set-3 | 47 | | | |
| 1.2 | Set-1 | 39 | 43 | 4.56 | 11.33 |
| | Set-2 | 43 | | | |
| | Set-3 | 48 | | | |

A27: Regressions analysis of varying applied reverse voltage desorption data in single-pass method:

| <i>Regression Statistics</i> | |
|------------------------------|---------|
| Multiple R | 0.00259 |
| R Square | 6.7E-06 |
| Adjusted R Square | -0.0769 |
| Standard Error | 3.31774 |
| Observations | 15 |

| ANOVA | | | | | |
|------------|-----------|-----------|-----------|----------|-----------------------|
| | <i>df</i> | <i>SS</i> | <i>MS</i> | <i>F</i> | <i>Significance F</i> |
| Regression | 1 | 0.00096 | 0.00096 | 8.7E-05 | 0.99269 |
| Residual | 13 | 143.096 | 11.0074 | | |
| Total | 14 | 143.097 | | | |

| | <i>Coefficients</i> | <i>Standard Error</i> | <i>t Stat</i> | <i>P-value</i> | <i>Lower 95%</i> | <i>Upper 95%</i> |
|-----------------|---------------------|-----------------------|----------------|----------------|------------------|------------------|
| Intercept | 42.2438 | 1.48374 | 28.4712 | 4.2E-13 | 39.0384 | 45.4492 |
| Applied Voltage | 0.01886 | 2.01911 | 0.00934 | 0.99269 | -4.3432 | 4.38088 |

| | | | |
|-----------------------------|-------------|---------|---|
| $t_{\frac{\alpha}{2}, n-2}$ | 2.16 | Comment | absolute value of t-stat smaller, not significant |
|-----------------------------|-------------|---------|---|

A28: Desorption data for duration of applying voltage tests – single pass method.

| Time Length | Conductivity drop in adsorption ($\mu S/cm$) | Conductivity rise in desorption ($\mu S/cm$) | % Regeneration | Conductivity drop in adsorption ($\mu S/cm$) | Conductivity rise in desorption ($\mu S/cm$) | % Regeneration | Conductivity drop in adsorption ($\mu S/cm$) | Conductivity rise in desorption ($\mu S/cm$) | % Regeneration |
|-------------|--|--|----------------|--|--|----------------|--|--|----------------|
| | Set 1 | | | Set 2 | | | Set 3 | | |
| 0 | 61 | 25.88 | 42 | 25 | 14.62 | 58 | 26 | 14.67 | 56 |
| 3S | 23 | 16.4 | 71 | 38 | 27.67 | 73 | 41 | 24.97 | 61 |
| 30S | 55 | 28.7 | 52 | 40 | 27.43 | 69 | 32 | 23.47 | 73 |
| 1 M | 53 | 30.1 | 57 | 40 | 25.00 | 63 | 30 | 22.30 | 74 |
| 3M | 53 | 32.3 | 61 | 36 | 23.33 | 65 | 29 | 21.52 | 74 |
| 5 M | 50 | 33.6 | 67 | 37 | 24.00 | 65 | 25 | 19.80 | 79 |

| Time Length | Trials | Results (%) | Average Regeneration (%) | Standard Deviation | 95% Confidence Interval |
|-------------|--------|-------------|--------------------------|--------------------|-------------------------|
| 0 | Set-1 | 42 | 42 | 8.74 | 21.70 |
| | Set-2 | 58 | | | |
| | Set-3 | 56 | | | |
| 3 sec | Set-1 | 71 | 72 | 6.49 | 16.12 |
| | Set-2 | 73 | | | |
| | Set-3 | 61 | | | |
| 30 sec | Set-1 | 52 | 65 | 11.10 | 27.57 |
| | Set-2 | 69 | | | |
| | Set-3 | 73 | | | |
| 1 min | Set-1 | 57 | 65 | 8.95 | 22.23 |
| | Set-2 | 63 | | | |
| | Set-3 | 74 | | | |
| 3 min | Set-1 | 61 | 67 | 6.82 | 16.94 |
| | Set-2 | 65 | | | |
| | Set-3 | 74 | | | |
| 5 min | Set-1 | 67 | 70 | 7.69 | 19.11 |
| | Set-2 | 65 | | | |
| | Set-3 | 79 | | | |

A29: Regressions analysis of varying time duration of applied reverse voltage desorption data in single-pass method:

| <i>Regression Statistics</i> | |
|------------------------------|---------|
| Multiple R | 0.36774 |
| R Square | 0.13523 |
| Adjusted R Square | 0.08118 |
| Standard Error | 8.86504 |
| Observations | 18 |

| ANOVA | | | | | |
|------------|-----------|-----------|-----------|----------|-----------------------|
| | <i>df</i> | <i>SS</i> | <i>MS</i> | <i>F</i> | <i>Significance F</i> |
| Regression | 1 | 196.632 | 196.632 | 2.50203 | 0.13326 |
| Residual | 16 | 1257.42 | 78.589 | | |
| Total | 17 | 1454.06 | | | |

| | <i>Coefficients</i> | <i>Standard Error</i> | <i>t Stat</i> | <i>P-value</i> | <i>Lower 95%</i> | <i>Upper 95%</i> |
|-------------------------|---------------------|-----------------------|----------------|----------------|------------------|------------------|
| Intercept | 61.6384 | 2.77051 | 22.248 | 1.8E-13 | 55.7652 | 67.5116 |
| Time of applied voltage | 0.03013 | 0.01905 | 1.58178 | 0.13326 | -0.0103 | 0.07052 |

| | | | |
|-----------------------------|-------------|---------|---|
| $t_{\frac{\alpha}{2}, n-2}$ | 2.12 | Comment | absolute value of t-stat smaller, not significant |
|-----------------------------|-------------|---------|---|

A30: Desorption data for time temperature tests – single pass method.

| Temperature (°C) | Conductivity drop in adsorption ($\mu S/cm$) | Conductivity rise in desorption ($\mu S/cm$) | % Regeneration | Conductivity drop in adsorption ($\mu S/cm$) | Conductivity rise in desorption ($\mu S/cm$) | % Regeneration | Conductivity drop in adsorption ($\mu S/cm$) | Conductivity rise in desorption ($\mu S/cm$) | % Regeneration |
|------------------|--|--|----------------|--|--|----------------|--|--|----------------|
| | Set 1 | | | Set 2 | | | Set 3 | | |
| 9.7±1.24 | 30 | 19.2 | 64 | 25 | 14.62 | 58 | 26 | 14.67 | 56 |
| 23±0.43 | 54 | 20.67 | 38 | 38 | 27.67 | 73 | 41 | 24.97 | 61 |
| 34±1.21 | 55 | 28.7 | 52 | 40 | 27.43 | 69 | 32 | 23.47 | 73 |

| Temperature (°C) | Trials | Results (%) | Average Regeneration (%) | Standard Deviation | 95% Confidence Interval |
|------------------|--------|-------------|--------------------------|--------------------|-------------------------|
| 9.7±1.24 | Set-1 | 64 | 61 | 3.92 | 9.73 |
| | Set-2 | 58 | | | |
| | Set-3 | 56 | | | |
| 23±0.43 | Set-1 | 38 | 57 | 17.54 | 43.57 |
| | Set-2 | 73 | | | |
| | Set-3 | 61 | | | |
| 34±1.21 | Set-1 | 52 | 65 | 11.10 | 27.57 |
| | Set-2 | 69 | | | |
| | Set-3 | 73 | | | |

A31: Regressions analysis of varying temperature level desorption data in single-pass method:

| <i>Regression Statistics</i> | |
|------------------------------|---------|
| Multiple R | 0.18616 |
| R Square | 0.03466 |
| Adjusted R Square | -0.1032 |
| Standard Error | 11.6111 |
| Observations | 9 |

| ANOVA | | | | | |
|------------|-----------|-----------|-----------|----------|-----------------------|
| | <i>df</i> | <i>SS</i> | <i>MS</i> | <i>F</i> | <i>Significance F</i> |
| Regression | 1 | 33.8809 | 33.8809 | 0.25131 | 0.63153 |
| Residual | 7 | 943.717 | 134.817 | | |
| Total | 8 | 977.598 | | | |

| | <i>Coefficients</i> | <i>Standard Error</i> | <i>t Stat</i> | <i>P-value</i> | <i>Lower 95%</i> | <i>Upper 95%</i> |
|-------------|---------------------|-----------------------|----------------|----------------|------------------|------------------|
| Intercept | 56.2115 | 9.48661 | 5.92535 | 0.00058 | 33.7792 | 78.6437 |
| Temperature | 0.19529 | 0.38956 | 0.50131 | 0.63153 | -0.7259 | 1.11645 |

| | | | |
|-----------------------------|--------------|---------|---|
| $t_{\frac{\alpha}{2}, n-2}$ | 2.365 | Comment | absolute value of t-stat smaller, not significant |
|-----------------------------|--------------|---------|---|

A32: Desorption data for flow rate tests – single pass method.

| Flow rates (mL/min) | Conductivity drop in adsorption ($\mu S/cm$) | Conductivity rise in desorption ($\mu S/cm$) | % Regeneration | Conductivity drop in adsorption ($\mu S/cm$) | Conductivity rise in desorption ($\mu S/cm$) | % Regeneration | Conductivity drop in adsorption ($\mu S/cm$) | Conductivity rise in desorption ($\mu S/cm$) | % Regeneration |
|------------------------|---|---|-------------------|---|---|-------------------|---|---|-------------------|
| | Set 1 | | | Set 2 | | | Set 3 | | |
| 12 | 23 | 16.40 | 71 | 38 | 27.67 | 73 | 41 | 24.97 | 61 |
| 18 | 78 | 30.07 | 39 | 45 | 18.67 | 41 | 56 | 24.32 | 43 |
| 24 | 56 | 26.77 | 48 | 48 | 17.50 | 36 | 73 | 23.50 | 32 |
| 30 | 51 | 21.34 | 42 | 30 | 17.00 | 57 | 53 | 16.50 | 31 |

| Flow rate (mL/min) | Trials | Results (%) | Average regeneration (%) | Standard Deviation | 95% Confidence Interval |
|--------------------|--------|-------------|--------------------------|--------------------|-------------------------|
| 12 | Set-1 | 71 | 71 | 6.49 | 16.12 |
| | Set-2 | 73 | | | |
| | Set-3 | 61 | | | |
| 18 | Set-1 | 39 | 40 | 2.46 | 6.11 |
| | Set-2 | 41 | | | |
| | Set-3 | 43 | | | |
| 24 | Set-1 | 48 | 39 | 8.07 | 20.04 |
| | Set-2 | 36 | | | |
| | Set-3 | 32 | | | |
| 30 | Set-1 | 42 | 43 | 12.82 | 31.86 |
| | Set-2 | 57 | | | |
| | Set-3 | 31 | | | |

A33: Regressions analysis of varying flow rate desorption data in single-pass method:

| <i>Regression Statistics</i> | |
|------------------------------|----------|
| Multiple R | 0.633369 |
| R Square | 0.401156 |
| Adjusted R Square | 0.341271 |
| Standard Error | 11.62836 |
| Observations | 12 |

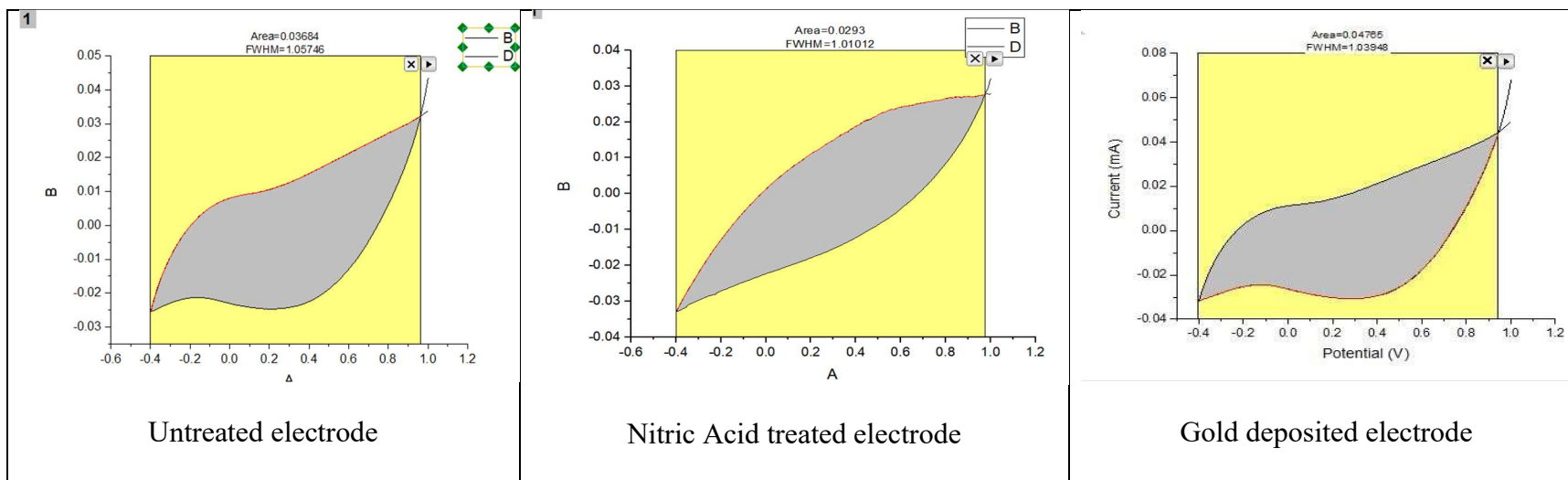
| ANOVA | | | | | | |
|------------|-----------|-----------|-----------|----------|-----------------------|--|
| | <i>df</i> | <i>SS</i> | <i>MS</i> | <i>F</i> | <i>Significance F</i> | |
| Regression | 1 | 905.809 | 905.809 | 6.698837 | 0.027033 | |
| Residual | 10 | 1352.188 | 135.2188 | | | |
| Total | 11 | 2257.997 | | | | |

| | <i>Coefficients</i> | <i>Standard Error</i> | <i>t Stat</i> | <i>P-value</i> | <i>Lower 95%</i> | <i>Upper 95%</i> |
|-----------|---------------------|-----------------------|---------------|----------------|------------------|------------------|
| Intercept | 75.07767 | 11.03163 | 6.805671 | 4.71E-05 | 50.49766 | 99.65768 |
| Flow rate | -1.29515 | 0.500405 | -2.58821 | 0.027033 | -2.41013 | -0.18018 |

| | | | |
|-----------------------------|--------------|---------|--------------------------------------|
| $t_{\frac{\alpha}{2}, n-2}$ | 2.228 | Comment | absolute t-stat greater, significant |
|-----------------------------|--------------|---------|--------------------------------------|

A34: Specific capacitance calculations

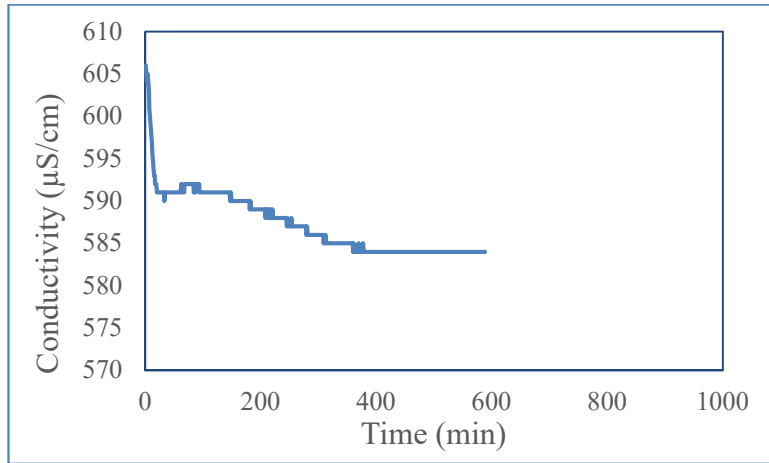
Area calculation from Current vs. Voltage graph in cyclic voltammetry



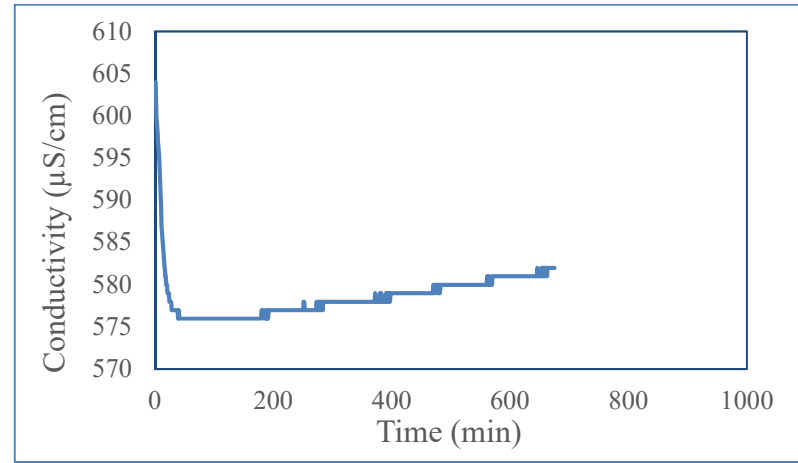
| Sample | Area of the CV graph | Mass (g) | Voltage range (V) | Scan rate (V/s) | Capacitance (F/g) |
|----------------|----------------------|----------|-------------------|-----------------|-------------------|
| Untreated | 0.03684 | 0.071516 | 1.4 | 0.005 | 37 |
| Acid treated | 0.0293 | 0.07575 | 1.4 | 0.005 | 28 |
| Gold deposited | 0.04765 | 0.06898 | 1.4 | 0.005 | 49 |

APPENDIX B

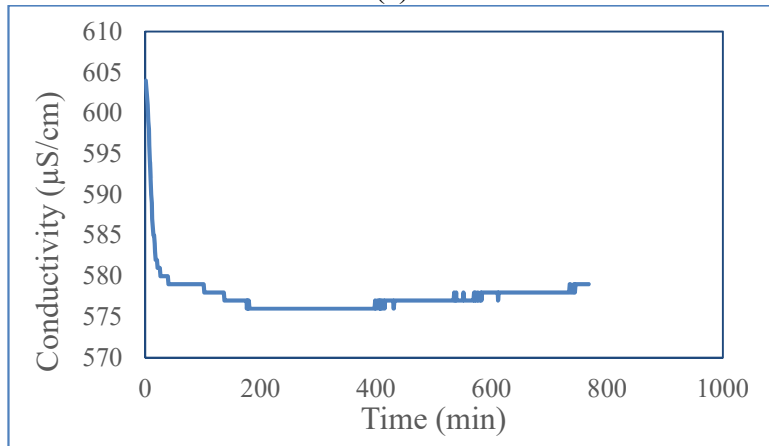
B1: Tests before acetone wash:



(a)

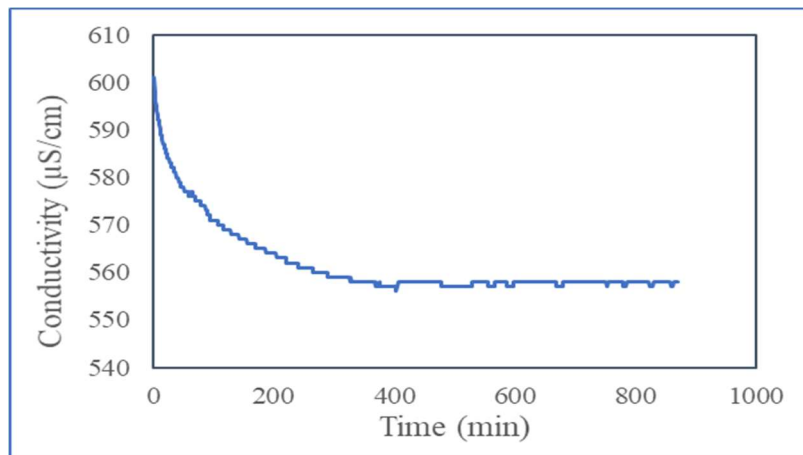


(c)

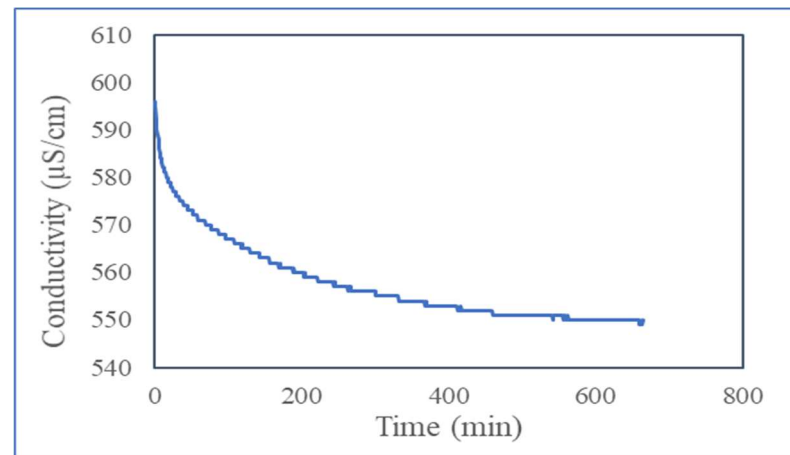


(b)

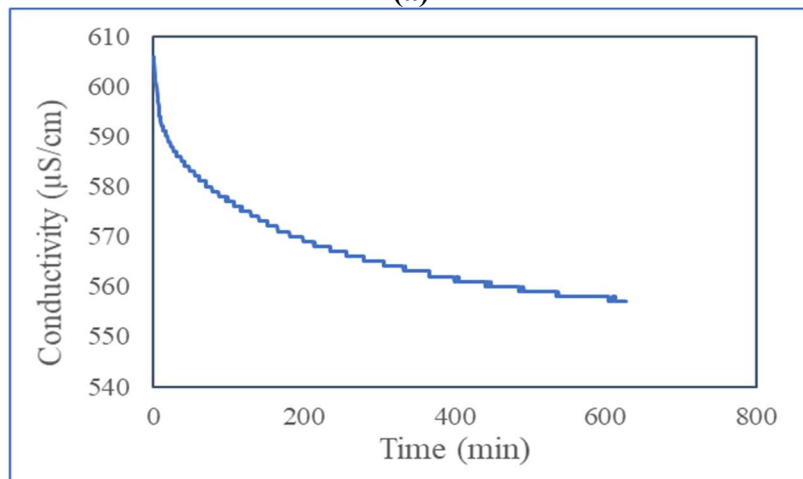
B2: Tests for Voltage = 0.6 V



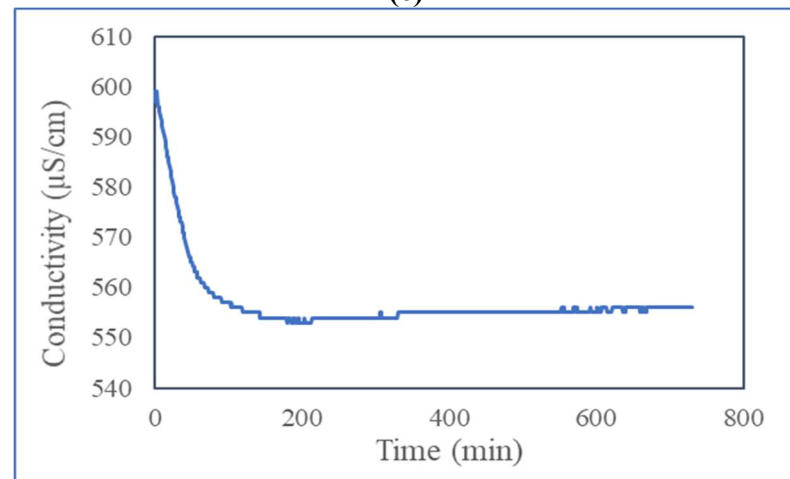
(a)



(c)

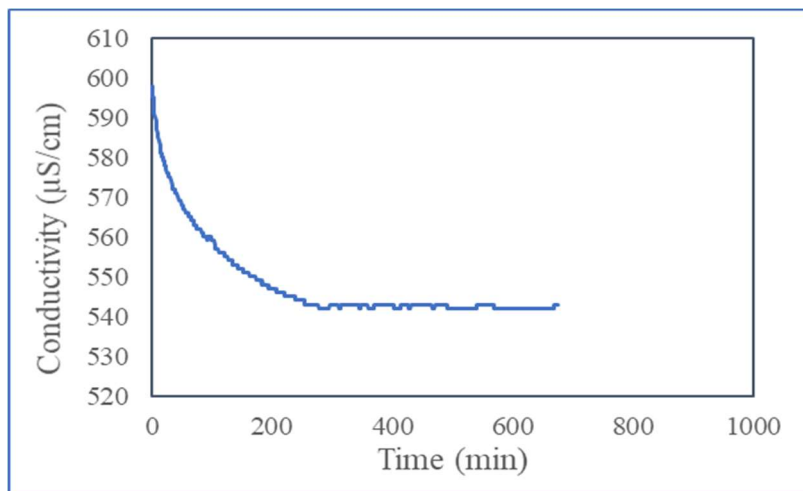


(b)

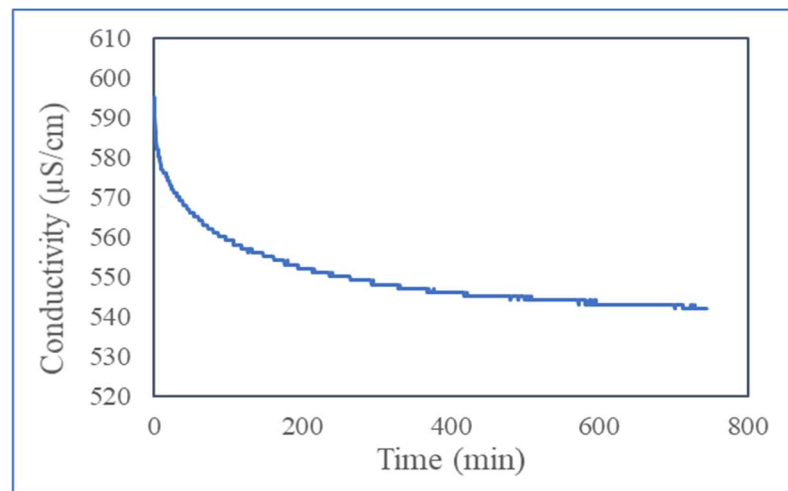


(d)

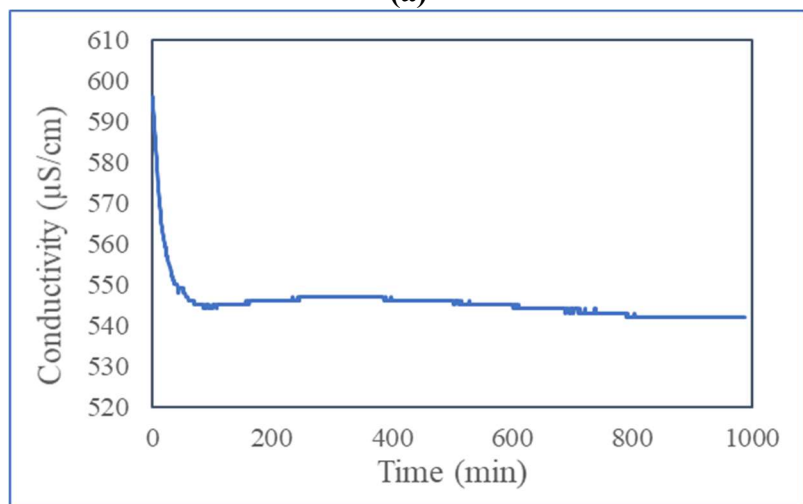
B3: Tests for Voltage = 0.8 V



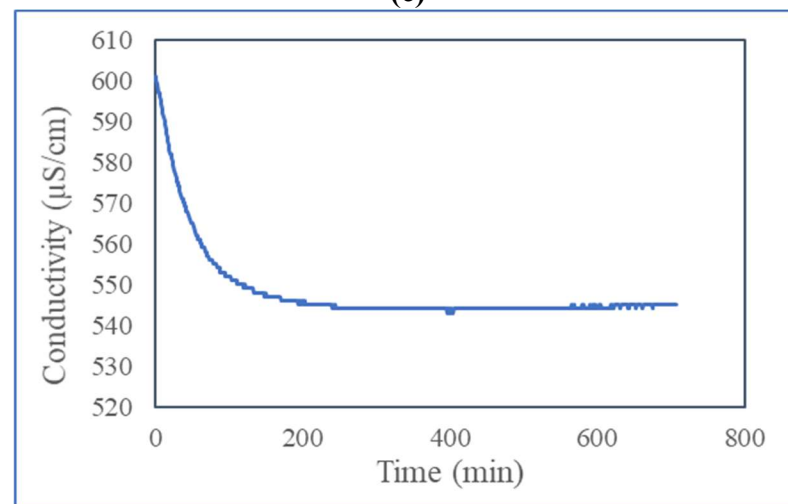
(a)



(c)

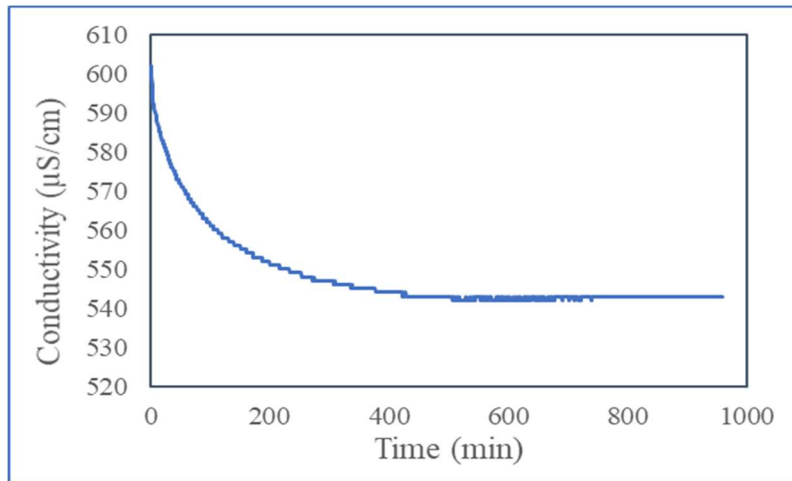


(b)

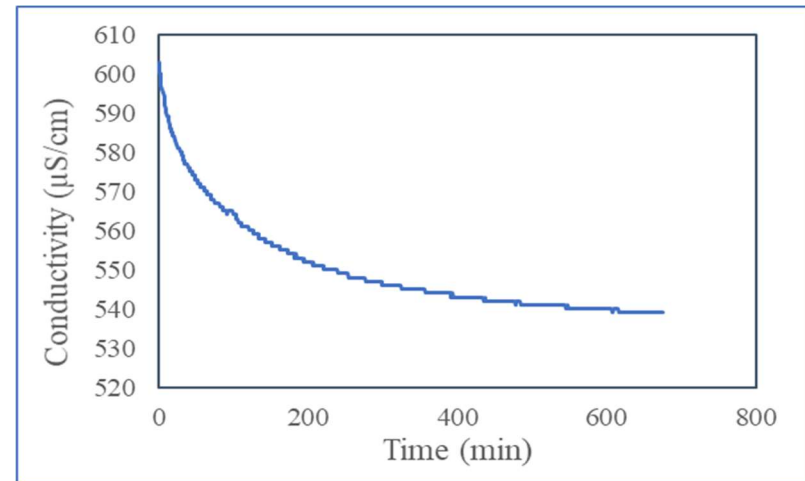


(d)

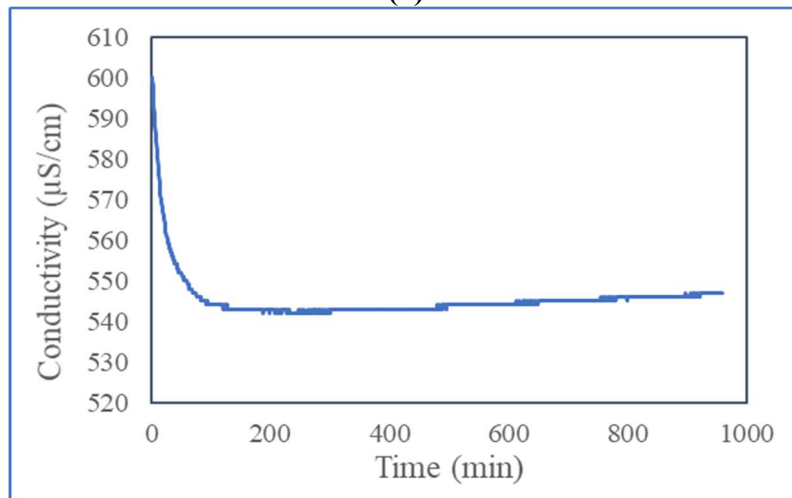
B4: Tests for Voltage = 1 V



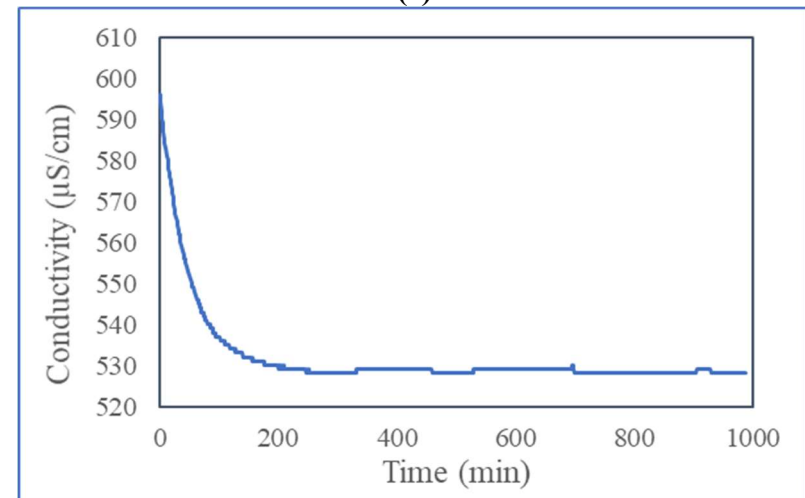
(a)



(c)

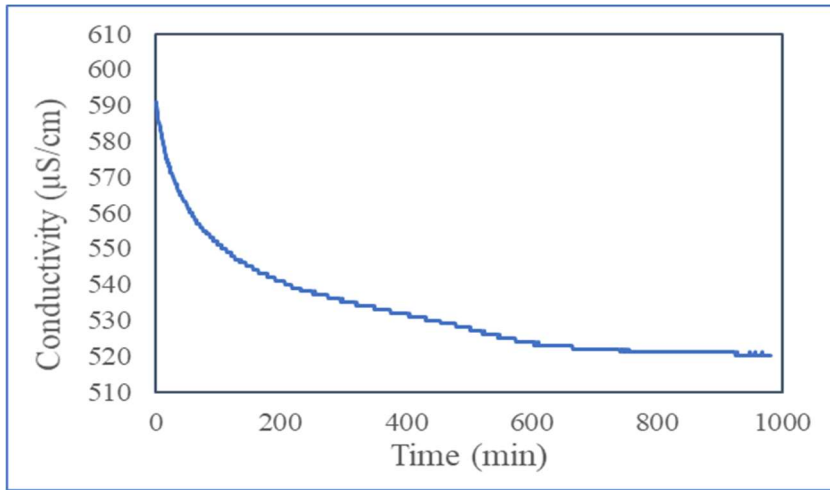


(b)

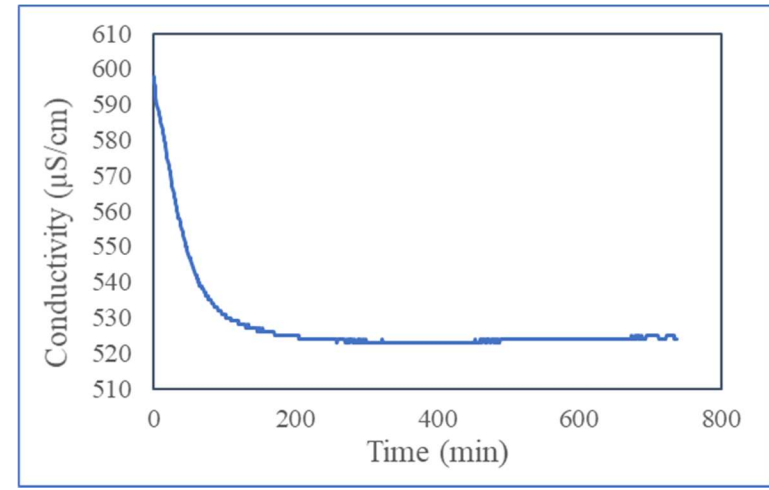


(d)

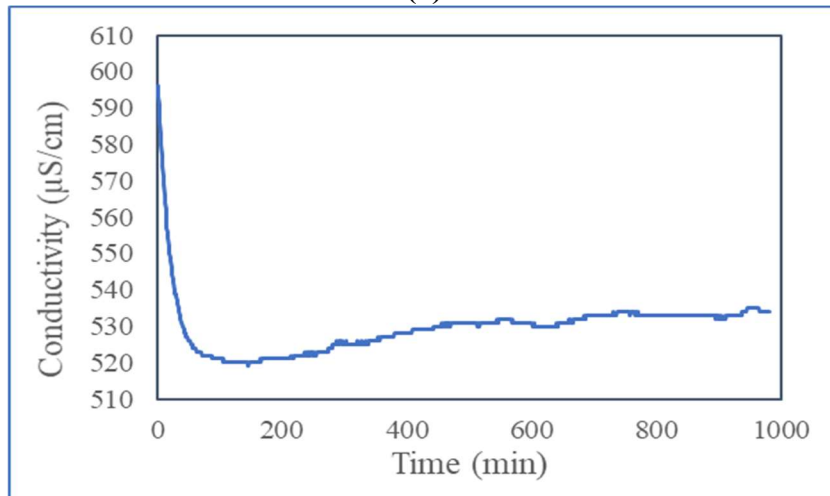
B5: Tests for Voltage = 1.2 V



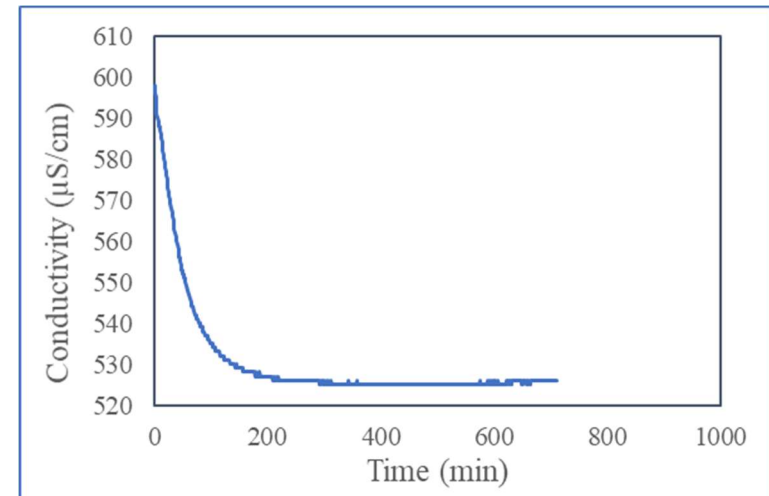
(a)



(c)

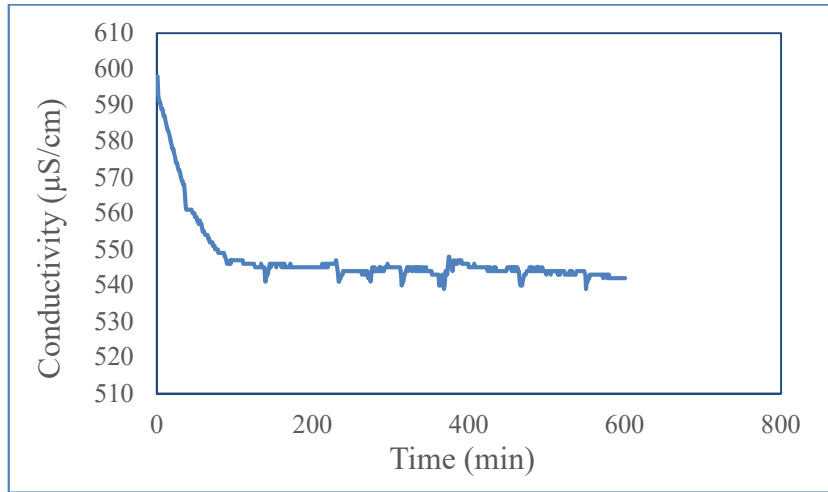


(b)

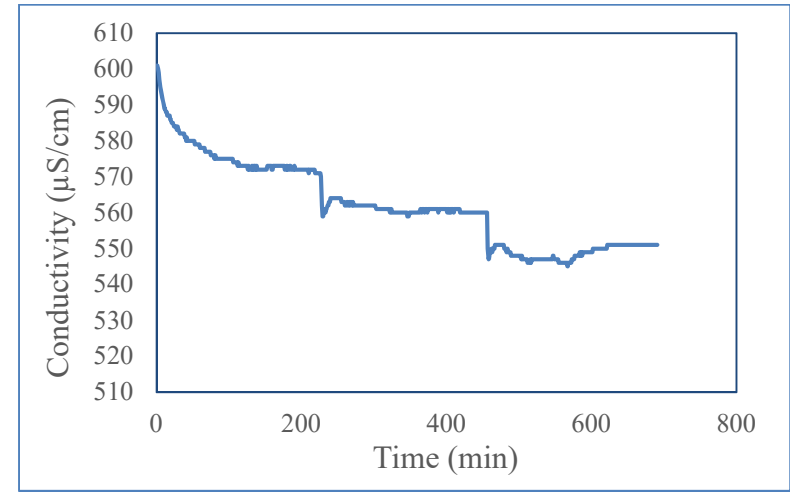


(d)

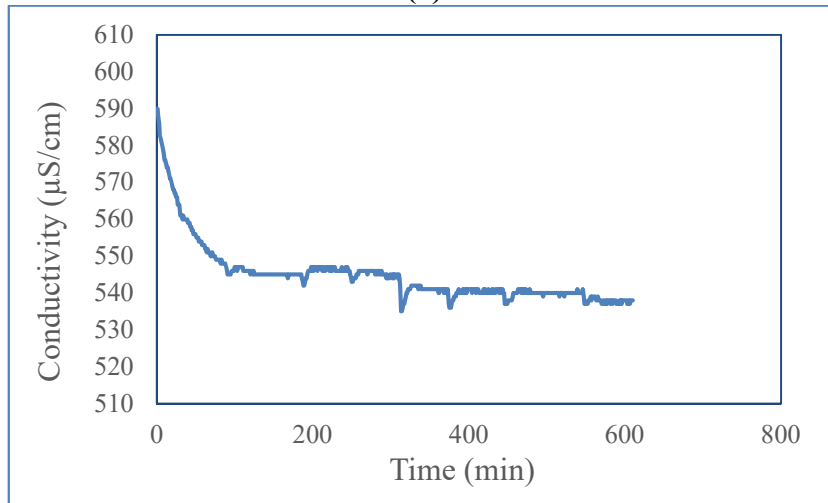
B6: Tests for Temperature Level = 9.7°C



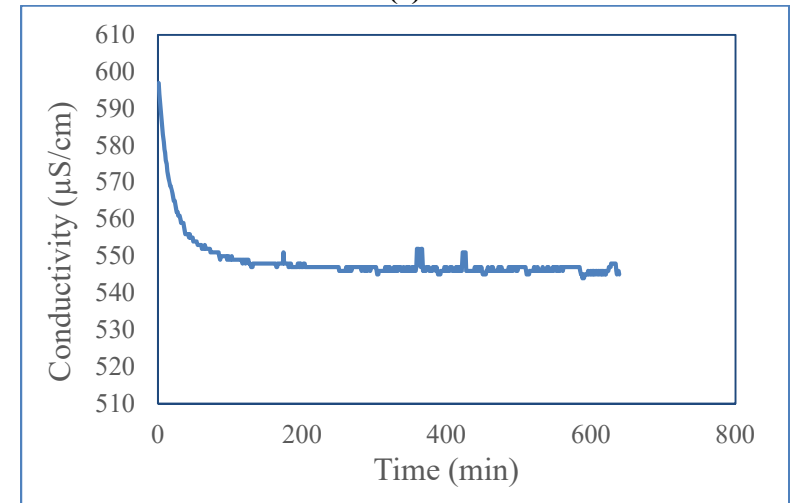
(a)



(c)

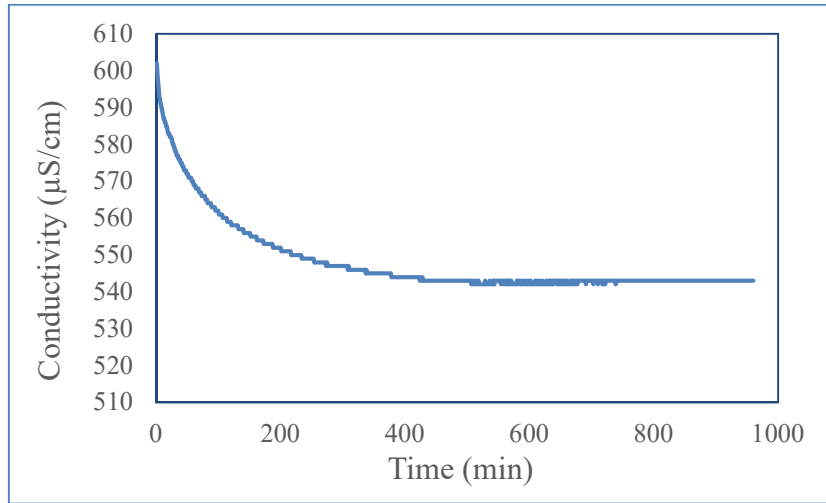


(b)

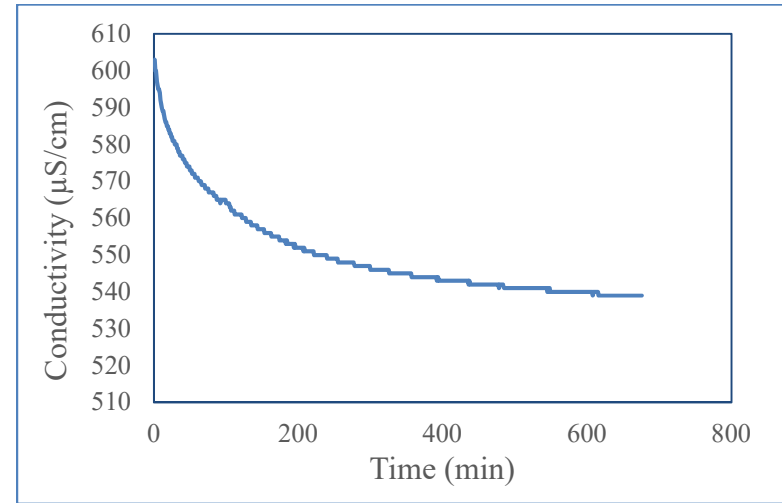


(d)

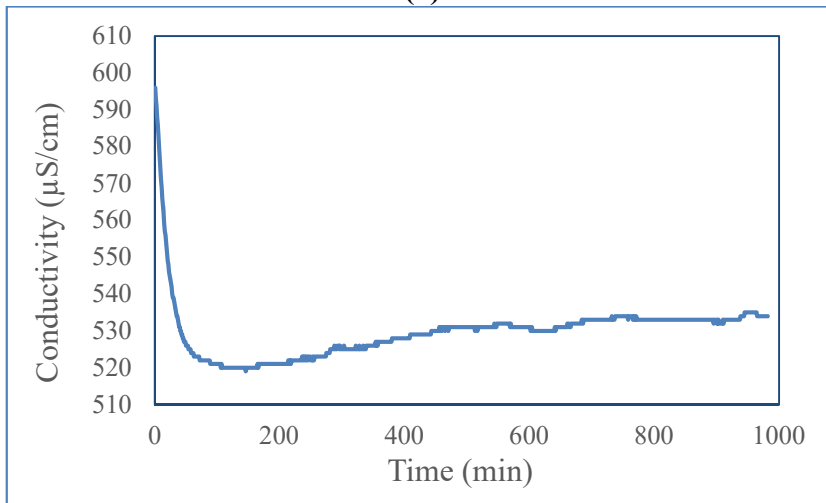
B7: Tests for Temperature Level = 23°C



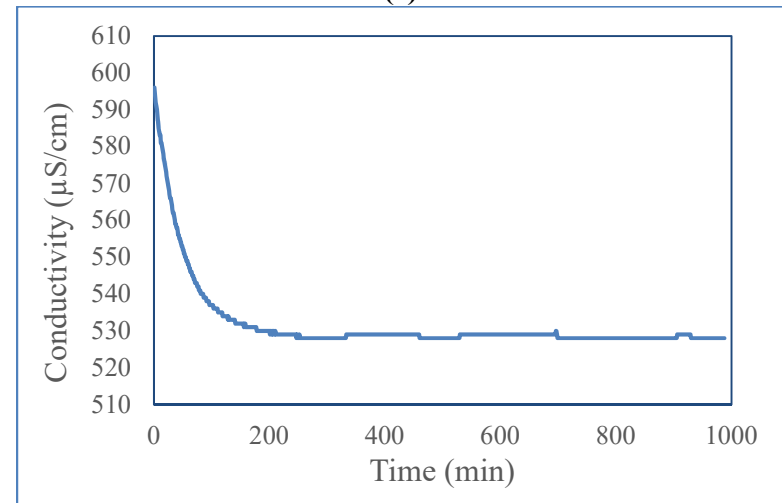
(a)



(c)

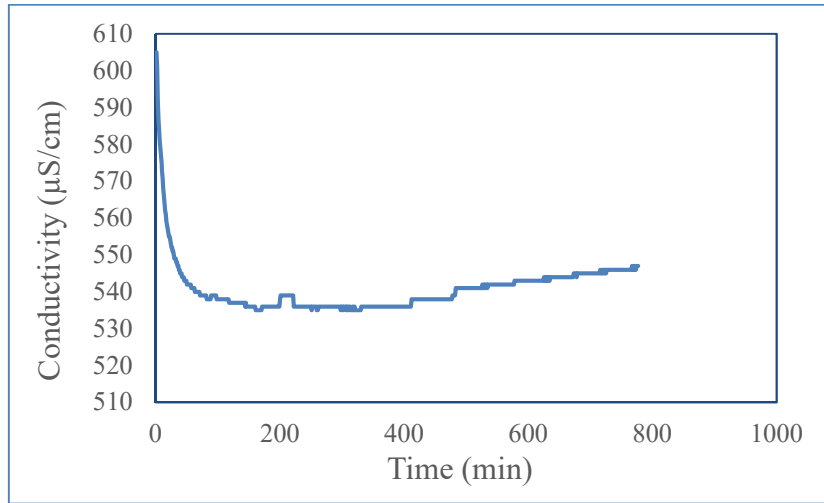


(b)

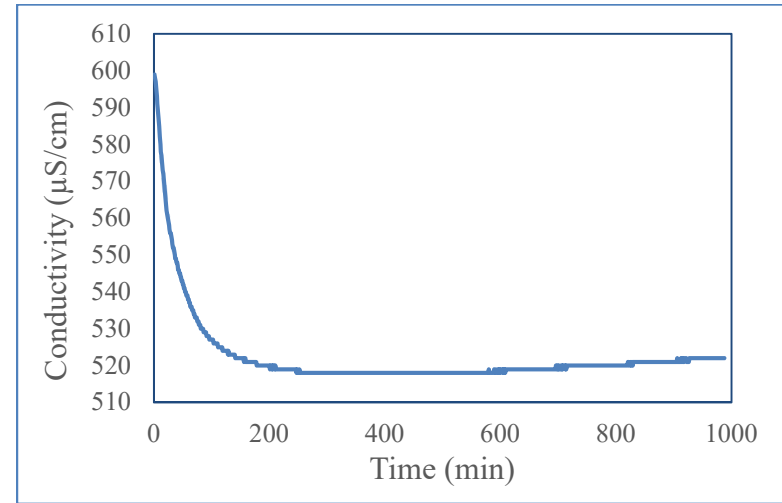


(d)

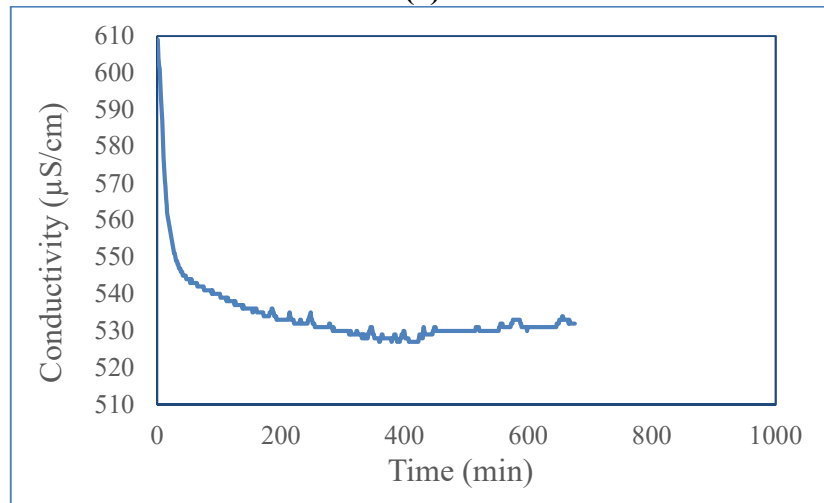
B8: Tests for Temperature Level = 34°C



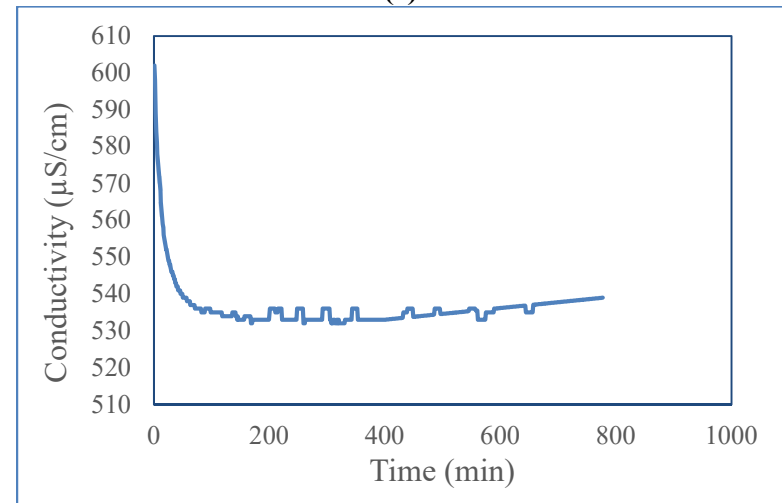
(a)



(c)

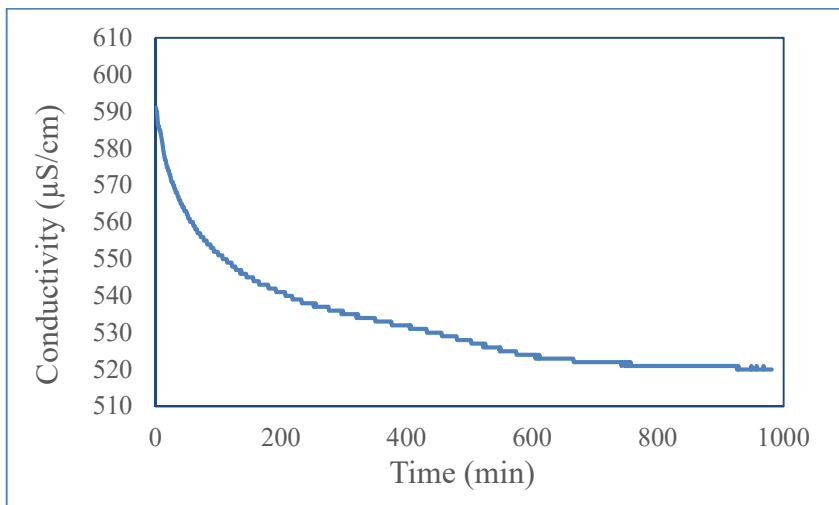


(b)

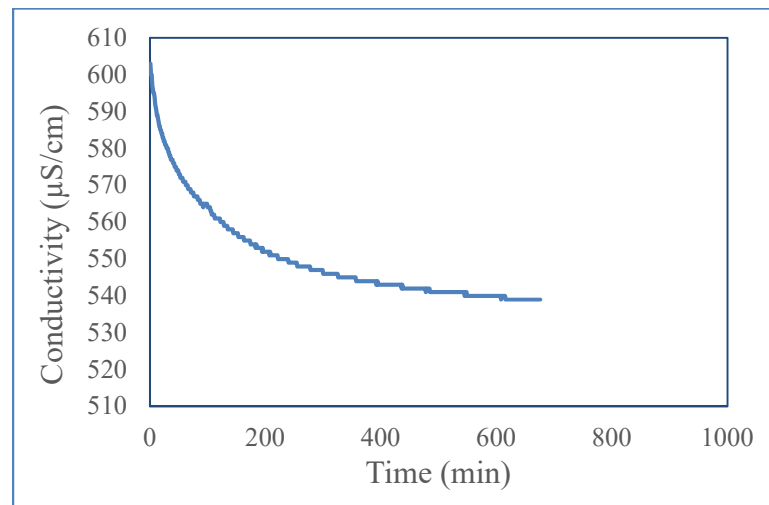


(d)

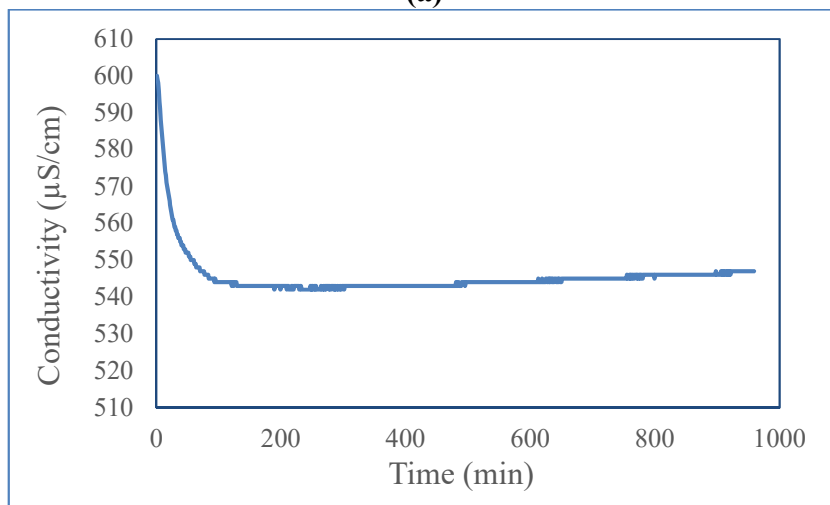
B9: Tests for Flow Rate = 12 mL/min



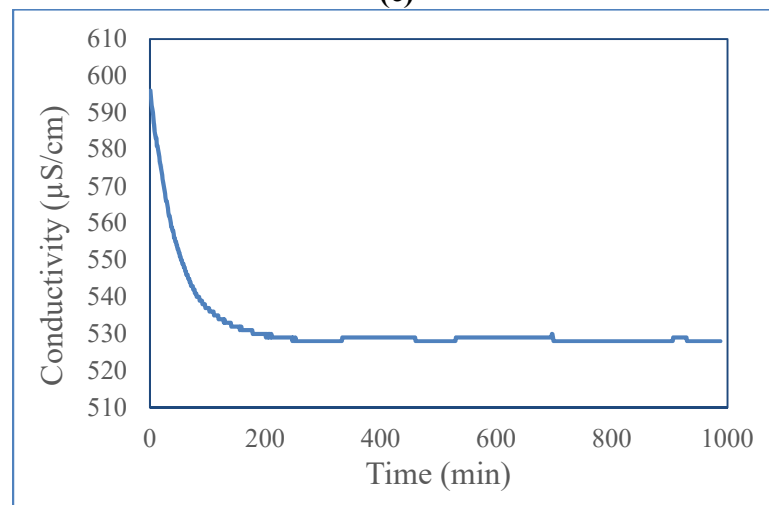
(a)



(c)

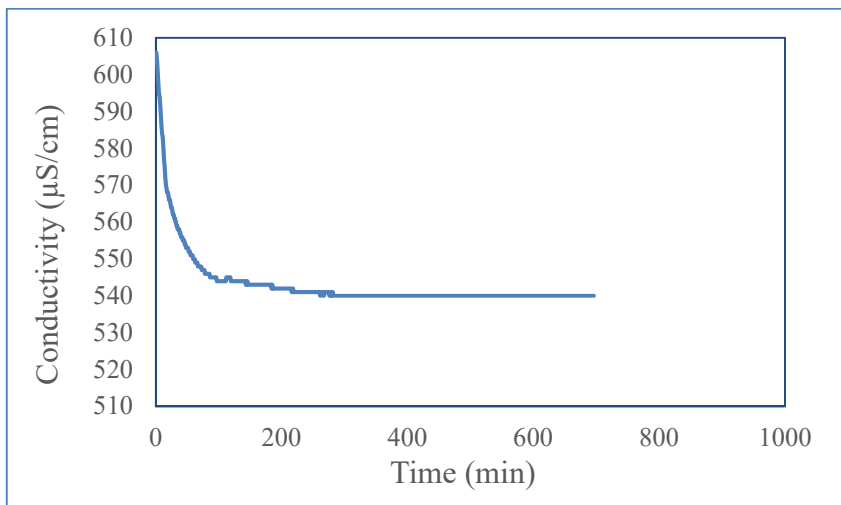


(b)

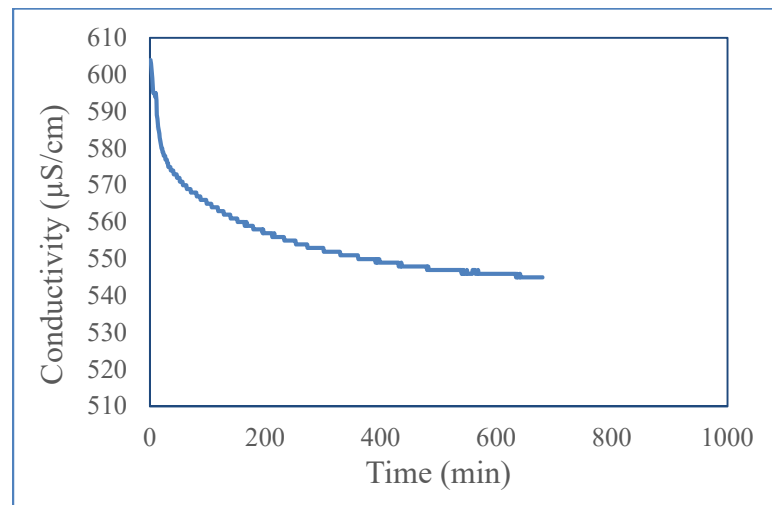


(d)

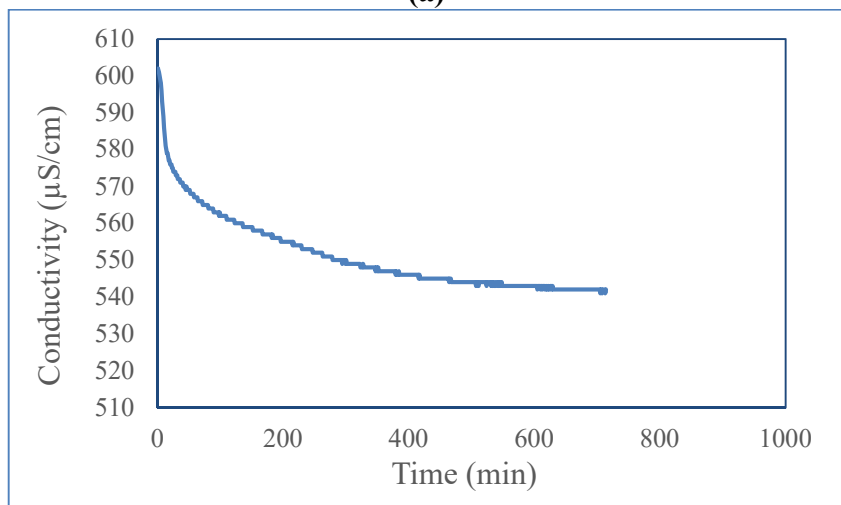
B10: Tests for Flow Rate = 18 mL/min



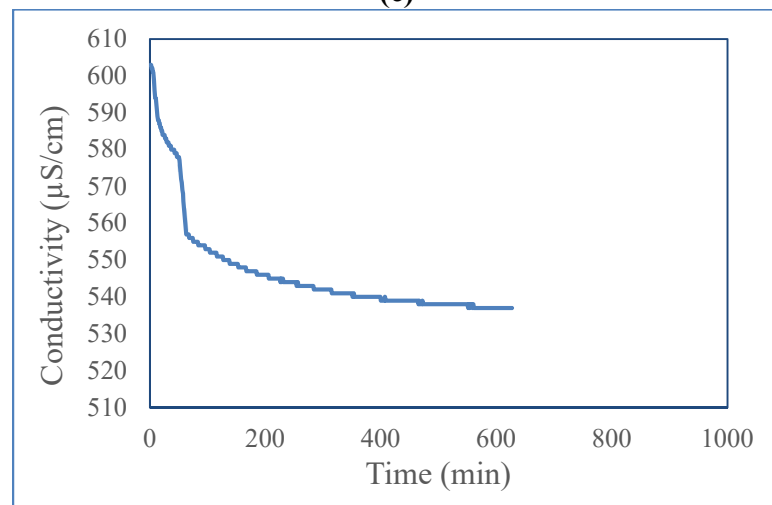
(a)



(c)

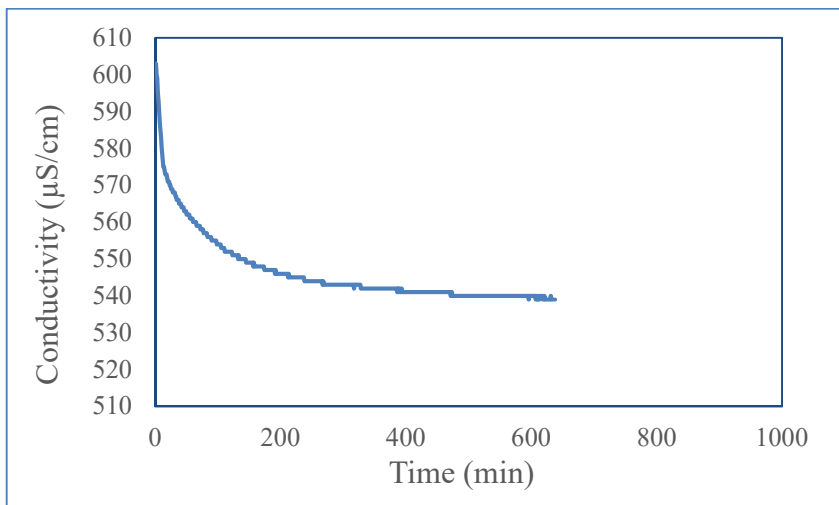


(b)

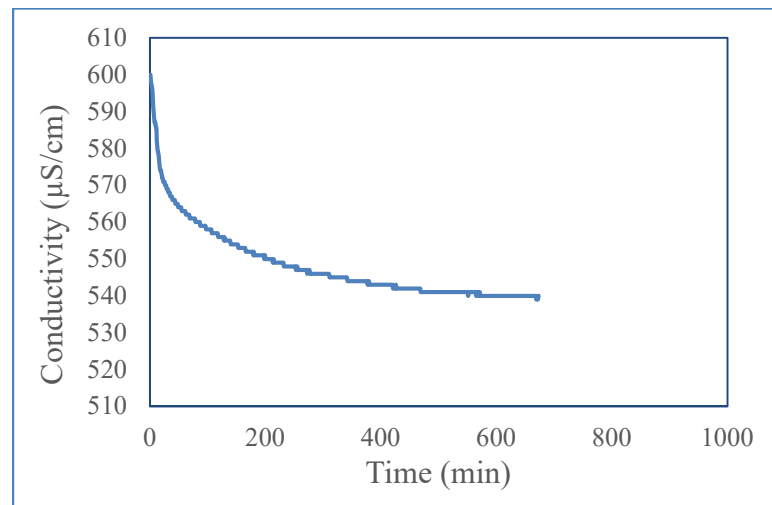


(d)

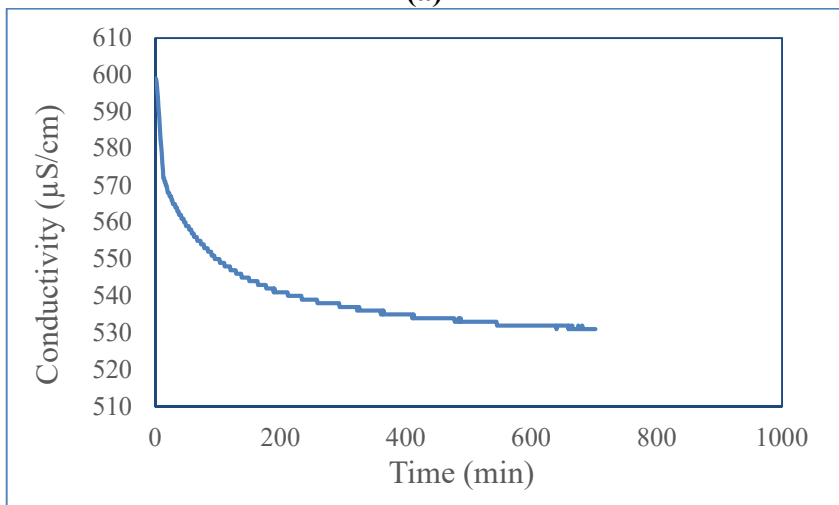
B11: Tests for Flow Rate = 24 mL/min



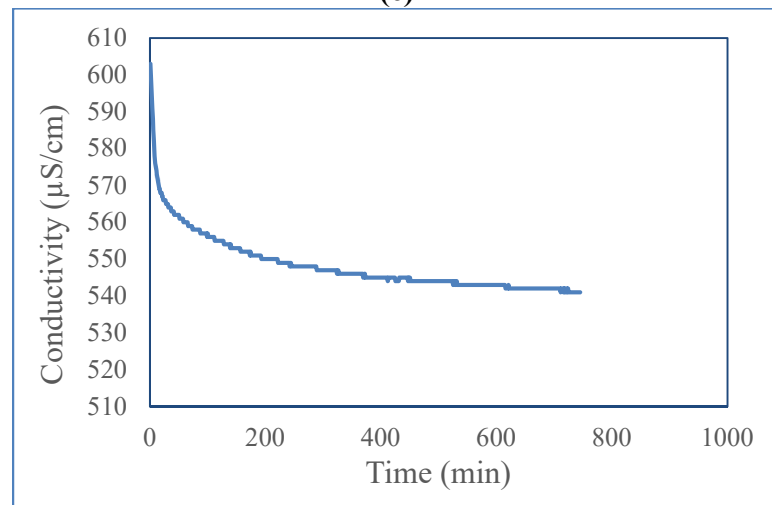
(a)



(c)

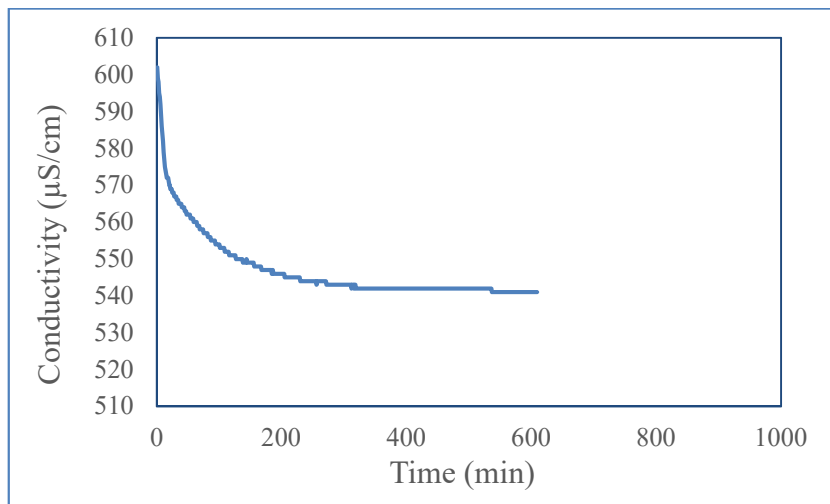


(b)

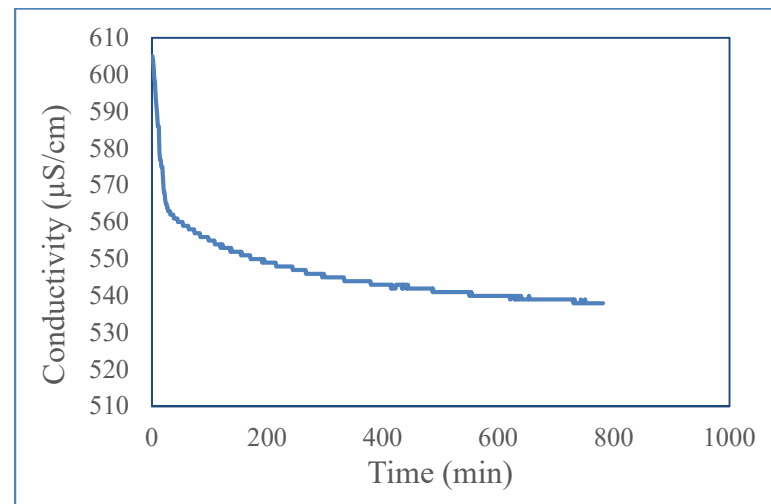


(d)

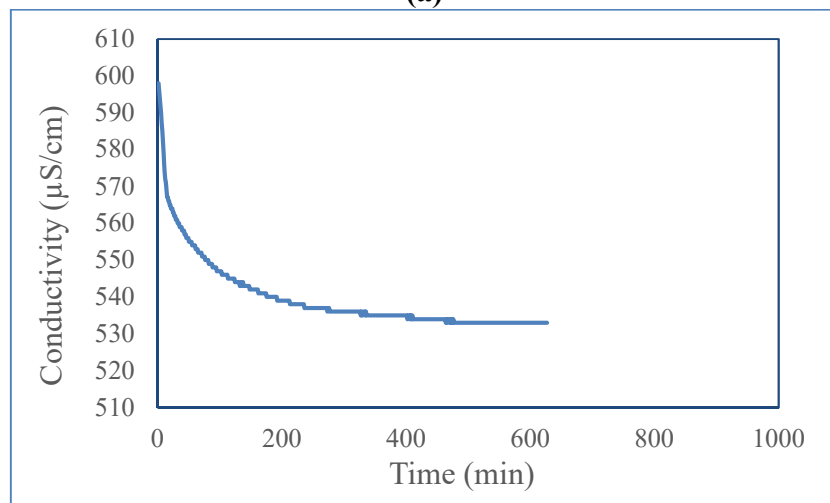
B12: Tests for Flow Rate = 30 mL/min



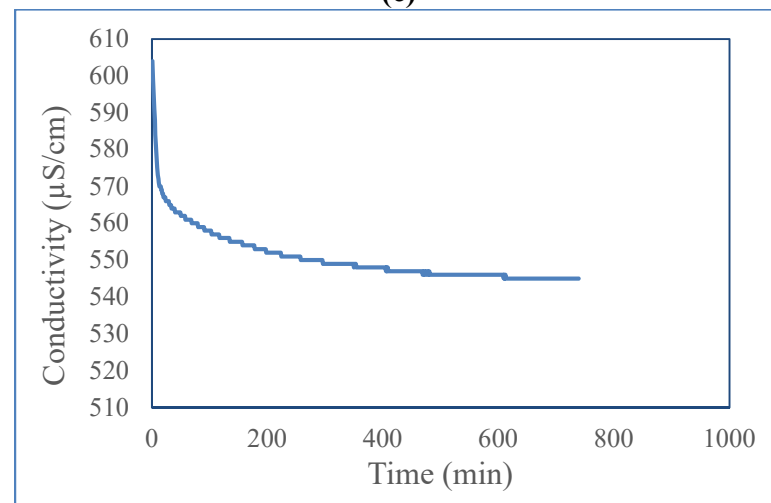
(a)



(c)

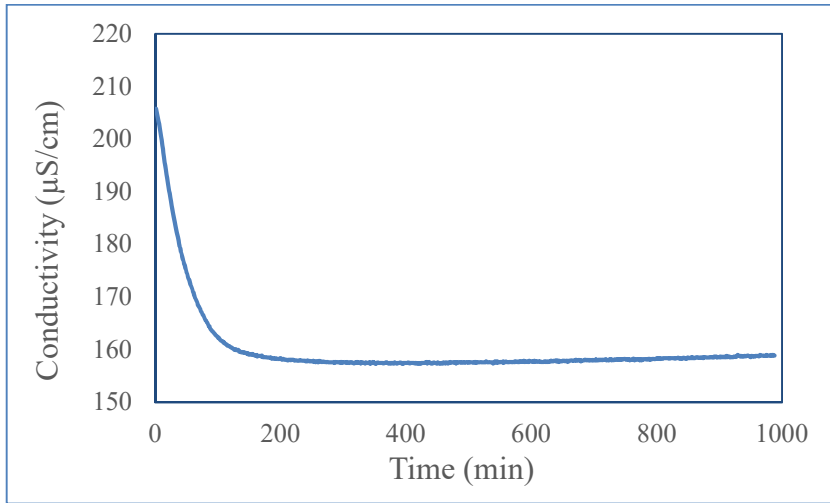


(b)

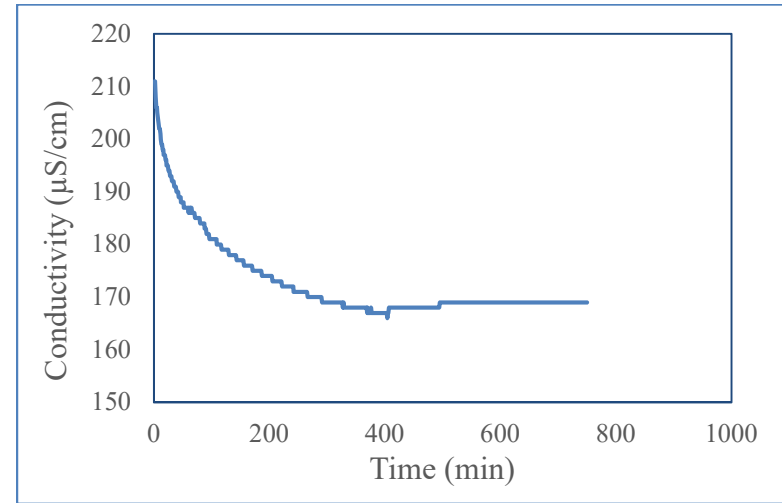


(d)

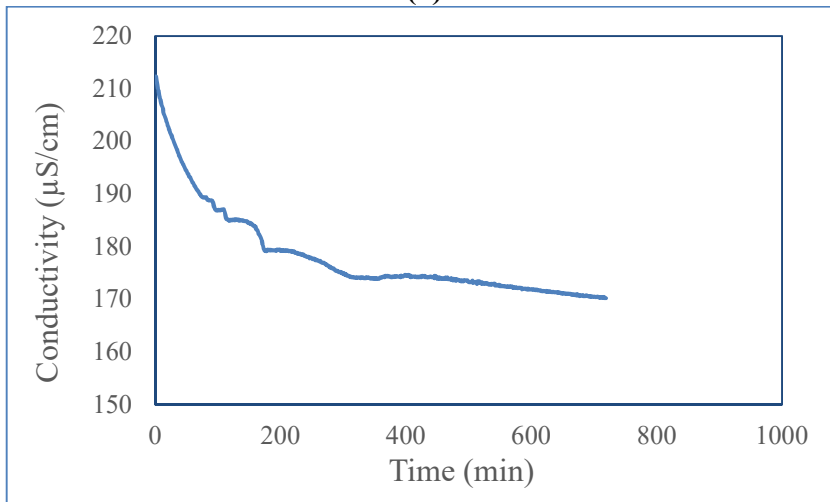
B13: Tests for initial concentration = 100 mg/L



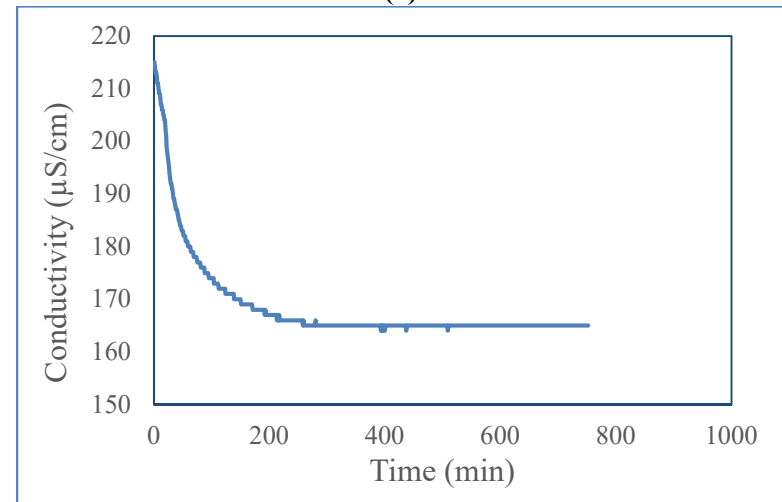
(a)



(c)

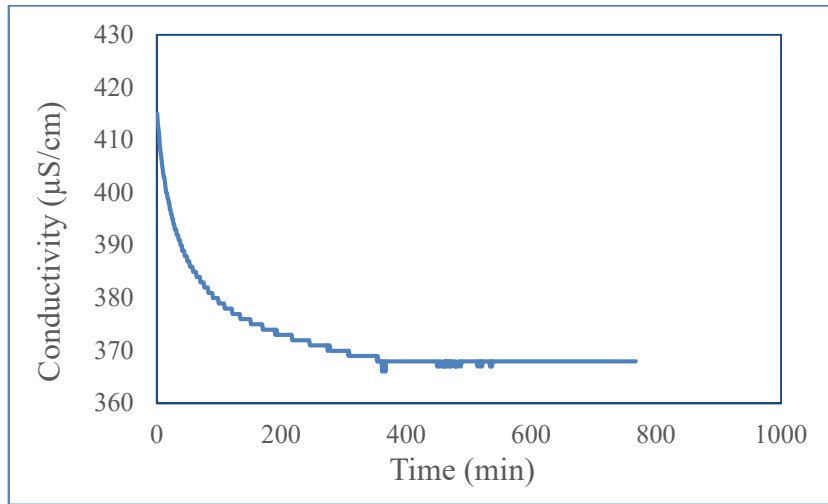


(b)

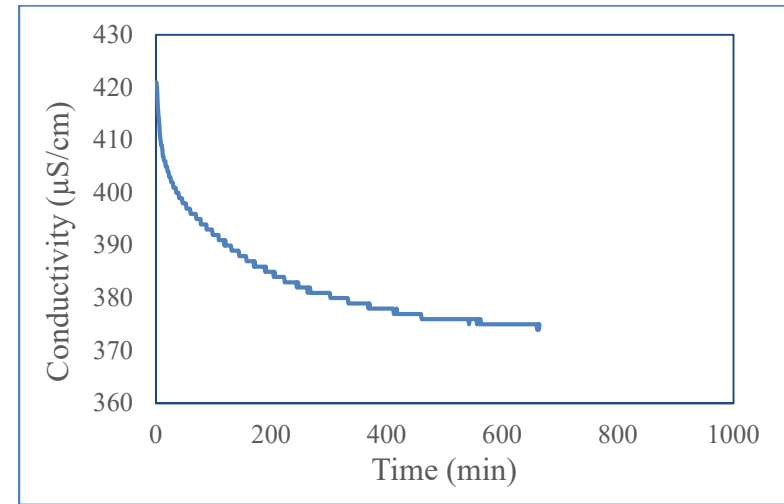


(d)

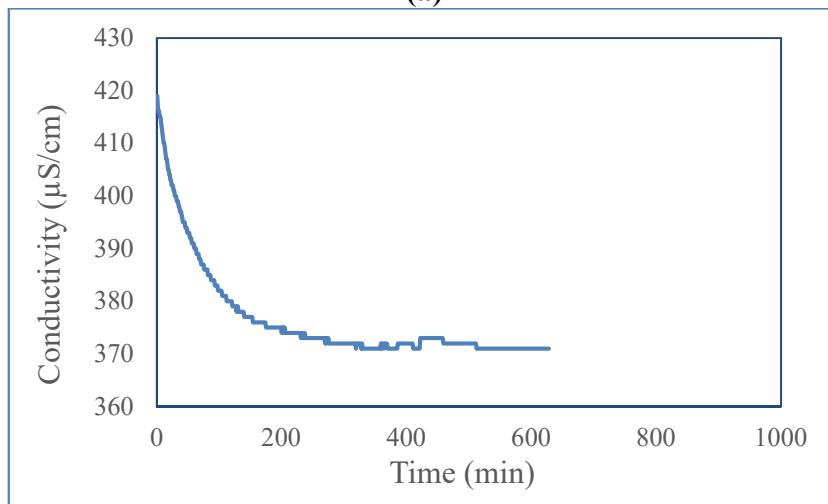
B14: Tests for initial concentration = 200 mg/L



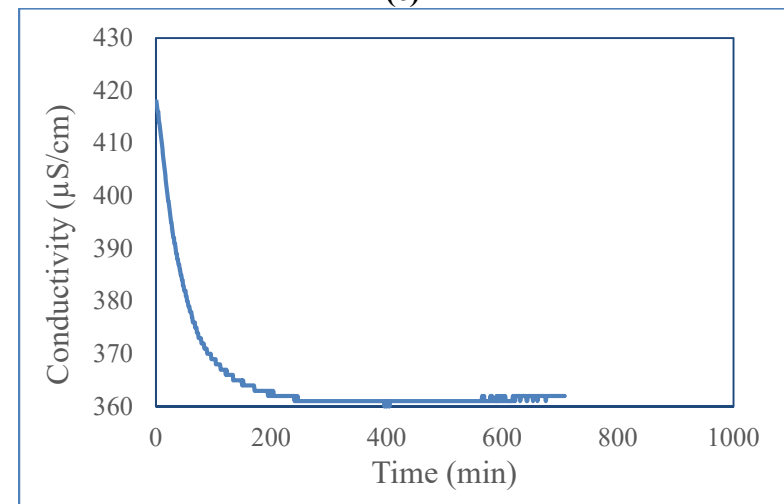
(a)



(c)

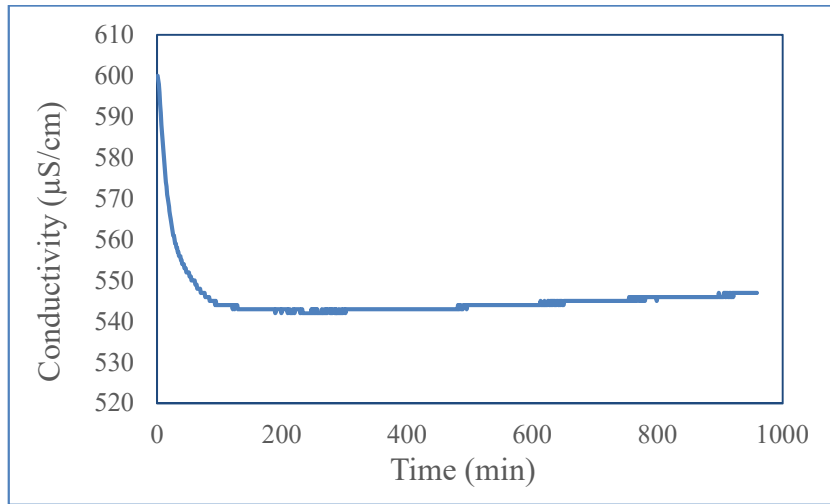


(b)

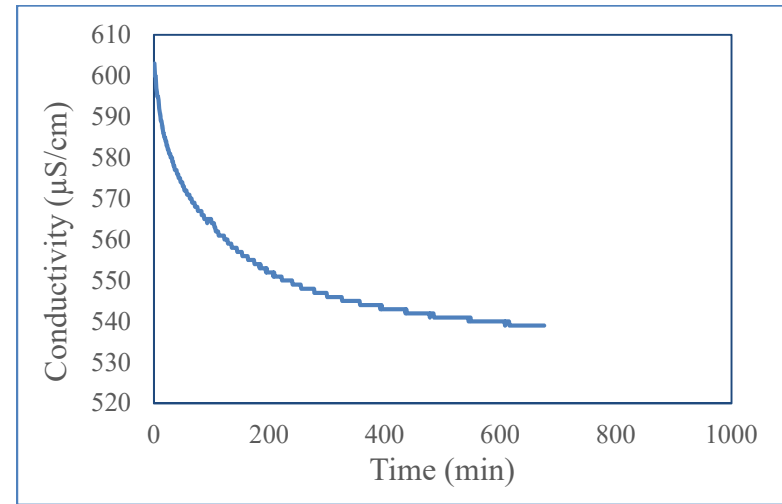


(d)

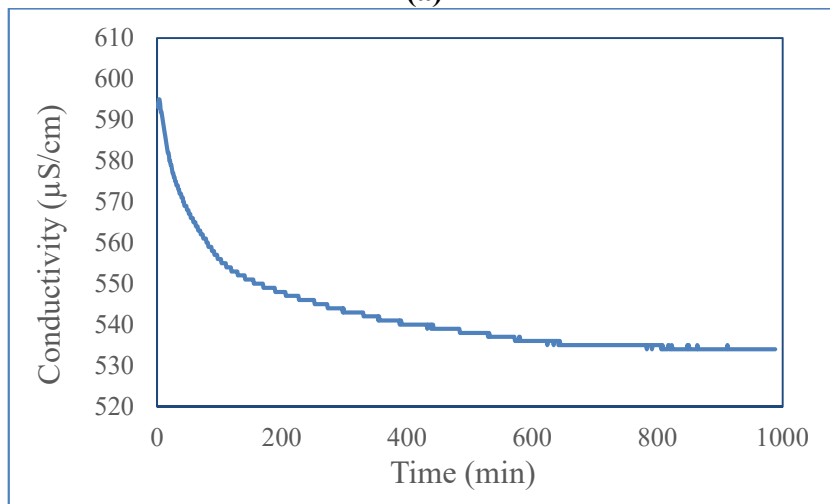
B15: Tests for initial concentration = 300 mg/L



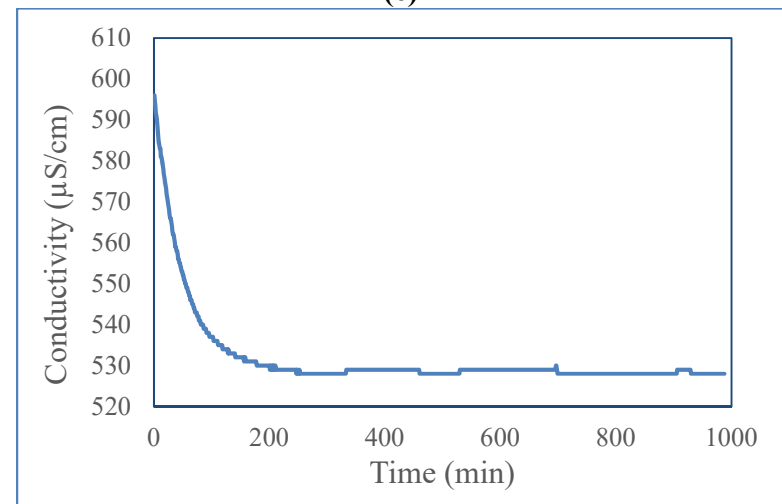
(a)



(c)

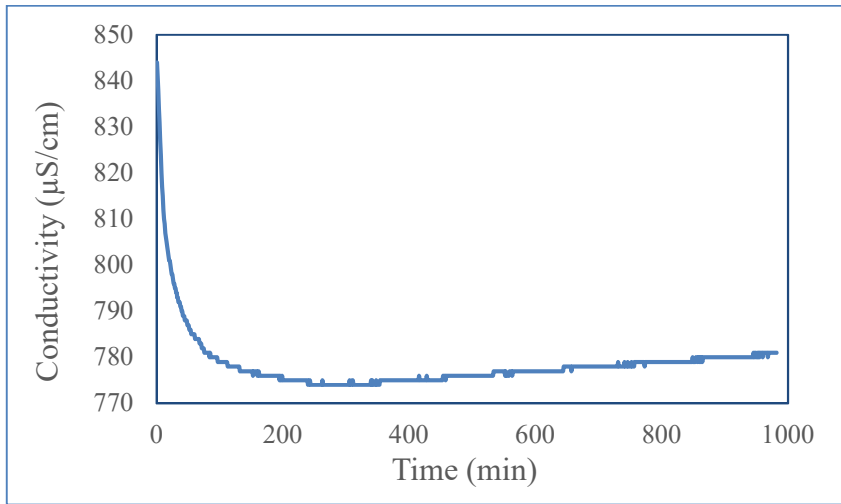


(b)

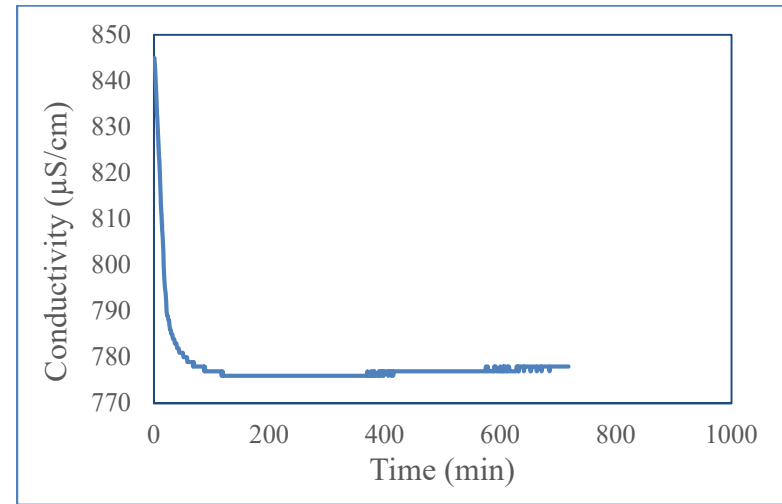


(d)

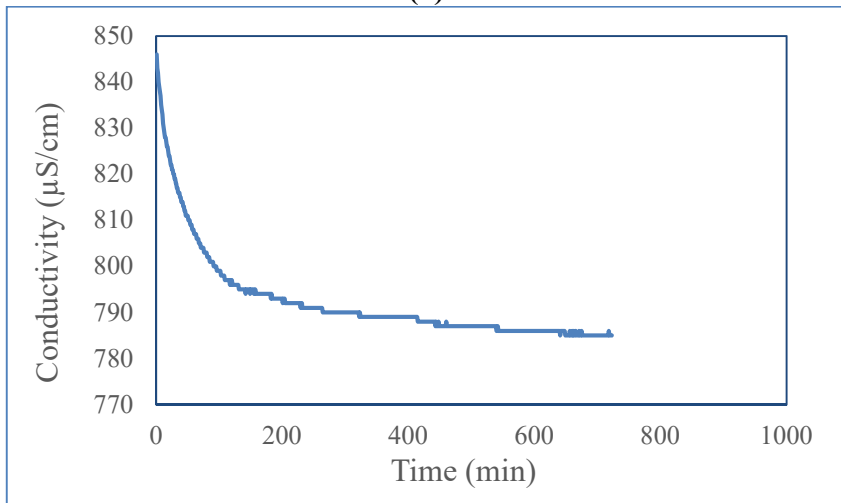
B16: Tests for initial concentration = 400 mg/L



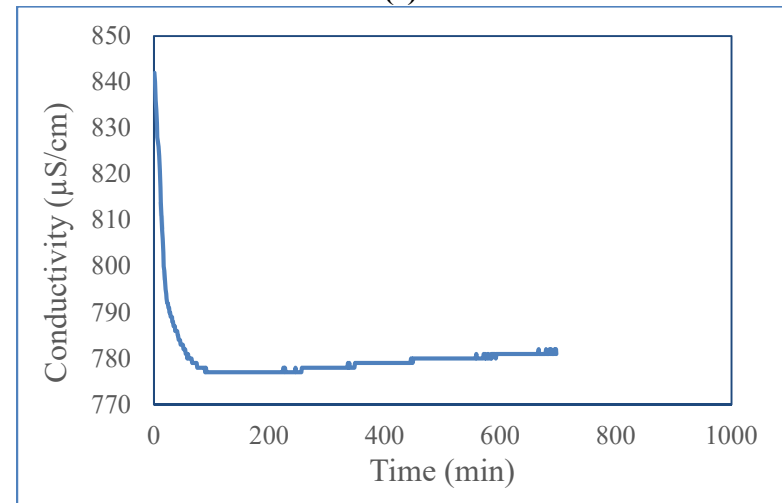
(a)



(c)

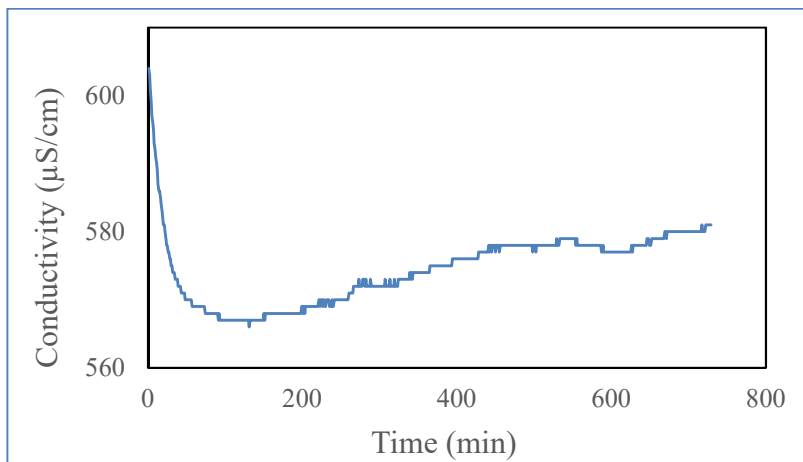


(b)

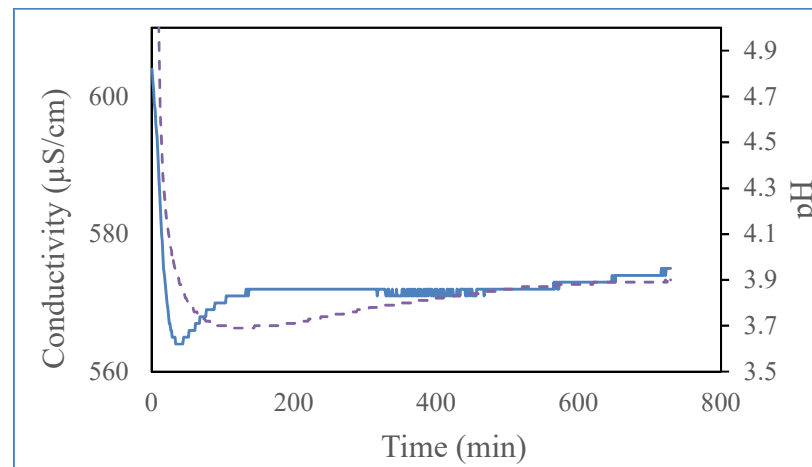


(d)

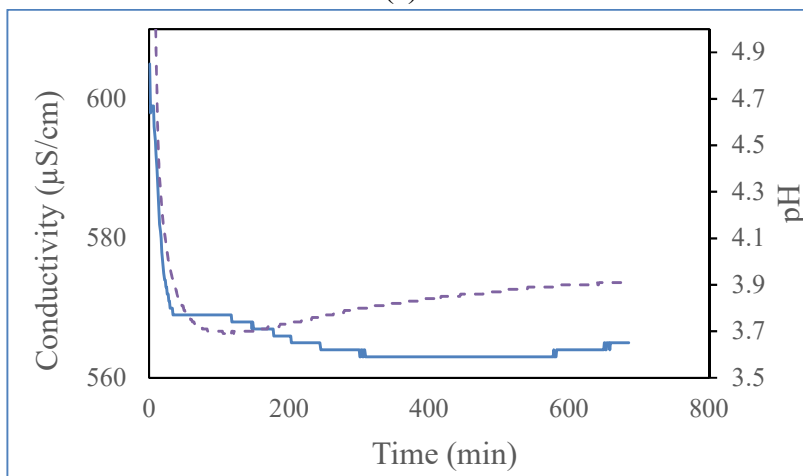
B17: Both acid tests



(a)*



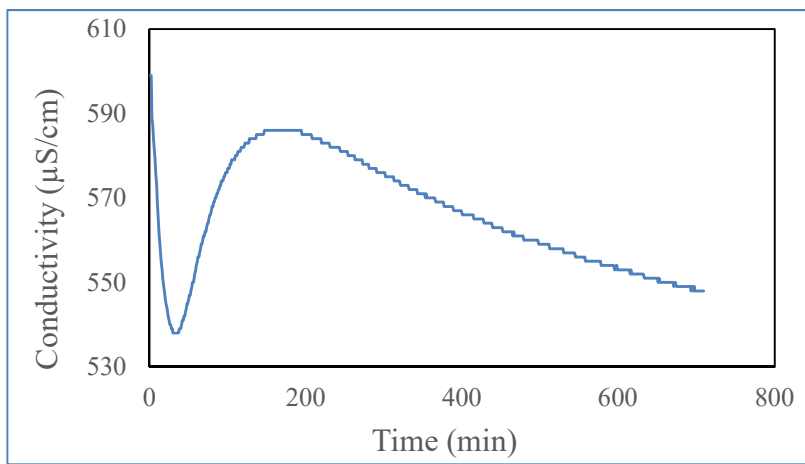
(c)



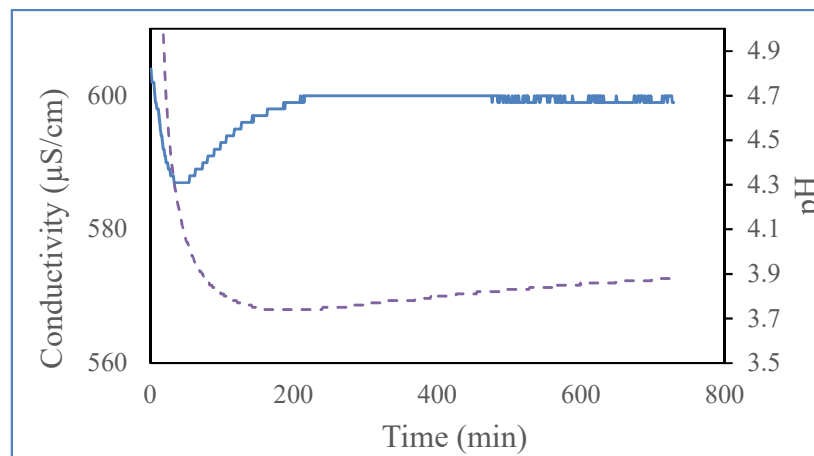
(b)

*pH data was not collected initially.

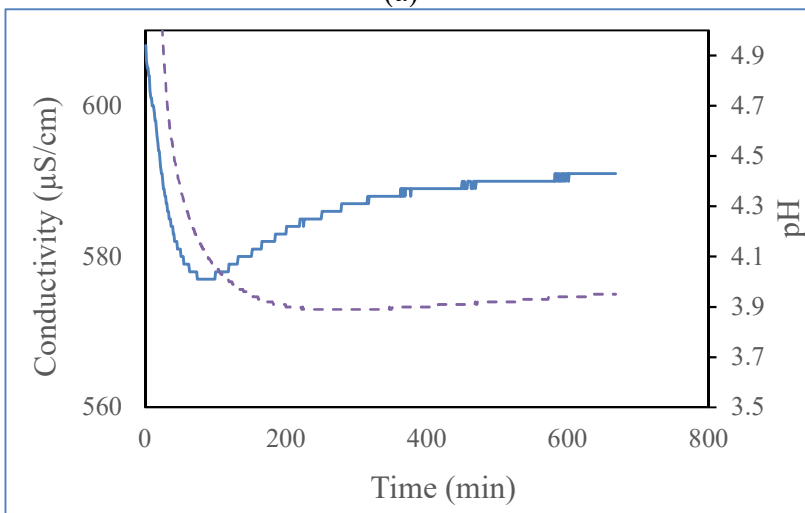
B18: Tests with - nitric acid treated electrode as cathode and untreated electrode as anode



(a)*



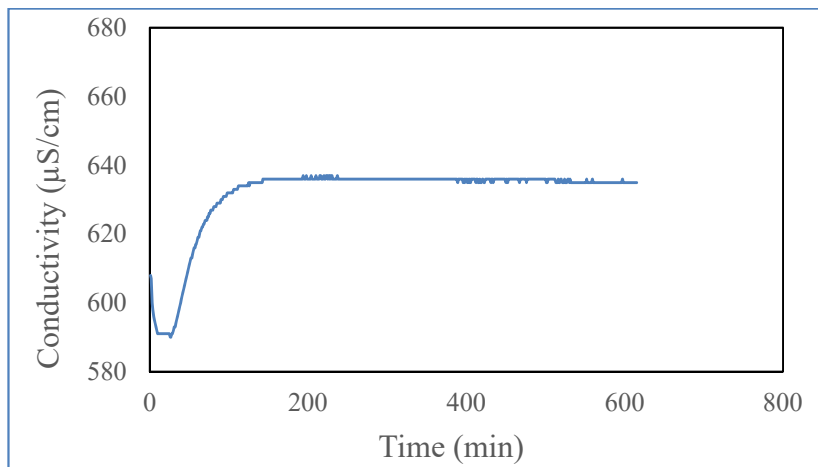
(c)



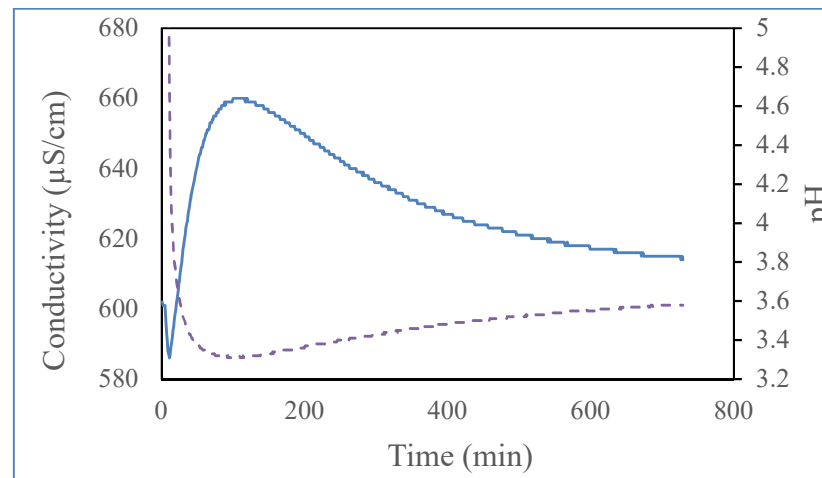
(b)

*pH data was not collected initially.

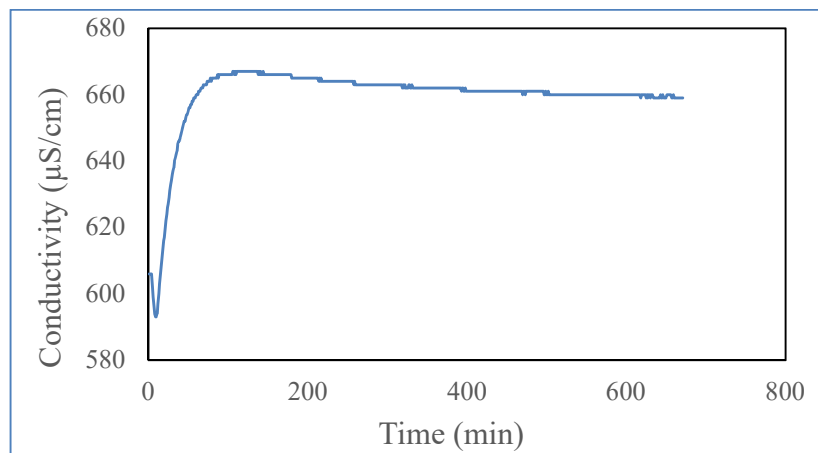
B19: Tests with - nitric acid treated electrode as anode and untreated electrode as cathode



(a)*



(c)



(b)*

*pH data was not collected initially.

REFERENCES

1. Hatzell, K.B., et al., *Capacitive deionization concept based on suspension electrodes without ion exchange membranes*. *Electrochemistry Communications*, 2014. 43(0): p. 18-21.
2. Zhao, Y., et al., *Optimization of the operational parameters for desalination with response surface methodology during a capacitive deionization process*. *Desalination*, 2014. 336(0): p. 64-71.
3. Porada, S., et al., *Review on the science and technology of water desalination by capacitive deionization*. *Progress in Materials Science*, 2013. 58(8): p. 1388-1442.
4. Zhao, R., et al., *Energy consumption in membrane capacitive deionization for different water recoveries and flow rates, and comparison with reverse osmosis*. *Desalination*, 2013. 330(0): p. 35-41.
5. Bouhadana, Y., et al., *Capacitive deionization of NaCl solutions at non-steady-state conditions: inversion functionality of the Carbon electrodes*. *The Journal of Physical Chemistry C*, 2011. 115(33): p. 16567-16573.
6. Gao, X., et al., *Modification of Carbon Xerogel electrodes for more efficient asymmetric capacitive deionization*. *Journal of The Electrochemical Society*, 2013. 160(9): p. E106-E112.
7. Yeo, J.-H. and J.-H. Choi, *Enhancement of nitrate removal from a solution of mixed nitrate, chloride and sulfate ions using a nitrate-selective carbon electrode*. *Desalination*, 2013. 320(0): p. 10-16.
8. Villar, I., et al., *Capacitive deionization of NaCl solutions with modified activated Carbon electrodes*. *Energy & Fuels*, 2010. 24(6): p. 3329-3333.
9. Zafra, M.C., et al., *Electrosorption of environmental concerning anions on a highly porous carbon aerogel*. *Journal of Electroanalytical Chemistry*, 2013. 708(0): p. 80-86.
10. Ahmed, M.A. and S. Tewari. *Effect of pretreatment of Carbon based electrodes in their adsorption performance in capacitive deionization*. in *World Environmental & Water Resources Congress*. 2017. ASCE.
11. Długolecki, P. and A. van der Wal, *Energy recovery in membrane capacitive deionization*. *Environmental Science & Technology*, 2013. 47(9): p. 4904-4910.

12. Liu, Y., et al., *Enhanced desalination efficiency in modified membrane capacitive deionization by introducing ion-exchange polymers in carbon nanotubes electrodes*. *Electrochimica Acta*, 2014. 130(0): p. 619-624.
13. Jande, Y.A.C. and W.S. Kim, *Modeling the capacitive deionization batch mode operation for desalination*. *Journal of Industrial and Engineering Chemistry*, 2014. 20(5): p. 3356-3360.
14. Zhao, R., et al., *Charge efficiency: a functional tool to probe the double-layer structure inside of porous electrodes and application in the modeling of capacitive deionization*. *The Journal of Physical Chemistry Letters*, 2009. 1(1): p. 205-210.
15. Cohen, I., et al., *Enhanced charge efficiency in capacitive deionization achieved by surface-treated electrodes and by means of a third electrode*. *The Journal of Physical Chemistry C*, 2011. 115(40): p. 19856-19863.
16. Zhang, W., et al., *A statistical experimental investigation on arsenic removal using capacitive deionization*. *Desalination and Water Treatment*, 2016. 57(7): p. 3254-3260.
17. Liu, P., et al., *Graphene-based materials for capacitive deionization*. *Journal of Materials Chemistry A*, 2017. 5(27): p. 13907-13943.
18. Huang, Z.-H., et al., *Carbon electrodes for capacitive deionization*. *Journal of Materials Chemistry A*, 2017. 5(2): p. 470-496.
19. Suss, M.E., et al., *Water desalination via capacitive deionization: what is it and what can we expect from it?* *Energy & Environmental Science*, 2015. 8(8): p. 2296-2319.
20. Thamilselvan, A., A.S. Nesaraj, and M. Noel, *Review on carbon-based electrode materials for application in capacitive deionization process*. *International Journal of Environmental Science and Technology*, 2016. 13(12): p. 2961-2976.
21. Welgemoed, T.J. and C.F. Schutte, *Capacitive Deionization Technology™: An alternative desalination solution*. *Desalination*, 2005. 183(1): p. 327-340.
22. Shi, W., et al., *Ultrahigh Performance of Novel Capacitive Deionization Electrodes based on A Three-Dimensional Graphene Architecture with Nanopores*. *Scientific Reports*, 2016. 6: p. 18966.
23. Han, L., et al., *Exploring the impact of pore size distribution on the performance of carbon electrodes for capacitive deionization*. *Journal of Colloid and Interface Science*, 2014. 430: p. 93-99.

24. Lado, J.J., et al., *Asymmetric capacitive deionization utilizing low surface area Carbon electrodes coated with nanoporous thin-films of Al₂O₃ and SiO₂*. Journal of The Electrochemical Society, 2013. 160(8): p. E71-E78.
25. Sun, Z., et al., *Membrane enhanced deionization capacitor device*. 2013, Google Patents.
26. Ahmed, M.A. and S. Tewari. *Preliminary investigation on the optimization of adsorption/desorption performance and operating parameters of capacitive deionization with Carbon Aerogel as electrodes and the effect of surface treatment with TiO₂/ZnO in World Environmental & Water Resources Congress*. 2016. ASCE.
27. Zou, L., G. Morris, and D. Qi, *Using activated carbon electrode in electrosorptive deionisation of brackish water*. Desalination, 2008. 225(1-3): p. 329-340.
28. Ryoo, M.-W. and G. Seo, *Improvement in capacitive deionization function of activated carbon cloth by titania modification*. Water Research, 2003. 37(7): p. 1527-1534.
29. Hou, C.-H., et al., *Development of multi-walled carbon nanotube/poly(vinyl alcohol) composite as electrode for capacitive deionization*. Separation and Purification Technology, 2014. 130(0): p. 7-14.
30. Porada, S., et al., *Water desalination using capacitive deionization with microporous Carbon electrodes*. ACS Applied Materials & Interfaces, 2012. 4(3): p. 1194-1199.
31. Li, H., et al., *Novel graphene-like electrodes for capacitive deionization*. Environmental Science & Technology, 2010. 44(22): p. 8692-8697.
32. El-Deen, A.G., N.A.M. Barakat, and H.Y. Kim, *Graphene wrapped MnO₂-nanostructures as effective and stable electrode materials for capacitive deionization desalination technology*. Desalination, 2014. 344(0): p. 289-298.
33. Avraham, E., et al., *Developing ion electroadsorption stereoselectivity, by pore size adjustment with chemical vapor deposition onto active Carbon fiber electrodes. case of Ca²⁺/Na⁺ separation in water capacitive desalination*. The Journal of Physical Chemistry C, 2008. 112(19): p. 7385-7389.
34. Macías, C., et al., *Improved electro-assisted removal of phosphates and nitrates using mesoporous carbon aerogels with controlled porosity*. Journal of Applied Electrochemistry, 2014. 44(8): p. 963-976.
35. Peng, Z., et al., *Comparative electroadsorption study of mesoporous Carbon electrodes with various pore structures*. The Journal of Physical Chemistry C, 2011. 115(34): p. 17068-17076.

36. Tsouris, C., et al., *Mesoporous Carbon for capacitive deionization of saline water*. Environmental Science & Technology, 2011. 45(23): p. 10243-10249.
37. Dong, Q., et al., *Electrospun composites made of reduced Graphene-Oxide and activated Carbon nanofibers for Capacitive deionization*. Electrochimica Acta, 2014. 137(0): p. 388-394.
38. Li, L., et al., *Ordered mesoporous carbons synthesized by a modified sol-gel process for electrosorptive removal of sodium chloride*. Carbon, 2009. 47(3): p. 775-781.
39. Huang, Z.-H., et al., *Relation between the charge efficiency of activated carbon fiber and Its desalination performance*. Langmuir, 2012. 28(11): p. 5079-5084.
40. Saleem, M.W., et al., *Hybrid CV-CC operation of capacitive deionization in comparison with constant current and constant voltage*. Separation Science and Technology, 2016. 51(6): p. 1063-1069.
41. Choi, J.-H., *Comparison of constant voltage (CV) and constant current (CC) operation in the membrane capacitive deionisation process*. Desalination and Water Treatment, 2015. 56(4): p. 921-928.
42. Zhi, M., et al., *Nanostructured carbon-metal oxide composite electrodes for supercapacitors: a review*. Nanoscale, 2013. 5(1): p. 72-88.
43. Bai, Y., et al., *Graphene oxide-embedded porous carbon nanofiber webs by electrospinning for capacitive deionization*. Colloids and Surfaces A: Physicochemical and Engineering Aspects, 2014. 444(0): p. 153-158.
44. Myint, M.T.Z., S.H. Al-Harhi, and J. Dutta, *Brackish water desalination by capacitive deionization using zinc oxide micro/nanostructures grafted on activated carbon cloth electrodes*. Desalination, 2014. 344(0): p. 236-242.
45. Chen, Y., et al., *Electrospun carbon nanofiber networks from phenolic resin for capacitive deionization*. Chemical Engineering Journal, 2014. 252(0): p. 30-37.
46. Laxman, K., et al., *Enhancement in Ion Adsorption Rate and Desalination Efficiency in a Capacitive Deionization Cell through Improved Electric Field Distribution Using Electrodes Composed of Activated Carbon Cloth Coated with Zinc Oxide Nanorods*. ACS Applied Materials & Interfaces, 2014. 6(13): p. 10113-10120.
47. Yang, L., Z. Shi, and W. Yang, *Enhanced capacitive deionization of lead ions using air-plasma treated carbon nanotube electrode*. Surface and Coatings Technology, 2014. 251(0): p. 122-127.

48. Zhao, S., et al., *Removal of NaCl from saltwater solutions using micro/mesoporous carbon sheets derived from watermelon peel via deionization capacitors*. RSC Advances, 2017. 7(8): p. 4297-4305.
49. Zhao, S., et al., *High capacity and high rate capability of nitrogen-doped porous hollow carbon spheres for capacitive deionization*. Applied Surface Science, 2016. 369(Supplement C): p. 460-469.
50. Peng, Z., et al., *High performance ordered mesoporous carbon/carbon nanotube composite electrodes for capacitive deionization*. Journal of Materials Chemistry, 2012. 22(14): p. 6603-6612.
51. Peng, Z., et al., *Three-dimensional micro/mesoporous carbon composites with carbon nanotube networks for capacitive deionization*. Applied Surface Science, 2013. 282(Supplement C): p. 965-973.
52. Xu, D., et al., *N,P-Codoped Meso-/Microporous Carbon Derived from Biomass Materials via a Dual-Activation Strategy as High-Performance Electrodes for Deionization Capacitors*. ACS Sustainable Chemistry & Engineering, 2017. 5(7): p. 5810-5819.
53. Wang, Z., et al., *Nitrogen-doped porous carbon derived from a bimetallic metal-organic framework as highly efficient electrodes for flow-through deionization capacitors*. Journal of Materials Chemistry A, 2016. 4(28): p. 10858-10868.
54. Wang, Z., et al., *In Situ Expanding Pores of Dodecahedron-like Carbon Frameworks Derived from MOFs for Enhanced Capacitive Deionization*. ACS Applied Materials & Interfaces, 2017. 9(17): p. 15068-15078.
55. Zhao, S., et al., *Creating 3D Hierarchical Carbon Architectures with Micro-, Meso-, and Macropores via a Simple Self-Blowing Strategy for a Flow-through Deionization Capacitor*. ACS Applied Materials & Interfaces, 2016. 8(28): p. 18027-18035.
56. Wen, X., et al., *Three-dimensional hierarchical porous carbon with a bimodal pore arrangement for capacitive deionization*. Journal of Materials Chemistry, 2012. 22(45): p. 23835-23844.
57. Wang, H., et al., *Creating Nitrogen-Doped Hollow Multiyolk@Shell Carbon as High Performance Electrodes for Flow-Through Deionization Capacitors*. ACS Sustainable Chemistry & Engineering, 2017. 5(4): p. 3329-3338.
58. Goh, P.S. and A.F. Ismail, *Graphene-based nanomaterial: The state-of-the-art material for cutting edge desalination technology*. Desalination, 2015. 356: p. 115-128.

59. Lee, S.-H., D. Kang, and I.-K. Oh, *Multilayered graphene-carbon nanotube-iron oxide three-dimensional heterostructure for flexible electromagnetic interference shielding film*. Carbon, 2017. 111(Supplement C): p. 248-257.
60. Wang, H., et al., *Graphene prepared via a novel pyridine-thermal strategy for capacitive deionization*. Journal of Materials Chemistry, 2012. 22(45): p. 23745-23748.
61. Wang, H., et al., *Three-dimensional macroporous graphene architectures as high performance electrodes for capacitive deionization*. Journal of Materials Chemistry A, 2013. 1(38): p. 11778-11789.
62. Wang, H., et al., *In situ creating interconnected pores across 3D graphene architectures and their application as high performance electrodes for flow-through deionization capacitors*. Journal of Materials Chemistry A, 2016. 4(13): p. 4908-4919.
63. Duan, H., et al., *A facile strategy for the fast construction of porous graphene frameworks and their enhanced electrosorption performance*. Chemical Communications, 2017. 53(54): p. 7465-7468.
64. Lei, H., et al., *Graphene-like carbon nanosheets prepared by a Fe-catalyzed glucose-blowing method for capacitive deionization*. Journal of Materials Chemistry A, 2015. 3(11): p. 5934-5941.
65. Lu, X., H. Dou, and X. Zhang, *Mesoporous carbon nanospheres inserting into graphene sheets for flexible supercapacitor film electrode*. Materials Letters, 2016. 178(Supplement C): p. 304-307.
66. Zhang, D., et al., *Enhanced capacitive deionization of graphene/mesoporous carbon composites*. Nanoscale, 2012. 4(17): p. 5440-5446.
67. Zhang, D., et al., *Enhanced capacitive deionization performance of graphene/carbon nanotube composites*. Journal of Materials Chemistry, 2012. 22(29): p. 14696-14704.
68. Wen, X., et al., *Three-dimensional graphene-based hierarchically porous carbon composites prepared by a dual-template strategy for capacitive deionization*. Journal of Materials Chemistry A, 2013. 1(39): p. 12334-12344.
69. Wang, H., et al., *Design of graphene-coated hollow mesoporous carbon spheres as high performance electrodes for capacitive deionization*. Journal of Materials Chemistry A, 2014. 2(13): p. 4739-4750.
70. Liu, P., et al., *Separation and recovery of heavy metal ions and salt ions from wastewater by 3D graphene-based asymmetric electrodes via capacitive deionization*. Journal of Materials Chemistry A, 2017. 5(28): p. 14748-14757.

71. Liu, P., et al., *Grafting sulfonic and amine functional groups on 3D graphene for improved capacitive deionization*. Journal of Materials Chemistry A, 2016. 4(14): p. 5303-5313.
72. Zhao, R., et al., *Optimization of salt adsorption rate in membrane capacitive deionization*. Water Research, 2013. 47(5): p. 1941-1952.
73. Liang, P., et al., *Coupling ion-exchangers with inexpensive activated carbon fiber electrodes to enhance the performance of capacitive deionization cells for domestic wastewater desalination*. Water Research, 2013. 47(7): p. 2523-2530.
74. Minhas, M.B., Y.A.C. Jande, and W.S. Kim, *Combined reverse osmosis and constant-current operated capacitive deionization system for seawater desalination*. Desalination, 2014. 344(0): p. 299-305.
75. Omosebi, A., et al., *Asymmetric Electrode Configuration for Enhanced Membrane Capacitive Deionization*. ACS Applied Materials & Interfaces, 2014.
76. Shi, K., M. Ren, and I. Zhitomirsky, *Activated Carbon-Coated Carbon Nanotubes for Energy Storage in Supercapacitors and Capacitive Water Purification*. ACS Sustainable Chemistry & Engineering, 2014. 2(5): p. 1289-1298.
77. Wang, J., et al., *Embedded Ag quantum dots into interconnected Co₃O₄ nanosheets grown on 3D graphene networks for high stable and flexible supercapacitors*. Electrochimica Acta, 2017. 224(Supplement C): p. 260-268.
78. Mossad, M., W. Zhang, and L. Zou, *Using capacitive deionisation for inland brackish groundwater desalination in a remote location*. Desalination, 2013. 308(Supplement C): p. 154-160.
79. Kim, T.Y., et al., *High-Performance Supercapacitors Based on Poly(ionic liquid)-Modified Graphene Electrodes*. ACS Nano, 2011. 5(1): p. 436-442.
80. Hatzell, K.B., et al., *Effect of Oxidation of Carbon Material on Suspension Electrodes for Flow Electrode Capacitive Deionization*. Environmental Science & Technology, 2015. 49(5): p. 3040-3047.
81. Gao, X., et al., *Surface charge enhanced carbon electrodes for stable and efficient capacitive deionization using inverted adsorption-desorption behavior*. Energy & Environmental Science, 2015. 8(3): p. 897-909.
82. Gao, X., et al., *Enhanced Salt Removal in an Inverted Capacitive Deionization Cell Using Amine Modified Microporous Carbon Cathodes*. Environmental Science & Technology, 2015. 49(18): p. 10920-10926.
83. Seo, S.-J., et al., *Investigation on removal of hardness ions by capacitive deionization (CDI) for water softening applications*. Water Research, 2010. 44(7): p. 2267-2275.

84. Huang, S.-Y., C.-S. Fan, and C.-H. Hou, *Electro-enhanced removal of copper ions from aqueous solutions by capacitive deionization*. Journal of Hazardous Materials, 2014. 278(0): p. 8-15.
85. Zhang, W., M. Mossad, and L. Zou, *A study of the long-term operation of capacitive deionisation in inland brackish water desalination*. Desalination, 2013. 320(Supplement C): p. 80-85.
86. Zhang, W. and B. Jia, *Toward anti-fouling capacitive deionization by using visible-light reduced TiO₂/graphene nanocomposites*. MRS Communications, 2015. 5(4): p. 613-617.
87. Laidler, K.J. and J.H. Meiser, *Physical chemistry*. 1982, Menlo Park, Calif.: Benjamin/Cummings Pub. Co.
88. Popov, B., *Chapter 3. Electrochemical Kinetics of Corrosion*. 2015. 93-142.
89. Schweiss, R., A. Pritzl, and C. Meiser, *Parasitic hydrogen evolution at different carbon fiber electrodes in vanadium redox flow batteries*. Journal of The Electrochemical Society, 2016. 163(9): p. A2089-A2094.